University of Glasgow

Huang, Mian (2022) *Constitutive modelling of fibre-reinforced sand based on the concept of effective skeleton stress and void ratio.* PhD thesis.

http://theses.gla.ac.uk/82671/

Copyright and moral rights for this work are retained by the author

A copy can be downloaded for personal non-commercial research or study, without prior permission or charge

This work cannot be reproduced or quoted extensively from without first obtaining permission in writing from the author

The content must not be changed in any way or sold commercially in any format or medium without the formal permission of the author

When referring to this work, full bibliographic details including the author, title, awarding institution and date of the thesis must be given

Enlighten: Theses
https://theses.gla.ac.uk/
research-enlighten@glasgow.ac.uk

Constitutive modelling of fibre-reinforced sand based on the concept of effective skeleton stress and void ratio

Mian Huang

Submitted in fulfilment of the requirement for the degree of

Doctor of Philosophy

School of Engineering

University of Glasgow

Dec 2021

Declaration

I declare that this thesis is a record of original work carried out by myself under the supervision of Dr Zhiwei Gao and Dr Thomas Shire in the Infrastructure & Environment Research Division of the School of Engineering at the University of Glasgow, United Kingdom. This research was undertaken during the period of Jan 2018 to May 2021. The copyright of this thesis belongs to the author under the terms of the United Kingdom Copyright Acts. Due acknowledgment must always be made of the use of any material contained in, or derived from, this thesis. The thesis has not been presented elsewhere in consideration for a higher degree.

Parts of the work have been published or are in the process of being published under joint authorship with the supervisor.

Gao, Z. , Lu, D. and Huang, M. (2020) Effective skeleton stress and void ratio for constitutive modelling of fiber-reinforced sand. *Acta Geotechnica*, 15, pp. 2797-2811. (doi: 10.1007/s11440-020-00986-w)

Gao, Z. and Huang, M. (2021) Effect of sample preparation method on mechanical behaviour of fibre-reinforced sand. *Computers and Geotechnics*, 133, 104007. (doi: 10.1016/j.compgeo.2021.104007)

Acknowledgement

It is an opportunity to express my gratitude and respect to my supervisor Dr Zhiwei Gao and Dr Thomas Shire, for their support and input throughout this project. It has been a great pleasure working with Dr. Gao. He always provided help when I needed. He has given me a lot of valuable advice on doing a PhD and future career planning.

I want to acknowledge Mr. Timothy Montgomery for providing technical support for me in the soil mechanics lab. He has helped me to set up the equipment and fabricate sample preparation mould. I would not be able to complete the tests without his help.

I also want to thank Prof. Cindy Smith and Dr Stephanie Connelly for their advice during the mini vivas.

Finally, I would like to thank my parents for supporting me to do the PhD.

Contents

List of Symbols and Acronyms

A	Cross-section of the sample
C_u	Coefficient of uniformity
D	Dilatancy relation
D_0	Initial diameter of sample
D_t,D_m,D_b	Diameter at the top, middle and bottom of sample
D_{50}	Mean diameter of soil
D_r	Relative density
d_f	Equivalent diameter of fibre
E_m	Membrane stiffness
E	Young's modulus
e_{max}	Maximum void ratio for soil
e_{min}	Minimum void ratio for soil
e	Void ratio
e_{ini}	Void ratio after sample preparation (initial void ratio)
e_0	Void ratio after consolidation
e^s	Effective skeleton void ratio
F	Axial force
f	Yield function
f_b	Dimensionless sliding function of fibre
G	Shear modulus
G_s	Specific gravity of soil
G_f	Specific gravity of fibres
H	Current height of sample
H_0	Initial height of sample
ΔH_s	Sample height during saturation
ΔH_c	Sample height during consolidation
ΔH	Sample height during shear

I_b	Brittleness index of soil
K	Bulk modulus
l_f	Length of fibre
M_c	Critical failure stress ratio in triaxial compression
η, η^s	Stress ratio
η_a	Aspect ratio
q	Deviator stress
p	Mean effective stress
p_w	Water content
p_c	Maximum fibre contribution to mean effective skeleton stress
p_a	Atmospheric pressure
p_f	Mean effective stress contribution from fibres
p^s, q^s	Effective skeleton stress
V	Sample volume
V_0	Initial volume of sample
V_s	Volume of sand
ΔV_s	Sample volume during saturation
ΔV_c	Sample volume during consolidation
ΔV	Sample volume during shear
w_f	fibre content
W_f	Fibre weight
W_s	Total weight of sand
W_w	Total weight of water
ψ	State parameter
ν	The Poisson's ratio
ε_a	Axial strain
ε_q	Shear strain
ε_v	Volumetric strain
$\varepsilon_q^p, \varepsilon_v^p$	Plastic shear strain

ε_v^p	Plastic volumetric strain
ϕ	Frictional angle of soil
σ_3	Minor principal stress
σ_1	Major principal stress
σ_c	Cell pressure
σ_b	Back pressure

List of Figures

Chapter 1

Chapter 2

Chapter 3

Chapter 4

Chapter 5

Chapter 6

List of Tables

Chapter 3

Chapter 4

Chapter 5

Chapter 6

Abstract

The inclusion of flexible fibres such as polypropylene and waste or natural fibres is an effective method for soil improvement, as it can significantly enhance soil strength. Though a lot of research has been done on fibre-reinforced sand (FRS), a simple and practical constitutive model, essential for assessing the stability and serviceability of fibre-reinforced slopes/foundations, has not yet been developed. A new method for constitutive modelling of fibre-reinforced sand (FRS) is proposed in this study. The new model has also been used to simulate the mechanical behaviour of FRS prepared by different methods.

In the new modelling approach, FRS is considered as a composite material with host sand and flexible fibres. It is assumed that the strain of FRS is dependent on the deformation of the sand skeleton only. The effective skeleton stress and effective skeleton void ratio, which should be used in describing the dilatancy, plastic hardening and elastic stiffness of FRS, are affected by fibre inclusion. The effective skeleton stress is dependent on the shear strain level, and the effective skeleton void ratio is affected by the fibre content and sample preparation method. A critical state FRS model in the triaxial stress space is proposed using the effective skeleton stress and void ratio. Four parameters are introduced to characterise the effect of fibre inclusion on the mechanical behaviour of sand, all of which can be easily determined based on triaxial test data on FRS, without measuring the stress-strain relationship of individual fibres. Triaxial compression test results validate the model on fibre-reinforced sands under loading conditions with various confining pressures, densities and stress paths. Potential improvement in the model for incorporating fibre orientation anisotropy is discussed.

It is well known that the mechanical behaviour of pure sand depends on the internal soil structure, which can be affected by sample preparation methods. For FRS, the

sample preparation methods influence the internal structure of the sand skeleton and the distribution of fibre orientation and sand-fibre interaction. The effect of sample preparation methods on the mechanical behaviour of FRS has been investigated using comprehensive drained triaxial compression tests. The soil samples have been prepared by moist tamping (MT) and moist vibration (MV). There is a small difference in the stress-strain relationship of pure sand with different sample preparation methods. But the response of FRS is dramatically different. Under the same initial conditions of void ratio, confining pressure and fibre content, FRS prepared using the MV method shows 30–50% higher peak deviator stress and a much less dilative response. The newly developed constitutive model has been used to predict the mechanical behaviour of FRS prepared using the MT and MV methods.

Chapter 1: Introduction

Soil improvement is widely used in geotechnical engineering to enhance the bearing capacity of geotechnical structures such as foundations, retaining walls, embankments and airfields built on weak soils with inadequate shear strength. Using fibres ranging from man-made fibres like steel fibres, polypropylene, polyester, glass fibres, and natural fibres (e.g., coir and jute) has been found effective for soil reinforcement. Some recent research has also reported the use of waste materials such as tyre shred and waste plastics as reinforcing fibres (Zornberg et al. 2004). There have also been some practical applications of this technique (Santoni and Webster 2001; Shukla, 2017). The use of fibre-reinforced soils was inspired by the root reinforcement to the soil strength (Wu et al. 1979; Gray and Sotir 1995; Sonnenberg et al. 2010; Gao and Zhao, 2013). The fibres contribute to the soil strength when they are in tension. Therefore, the fibres can be placed in a direction that most fibres are subjected to tension under loading to achieve the maximum fibre-reinforcement. The fibre-reinforcement has several advantages over the existing methods for ground improvement:

(1) Fibres can be mixed with the soil using conventional construction equipment. It is easy to get the mechanical properties of FRS such as the shear strength, and large-scale tests are typically not needed for practical implementation (Hatami et al., 2018). This can help reduce the construction cost significantly.

(2) The use of fibre reinforcement in practical construction will not be restricted by weather or soil conditions. Different fibre types (natural, synthetic and waste) can be used for various situations. For example, FRS has been used in Malaysia because the fibres are not bio-degradable (Ahmad et al.,2012). Some recent studies have focused on fibre reinforced cement application in expansive soils (Puppala, 2000; Viswanadham et al., 2009; Wang et al., 2016). In Wang (2016), a reduction in shrinkage and swelling of expansive soil has been found. This was

attributed to jute fibre having a superior ability of effectively increasing the soil strength and reducing the soil expansion. In some tests, the soil behaviour changes from strain-softening to strain-hardening.

(3) Natural fibres can also be used for short-term soil stabilization (Aggarwal and Sharma, 2011). To make the natural fibres more durable, the surface of fibres can be treated by chemical additives, aiming to impair the fibre's hydrophilic nature (Aggarwal and Sharma, 2011).

(4) Some applications of fibre reinforcement for stabilisation of pavement and road construction have been reported by Santoni and Webster (2001a) and Grogan (1993). Besides, inspired by such advantages of fibre reinforcement, this technique has been applied for aircraft pavements construction. Compared with a sand grid filled with pure sand, filling with reinforced sand makes the required thickness half of grid-sand and reduces the construction cost. Repeated compaction is required to ensure that no voids exist in the grid cells (Santoni and Webster, 2001b).

(5) Finally, the inclusion of fibres can reduce the degree and width of desiccation cracks effectively (e.g., Zornberg et al., 2003; Ziegler et al.,1998). Ziegler et al. (1998) found that fibres give tensile strength for the soil, resulting more ductile soil behaviour. Besides, Fibre reinforcement can also lead to an improvement in erosion control and facilitate vegetation development, thus improving surface stability. It is appealing for building an evapotranspiration cover system for landfills (Zornberg et al., 2013).

(6) As shown in Fig. 1.1, compared to planar reinforcement, the FRS technique can effectively minimise the anchorage zone and required excavation, which is a major benefit of FRS. For example, planar reinforcement cannot be used in the embankment at the crest of the slope, as large excavation is required to satisfy

proper anchorage zone (Hatami et al., 2018). Instead, the use of FRS can reduce the disturbance from underground.

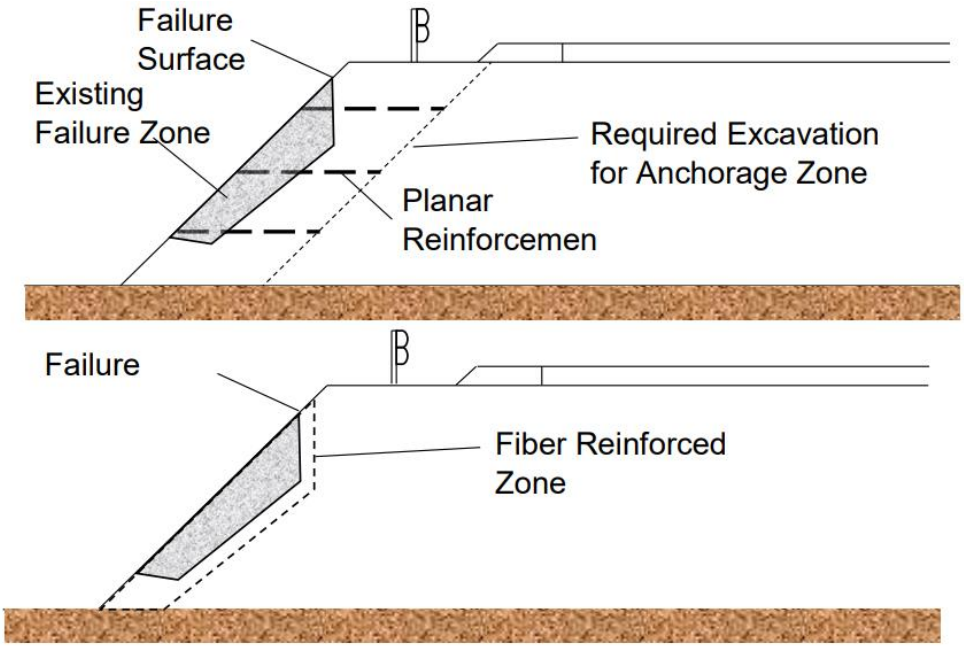

Fig. 1.1 Comparison of planar technique and FRS technique (Gregory and Chill, 1998)

Chapter 2: Literature Review

Since earlier times, soil as a multifunctional material was widely applied in various construction such as foundations and road. In the last two centuries, soil as a vital material in multiple industries has constantly developed to make it stronger and more economical in construction application. However, in general, the earth is weak in tension, and its shear strength may strongly depend on the environmental conditions (Ling et al., 2003). Consequently, due to natural effects, road subsidence and soil liquefaction have become the main problem for earth constructions. Therefore, many methods for soil improvement have been developed. In particular, the soil reinforcement using flexible fibres is found and cost-efficient effective in soil improvement. The earliest studies relating to natural fibre being used can be traced back to Gray (1970) and Waldron (1977). Plant roots were used to enhance the shear strength of the soil, resulting in strengthening natural slopes. Nowadays, this technique is maturing. Natural or synthetic materials, such as coir or polypropylene instead, can be widely applied in motorways, tunnels, bridges, and wall retaining structures, to mitigate the risk of soil liquefaction and slope failure. Though this technique has been studied and applied for many decades, more research is needed to further understand the potential benefits and limitations of this technique and explore more further observations in terms of its mechanical behaviour and thus allow it to be used in the construction of geotechnical structures.

2.1 Introduction of Fibres

Many kinds of fibres, which are more friendly for the environment and locally available are becoming an attractive means of enhancing soil performance. For example, synthetic fibres were used at the end of the 20th century, as they have superior erosion resistance and longer duration (e.g., Michalowski & Zhao, 1996; Gray & Ohashi, 1983). Besides, Gray and Ohashi (1983) conducted a series of triaxial shear experiments to

prove the effects of fibre properties on the soil. The results show that the increase of shear strength was directly proportional to the fibre content or aspect ratio. However, Shewbridge and Sitar (1989) found that the increase in shear strength was not proportional to the aspect ratio. Gray and Ohashi (1983) conducted a series of triaxial compression tests, aiming to investigate the influence of fibre properties on soil response. The results showed that fibre properties such as aspect ratio and surface friction can affect the mechanical behaviour of soil. More details regarding the fibre properties will be discussed in the following section.

2.1.1 Fibre Types

Many types of fibres have been used in soil reinforcement, including artificial fibres and natural fibres. This section will review the fibres which have been used in lab tests and field trials.

Natural Fibres

They are generally friendly to the environment, locally available and relatively cheap. The common choices include coir, jute and bamboo fibres (Rao & Balan, 2000; Swamy, 1984; Huang & Lin, 2009). According to Rao and Balan (2000), the organic fibre material coir contains 40% lignin and 54% cellulose. This high lignin content leads to coir degrading slowly and can be widely applied in different situations. For instance, many studies (e.g., Sivakuamr Babu & Vasudevan,2008; Hejazi et al.,2012) outlined the use of these materials in temporary constructions where the reinforcement effect need to last at least three years or up to 10 years.

Furthermore, Sivakuamr Babu and Vasudevan (2007) conducted a series of triaxial compression tests to evaluate the effect of coir on the strength and stiffness of FRS (Fig 2.1). The results indicate the stiffness of FRS depends on not only the fibre content,

but also other factors such as strain level and confining pressure. A similar observation can be found in Zornberg (2002), in which the fibre-induced tension was associated with the fibre content. Besides, the critical normal stress is independent of the fibre content. Though natural fibres are widely applied in various projects, the possibility that chemicals may erode them should be considered, as most natural fibres added to the soil are impacted by chemical ions in oxygen or water (Hejazi et al., 2012).

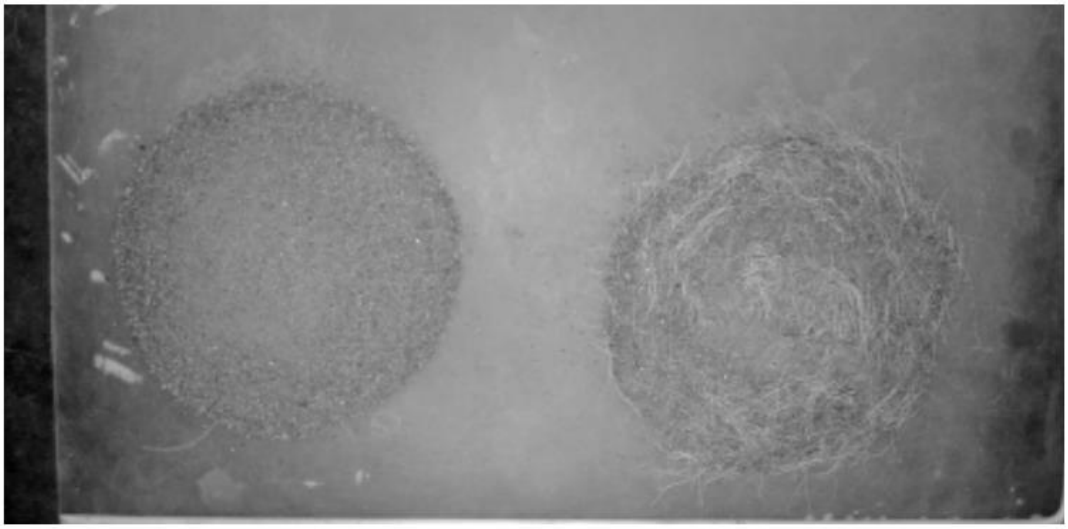

Fig. 2.1 (a) host sand and (b) sand with fibres (Sivakuamr Babu and Vasudevan, 2007)

Synthetic Fibres

Synthetic fibres, such as polypropylene and polyester, which have high tensile strength, can be added to the soil (Biswas et al., 2013; Gray & Ohashi, 1983; Li et al., 2014; Hejazi et al., 2012). The fibres can significantly increase the Young's modulus and shear strength, reduce swelling and shrinkage potentials, and are more durable than the natural fibres. A significant difference in the failure mode in a drained triaxial test (Fig. 2.2) between polypropylene fibre-reinforced specimens (PPFRS) and unreinforced samples can be found in Freilich and Zornberg (2010). The PPFRS show a remarkable hardening behaviour at very large axial strain ($\varepsilon_a = 13\%$), whereas the unreinforced

one reaches the failure stress state at that strain level (Fig. 2.3). Consoli et al. (2009) showed that the fibre-reinforcement can be further enhanced by adding cement in the soil.

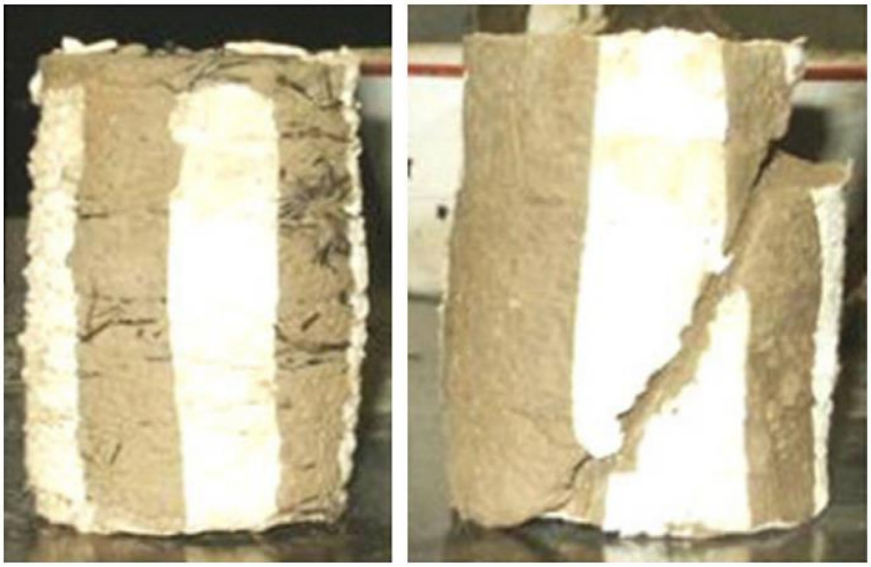

(a) (b)

Fig. 2.2 Deformation pattern for (a) soil reinforced with 0.25% polypropylene fibres and (b) unreinforced clay soil (Freilich and Zornberg, 2010)

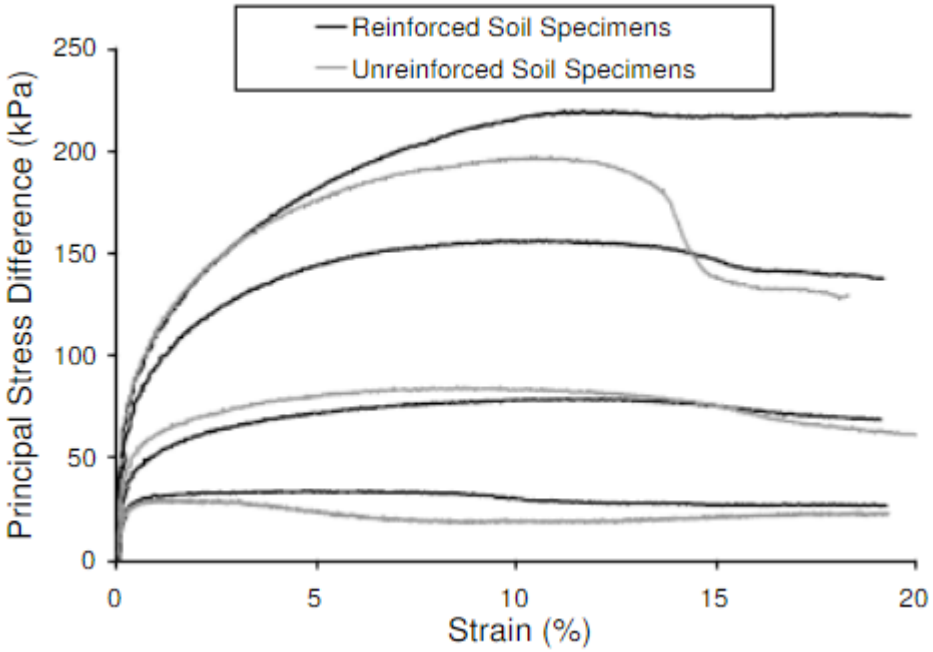

Fig. 2.3 The stress-strain relationship of fibre-reinforced and unreinforced soil in a drained triaxial compression test (Freilich and Zornberg, 2010)

Waste Fibres

Glass, steel and rubber fibres have been used in several studies. These fibres have higher Youngs' modulus and ductility than the natural and synthetic fibres (Hejazi et al., 2012; Mather, 1994; Colombo et al, 2003). Most studies on fibres show that the glass-based reinforced material can be used in condition of high temperature up to 500℃(Mayes, 2005). On the other hand, Ahmad et al. (2012) studied this unique property of glass fibres. It is found that they can retain about 70%-75% of their elastic modulus and tensile strength, even under the effect of temperature of 450℃. Unlike the polypropylene fibres, the inclusion of glass fibres slightly reduces the brittleness (Ahmad et al., 2012). Furthermore, due to its reduction of landfill and providing a lower cost of disposal, it has become a prior option for developing countries (Asokan et al., 2009; Axinte, 2011;). However, further investigation on the application of waste fibres is needed, as many potential chemical processes between waste fibres and soil may cause degradation of the fibres.

2.2.2 Influence of Fibres Characteristics

Although the practical application of FRS has been increasing, laboratory investigations have confirmed the mechanical behaviour of FRS is strongly dependent on many factors, including the properties of fibre (e.g., aspect ratio, length, stiffness and tensile strength), properties of host sand (particle size and friction between sand and fibres) and sample preparation methods (Michalowski & Čermák, 2002; Consoli et al., 2007; Diambra, 2010). Similar to pure sand, the FRS behaviour is also dependent on the soil density and confining pressure (e.g., Vaid and Thomas, 1995; Verdugo and Ishihara, 1996).

Fibre Length

The fibre length has a significant effect on the behaviour of FRS. Ahmad et al. (2010) have studied the behaviour of FRS with different fibre lengths (15mm, 30mm and 45mm) at the same fibre diameter and fibre content using consolidated-drained (CD) triaxial tests (Fig. 2.4). It is evident that higher peak shear strength is observed when the fibres are longer. Similar results have been reported in other studies (Consoli et al., 2007; Wang et al., 2016). However, Diambra (2010) and Consoli et al. (2007) have pointed out that the fibre-reinforcement effect can be mobilised at larger strain when the fibres are longer. Therefore, the optimum fibre length has to be chosen in real applications.

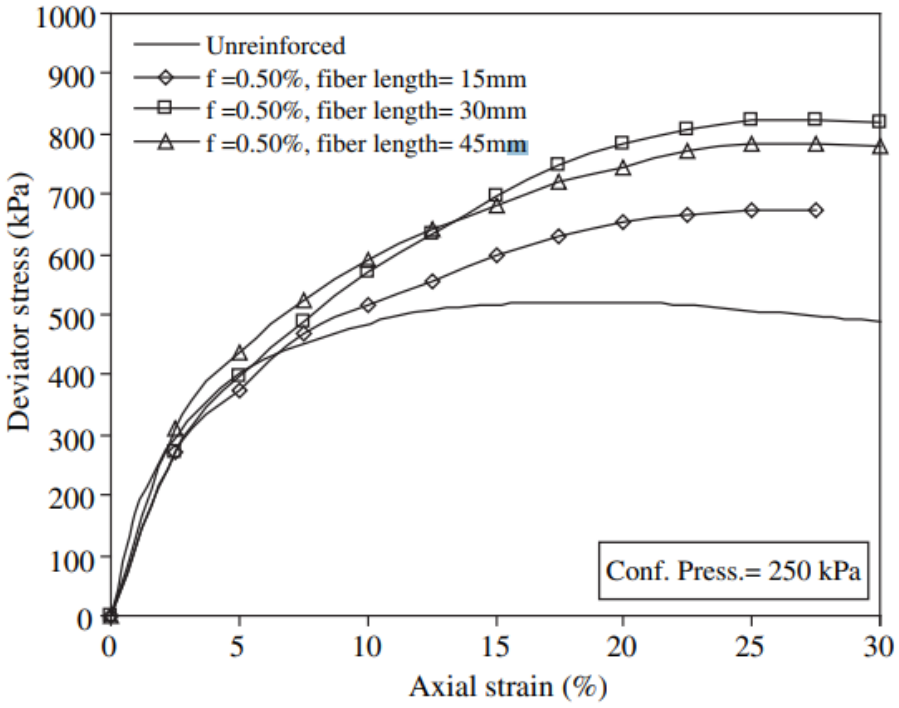

Fig. 2.4 Typical stress-strain response of reinforced soil with different fibre length (Ahmad et al., 2010)

Fibre Content

Besides, the shear strength of FRS is dependent on the fibre content (w_f). In general, higher elastic stiffness and shear strength can be observed at higher fibre content. However, as shown in Fig. 2.5, higher fibre content, which exceeds 0.60%, can have a negative effect on cohesion and friction angle in drained triaxial compression tests (Wang et al., 2016). A similar result can be found in Maheshwari et al. (2011), in which 0.5% of maximum fibre content was recommended, or it would have a negative effect on soil strength (Ranjan et al., 1996; Al-Refeai, 1990).

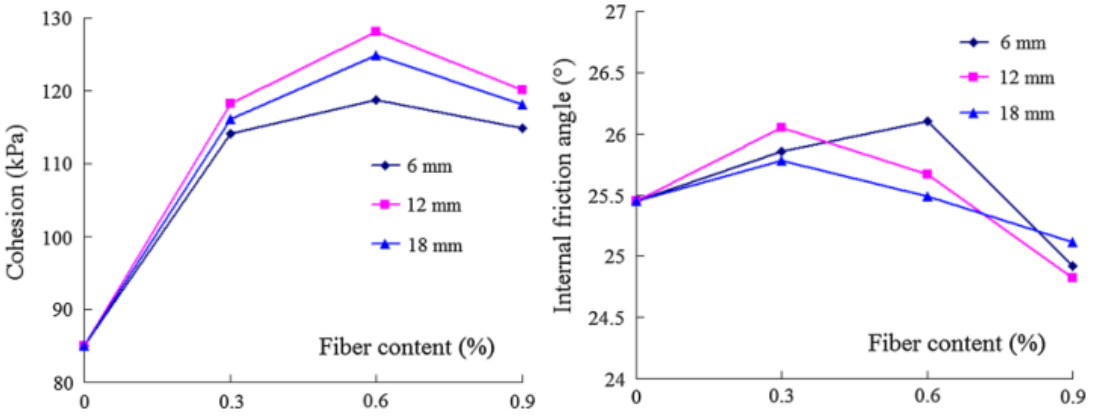

(a) (b)

Fig. 2.5 Strength parameters for (a) cohesion and (b) internal friction angle with fibre content (Wang et al., 2016)

Fibre Orientation

Fibre orientation in FRS depends on the sample preparation methods. When the FRS is prepared through vertical compaction, most fibres are oriented in the horizontal direction (Michalowski & Cermak,2002). When more fibres orient in the horizontal direction, the shear strength measured in a triaxial compression test is higher because more fibres are in tension in triaxial compression (Fig. 2.6). When most fibres oriented in the vertical direction, the shear strength of FRS is almost the same as that of host

sand, because very few or no fibres are in tension. The fibres contribute to the shear strength only when they are in tension. Diambra (2010) have developed a method for measuring the fibre orientation in FRS. It is found that the FRS prepared by moist vibration (MV) shows a less anisotropic orientation distribution compared with that prepared by moist tamping (MT). Besides, fibre orientation can also influence the elastic stiffness. It is found that the vertical fibre orientation can lead to reduction in the initial stiffness (Wang et al., 2017). However, less research has focused on the difference in the stress-strain relationship between the samples prepared by moist tamping and moist vibration.

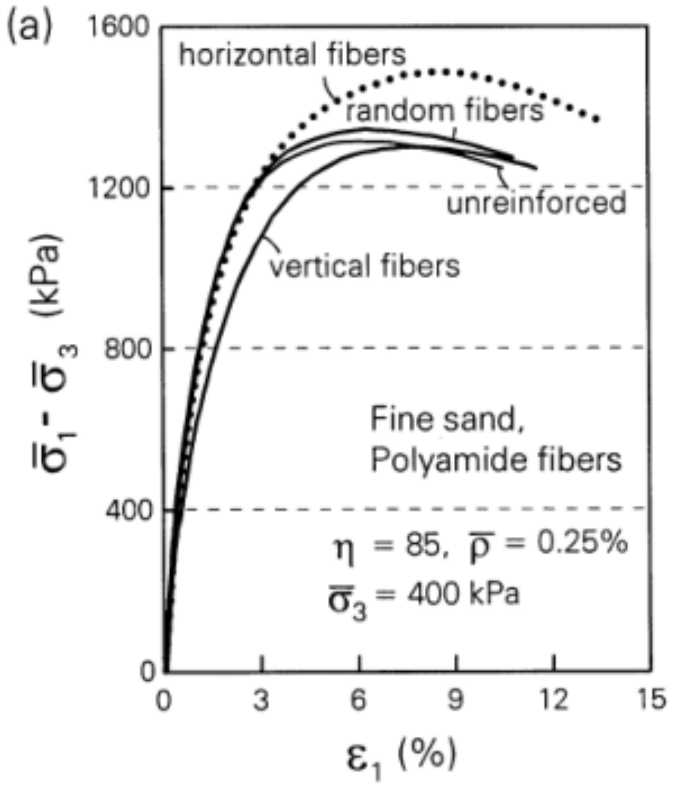

Fig. 2.6 Stress-strain behaviour of reinforced fine sand (Michalowski & Cermak, 2002)

Aspect Ratio

The aspect ratio (η_a) of fibre is defined as the ratio of its length (l_f)and equivalent diameter (d_f):

$$\eta_a = \frac{l_f}{d_f} \tag{2.1}$$

The aspect ratio should be within a reasonable range to avoid pullout failure (Gregory, 1999, Zornberg, 2004). When the aspect ratio is higher, which means a thin diameter for a given length of fibres, there is more friction between sand and fibres because of the increase in surface area of the fibre for a given fibre content. For example, Zornberg (2004) reported the number of fibres in FRS specimen having 3620 deniers (η_a =32, of which 1 denier = 1/9000 g/m) fibres, at 0.5% water content would approximately equal to 5000 threads. The sample reinforced with three deniers (η_a =1128) fibres at the same water content would contain over six million fibres. In addition to the aspect ratio affecting the contact area between fibres and soil particles, the relationship between aspect ratio and principal stress had been reported by Maliakal and Thiyyakkandi (2012). In this case, the effect of aspect ratio is evaluated by controlling other test conditions such as confining pressure and fibre content. Consequently, as shown in Fig. 2.7, 150 of aspect ratio, which corresponds to 36mm of fibre length, is the most effective in reinforcing the soil strength.

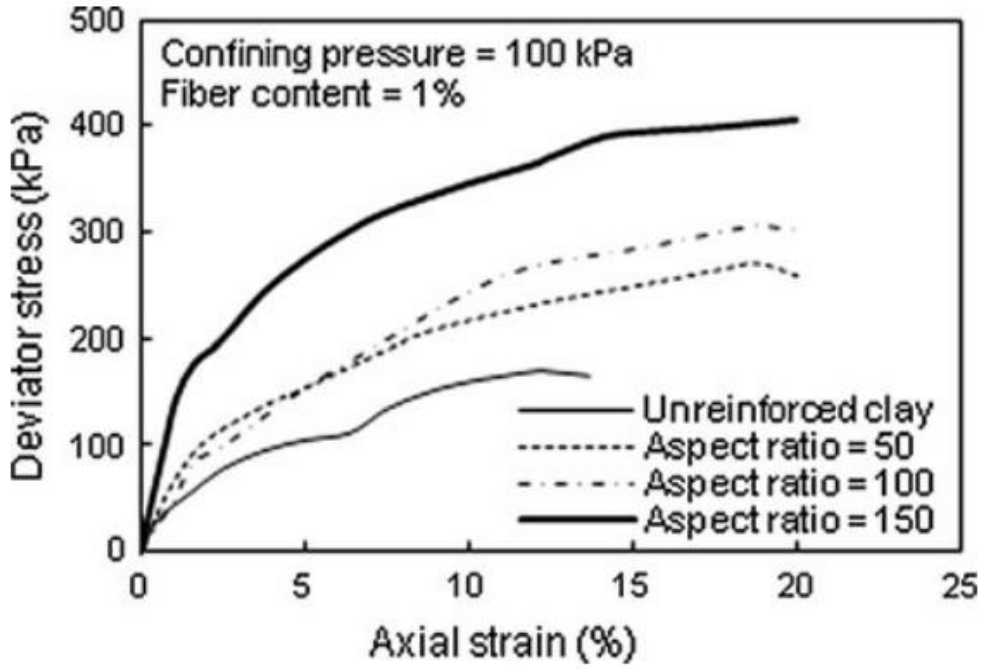

Fig. 2.7 Stress-strain relationship for fibre-reinforced soil with different aspect ratio (Maliakal & Thiyyakkandi, 2012)

2.3 Influence of Soil Properties

The behaviour of FRS is also affected by the properties of host sand, including the density, particle size and water content.

Soil Density

For unreinforced sand, a comparing result is given by Li (2014), showing the higher peak strength occurs at the specimen with higher density. Wang et al. (2016) analysed the effect of soil density based on the relationship between the fibre content and dry density, showing that fibre reinforcing effect is more apparent when density is higher. A series of plate load tests have been conducted by Consoli et al. (2007) on unreinforced and fibre reinforced sand under different states (loose, medium and dense). It is found that higher relative density suppresses the dilation, leading to higher effective stress and hence higher shear strength and stiffness of the soil. Besides,

Consoli et al. (2009b) performed plate-load tests on fibre-reinforced sand to evaluate the effects of dry density on cohesion and the internal friction angle. The study shows that higher relative density gives a higher overall stiffness and bearing capacity for fibre reinforced sand. Fig. 2.8 shows a schematic diagram of sand-fibre interaction. It is shown that a denser fibre-reinforced specimen implies a smaller void space, thus giving a greater effective contact area between fibres and soil particles, leading to higher reinforcement to the soil strength. However, due to the fibre inclusion, the initial soil density is changed because of the interaction between fibres and soil particles. Generally, fibres are regarded as a part of the solid phase, as fibres affect or 'occupy' the soil's void space (Michalowski & Zhao, 1996; Diambra, 2010; Gao & Huang, 2020).

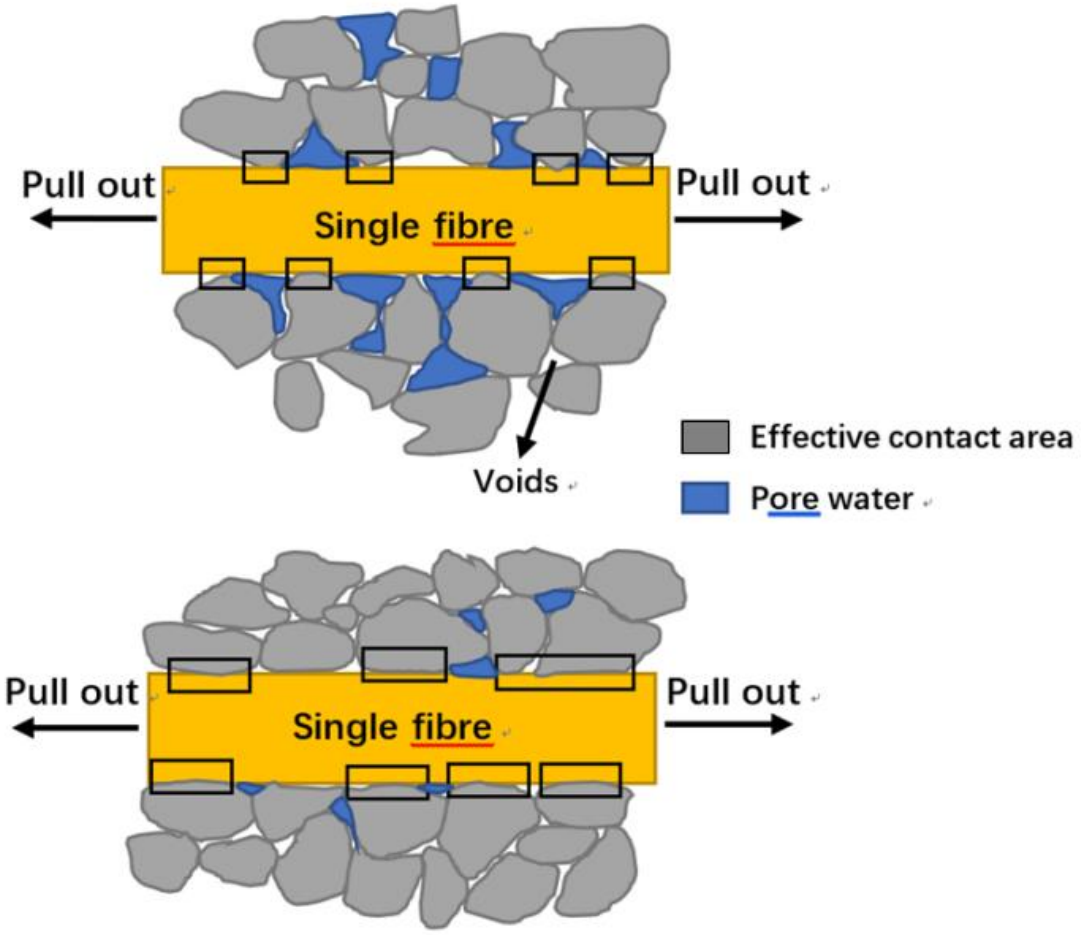

Fig. 2.8 Schematic diagram of different effective contact area in (a) lower dry density; (b) higher density

Water Content

Water content used during sample preparation is found to influence the behaviour of FRS, because the soil density after preparation is affected by water content for sample preparation. (Ladd, 1978; Wang et al., 2016; Tang et al., 2016). The shear strength of both reinforced and unreinforced specimens increases as the water content used during sample preparation decreases, when water content varies at a certain range (Tang et al., 2016; Wang et al., 2016; Li et al., 2013). This is because capillary force, which help keep the sample shape stabilised during sample preparation, decreases as water content increases.

If the soil density is very low, water content is one of the main factors that induce the sample collapse during sample preparation. Therefore, 5% and 10% of water content for moist tamping were proposed by Sze & Yang (2014), Diambra (2010) and Consoli et al. (2005). However, higher water content from 14.5% up to 20% is more reasonable and has been widely reported in earlier studies (e.g., Li et al., 2013; Wang et al., 2016).

2.4 Constitutive Models for FRS

Based on the experimental studies, several constitutive models for FRS have been developed (Gray & Ohashi,1983; di Prisco & Nova, 1993; Michalowski & Zhao, 1996; Zornberg, 2002; Ding & Hargrove, 2006; Sivakumar Babu et al., 2008). A brief introduction of the existing constitutive models will be discussed in this section.

Gray and Ohashi (1983) conducted a series of direct shear tests on sand with different fibre orientation and then proposed a simple force-equilibrium-based model for predicting the shear strength of FRS. The hypothesis in this model is that the shear strength of soil is caused by fibre tension (Fig. 2.9), in which the angle of shear

distortion (θ^d) and the orientation angle of the distorted fibres (ψ^{d}) are mainly employed to establish a relative functional relationship with shear strength. But it has been pointed out that the thickness of the shear zone is difficult to quantify, which is being used here as an input parameter in this model (Diambra, 2010; Li, 2005). Besides, their derivation assumes that the fibres must be long enough to avoid fibre pullout. Therefore, this model does not work when the fibre pullout occurs in FRS.

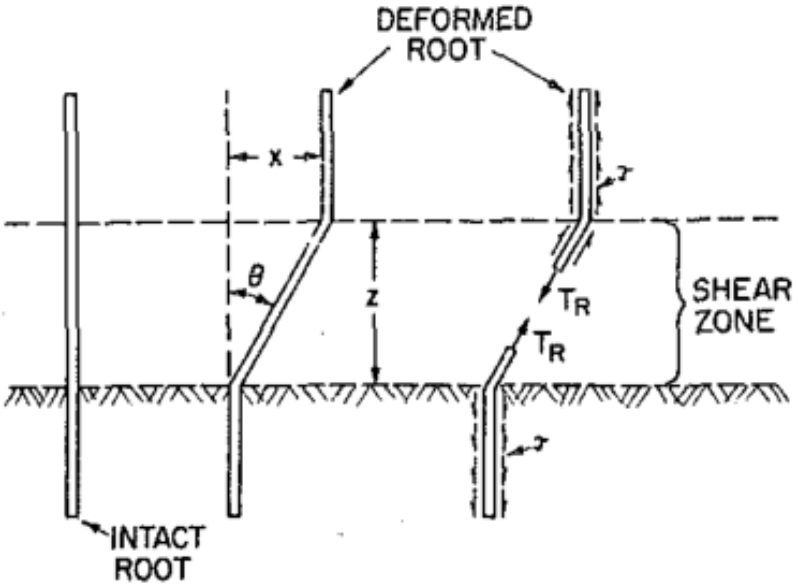

(a)

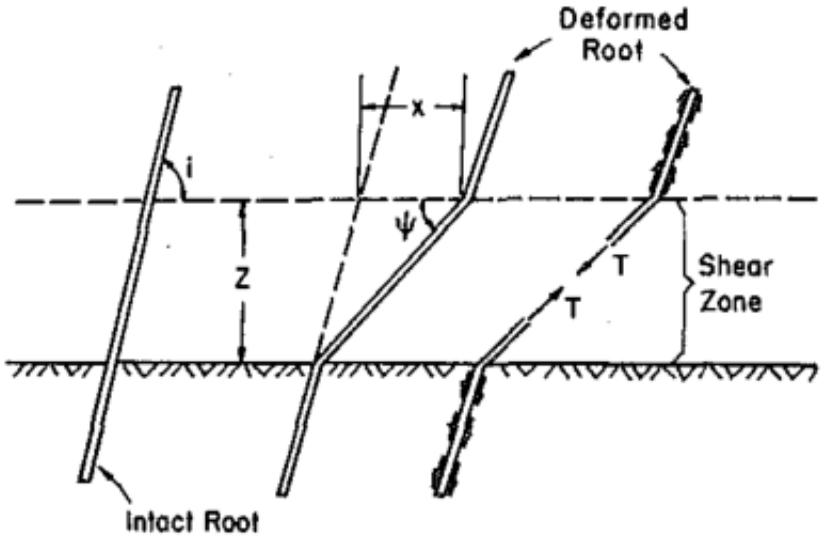

(b)

Fig.2.9 The hypothesis of fibre distortion in (a) vertical direction and (b) oriented at angle to shear surface (Gray & Ohashi, 1983)

di Prisco and Nova (1993) later developed a simple model based on the superposition theory of sand and fibre. A series of drained triaxial compression tests on reinforced and pure sand samples are conducted to compare and validate the constitutive model. The model can give qualitative description of sand behaviour only. For the FRS, the solid lines representing model prediction are far from the test results (Fig. 2.10). In this model, although the dilatancy angle has been considered, the parameters of the material are ignored. On the other hand, Fibre inclusion can significantly induce a significant effect on dilatancy so that the model dose not capture well the volumetric behaviour (Gao et al., 2020).

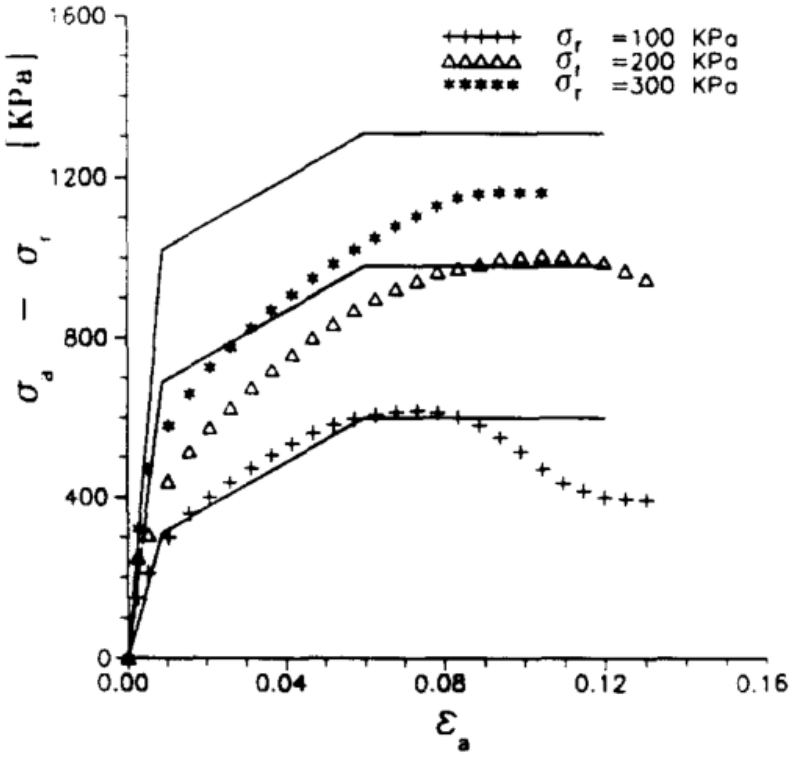

(a)

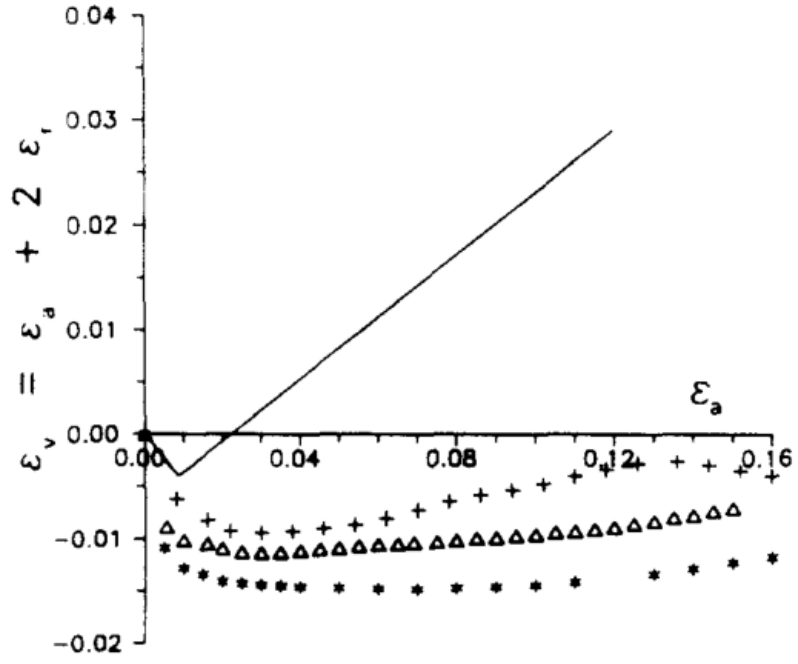

(b)

Fig.2.10 Comparison between experimental data and model simulation on reinforced sand: (a) stress-strain, and (b) volumetric response (di Prisco & Nova, 1993)

Michalowski and Zhao (1996) proposed an energy-based homogenisation technique to describe the failure of FRS. In this case, fibres are treated as a cylindrical shape, and two failure patterns are given, as shown in Fig. 2.11. The figure indicates fibres are considered one-dimensional elements. The distribution of shear stress on the fibre surface and the fibre's axial stress is determined based on the analysis of fibre slippage and tensile rupture. During plastic deformation, the associative flow rule is zero, determined by the energy dissipation rate.

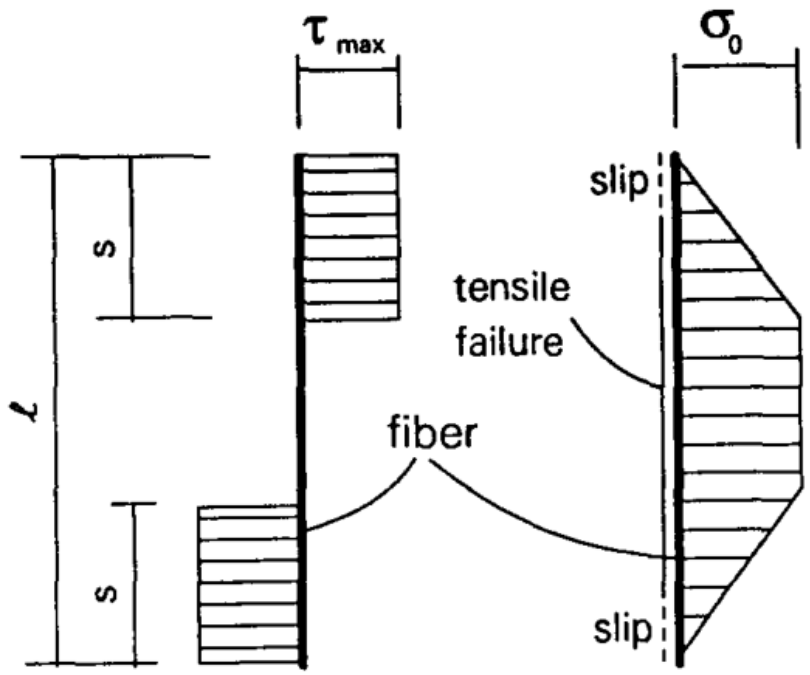

Fig. 2.11 The distribution of shear stress and axial stress in rigid-perfectly plastic fibre (Michalowski & Zhao, 1996)

Further work on FRS with anisotropic fibre orientation has been carried out by Michalowski and Cermak (2002). In this study, a series of conventional triaxial compression tests are conducted. Kinematic hardening is found at large strain due to fibre orientation distribution evolution (Fig. 2.12). The model based on frictional interaction of fibres and sand, built on these earlier studies, is then developed by Michalowski and Cermak (2003). A macroscopic internal friction angle is introduced initially, especially fibres are considered isotropic. The anisotropic frictional angle is

then explained in the kinematic-based analysis for FRS, in which it shows that the anisotropic frictional angle (ϕ_a) is a function of the major principal stress direction. The use of the kinematic approach in solving retaining wall loading and the bearing capacity of a strip footing has also been reported (Michalowski, 2008).

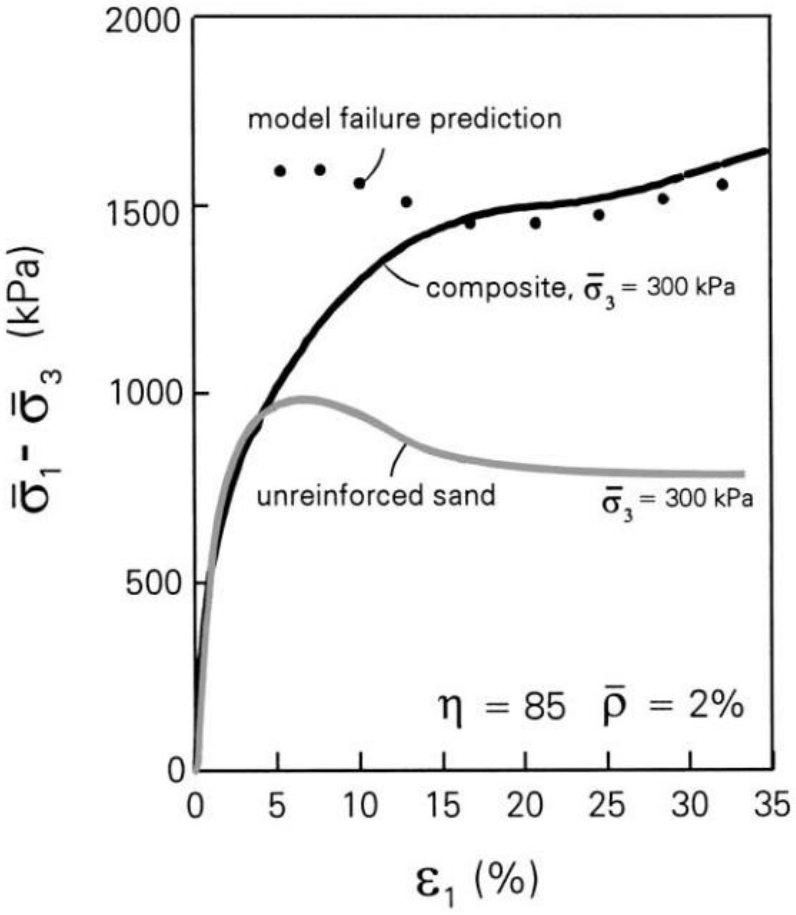

Fig. 2.12 A kinematic hardening for model prediction found at around 10% of strain (Michalowski and Cermak, 2002)

Zornberg (2002) recently proposed a discrete framework for fibre-reinforced soil (FRS) to characterise the contribution of randomly distributed fibres to soil strength. In this model, fibres and soil are treated as discrete (or individual) elements to characterise the shear strength of FRS. This model is mainly designed for the engineer to calculate the enhancement on shear strength of FRS slopes by predicting the increase in cohesion and friction angle with reasonable accuracy.

Ding and Hargrove (2006) developed a constitutive model for FRS wherein soil and reinforced material is described by nonlinear and linear elastic stress-strain relationship. In this case, the shear modulus is dependent on the fibre content, distribution and interaction. However, Consoli et al. (2006) suggested in terms of the theoretical analysis of the equivalent homogeneous bulk modulus of geofibre-reinforced soil cannot be considered as a general rule, of which $K^a = K^s$ (where K^a and K^s are the bulk modulus of FRS and host soil). Since a higher bulk modulus of FRS can be found in isotropic compression due to the fibres subjected to tensile stress induced by the relative movement of soil particles (Fig. 2.13). Furthermore, this model is limited to predicting FRS's stress-strain response at small strains (Diambra, 2010).

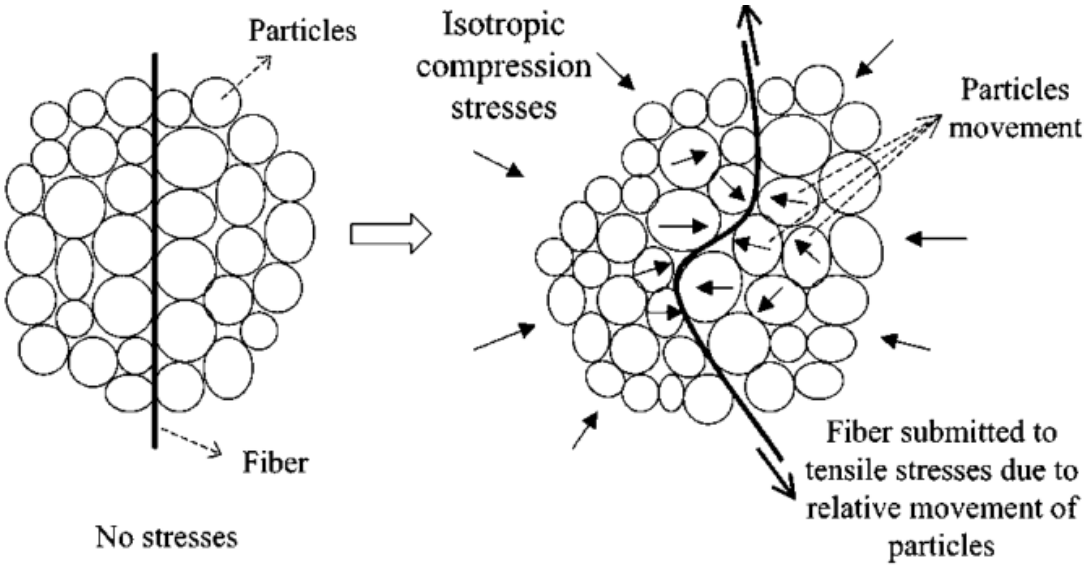

Fig. 2.13 Illustration of proposed mechanism of fibre submitted to tensile stress due to relative movement of particles (Consoli et al., 2005)

Sivakumar Babu et al. (2008) have used the finite element method to simulate the stress-strain relationship of FRS in triaxial compression. In this study, the specimen consists of 1000 elements. Fibres are modelled as line elements, wherein they are uniformly distributed within 0 to 180°. As a result, the model has a good simulation for the shear stress and strain relationship on both reinforced and unreinforced soil (Fig. 2.14). A comparison of failure mechanisms between host soil and reinforced soil

has also been shown. It is found that the fibres with random distribution can affect the microstructure and prevent the formation of a shear band, leading to a pronounced increase in shear strength and elastic stiffness. But the prediction of soil volume change has not been presented.

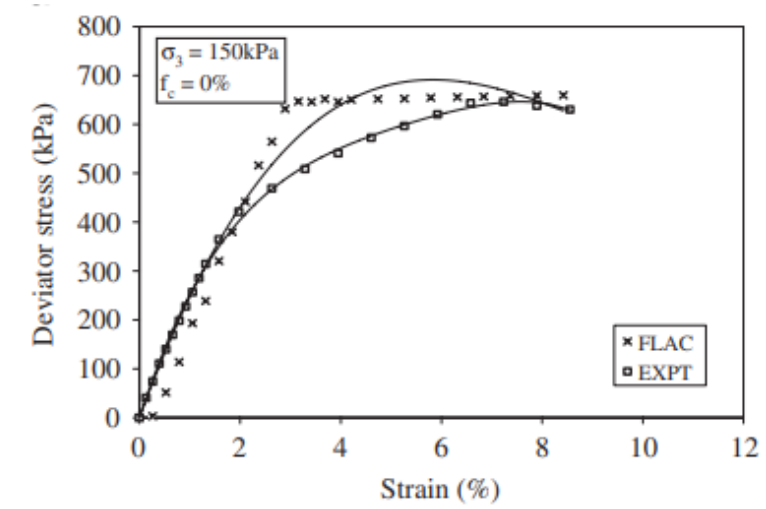

(a)

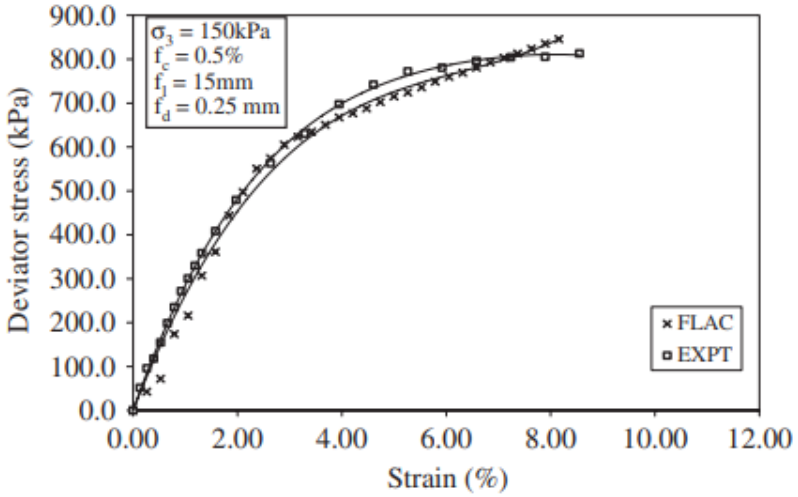

(b)

Fig. 2.14 Experimental and simulating stress-strain plane on (a) unreinforced soil and (b) fibre-reinforced soil (Sivakumar Babu et al., 2008)

2.4.1 Diambra's General Constitutive Model for Fibre Reinforced Sand (FRS)

Diambra (2010) proposed an elastoplastic model, in which FRS is considered as a composite with three phases, including sand, fibres and voids. Meanwhile, the fibres might generate a network (due to entanglement among the fibres) within the soil matrix. As a result, the volume of voids (V_v) upied' by the fibres and the grains can be calculated by:

$$V_v = V_{vs} + V_{vf} \tag{2.2}$$

where V_{vs} and $\mathrm{V_{vf}}$ represent the volume of sand void and fibre void, respectively. The basic assumption in terms of the volume in this model is shown in Fig. 2.15, where the composite volume is divided into two parts, soils and voids, which both include the contribution of fibres.

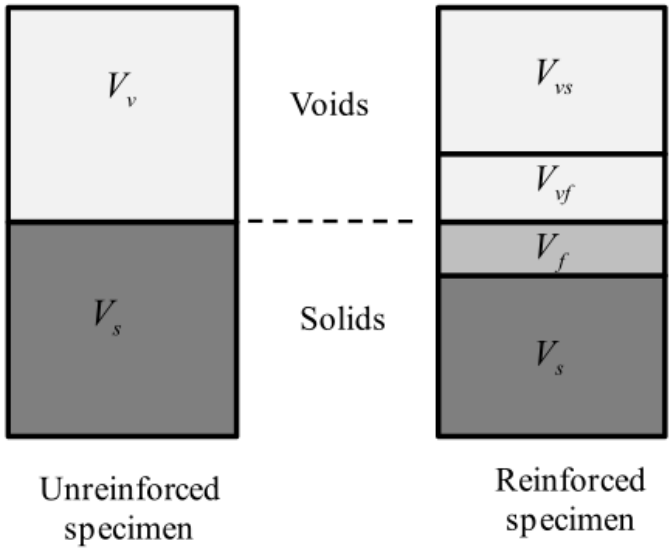

Fig. 2.15 Schematic drawing of volume distribution for both unreinforced and reinforced samples (Diambra, 2010)

The fibres are assumed to have no contributions to the soil strength when they are in compression. Their contribution to soil stiffness and strength is only active when they are in tension. The stress and strain relationship for host sand and fibre matrix can be

expressed as below (Diambra, 2010):

For sand: $$\dot{\boldsymbol{\sigma}}' = [M_m]\dot{\boldsymbol{\varepsilon}}_{\boldsymbol{m}} \quad (2.3)$$

For fibre: $$\dot{\boldsymbol{\sigma}}_{\boldsymbol{f}}{}' = \left[M_f\right]\dot{\boldsymbol{\varepsilon}}_{\boldsymbol{f}} \quad (2.4)$$

where $\dot{\boldsymbol{\varepsilon}}_{\boldsymbol{m}}$ and $\boldsymbol{\varepsilon}_{\boldsymbol{f}}$ are strain increment of sand skeleton and fibre matrix; M_m and M_f are the stiffness matrix for sand and fibres, respectively.

Due to the non-uniformity of the orientation distribution of fibres, the fibre orientation distribution function $\rho(\theta)$ is introduced to describe the fibre orientation. Only those fibres which are pulled in tension are included in the constitutive model ($0 \leq \theta \leq \theta_0$), where θ_0 is the direction of zero incremental strains, which is defined as

$$\theta_0 = \arctan\sqrt{-\frac{\dot{\varepsilon_r}}{\dot{\varepsilon_a}}} \quad (2.5)$$

where $\dot{\varepsilon_r}$ and $\dot{\varepsilon_a}$ are the vertical and horizontal strain increment, respectively. Note that this equation works in triaxial tests only. More details of this can be found in Diambra (2010). Similar to Michalowski's model (Michalowski & Zhao, 1996), Diambra (2010) has assumed that the stress distribution (or mobilised stress) on a single fibre is not constant along the length. Instead, it must tend to be zero at its end. Furthermore, the dimensionless sliding function (f_b), is employed to describe the imperfect interfacial bond between fibres and sand grains, which can be varied between 0 and 1 with f_b=1 for perfect bonding and f_b=0 for fully sliding, thus reflecting the fibre skeleton's deformation ($\dot{\varepsilon_f}$) to the deformation of the specimen (Eq. 2.6):

$$\dot{\varepsilon_f} = f_b\dot{\varepsilon} \quad (2.6)$$

where f_b is the dimensionless sliding function for fibre, and $\dot{\varepsilon}$ is the strains of the sand skeleton.

The stress increment of FRS expressed in terms of the fibre concentration factor μ_f as below:

$$\dot{\sigma} = \dot{\sigma}' + \mu_f\dot{\sigma}_f \quad (2.7)$$

where $\dot{\sigma}'$ is the stress increment of the sand skeleton; μ_f and $\dot{\sigma}_f$ are the fibres concentration factor and the stress increment of the fibre matrix. Since the volume of fibres is negligible for FRS, which means $\mu_f = 0$ can be used in the model. It is assumed that the strain of the FRS and sand skeleton is the same

$$\dot{\varepsilon} = \dot{\varepsilon}_m \tag{2.8}$$

where $\dot{\varepsilon}$ is the strain of the sand skeleton and $\dot{\varepsilon}_m$ is the strain of the fibre matrix.

The model has been validated by a series of drained and undrained triaxial tests on FRS and some of the simulations are shown in Fig. 2.16-2.18, where the density from loose to dense state are noted as L, M and D. It is noted that the stress-strain relationship of host sand is assumed to be elastic perfectly plastic in these simulations.

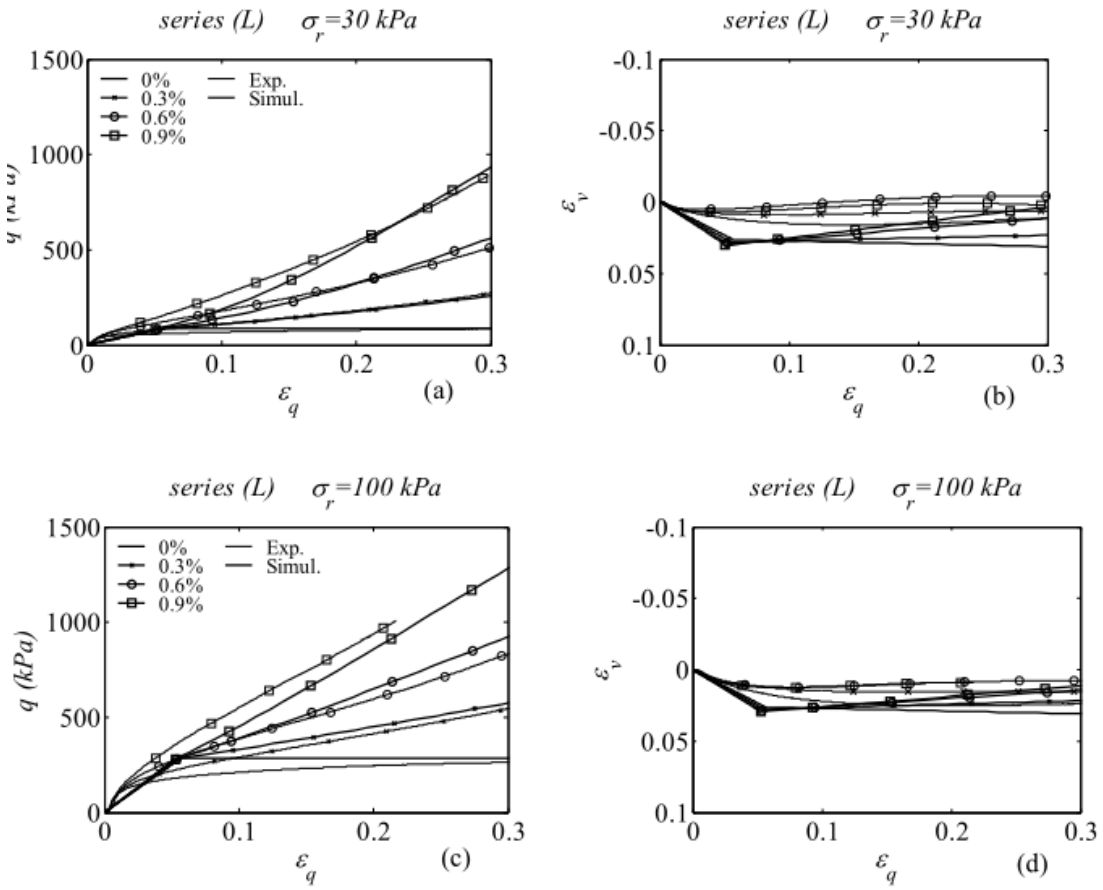

Fig 2.16 Compression between the drained triaxial test data and model simulations for unreinforced and reinforced loose sand (Diambra, 2010)

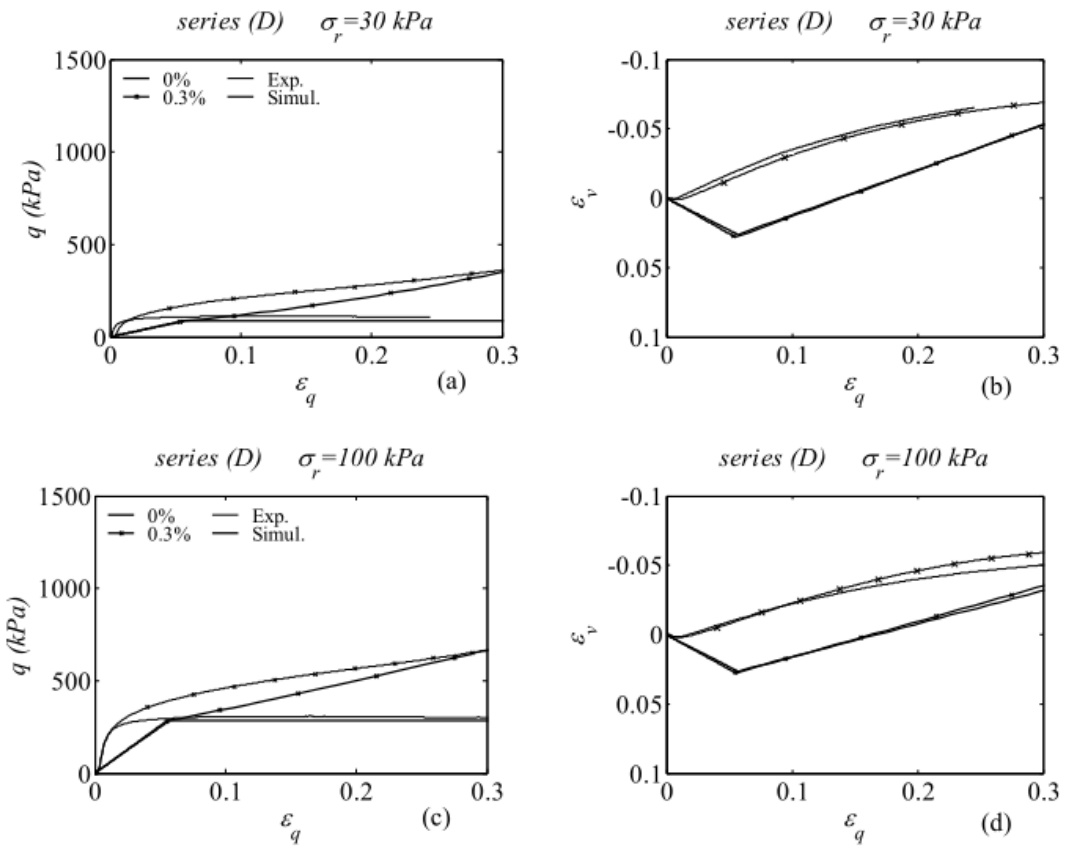

Fig. 2.17 Compression between the drained triaxial test data and model simulations for unreinforced and reinforced dense sand (Diambra, 2010)

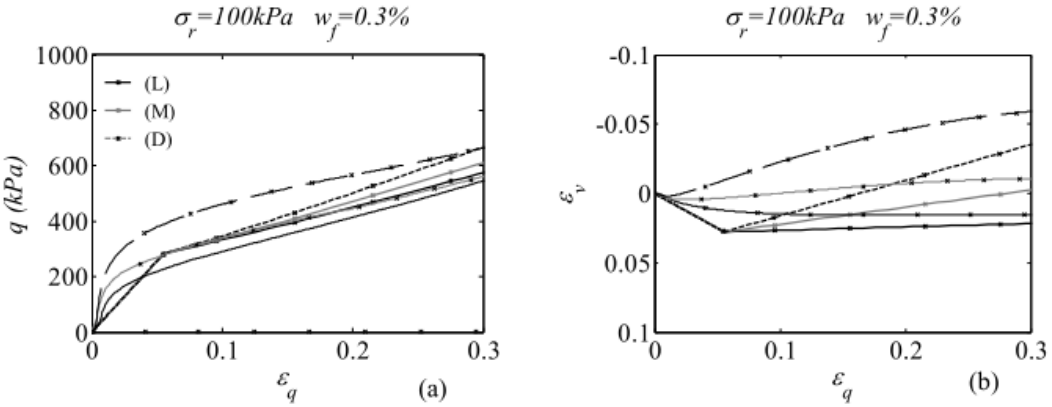

Fig. 2.18 Comparison between the drained triaxial compression test data and model simulations for sand and fibre-reinforced sand (Diambra, 2010)

One of the differences between the test results and model simulations can be observed at lower strains (or incipient stage), where the model fails to capture well the initial stiffness of the specimens. Diambra (2010) explained that the fibre

contribution to the stress of composite is relatively small at the developing stage ($\varepsilon_q < 5\%$ in the figures). At the large strains, the shear stress given by the model is able to fit the test results, attributable to the dependency of the sliding function f_b on the stress in the FRS. Though the model gives reasonable prediction of the shear stress and strain relationship, the soil dilatancy is not well captured. The main reason is the use of a simple Mohr-Coulomb model, in which the elastic stress-strain relationship is given below:

$$\begin{bmatrix} \dot{p}' \\ \dot{q}' \end{bmatrix} = \begin{bmatrix} K & 0 \\ 0 & 3G \end{bmatrix} \begin{bmatrix} \dot{\varepsilon_v} \\ \dot{\varepsilon_q} \end{bmatrix} \tag{2.9}$$

where K and G are the elastic bulk modulus and material constant, respectively.

Further improvement in the model formulations have been done using the Severn-Trent model for sand. Gajo and Muir Wood (1999) developed the basic concepts of the Severn-Trent model, which uses the state parameter ξ (Been & Jefferies, 1985) for modelling the shear strength and dilatancy of sand. The Severn-Trent sand model can be classified as an elastoplastic model, which includes the four main elements: elastic stress-strain relationship, yield function, flow rule and hardening law. For the parameters input in the Severn-Trent model, there are 14 model parameters employed to describe the stress-strain relationship of the fibre-reinforced sand, of which 4 of those model parameters, sliding function (f_b), fibre orientation distribution function ($\rho(\theta)$), elastic modulus (E_f) and specific volume of the fibres (V_f) are used to describe the contribution of fibres. As a result, the improved model can better reproduce the non-linearity of the deviatoric response (Fig. 2.19). However, the model simulation in Fig. 2.19(d) reproduces an opposite trend on the volumetric response, where the test results exhibit dilative response, but the solid lines representing model simulation show more contraction. Diambra (2010) stated some of the voids generated by fibre agglomeration enable the sand matrix much denser, resulting in a more dilative behaviour in the reinforced specimen's volumetric change.

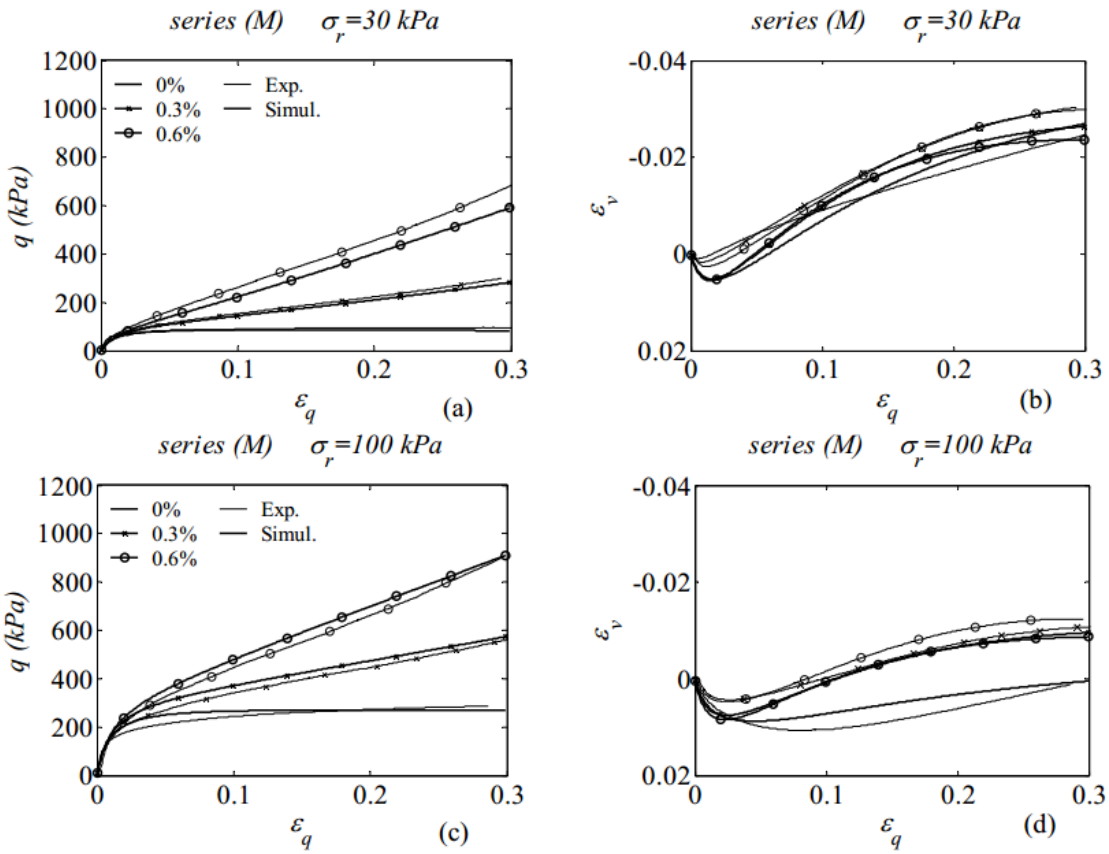

Fig. 2.19 Comparison between the drained triaxial tests data for pure and fibre-reinforced medium dense sand (Diambra, 2010)

Overall, the model developed by Diambra (2010) does well in predicting the stress-strain relationship of FRS. The versatility of the model has been highlighted through the comparison with experimental results. The model not only can be used in the tension condition but also it can perform well in compression condition. Also, for the model's basic concepts, fibres and sand grains are separated to analyse, which means they are independent elements. Except for fibres having contributions to the composite only when they are pulled in tension, sand grains also provide stress to the composite. Therefore, four model parameters are introduced to describe fibre contributions to the composite matrix, determined through the testing results. However, although the improved model (The Severn-Trent sand matrix) can better reproduce the stress-strain relationship, more model validations are needed under triaxial undrained condition.

2.5 Limitations of Existing Constitutive Model

There has also been some development in constitutive modelling of FRS. But they all have some limitations which make them hard to use in finite element analysis of geotechnical problems. Gray and Ohashi di Prisco and Nova (1993) were among the first to develop a constitutive model for soil reinforced by fibres using a composite approach. This model gives reasonable prediction of soil failure but poor simulation of dilatancy and plastic hardening. Ding and Hargrove (2006) have derived a nonlinear elastic stress–strain relationship for FRS based on nonlinear elastic stress–strain relationship for soil and a linear elastic stress–strain relationship for fibres. Therefore, the model is not capable of modelling the failure of FRS. Sivakumar Babu et al. (2008) used the finite element method to simulate the stress–strain relationship FRS in triaxial compression wherein the soil–fibre interaction and fibre orientation is considered. Though good simulation for the shear stress and strain relationship has been shown, the capability of this method in modelling the volume change of FRS has not been verified. Diambra et al. (2013) were the first to develop a constitutive model for FRS which can satisfactorily describe the stress–strain relationship in triaxial compression and extension. The constitutive relation is derived based on the interaction between sand and fibres, and therefore, it can explain the micromechanical mechanism of the FRS behaviour (Diambra et al., 2013; Ibraim et al., 2012; Li & Dafalias, 2000). Since a complex integration is needed to get the stress-strain relationship of FRS which can only be performed under triaxial loading conditions, the model cannot be extended to the general multi-axial stress space. In addition, extra tests on the stress–strain relationship of individual fibres need to be done to get some of the model parameters. But their tests cannot be performed in a conventional soil laboratory.

2.5.1 Sand Model with State-Dependent Dilatancy (Li and Dafalias, 2000)

The new constitutive model for FRS is based on the sand model developed by Li and Dafalias (2000). The model employs a Mohr-Coulomb yield function and state-dependent dilatancy and hardening law.

Dilatancy is one of the essential elements for modelling the stress-strain relationship of soils. It is assumed that sand dilatancy is dependent on the stress state only, and therefore, a dilatancy equation expressed as below is used: (Rowe, 1962; Taylor, 1948).

$$d = d(\eta, C) \tag{2.10}$$

where η is the stress ratio, and C represents some material constants. However, it is found that the dilatancy of sand is highly dependent on the void ratio (Fig. 2.20). In Li and Dafalias (2000), the mechanism of sand dilatancy with different stress states and soil densities has been analysed. A new dilatancy equation accounting for the effect of void ratio e and stress p has been proposed, which employs the effect of state parameter ψ (Been & Jefferies, 1985).

$$d = d\ (\eta, e, Q, C) \tag{2.11}$$

where Q is internal state variable.

The yield function of this model can be written as:

$$f = q - \eta p' = 0 \tag{2.12}$$

where q and p' are deviatoric stress and mean effective stress, respectively. The yield function indicates that it only considers yield in shear but not in compression. But it has been shown by many studies that such yield function works well for sand because compression causes relatively small plastic deformation in sand. The hardening law for the yield function (the plastic modulus) is also expressed in terms of the state parameter ψ, which allows the model to describe the strain-hardening and strain-softening response of sand.

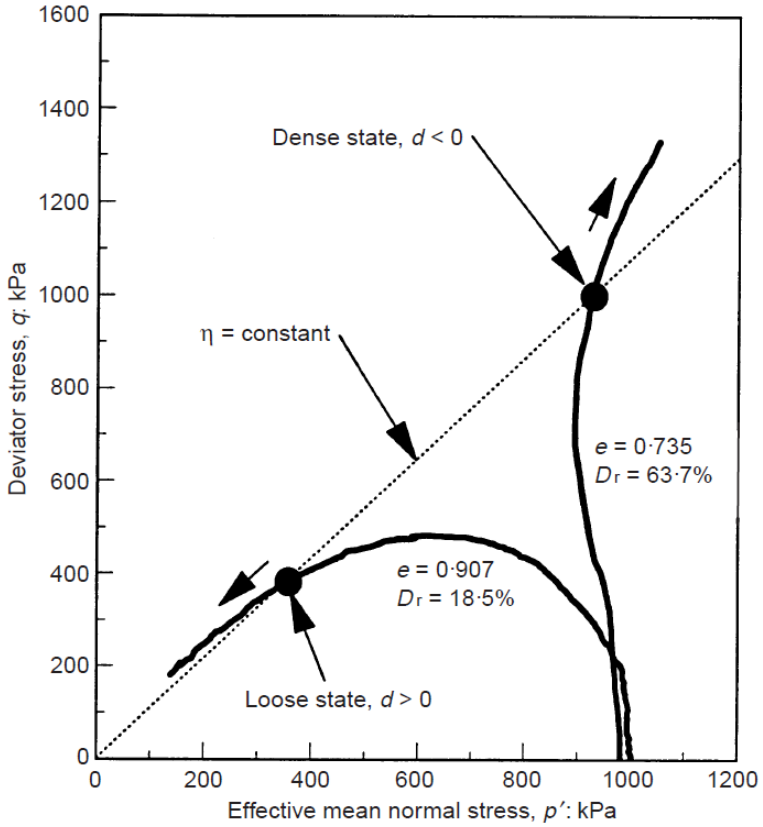

Fig 2.20 The different densities of sand exhibit different stress paths (Li & Dafalis, 2000)

In this model, 11 model parameters are employed. Fig. 2.21 shows some model predictions for the response of Toyoura sand in triaxial compression.

In this study, the Li and Dafalias (2000) model will be used for pure sand. To account for the effect of fibre including on sand behaviour, the concept of effective skeleton stress and void ratio will be used. In this concept, it is assumed that the deformation of FRS is affected by the soil particle movement only, but the mechanical response of FRS should be described using the effective skeleton stress and void ratio, which is dependent on the loading history and fibre content. Specifically, the effective skeleton stress and void ratio should be used to replace those in the dilatancy and hardening law of Li and Dafalias (2000) model.

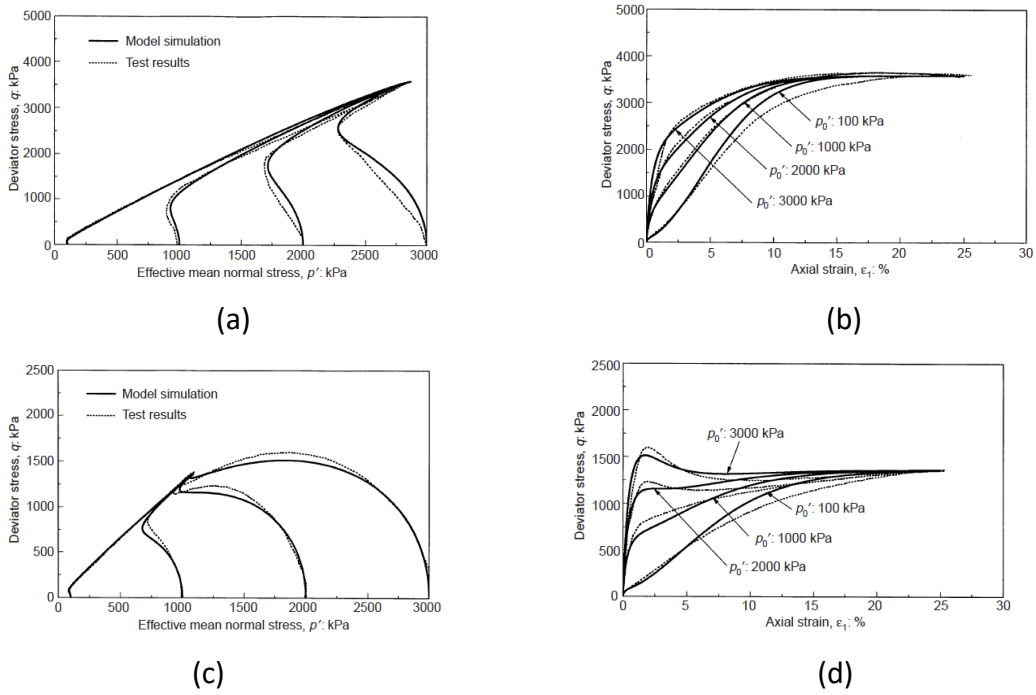

Fig 2.21 Comparison between model simulations and undrained triaxial compression testing results for (a-b) e=0.735 and (b-c) e=0.833 (Li & Dafalias, 2000)

2.5.2 A Failure Criterion for Fibre-Reinforced Sand

To describe the mechanical behaviour of FRS, a proper failure criterion is needed. In this study, the failure criterion developed by Gao and Zhao (2013) will be employed.

$$q = M_c[(p + \sigma_0^u) + f_c] \tag{2.13}$$

with

$$f_c = cp_a[1 - \exp(-\kappa \frac{p+\sigma_0^u}{p_a})] \tag{2.14}$$

where c and κ are two material constants for modelling the failure of FRS, p_a is the atmospheric pressure, with $p_a = 101$ kPa, σ_0^u is triaxial tensile strength of host sand. As shown in Fig. 2.22, the two materials constant play different role in describing the failure curve, where c characterises the maximum or limited fibre reinforcement, and κ controls the magnitude of the critical mean stress, at which there is a sudden change in the curvature of the failure curve (Zornberg, 2004). Both material constants

depend on the fibre properties such as fibre content and fibre length. Fig. 2.23 shows the prediction of the failure criterion for two FRS (Heineck & Consoli, 2004)

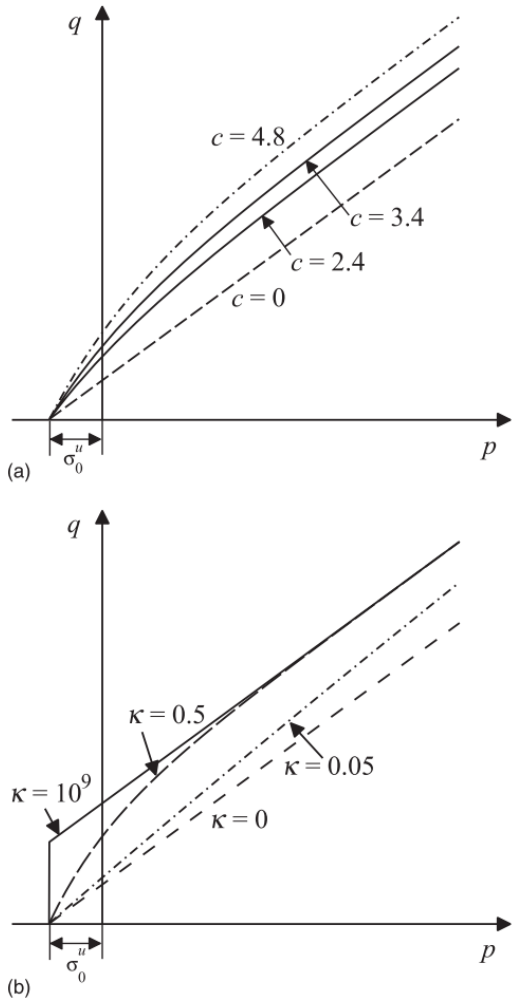

Fig. 2.22 The effect of parameter c and κ on the critical state line (Gao & Zhao, 2013)

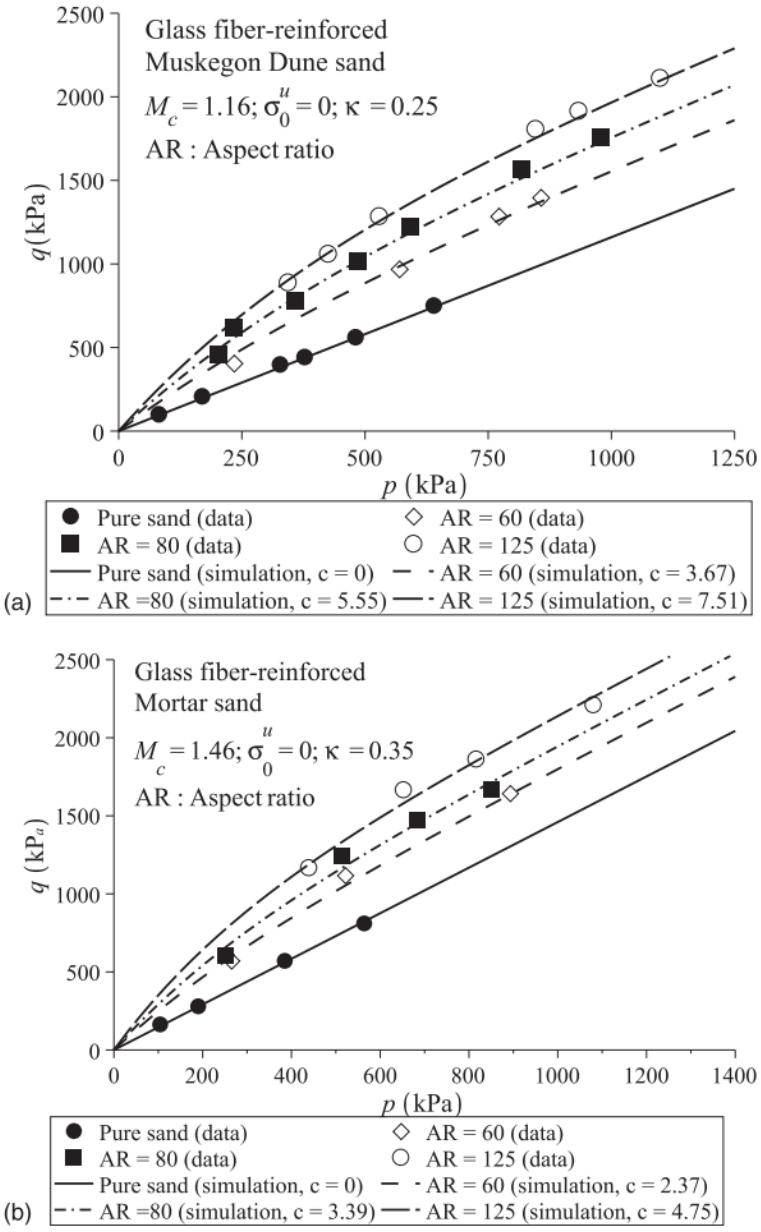

Fig. 2.23 Comparing results between the prediction of the proposed failure criterion and the test results on two glass fibre-reinforced sands (a) Muskegon Dune sand and (b) Mortar sand (Figure from Gao & Zhao, 2013)

A new method for constitutive modelling of fibre-reinforced sand (FRS) is proposed in this study. It assumes that the strain of FRS is dependent on the deformation of the sand skeleton only, while the effective skeleton stress and effective skeleton void ratio, which should be used in describing the dilatancy, plastic hardening and elastic stiffness of FRS, are affected by fibre inclusion. The effective skeleton stress is dependent on the shear strain level, and the effective skeleton void ratio is affected by the fibre

content and sample preparation method. A critical state of FRS model in the triaxial stress space is proposed using the concept of effective skeleton stress and void ratio. Four parameters will be introduced to characterise the effect of fibre inclusion on the mechanical behaviour of sand, all of which can be easily determined based on triaxial test data on FRS, without measuring the stress-strain relationship of individual fibres. The model can be easily extended to the multi-axial stress space and then used in finite element analysis of practical geotechnical problems (Gao & Diambra, 2020).

2.6 Summary and Research Objective

This chapter has given a review of previous research on FRS, including the fibres used in FRS, the basic mechanical behaviour of FRS and the constitutive modelling.

Different fibres have been used in FRS, such as man-made fibres and natural fibres. The man-made fibres are durable and have higher tensile strength. They can thus be used in some tough environment. Since these fibres do not degrade and harm the environment when the soil does not fail, but these fibres are plastic, resulting in a problem in the long-term. For instance, when the foundation or slope fails, the fibres cannot be removed from the soil. Natural fibres are more environmentally friendly but not durable. In most cases, they are just used for short-term stabilization. Methods for increasing the durability of natural fibres are being explored.

The mechanical behaviour of FRS is dependent on the fibre properties, including the fibre content, fibre aspect ratio and fibre length. The soil strength is higher as the fibre content increases. But when the fibre content is too high, the fibres can have a negative effect on the soil stiffness and strength. The fibres should be long enough to prevent pullout failure in shear. (e.g., Michalowski, 2008; Zornberg, 2002; Gregory, 2006). The properties of host sand can also affect the response of FRS, such as the density, particle size and water content.

Many constitutive models for fibre reinforced soil (FRS) have been proposed in literature. Though some of these constitutive models can give reasonable prediction of the behaviour of FRS, but they all have some limitations which make them hard to use in practical geotechnical problems. The objective of this study is to investigate the mechanical behaviour of fibre-reinforced sand through laboratory tests (FRS), and develop a new constitutive model for FRS that can be used for finite element analysis of geotechnical problems. The objectives of this research include:

1) Experimental tests:

- To investigate pure sand and the FRS in drained triaxial compression tests.
- To investigate the effect of sample preparation methods on the stress-strain relationship of FRS.

2) Constitutive modelling:

- To develop a new constitutive model that can predict mechanical behaviour of fibre-reinforced sand in triaxial compression.
- To validate the constitutive model using the test data from this research and the literature.

This dissertation includes 7 chapters and is organised as below:

Chapter 1 gives a brief introduction to the FRS.

Chapter 2 gives a review of existing studies on FRS, including the laboratory tests and constitutive modelling.

Chapter 3 presents the triaxial compression test equipment and the sample preparation methods employed in this project.

Chapter 4 presents the test results.

Chapter 5 introduces the new constitutive model for FRS, including the model framework, model formulations and validation.

Chapter 6 explores the effect of the sample preparation methods on the mechanical behaviour of FRS using drained triaxial compression tests. The new constitutive model is used to predict and analyse the stress-strain relationship of FRS.

Chapter 7 is the conclusion of the thesis. The limitation of the new constitutive model and the recommendation for further research is discussed.

CHAPTER 3: Experiment: Apparatus, Materials and Sample Preparation

The experimental testing program aims to investigate the mechanical behaviour of FRS. A series of drained triaxial compression tests have been conducted with different confining pressure, void ratio and fibre content. The experimental programme will be presented in this chapter, including the equipment, sand and fibres used in the tests, and sample preparation methods.

3.1 Triaxial test apparatus

3.1.1 General Introduction to Triaxial Test

There are three types of triaxial tests: consolidated drained test (CD), consolidated undrained test (CU) and unconsolidated undrained test (UU). Baldi et al. (1988) have discussed the major advantages of these tests:

- The stress and strain in the samples is approximately uniform before failure.
- Since the pore pressure and volumetric changes are possible to be measured directly, soil response under different drainage conditions can be investigated.

3.2.2 Introduction to Testing Instruments

The triaxial test apparatus used in this study is shown in Fig. 3.1 and Fig. 3.2. The equipment mainly consists of a TriSCAN-50 triaxial loading frame (VJ Tech) and two automatic pressure controllers, one is to apply confining preesure, the other one is for measuring the volume change or controlling the back pressure (Fig. 3.3).

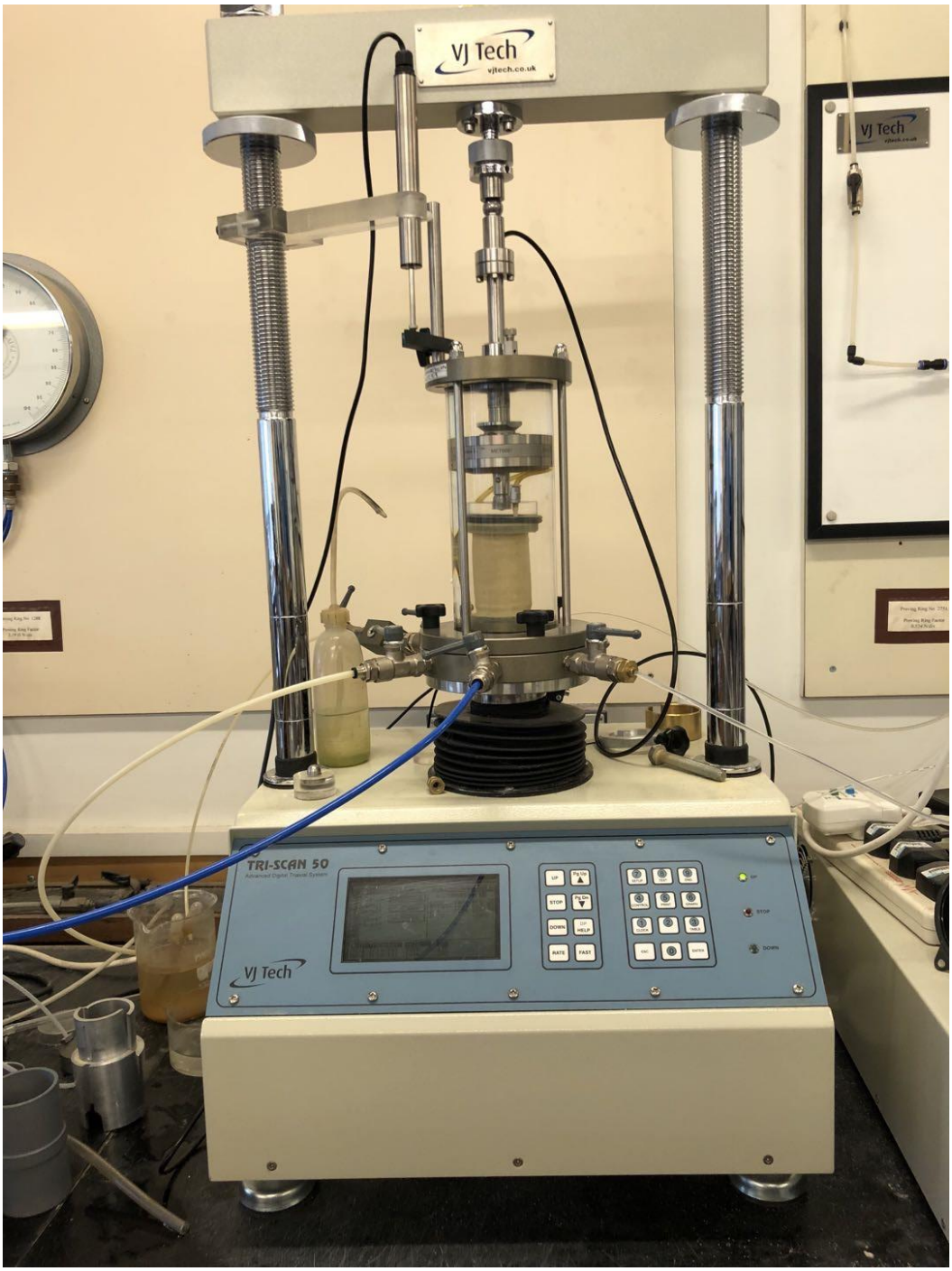

Fig 3.1 The loading frame of VJ Tech (https://www.vjtech.co.uk/)

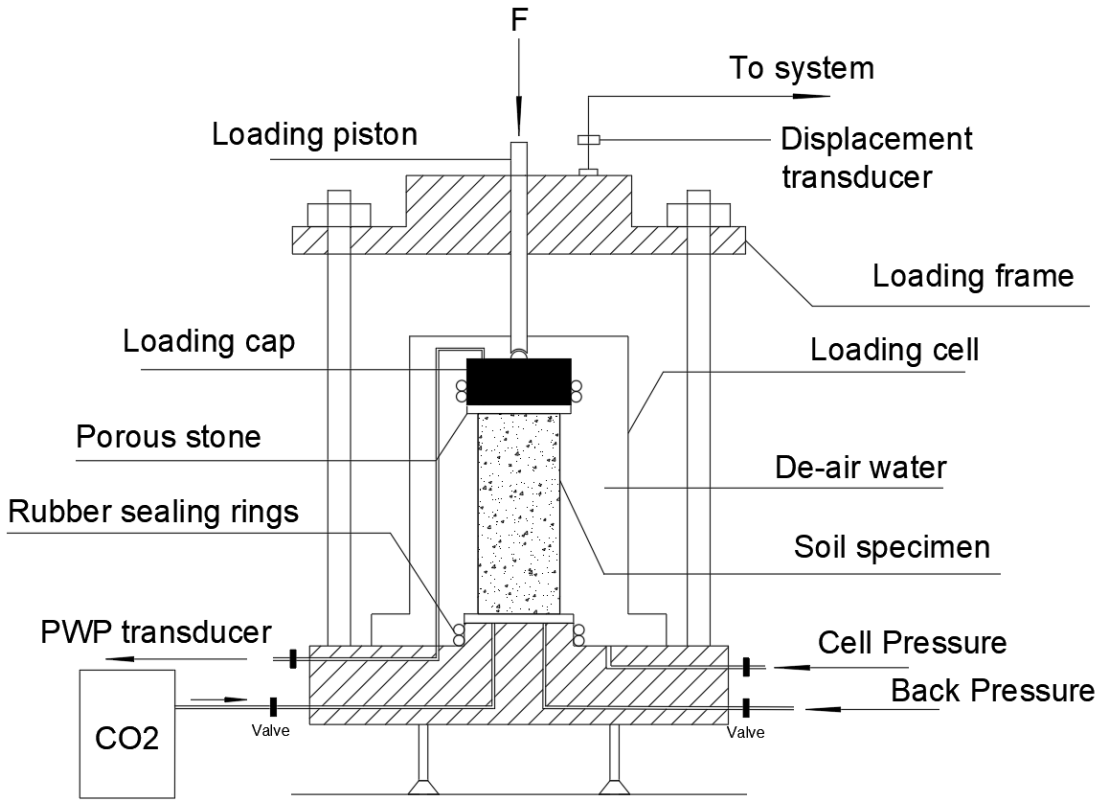

Fig. 3.2 The schematic drawing of the experimental instrument

The triaxial cell is suitable for a range of specimen sizes, which the maximum size is 50mm, and are capable of withstanding confining pressure up to 3200 kPa. However, the pressure value is limited by the software (CLISP studio), which is less than 80% of maximum pressure, to prevent the equipment damage. The base of the triaxial cell provides 5 exit holes, which can be used for controlling the cell pressure, back pressure and CO_2 saturation.

Figure. 3.3 The equipment used in the project

Loading Frame

The TriSCAN-50 loading frame can provide fully automatic triaxial testing and withstand the maximum load up to 50 kN. Some of the testing options such as loading rate can be controlled through 'CLISP' software or a touchscreen on the loading frame. For a triaxial compression test, both the loading piston and the top of the specimen are fixed, meanwhile the loading movement is applied from the bottom of the specimen. Besides, four main parameters (axial force, pore water pressure, axial displacement and volume change) are monitored during the tests and recorded by the machine's control panel.

Transducer

The transducers for this apparatus include (shown as Fig 3.4):

- LSCT Dynamic Displacement Transducers (DT) (Fig 3.4a) were placed outside the loading cell to record the vertical displacement of the specimen. (Unit: mm)
- Dynamic Internal Submersible Load Cell (LC) (Fig 3.4b), for measuring the value of vertical force. (Unit: N)
- Two Automatic Pressure Controllers (APC) (Hydraulic) - 3000 series (Fig 3.4c), one is for applying and monitoring the value of cell pressure, and the other one is for applying the back pressure and sample volume change during the test. The back pressure controller is mainly accompanied by an automatic solenoid valve, aiming to operate the back pressure valve switch automatically. (Unit: kPa for pressure; cc for volume). This pressure controller can withstand pressure up to 3000 kPa.
- Pressure Transducers for Dynamic Systems (PT) (Fig. 3.4d), measuring the pore water pressure (PWP) inside the specimen.

(a)

(b)

(b)

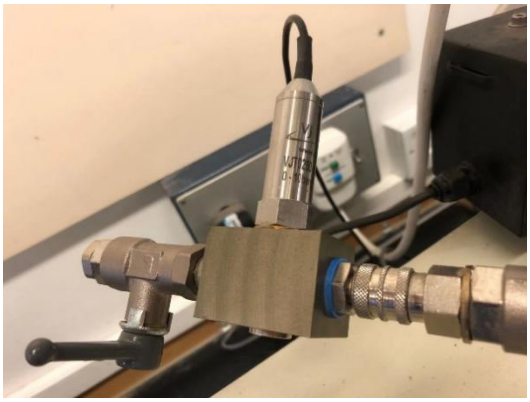

(d)

Fig. 3.4 The main transducers used in the study

The transducers used in this study are shown in Fig. 3.4 and their technical details are given in Table 3.1. Meanwhile, calibration for all transducers has been carried out weekly following the instructions provided by VJ Tech Limited. In addition, the back pressure controller is calibrated before calibrating PWP transducer. Since the controller can be used as a reference for the PWP transduce once the controller is calibrated by the gauge (Fig. 3.5). According to the guidance, the back pressure controller's value is required to be 0 kPa when disconnecting the pipe, or it will be recalibrated using a mechanical reference device such as a pressure gauge (Fig. 3.5). In general, the value of PWP is required to keep the same as that of backpressure throughout the drained

triaxial test. However, due to the PWP transducer's sensitivity, a slight deviation between them within ±2 kPa is observed, meaning that the result of PWP is slightly affected.

Fig. 3.5 The pressure gauge is used to recalibrate the controllers

Table 3.1 The technical details of the transducers

Device	Manufacturer	Model	Max Capacity	Precision
Load Cell	VJ Tech	VJ0352B	15 kN	±0.1 N
Displacement Transducer	VJ Tech	VJ0271	25 mm	±0.01 mm
Pressure Transducer	VJ Tech	VJT0250	1000 kPa	±1.0 kPa
Automatic Pressure Controller	VJ Tech	-	250cc/ 3000 kPa	±0.001cc/ ±1.0 kPa

The software and data acquisition

The 'CliSP. studio' software is the control centre of all the devices. The triaxial test module in this software has three stages: saturation, consolidation and shearing. The configuration of the testing can be personalised. For example, it is flexible to set the time log and stop condition in each stage. During the tests, the status and condition of the tests can be monitored (Fig. 3.6). For the test result, it can produce various results such as deviator stress, stress ratio and axial strain.

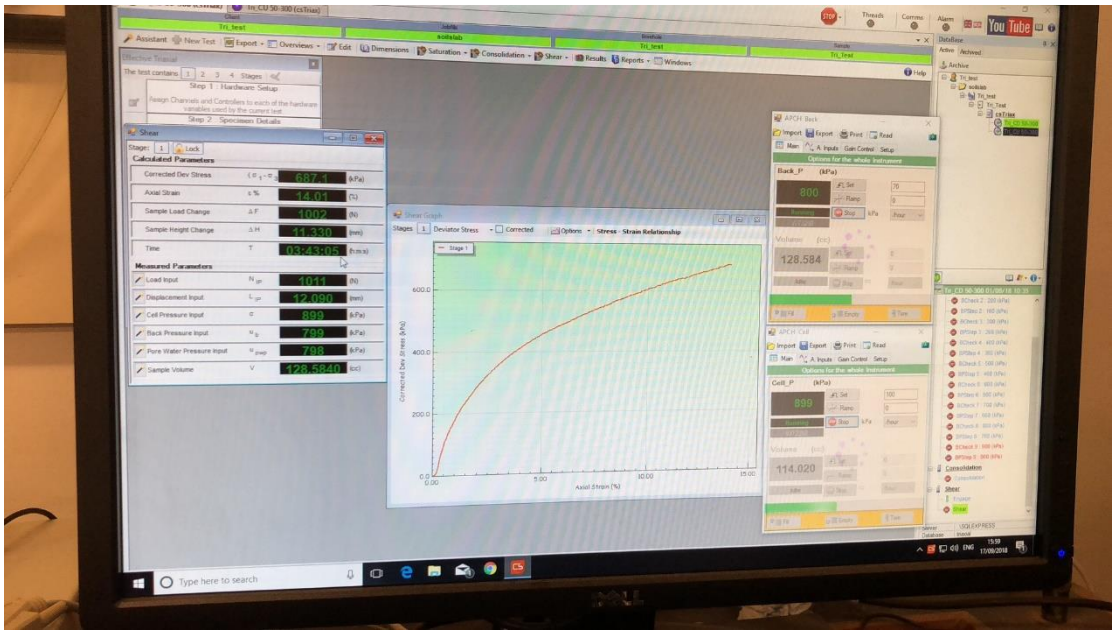

Fig 3.6 The software is monitoring the status and condition of the test

3.3 Mechanism of Saturation, Consolidation and Shearing

De-aired water is used, aiming to generate a testing condition with as few air bubbles as possible. Both the cell and back pressure controllers provide pressures for the sample through a 4-way air-water distribution panel (Fig. 3.7). This air-water distribution panel not only accesses the pressures to the cell but also can be used for the work of de-airing or calibrating the pressure transducer. Furthermore, the triaxial cell is filled with de-aired water supplied by the water tank hanging on the ceiling. This will produce a natural pressure for the water to transfer into the cell due to a height difference between the cell and water tank. As shown in Fig. 3.8, carbon dioxide (CO_2) is supplied to the sample for saturation through the connection (blue pipe) with the base of the triaxial cell. However, it is realised that the carbon dioxide tank is only supporting manual regulation. More details regarding the three stages are introduced below:

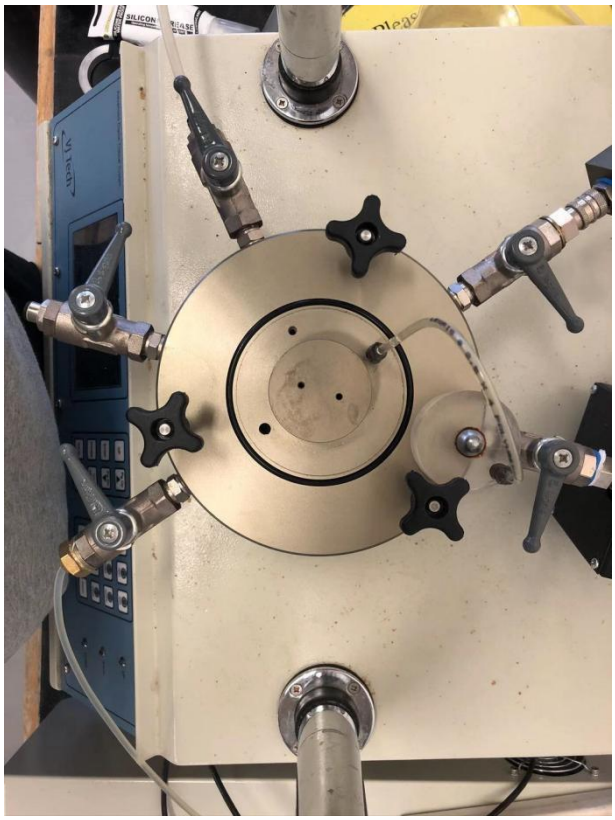

Fig. 3.7 The air water distribution panel used in this study

Saturation

Since the density of carbon dioxide is higher than air, air can be replaced by carbon dioxide when it is flushed at the bottom of the sample. Due to the high solubility of carbon dioxide in water, the soil can then be saturated by increasing the back pressure. Therefore, CO_2 has been frequently used to saturated sand samples. (Diambra, 2010; Noyes, 1914)

Saturation is done with the following steps. Firstly, the sample is flushed by de-aired water. During this process, the water is collected from the top of the sample. When there are no visible air bubbles in the collected water, the flushing stops (Fig. 3.9). This brings the sample to a higher degree of saturation. The sample is flushed by CO_2 from the bottom of the sample. The back and cell pressure controller valves, and the PWP transducer are closed. The intension is to use CO_2 to replace the air, which can be easily dissolved in higher confining pressure. This takes at least 30 minutes until regular bubbles could not be observed through the tube. It implies that the air inside the sample has been pushed out and CO_2 has filled the void in the specimen. Meanwhile, the valve of cell pressure controller was open, imposing a cell pressure about 30 kPa to prevent the sample from being damaged by CO_2. Besides, if the value of cell pressure was maintained at a constant, the back pressure controller's volume still decreases rapidly, it implies that there is some water leakage from the sample. The test had to be stopped. Finally, the air inside the tube was removed through a de-airing block on the PWP transducer. Meanwhile, the PWP transducer was then flushed by de-air water to ensure air inside the transducers was fully removed. Before starting the test, all transducers' valves (back, cell pressure controller and PWP transducer) were maintained open. In the meantime, ensuring the value of PWP and back pressure is almost the same, indicating no more air is remaining in the PWP transducer.

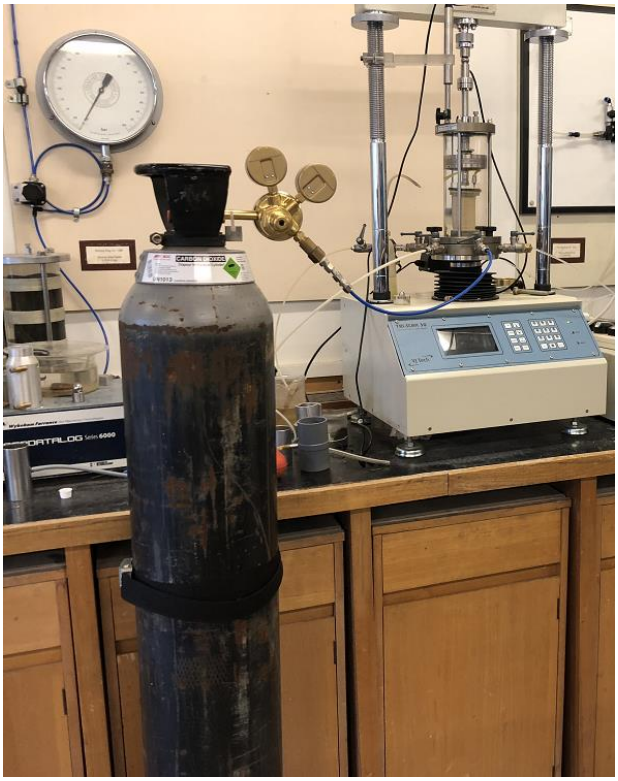

Fig. 3.8 Carbon dioxide are transferring into the sample

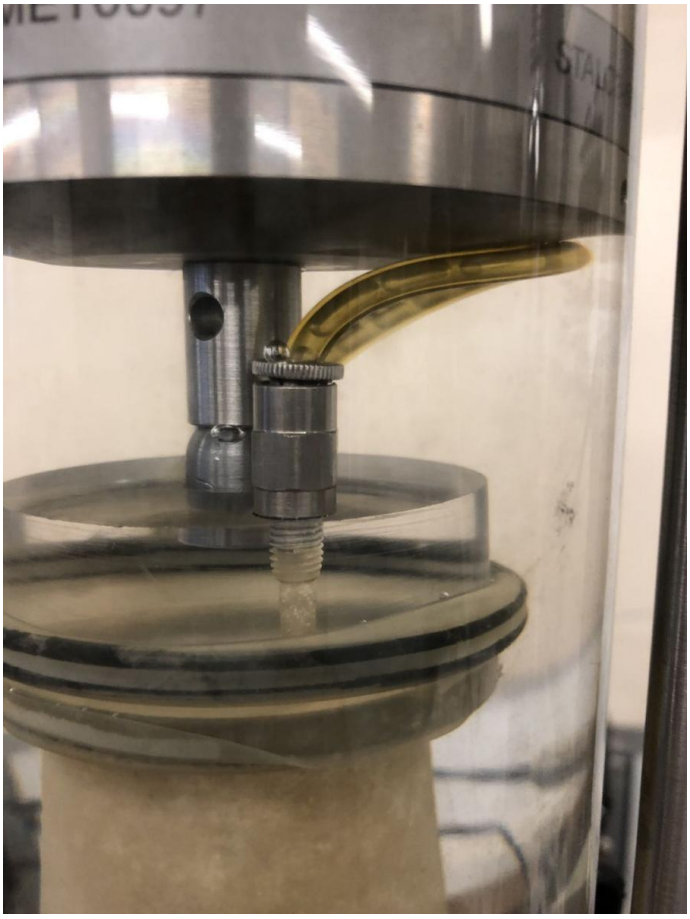

Fig. 3.9 Regular bubbles inside the sample are pushed out

During this stage, the pore pressure coefficient B (B-value) determines the degree of saturation. This step is denoted as the B-check step in the software. Skempton first introduced the B-value (1954), defined as the ratio between the pore pressure change and the total mean stress variation under undrained isotropic loading condition. Therefore, a B-value greater than 0.97 indicates that a sample is sufficiently saturated (the maximum B value is 1.0).

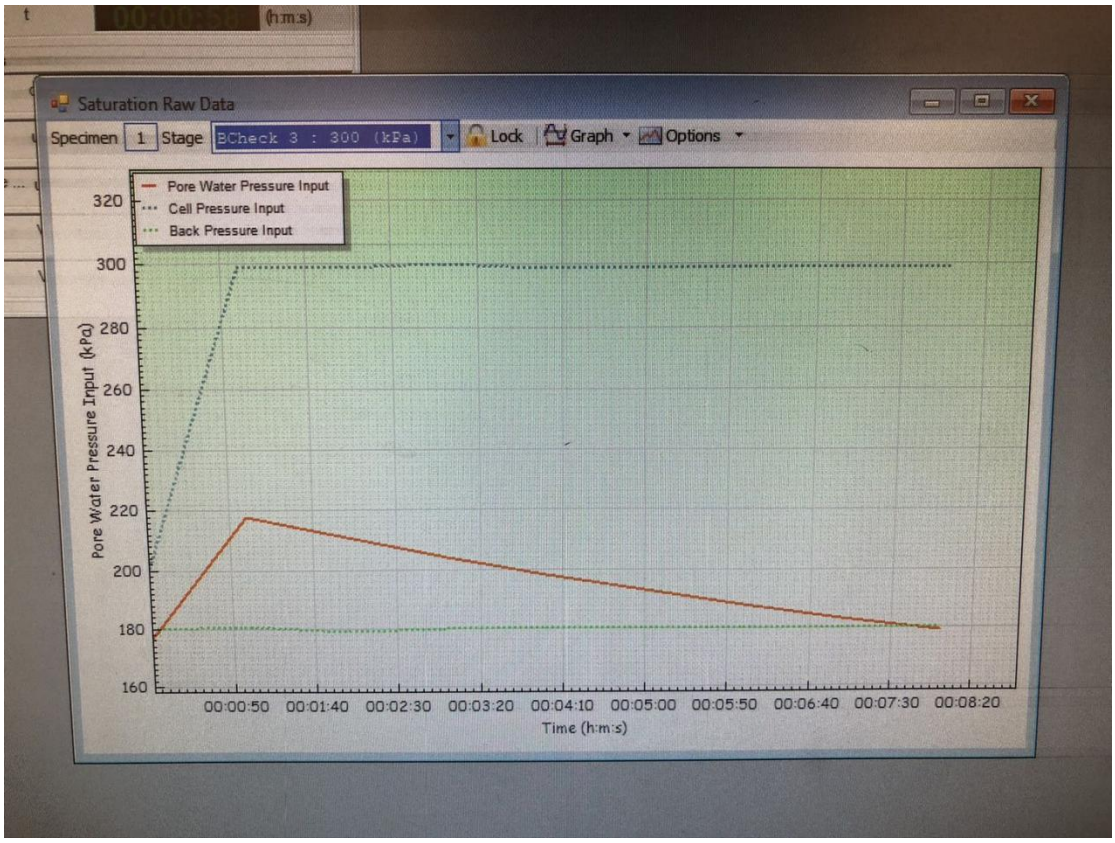

Fig. 3.10 PWP dramatically drops due to CO_2 dissolved under high pressure

The B-check step was prior to starting of the test. During this step, the back pressure valve is always closed, controlled by an attachment called a solenoid valve. The cell pressure is then gradually increased to the target value, while the value of PWP is also gradually increasing. For instance, the cell pressure value is expected to increase from the initial value (less than 10 kPa) up to 100 kPa, while the PWP value is also changing with cell pressure, but the value of back pressure keeps a constant. However, as shown in Fig. 3.10, due to carbon dioxide inclusion, it is a fact that the curve representing

PWP change dramatically drops, since CO_2 can be dissolved under higher pressure. This situation would be last until the sample reach full saturation (B-value > 0.97). During the saturation stage, the specimen is saturated under the effective confining pressure maintained at 20 to 50 kPa, depending on the relative density of the specimen. Higher confining pressure is required for samples with lower density, as the loose samples are more vulnerable to collapse under smaller confining pressure. In contrast, the denser sample could be more easily saturated under smaller confining pressure. Fig. 3.11 indicates when the sample is reaching full saturation, the PWP curve would be maintained at a level, which means the PWP change is zero. Meanwhile, it is implied CO_2 inside the sample is mostly dissolved in the water.

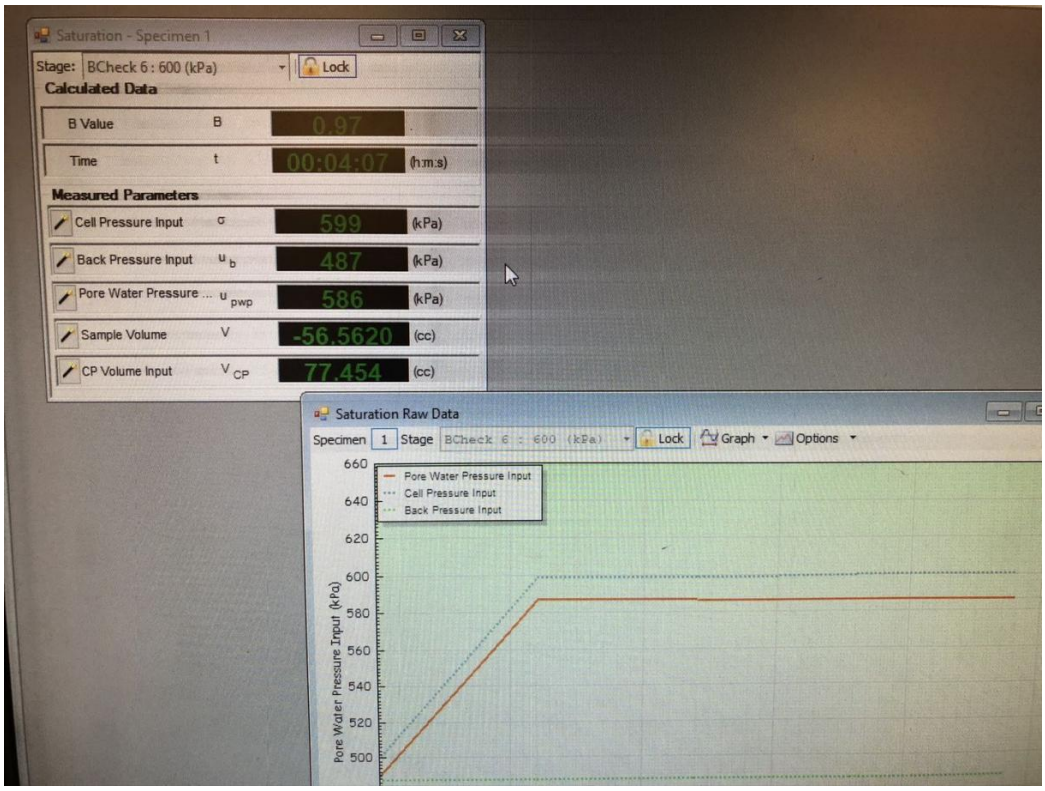

Fig. 3.11 The curve of PWP stabilised a level indicating the gas bubbles are almost eliminated

In addition to the B-check step, a back pressure step (BP step) is accompanied during this process. This step is to push de-aired water from the back pressure controller into the sample for saturation. Consequently, the sample is filled with de-aired water

instead of the water from CO_2 dissolution. During this step, the back pressure valve is open, meaning both PWP and back pressure value would be increasing simultaneously and stabilise at the same level (Fig. 3.12). In terms of the stop condition, if the volume change of back pressure stabilises at a constant, or a slight change by less than 3 kPa of PWP within 5 minutes, will be treated as a condition for the next step (B-check step). Both steps are repeated until the sample is fully saturated (B value≥0.97).

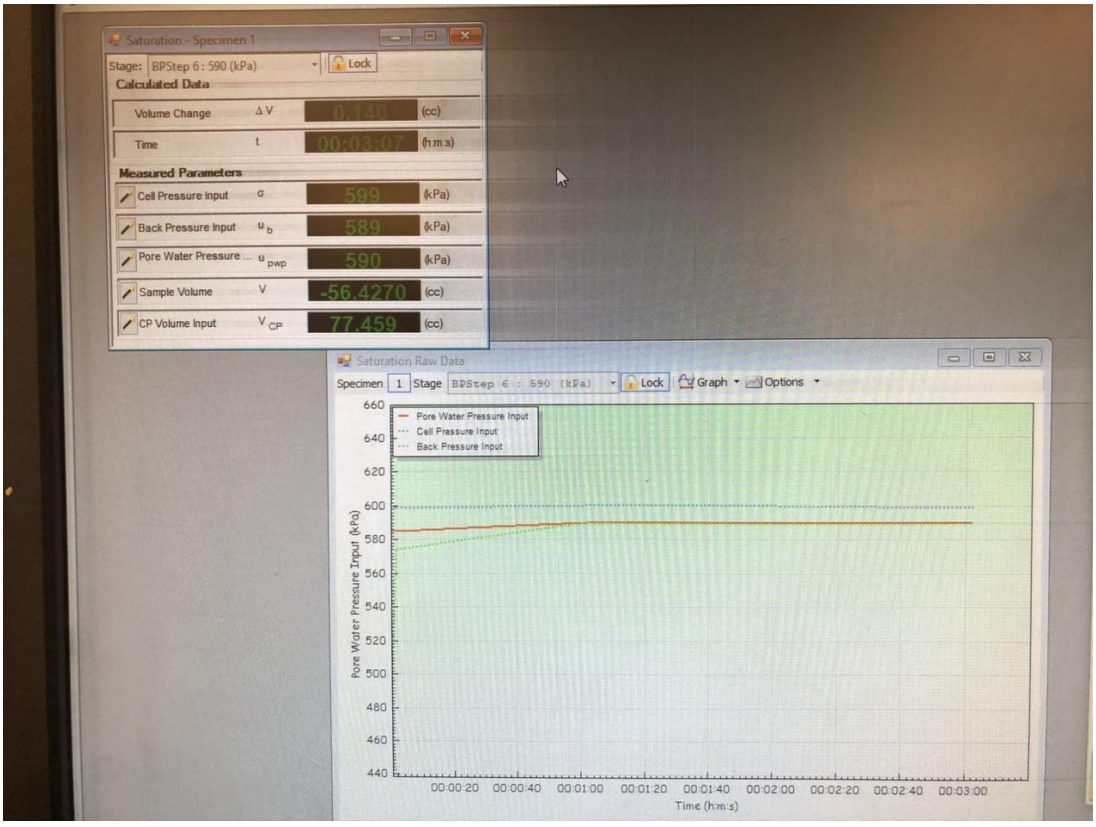

Fig 3.12 The curve of PWP is close to the back pressure at BP step

Consolidation

In this stage, the target effective confining pressure, which would be used in the shear stage, is achieved by maintaining back pressure and increasing cell pressure. Similarly, this stage's stop condition requires the sample's volume changes by less than a specified amount within a selected time.

Shear stage

The shear stage is carried out according to the type of triaxial test (drained or undrained). Before shearing, setting up the thickness of the membrane is required in the software, default as 0 mm. The membrane with 0.45 mm thickness was applied in this study. The test would be conducted at a loading rate of 0.05 mm/min. The test data is recorded in the control software. This stage lasts about 8 hours until the axial strain of the sample reaches at least 30%. Constant back pressure is used during shear.

3.4 Sample Preparation

3.4.1 Materials

Hostun sand

Hostun sand is a commercially available sand in Europe and has been widely used for experimental research and constitutive modelling (Doanh and Ibraim, 2000; Diambra, 2010). Hostun sand is a fine-grained and uniformly graded sand with sub-angular to angular particles. Its grain size has been classified by sieve analysis and shown in Fig 3.13. The Hostun sand properties are shown in Table 3.2.

Table 3.2 Hostun sand properties

Properties	Hostun sand
D_{50}	0.33 mm[a]
C_u	1.4[a]
G_s	2.62
e_{max}	1.0
e_{min}	0.66

a: Data from Azeiteiro et al. (2017)

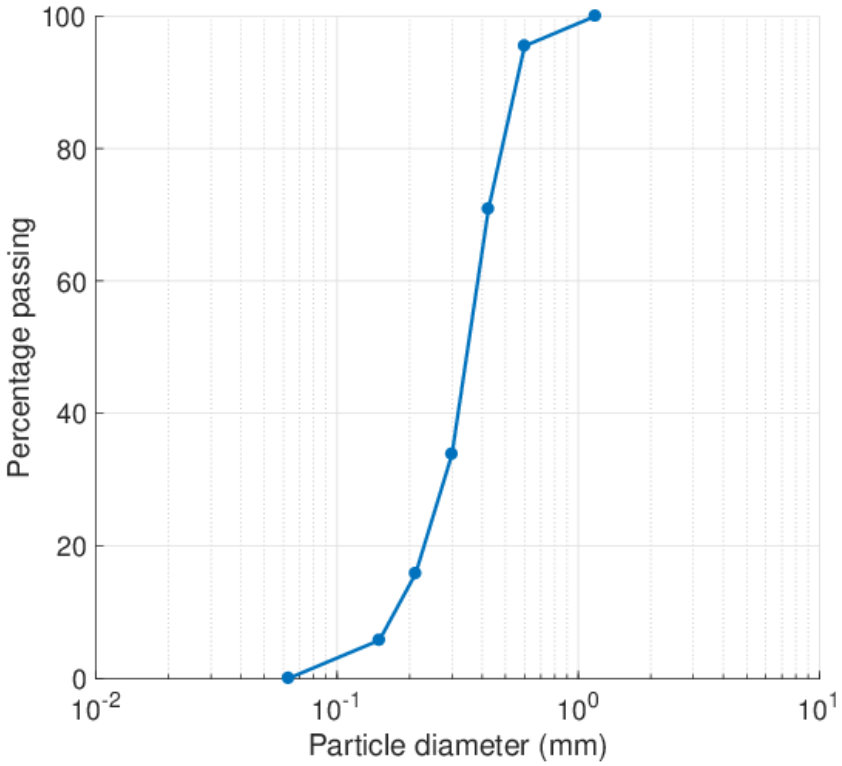

Fig.3.13 Grain size distribution of Hostun sand

Leighton Buzzard Sand

Leighton Buzzard (LB) sand is one of the coarse sand used in laboratory test in the UK. Its mean particle diameter (D_{50}) was found to be 0.53mm, which larger than that of Hostun sand, which has been introduced in chapter 3. Other properties of LB sand are shown in Table 3.3 and Fig. 3.14. More details regarding LB sand will be given in the following Chapter 6.

Table 3.3 Leighton Buzzard sand properties

Properties	Hostun sand
D_{50}	0.53
C_u	2.13
G_s	2.81
e_{max}	0.86
e_{min}	0.61

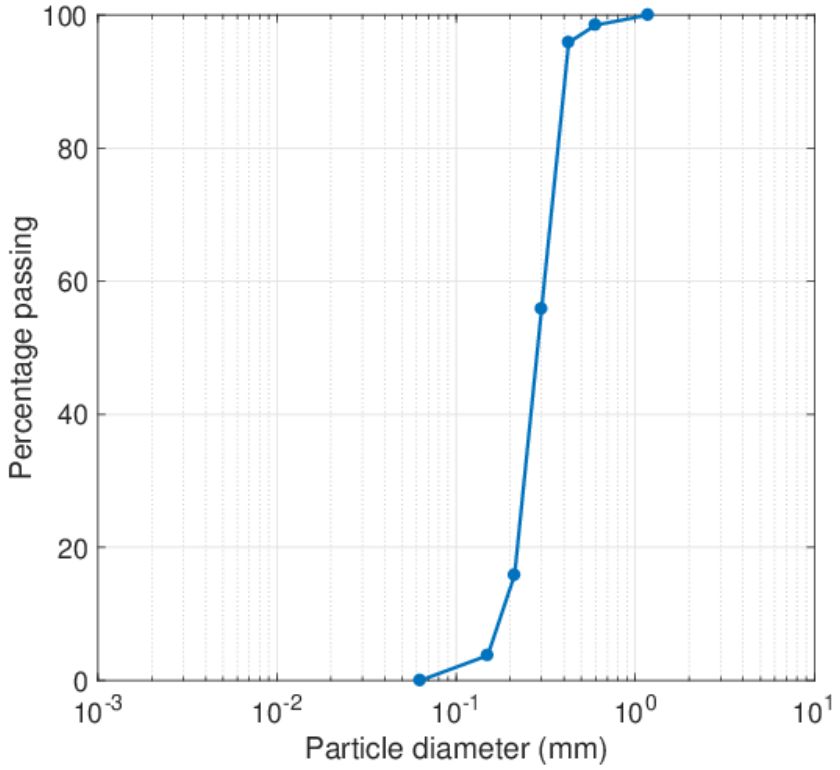

Fig. 3.14 Particle size distribution curve of Leighton Buzzard Sand

Fibres

Fibre: The Loksand™ fibres are used in the project, with the properties being shown in Table 3.4. Loksand™ fibre has been used in reinforcing the turf at Leeds Camegie Stadium in the UK, where it gives a strong and load-bearing surface, and significantly reduces the maintenance cost due to its superiorities such as high tensile strength and ease of operation (e.g., mixing with sand and compaction) (Hajazi et al., 2012). Existing studies also show that this fibre gives effective reinforcement to sand (Diambra, 2010; Ibraim et al., 2010). Therefore, this fibre has been used in the tests. Since the focus of this study is constitutive modelling, tests on FRS with different fibres have not been done. But some test data on FRS with different fibres have been used in the model validation.

Table 3.4 Characteristics of $\mathbf{Loksand}^{\mathbf{TM}}$ fibres

Parameter	Value
Length	35 mm
Diameter	0.088 mm
Specific gravity G_f	0.91
Tensile strength	200 MPa

The motivation of using Hostun sand and Leighton Buzzard sand in this study is to investigate whether the sand properties such as the mean diameter of sand and uniformity coefficient influence the shear strength of FRS. They are two commonly used commercial sands in Europe.

3.4.2 Data Correction and Sample Preparation Method

The moist tamping technique was first introduced by Ladd (1978). This technique was then improved by Michalowski and Zhao (1996), where sand and fibres are separately dropped into the mould to control the orientation of the fibres

After sample preparation, the sample is not a perfect cylinder, and therefore, the diameter of sample is determined based on the measurement at three locations as shown in Fig. 1.

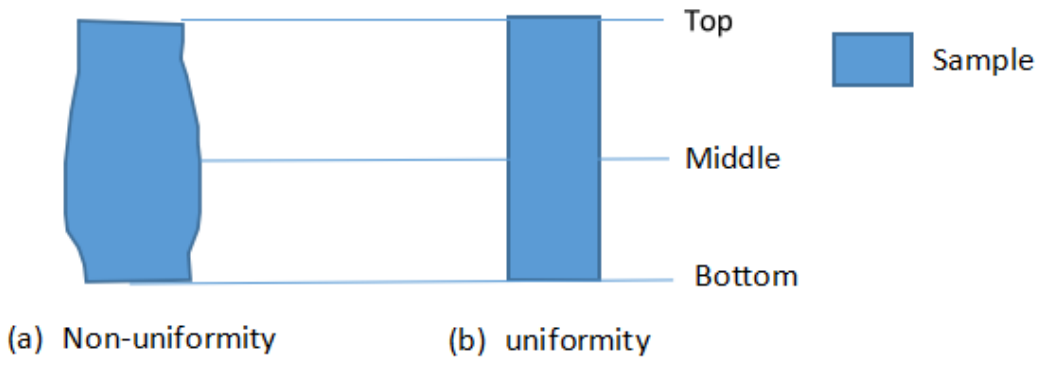

Figure. 3.15 Schematic drawing of (a) non-uniformity sample caused and (b) uniformity sample

Specifically, the sample diameter is taken as the average of the three values at the top (D_t), middle (D_m) and bottom (D_b). The initial diameter of the sample is:

$$D_0 = \frac{(D_t + D_m + D_b)}{3} \tag{3.1}$$

The volume of sand is given by:

$$V_s = \frac{W_s}{G_s \rho_w} \tag{3.2}$$

where W_s is weight of dry sand; G_s is the specific gravity of sand, and ρ_w is density of water. The volume of sand is assumed constant during the test because the sand particles are incompressible. The initial sample volume is:

$$V_0 = \pi D_0^2 H_0 \tag{3.3}$$

where H_0 is the initial height of the sample.

During the test, the sample volume is calculated using the equation below:

$$V = V_0 - \Delta V_s - \Delta V_c - \Delta V \tag{3.4}$$

where V_0 is the initial volume of the sample (based on the measured sample diameter and height at the start of the test), ΔV_s is the sample volume during the saturation stage, ΔV_c is the sample volume during the consolidation stage, ΔV is the sample volume during the part of the shear stage up to the current point.

The sample volume change ΔV is measured based on the water flow in or out of the sample. This has some error because there is extra volume change of the plastic pipe connecting the sample and pressure controller. In addition, the plastic cylinder of the cell can also absorb water. ΔV_s is not measure and assumed to be zero. But there must be some volume change during saturation, which can cause errors for the measurement.

The cross-section area of the sample is calculated as:

$$A = \frac{V}{H} \tag{3.5}$$

where H is the current height of sample, with:

$$H = H_0 - \Delta H_s - \Delta H_c - \Delta H \tag{3.6}$$

where H_0 is the initial height of sample, ΔH_s is the sample height during saturation stage, ΔH_c is the sample height during consolidation stage, ΔH is the sample height during the shear stage.

The axial strain and volumetric strain are calculated as below:

$$\varepsilon_a = \frac{H-H_0}{H_0} \tag{3.7}$$

$$\varepsilon_v = \frac{V-V_0}{V_0} \tag{3.8}$$

The void ratio is determined based on the current sample volume and dry sand volume:

$$e = \frac{V_v}{V_s} \tag{3.9}$$

where $V_v = (V_0 - V_s) - (\Delta V_s - \Delta V_c - \Delta V)$

The deviatoric stress is:

$$q = \frac{F}{A} \tag{3.10}$$

where F is the axial force. The radial and axial effective stress is:

$$\sigma_r = \sigma_3 = \sigma_{cell} - \sigma_{back} \tag{3.11}$$

$$\sigma_1 = \sigma_3 + q \tag{3.12}$$

where σ_{cell} and σ_{back} are cell pressure and back pressure during the shear stage, respectively.

The fibre content is given by:

$$w_f = \frac{W_f}{W_s} \times 100\% \tag{3.13}$$

where W_f is the weight of fibre.

Previous studies have shown that the fibre content of FRS should be chosen between 0.25% and 0.60% for the optimum reinforcing effect. When the fibre content is over w_f =0.90%, there is significant segregation between sand and fibres, which has a negative effect on the soil stiffness and shear strength (Wang et al., 2017; Santoni et al., 2001; Michalowski & Cermak, 2003). Therefore, 0.25% and 0.50% of fibre content are used in this study.

Table 3.5 Amount of sand and fibres used for sample preparation

Test ID	W_f (g)	W_s (g)
Sand_MT50	-	180.03
Sand_MT100	-	180.01
Sand_MT150	-	180.00
Sand_MT200	-	180.00
Sand_MT300	-	180.00
FRS_025MT50	0.432	180.00
FRS_025MT100	0.441	179.98
FRS_025MT150	0.453	180.01
FRS_025MT200	0.428	180.00
FRS_025MT300	0.435	180.00
FRS_050MT50	0.836	180.00
FRS_050MT100	0.887	180.00
FRS_050MT150	0.893	180.00
FRS_050MT200	0.874	180.01
FRS_050MT300	0.842	179.98

The triaxial compression tests were conducted on cylindrical specimens with 40 mm of diameter and 80 mm of length. All specimens were assembled into a split mould with outer and inner diameter of 45 mm and 40 mm respectively, and 80 mm height. Silicone grease and two latex rubber disks respectively were placed at the bottom and top of the specimen to reduce the friction between the porous stones and sample ends (Omar & Sadrekarimi, 2014; Diambra, 2010). There was also a 15 mm diameter hole in the centre of the latex rubber disks to permit the drainage of the specimen. All the triaxial compression tests were terminated when the axial strain (ε_a) is over 30%. The effects of membrane on FRS behaviour have been neglected in the tests.

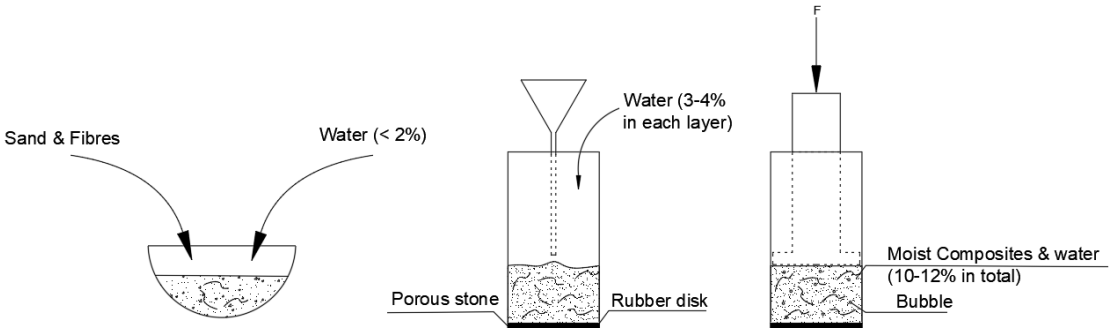

Fig. 3.16 A simple schematic illustration of the MT procedure

Fig. 3.16 shows the moist tamping technique used in the study. The amount of sand and fibres used for sample preparation have been shown in Table 3.5, where the test ID is consisted of the soil type (reinforced or unreinforced), fibre content (0.25% or 0.50%), sample preparation method (MT-moist tamping or MV-moist vibration) and the confining pressure (50kPa up to 300kPa). The following procedure was used for the sample preparation:

1. The sand and fibres were manually mixed with a small amount of water (about 2% of the weight of dry sand) to prevent the segregation between sand and fibres. Mixing was stopped when fibres were evenly distributed through visual examination (Fig 3.17).

Fig. 3.17 The sand fibre mixture before sample preparation

2. A membrane with 38 mm diameter and 200 mm length, a rubber latex disk with silicon grease coated and a porous stone were placed on the triaxial cell base (Fig. 3.18a). Both diameters of stone and the base plate were 50 mm. The bottom of the membrane was fixed by two plastic O-rings (Fig 3.18b). Meanwhile, as shown in Fig 3.18b, due to the different sizes of the membrane and the base plate, this produces a space that allows flexible movement of the specimen during the shearing stage.

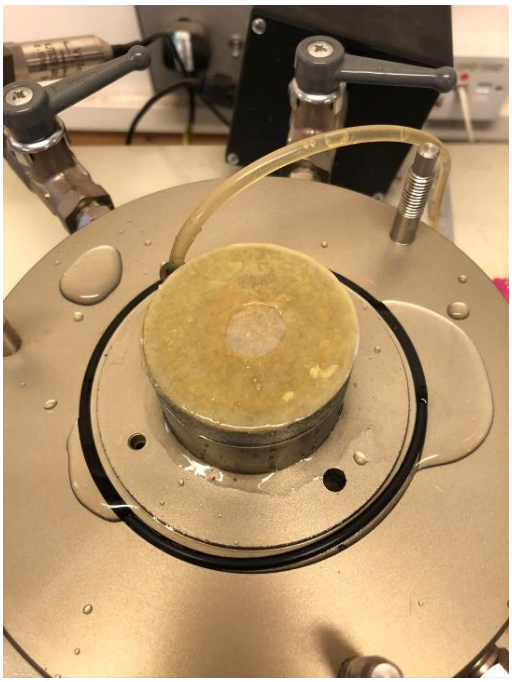

Fig 3.18a The bottom of the specimen consists of porous stone and a latex disk

Fig 3.18b Membrane is fixed at the base of the triaxial cell

3. Before assembling the specimen, an air bulb was used to suck out the air between the mould and membrane, reducing the gap between them (Fig. 3.19).

Fig 3.19 Eliminating the gap between the membrane and the split mould

4. All samples were prepared in 3 layers of equal thickness. Firstly, one-third of the sand and fibre mixture was dropped into the mould through a funnel, which was maintained at a minimum drop height above the sand surface. The sand-fibre mixture was then compacted manually by a hammer with 38 mm of diameter until an even distribution of fibres on the sand surface was produced. A certain amount of water for each layer, around 2% to 4% of the weight of dry sand, is added during compaction.

5. Another one-third of the mixture was dropped into the mould, and step 4 was repeated. If the specimen's height reached the top of the split mould, but the void ratio was not satisfied, the specimen would be compacted manually until it reached the target void ratio (Fig. 3.20).

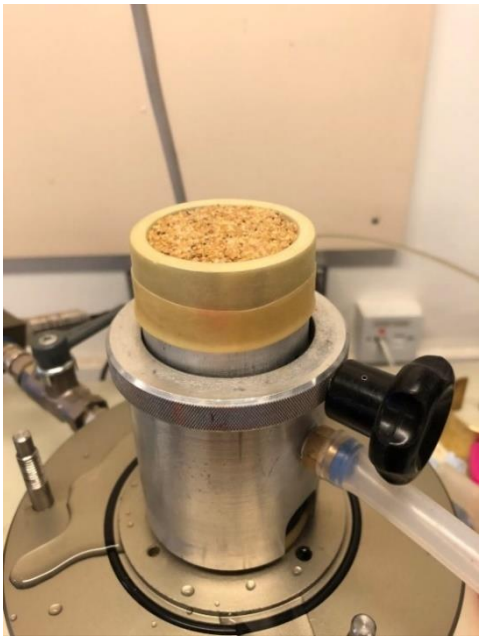

Fig 3.20 The height of the sample is equal to the height of the split mould

6. Once the specimen fabrication was complete, another latex disk and porous stone were placed on the top of the specimen. Two O-rings fixed the top of the membrane. After removing the split mould with minimal disturbance of the sand-fibres mixture, the specimen's diameter was measured from the bottom, medium, and top. A complete sample is displayed as Fig. 3.21.

Fig. 3.21 Sample preparation completed

The details of the specimens are shown in Table 3.6.

Table 3.6: The details of the specimens

Number of Test/Test ID		w_f (%)	Height Spec(mm)	Diam Spec(mm)	σ_3 (kPa)	e_0	D_r
01	Sand_MT50	-	80.4	39.31	50	0.80	59%
02	Sand_MT100	-	79.7	39.44	100	0.79	61%
03	Sand_MT150	-	80.7	39.67	150	0.81	56%
04	Sand_MT200	-	80.1	39.41	200	0.80	59%
05	Sand_MT300	-	80.1	39.63	300	0.78	65%
06	FRS_025MT50	0.25	79.7	40.31	50	0.78	65%
07	FRS_025MT100	0.25	80.1	40.26	100	0.79	62%
08	FRS_025MT150	0.25	80.1	39.77	150	0.79	62%
09	FRS_025MT200	0.25	79.7	39.23	200	0.83	50%
10	FRS_025MT300	0.25	80	39.46	300	0.81	56%
11	FRS_050MT50	0.5	80.1	39.51	50	0.78	65%
12	FRS_050MT100	0.5	80	40.11	100	0.78	65%
13	FRS_050MT150	0.5	80	39.67	150	0.79	61%
14	FRS_050MT200	0.5	80.1	39.45	200	0.79	61%
15	FRS_050MT300	0.5	80	39.68	300	0.80	59%

3.5 Error Analysis

The triaxial tests have been enhanced with the continuous advent and wider use of electronic transducer, thus improving the quality of the test results through the enhancement of the precision. However, other potential factors such as specimen size effect, membrane effect and boundary effect can also cause errors associated with triaxial tests (e.g., Omar & Sadrekarimi, Baldi & Nova, 1984; Garga & Zhang, 1997). The following section will mainly discuss the potential errors during the tests.

Effect of Volume Change during Saturation

In this study, moist-tamped samples are saturated by first percolating carbon dioxide (CO_2) and then de-aired water through the sample by applying back pressure. As mentioned earlier, the void ratio used should be the final void ratio before shear by deducting the volume change during consolidation. However, the volume change occurring during saturation is neglected. The sample volume change during saturation has been considered by Castro (1969). Zhang (1997) reported this void ratio change may cause a significant error in the triaxial undrained tests.

Effect of Sample Size

Though most previous studies have introduced specimen size ranging from 36 to 70 mm in diameter and 71 to 150 mm in length (Diambra, 2010; Michalowski & Cermak, 2002; Ladd, 1978; Zornberg & Li, 2010; Omar & Sadrekarimi, 2015), several researchers have studied the effect of sample size on the behaviour of soil in triaxial tests. For instance, a series of drained triaxial compression tests carried out using Leighton Buzzard sand assembling specimen of 38 mm and 100 mm diameter have been reported by Scott (1987). In this study, higher peak strength and initial shear modulus are found, while smaller post-peak shear strength mobilised in the larger sample. Omar and Sadrekarimi (2015) has reported other similar observations, where a significant difference in shear strength only can be found in higher confining pressure, whereas the effect of sample size is negligible (Fig. 3.22a). In contrast, volumetric responses for all specimen sizes exhibit contraction with a steady reduction under different confining pressures (Fig. 3.22b). Furthermore, the effect of sample size is found to be associated with localised deformation and specimen boundary conditions (Lade & Wang, 2011).

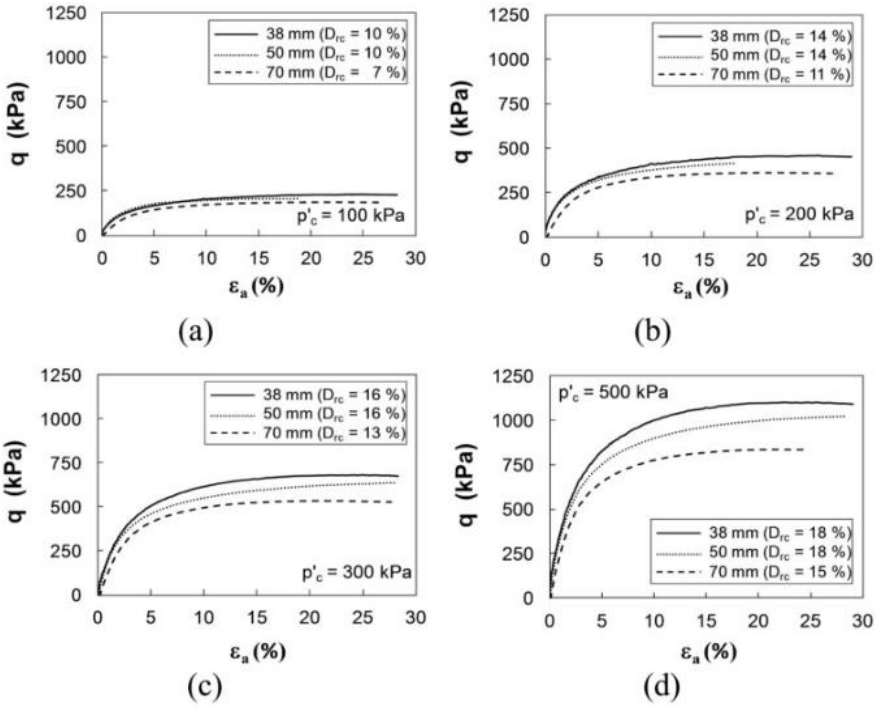

(a)

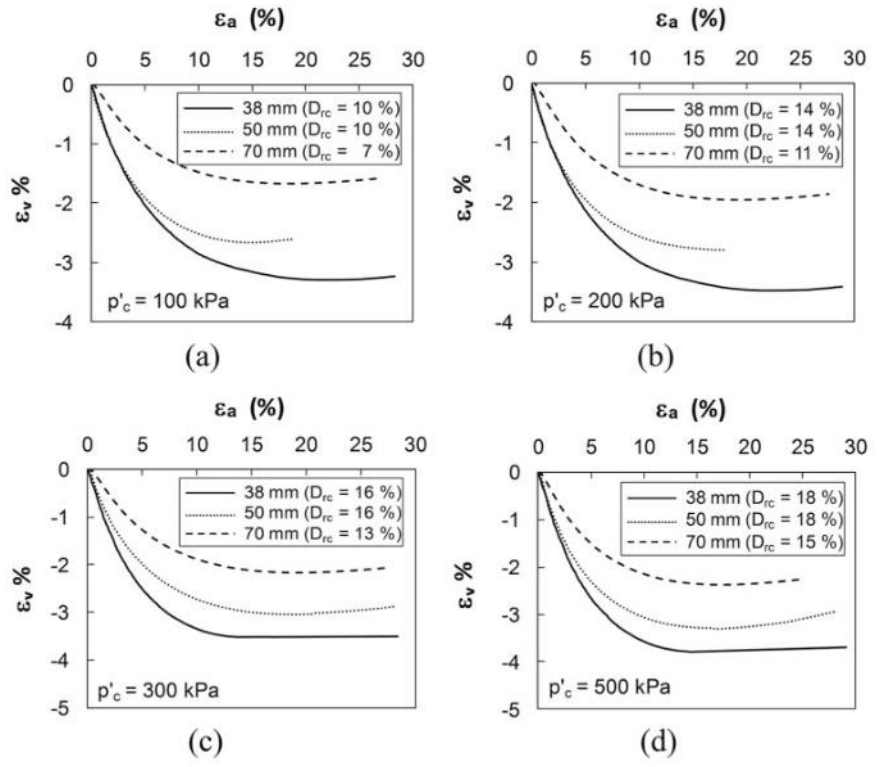

(b)

Fig. 3.22 Effect of the sample size on the measured soil response: (a) stress response and (b) volumetric response (Omar & Sadrekarimi, 2015)

Non-uniform deformation

Shear band is typically observed in both sand and FRS as shown in Fig. 3.23. It can result from friction at the specimen end, which prevents the soil from moving outward and inducing shear stress (Bishop & Green, 1965; Sheng et al., 1997). In particular, Omar and Sadrekarimi (2014) stated that the sample exhibiting bulging deformation at large strain might produce non-uniform stress and strains, which could significantly influence the mechanical behaviours of a soil sample (e.g., pore pressure, strain softening and volume change). A ratio between the height and diameter ($^{H_s}/_{D_s}$) of a sample that affects the bulging deformation have been discussed by Bishop and Green (1995), where samples with lubricated ends could deform nearly uniformly in the drained condition when the ratio equal to 1, while slender sample ($^{H_s}/_{D_s} = 2$) exhibits bulging deformation irrespective of end restraints. Many earlier studies (e.g., Zhang, 1997; Desrues et al., 1996; Liu et al., 2013) stated shear band development depends on sample density and soil types. In Desrues's study, the shear band mainly occurs in the dense sample (Desrues, 1996). But some studies show that shear band can be observed even in loose masonry-sand samples (Finno et al., 1996). Furthermore, the void ratio within the shear band would be larger than the global void ratio of the sample due to more volume expansion (Zhang, 1997).

Enlarged and lubricated end platens were first employed by Rowe (1962), aiming to allow homogeneous stress distribution and a uniform deformation of the sample. The results of drained triaxial tests using lubricated end platens indicate the shear strength is smaller than the one without the lubricated technique (Bishop & Green, 1965). Similarly, in undrained tests, as shown in Fig. 3.24, the sample with lubricated technique exhibits the peak shear strength slightly lower than that without lubrication (Omar & Sadrekarimi, 2014). Conversely, the effect of lubrication technique on the peak shear strength was carried out by Lee (1978), as a result, due to the change of

pore pressure at failure, an unreinforced sample with the lubricated end in undrained tests exhibits higher peak shear strength and lower pore pressure than those with non-lubricated end. Also, Liu et al (2013) suggested that although the use of the lubricated platens would be an effective way to eliminate the end restrain it in triaxial tests, the specimen tended to slice due to the existence of end lubrication.

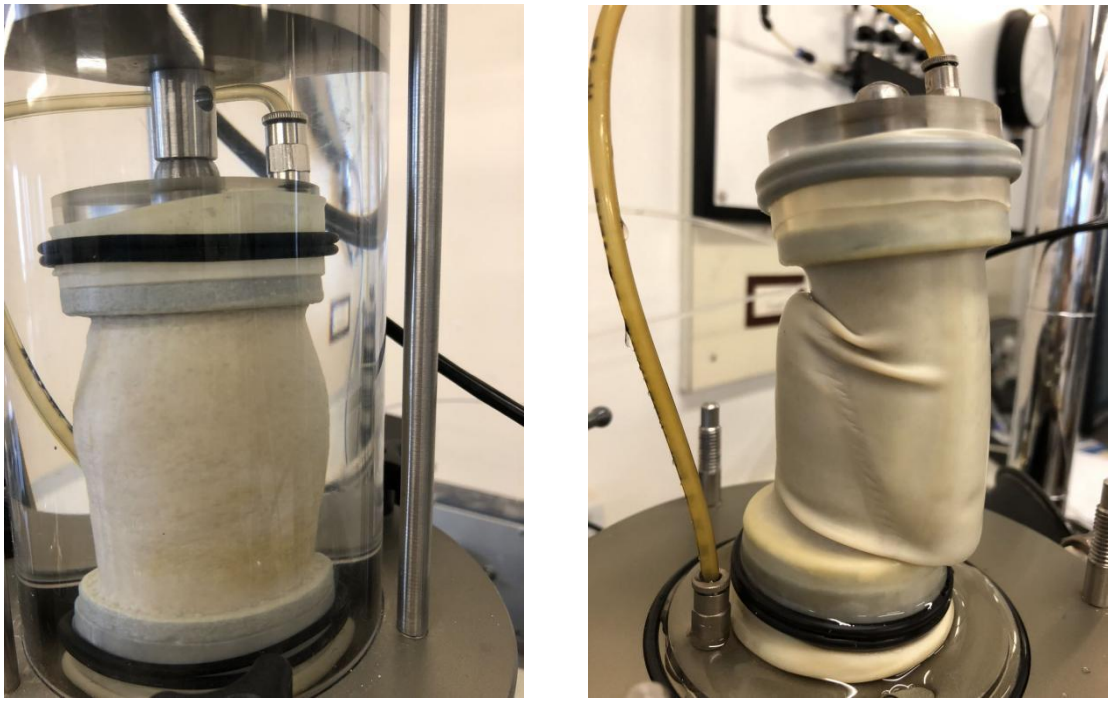

(a) (b)

Fig. 3.23 Typical sample deformation in drained triaxial compression test (a) bulging and (b) shear band

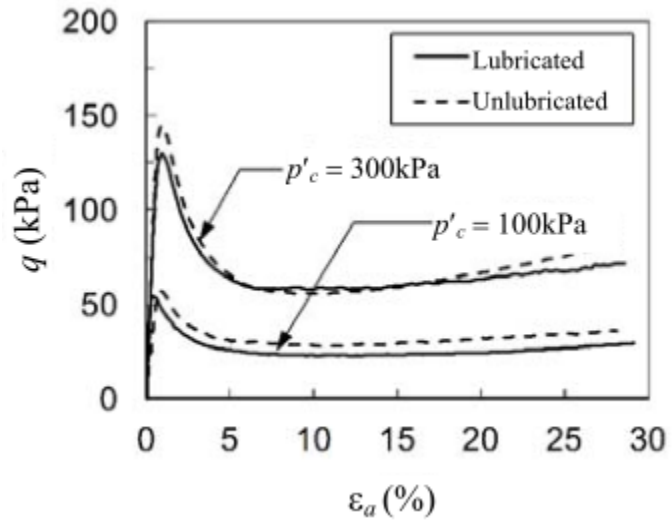

Fig. 3.24 Effect of lubricated end platens on stress-strain behaviour in undrained tests (Omar & Sadrekarimi, 2014).

Membrane Penetration

In a traditional triaxial test, the soil specimen is usually enclosed in a latex membrane to isolate it from the cell water. This implies the membrane is involved in the whole process of the test, which means the rubber membrane has a significant effect on the behaviour of the sample, such as volume change (drained condition), pore pressure (undrained) and deviatoric stress. Fig. 3.25a shows that the membrane penetrates the soil specimen under high confining pressure. The membrane penetration can cause some measurement errors. For instance, the sample's pore pressure will be increased because of an increase in cell pressure during the saturation stage, even though the volume is constant. As a result, as shown in Fig 3.25b, the sample not only withstands the stress caused by the cell pressure, but also extra stress given by the membrane penetration, which depends on the elastic modulus and thickness of the membrane. Consequently, the measured results might be overestimated or underestimated.

(a)

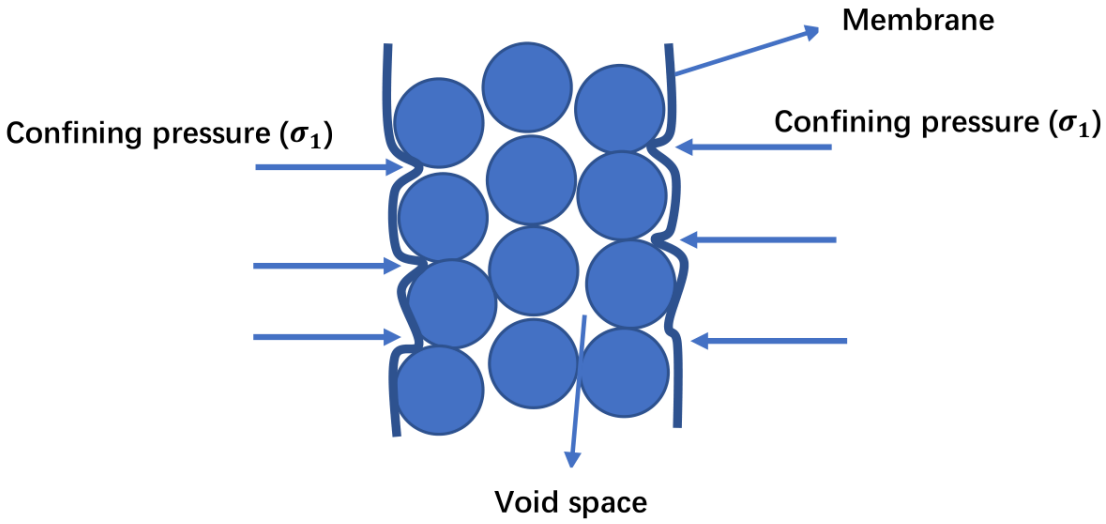

(b)

Fig 3.25 (a) A possible membrane penetration on soil specimen during saturation and (b) a possible schematic diagram of the soil specimen compressed by confining pressure and the stress given by membrane penetration.

Newland and Allely (1957) were among the first to recognise the effect of the membrane penetration in triaxial tests. They found that it would result in an overestimation of the volume change and underestimating the void ratio after consolidation. Therefore, many later studies (Raju & Sadasivan, 1974; Baldi & Nova, 1984; Nicholson et al., 1993; Ansal & Erken, 1996; Zhang, 1997) have investigated the factors affecting the membrane penetration in a soil specimen:

- Effective confining pressure
- The grain size, sample density and gradation of the sample
- The membrane thickness and its elastic modulus

Based on such observations, several methods have been developed to account for the membrane effect's correction on the deviatoric stress and volume change.

The membrane stiffness ($\mathrm{E_m}$) was first mentioned by Henkel and Gilbert (1952), which is the major factor causing an additional increase in the deviatoric stress of the specimen. Later studies (e.g., Baldi & Nova, 1984; Raghunandan et al., 2012) have reported that membrane stiffness depends on the material type, thickness, and dimension of the membrane. ASTM has employed a common correction for the shear stress caused by the effect of membrane (ASTM D 4767-11):

$$\Delta q = \frac{4E_m t_m \varepsilon_a}{D_c} \tag{3.14}$$

where $t_m(\mathrm{mm})$, $E_m(\mathrm{kPa})$ and $\varepsilon_a(\%)$ are the thickness of the membrane, membrane stiffness and the axial strain, respectively; D_c $(\mathrm{mm})$is the sample diameter after consolidation. The test results from most previous studies (e.g., Raghunandan, 2012; Omar & Sadrekarimi, 2014; Greeuw et al., 2001) stated the thinner the membrane, the smaller the deviatoric stress is due to membrane penetration. However, the membrane's effect can be neglected when the error in deviatoric stress is less than 5% (Raghunandan, 2015).

In addition to the rubber membrane affecting the measurement of deviatoric stress, the volume change effect is also of concern by many researchers (Newland & Allely, 1959; Skempton, 1954; Raghunandan, 2011). For instance, Skempton (1954) highlighted the relationship between sample pore pressure and effective confining pressure using Skempton' B factor during the saturation stage. However, this is limited to the possible penetration of the membrane into the soil voids. Therefore, the effect of membrane penetration would be less during saturation (Raghunandan, 2011). Furthermore, a proposed method accounting for the volume change due to membrane penetration has been introduced by Baldi and Nova (1984):

$$\mathrm{V_m} = \left(\frac{\mathrm{D_{50}}}{2\times \mathrm{D_s}}\right) \times \left[\mathrm{V_0} \times \left(\frac{\sigma_3^{'} \times \mathrm{D_{50}}}{\mathrm{E_m} \times \mathrm{t_m}}\right)\right] \tag{3.15}$$

where D_{50} and D_s are the mean diameter of the sand and the diameter of the sample. According to Eq. (3.15), it is indicated that volume change is also affected by the mean diameter of sand D_{50} and the effective confining pressure σ_3'.

The common membrane correction methods above are not adopted in this study due to several reasons. Firstly, due to the lack of the Young's modulus of membrane, which is the most important property for membrane, the above correction method fails to estimate the precise results caused by the membrane effect and thus those correction methods have not been used in this study. Secondly, the membrane correction has been included in the 'CLISP studio' software, which only requires setting the membrane thickness at the shear stage. In other words, once the parameter of membrane thickness is set, the software can generate the testing data such as the deviator stress and volume change automatically. However, as sample uniformity affects test results, both the deviator stress and volume change need to be corrected.

Chapter 4: Test Results and Discussion

4.1 Test Results

A series of drained triaxial compression tests have been carried out using the apparatus with high-precision electronic transducers to understand the typical mechanical behaviour of fibre-reinforced sand. The results of host sand can be treated as a reference for understanding the effect of fibre inclusion on sand behaviour.

In general, the experimental results of triaxial tests from the previous studies (e.g., Michalowski & Cermak, 2002; Diambra, 2010; Wang et al., 2017; Muir Wood et al., 2016) focus on various aspects such as the effect of sand properties (e.g., sand type, particle size, density), fibre characteristics (e.g., fibre content, fibre length and fibre type) and loading conditions (e.g., confining pressure and loading rate), to explore the factors that may influence the mechanical behaviours of the soil. The analyses of the results in this chapter will focus on the following aspects:

- Stress-strain relationship
- Shear strength
- Dilatancy
- Critical state

The soil samples have been prepared using two different sands. This chapter will mainly focus on the test results of the samples prepared using Hostun sand and polypropylene fibres. A section of the test results on Leighton Buzzard sand are used to show the effect of sand type on the soil behaviour. Results of 21 tests are shown in this chapter, of which 13 of the test results are for host sand samples, the rest are for fibre-reinforced samples, covering a range of confining pressure from 50 kPa to 300 kPa. The samples are reinforced by polypropylene fibres and the fibre content varies from 0% to 0.50%. The test details, including fibre content and relative densities for the samples have been listed in Table 4.1.

Table 4.1 The basic details of tested specimens used in this Chapter

Test ID	w_f (%)	σ_3 (kPa)	e_0	D_r(%)
Repeatability of test results				
Hos_100	-	100	0.806	57.06
Hos_100_01	-	100	0.808	56.47
Hos_300	-	300	0.814	54.71
Hos_300_01	-	300	0.801	58.53
Soil type				
Hos_100_080_MT	-	100	0.789	62.06
Hos_200_080_MT	-	200	0.801	58.53
Hos_300_080_MT	-	300	0.780	64.71
LB_100_080_MT	-	100	0.801	23.60
LB_200_080_MT	-	200	0.793	26.80
LB_300_080_MT	-	300	0.786	29.60
Soil density				
LB_100_080_MT	-	100	0.801	23.60
LB_100_075_MT	-	100	0.753	42.80
LB_100_065_MT	-	100	0.658	80.80
Fibre content				
Hos_50_080	-	50	0.800	58.82
Hos_100_080	-	100	0.789	62.06
Hos_200_080	-	200	0.801	58.53
Hos_300_080	-	300	0.780	64.71
FRS_50_080_025	0.25	50	0.778	65.29
FRS_100_080_025	0.25	100	0.789	62.06
FRS_200_080_025	0.25	200	0.828	50.59
FRS_300_080_025	0.25	300	0.808	56.47
FRS_50_080_050	0.50	50	0.787	62.65
FRS_100_080_050	0.50	100	0.785	63.23

FRS_200_080_050	0.50	200	0.786	62.94
FRS_300_080_050	0.50	300	0.798	59.41

4.2 Stress-Strain Relationship of Host and Fibre-Reinforced Sand

4.2.1 Repeatability of Results for Pure Sand

The repeatability investigation has been performed using Hoston sand. All the samples have been consolidated under effective confining pressure of 100 kPa or 300 kPa. The void ratio after consolidation is approximately 0.81, corresponding to the relative density $D_r = 56\%$. More details of the tests are given in Table 4.2.

Table 4.2: The void ratio after consolidation used in the test

Sample ID	Method	Void ratio after sample preparation (e_{ini})	Volume change during consolidation (cc)	Void ratio after consolidation (e_0)
Hos_100	MT	0.808	0.188	0.806
Hos_100_01		0.811	0.110	0.808
Hos_300		0.819	0.347	0.814
Hos_300_01		0.811	0.628	0.801

Fig. 4.1 shows the repeatability of the test results on the host sand with effective confining pressure 100 kPa and 300 kPa. As can be seen in Fig 4.1(a), the results of host sand have a similar value in terms of the deviatoric stress. This difference in the stress-strain relationship can be attributed to a difference in the void ratio between them, at

e_0=0.814 versus the one with e_0= 0.801. However, the difference in the dilatancy behaviour (Fig. 4.1b) is more pronounced than that observed in the stress-strain response. Although the void ratios of the host sand specimens in 100 kPa confining pressure are approximately the same, with a deviation of 0.002, the results of volumetric response exhibit a significant difference. Besides, a higher deviation in the void ratio, causing a more significant difference in volumetric response, has been observed in the testing results under 300 kPa. Therefore, volumetric response is more sensitive to the void ratio than the stress response.

Although some difference can be observed, all the repeating results are exhibiting a similar trend in both plots (Fig. 4.1). Meanwhile, it is interesting to notice that a small variation of void ratio could be negligible on the stress-strain ($q - \varepsilon_a$) response, but it has a more remarkable effect on the dilatancy behaviour ($\varepsilon_v - \varepsilon_a$).

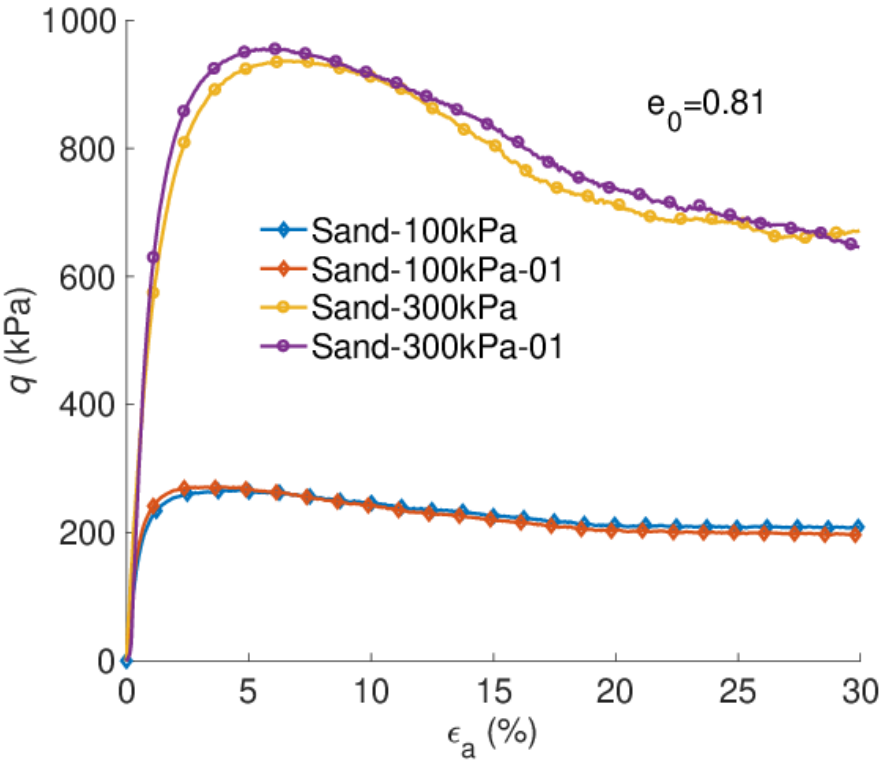

(a)

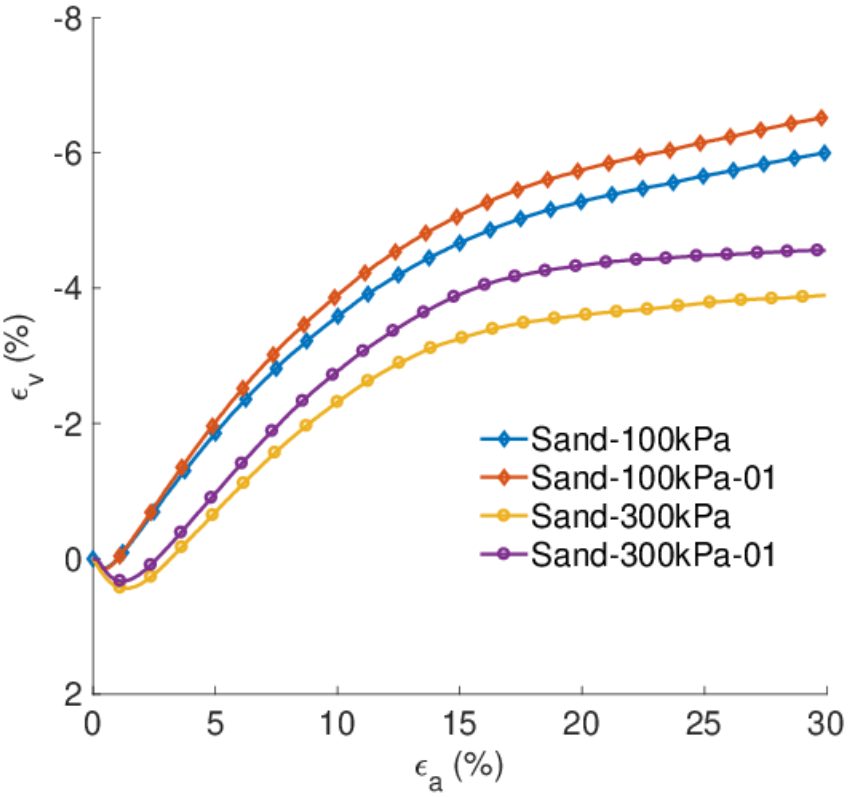

(b)

Fig. 4.1 The repeatability of test results in (a) stress-strain curve and (b) volume changes

4.2.2 Effect of Soil Type on The Stress-Strain Relationship

The effect of soil type on the response of sand has been reviewed in Chapter 2. In this study, the response of two sands (Hostun sand and Leighton Buzzard sand) has been investigated. The properties of two sands are shown in Table 4.3. Hostun sand is a fine-grained and uniformly graded sand with sub-angular to angular particles. The Leighton Buzzard sand is a uniformly graded sand with gravel.

Table 4.3: The properties of two different soil

Soil Type	D_{50}(mm)	C_u	G_s	e_{max}	e_{min}
Hostun Sand	0.33	1.4	2.62	1.0	0.66
Leighton Buzzard sand	0.53	2.13	2.81	0.86	0.61

Different mean diameter (D_{50}) of soil indicates they may affect the shape of the strength envelope. Consequently, this would induce an increase or reduction in the shear strength of the specimen. The details of the tests have been concluded in Table 4.4.

Fig. 4.2 shows a comparison between the stress-strain relationship of two different soil types with the confining pressure from 100 kPa to 300 kPa. At any given value of axial strain, the deviatoric stress of the Leighton Buzzard sand sample is always higher than that of the Hostun sand, though their void ratio is approximately the same. As discussed in Chapter 2, the gradation of soil is positively associated with the coefficient of uniformity (C_u), resulting in an increase in the strength when friction angle is larger (Diambra, 2010). Additional interesting observation can be found in Fig. 4.2(a): the initial stiffness of the sands is very close in the tests, though the soil type is different. In general, the Leighton Buzzard sand shows less dilative response (Fig. 4.2b)

Table 4.4 The void ratio after consolidation

Sample ID	Soil type	Void ratio after sample preparation (e_{ini})	Volume Change during consolidation (cc)	Void ratio after consolidation (e_0)
Hos_100_080_MT	Hostun	0.791	0.110	0.789
Hos_200_080_MT		0.803	0.154	0.801
Hos_300_080_MT		0.804	1.447	0.780
LB_100_080_MT	Leighton Buzzard	0.807	0.364	0.801
LB_200_080_MT		0.808	0.936	0.793
LB_300_080_MT		0.811	1.395	0.786

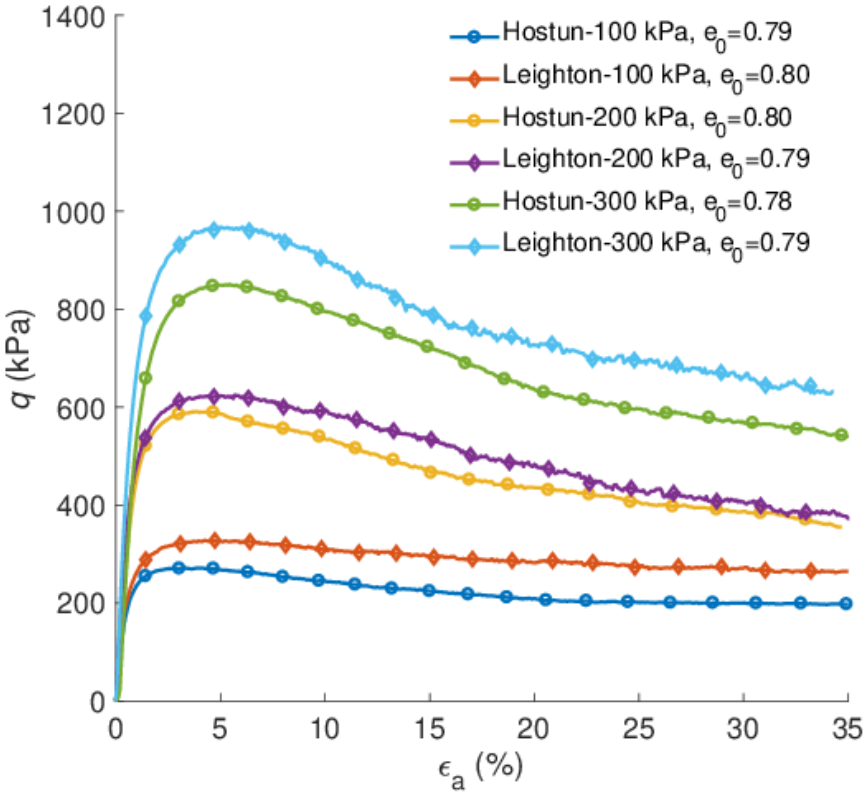

(a)

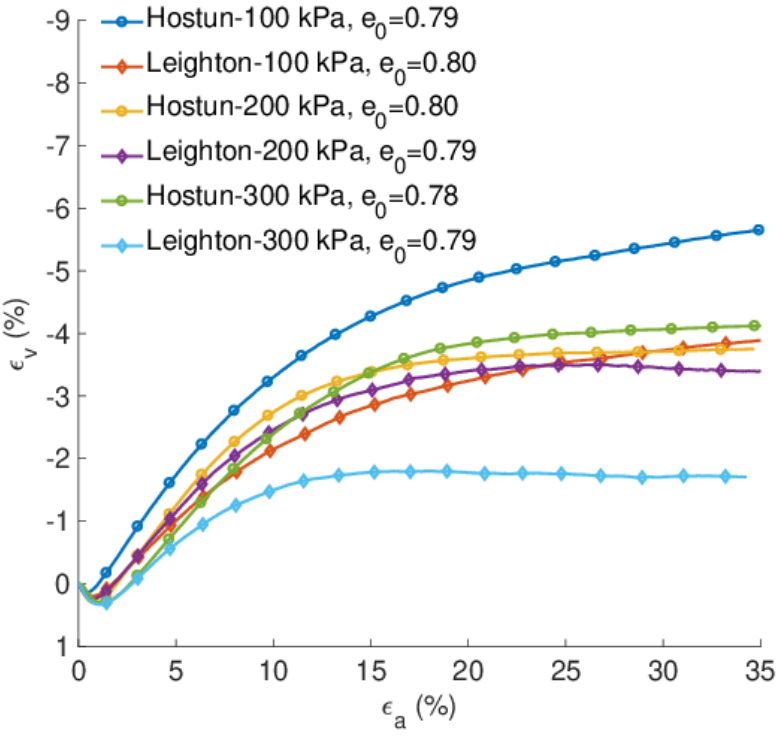

(b)

Fig. 4.2 A comparing results between Hostun sand and Leighton Buzzard sand on (a) the stress-strain response and (b) volumetric response.

4.2.3 Effect of Confining Pressure on The Stress-Strain Relationship

The confining pressure is found to have significant influence on the response of sand. As shown in Fig 4.3(a), the shear strength increases with an increase in confining pressure ranging from 100 kPa up to 300 kPa, even though they have a similar void ratio $e = 0.80$. Less strain softening can be observed when the density is lower.

Fig. 4.3(b) shows the volumetric response of the samples under different confining pressures. More dilative response can be observed in the sample with 100 kPa confining pressure. More contraction is observed when the confining pressure is 300 kPa. This is consistent with existing research findings.

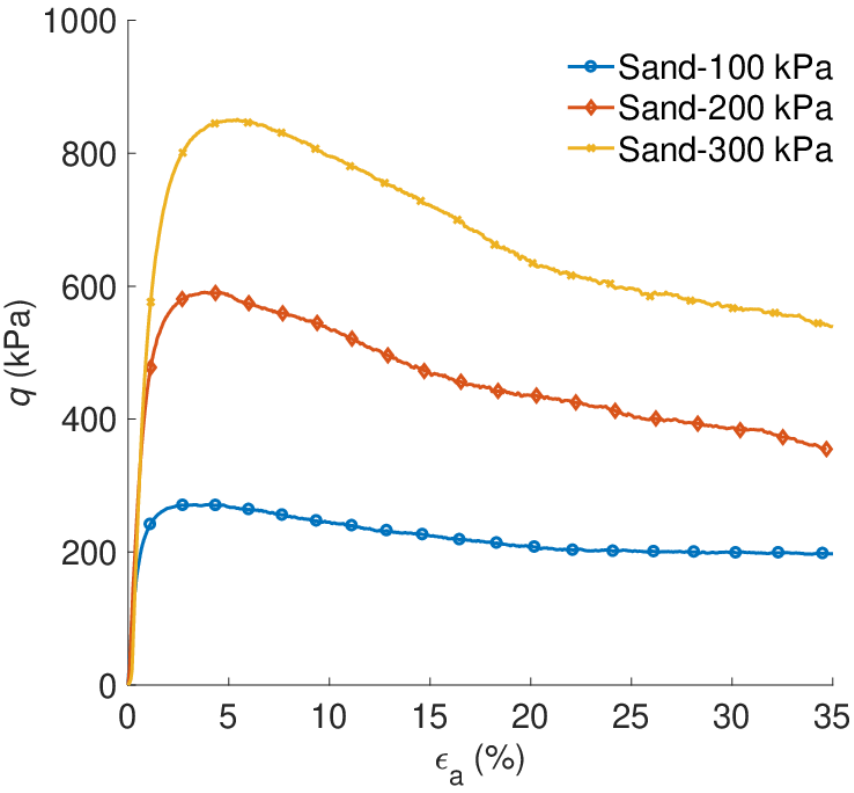

(a)

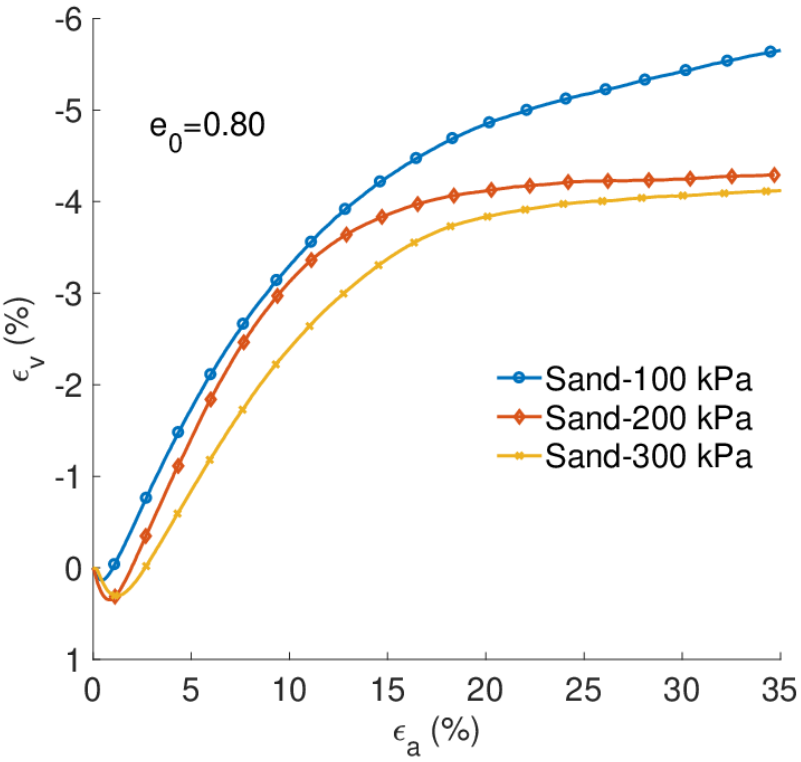

(b)

Fig. 4.3 The stress-strain relationship of Hostun sand tested at 100-300 kPa confining pressure in (a) the stress response and (b) volumetric behaviour

4.2.4 Effect of Void Ratio on The Soil Response

Fig. 4.4 shows the Leighton sand sample results with different void ratios, ranging from 0.66 to 0.80, under the confining pressure in 100 kPa. In Fig. 4.4(a), although the tested specimens have a different void ratio, resulting in a difference in the peak stress, the shear strength is approximately the same at the critical state ($\varepsilon_a > 25\%$). The void ratio has a noticeable effect on the peak deviator stress but negligible effect on the critical state one. It implies that the denser the sample is, the higher the peak deviator stress.

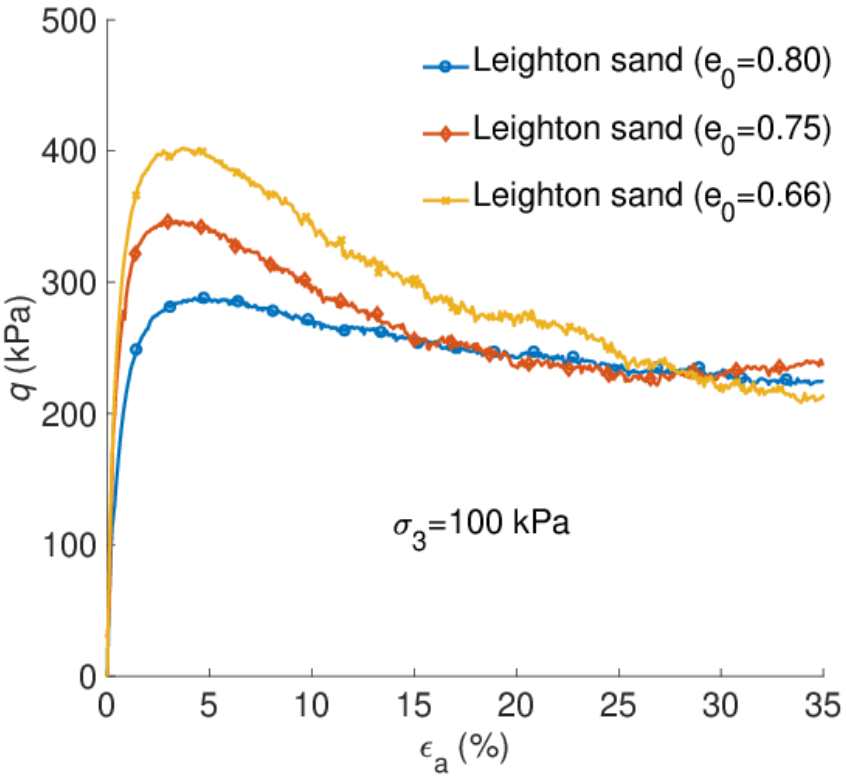

(a)

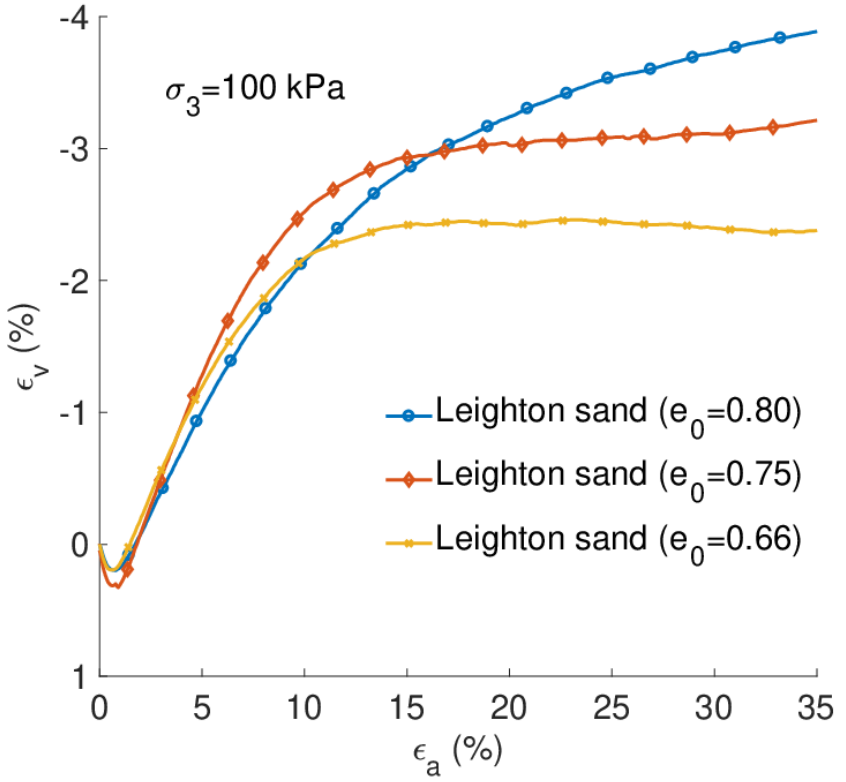

(b)

Fig. 4.4 The effect of void ratio on (a) the stress-strain response and (b) the volumetric response of sand

Been and Jefferies (1985) have introduced the state parameter for describing the effect of void ratio and confining pressure on the response of sand (Fig. 4.5). It can be used to measure the distance between the material state and the critical state line. As shown in Fig. 4.5, ψ can be either negative or positive. Sand is expected to show contractive and strain hardening response in a drained triaxial compression when ψ is positive. Dilatancy and strain softening can be observed in sand with negative value of state parameter ψ.

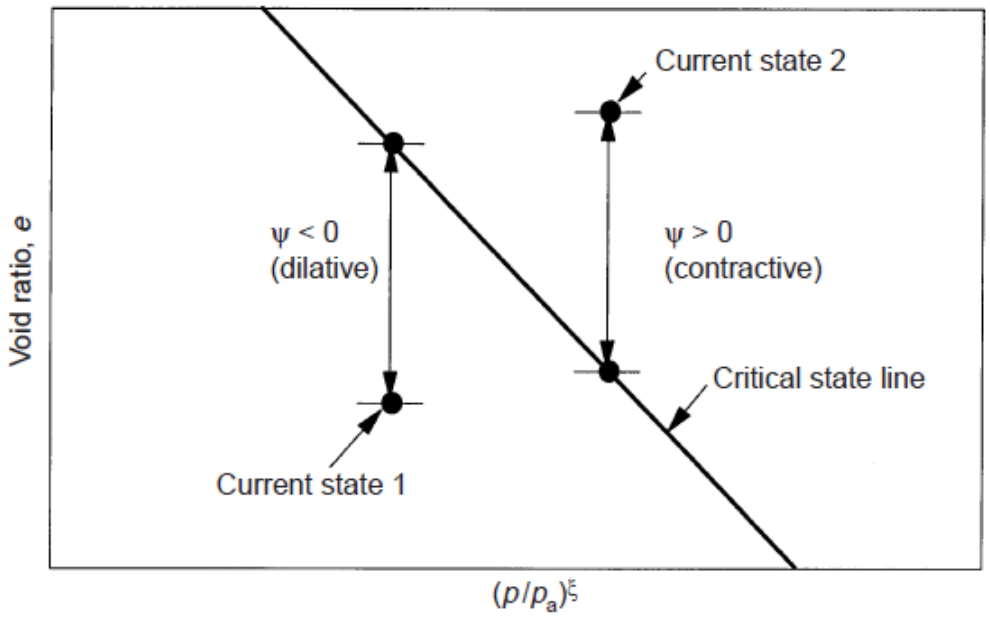

Fig 4.5 Critical state line and state parameter ψ (Been & Jefferies, 1985; Li & Dafallias, 2000)

4.2.5 The Stress-Strain Relationship of Fibre-Reinforced Sand

Fibre inclusion affects the mechanical behaviour of soils, such as the shear strength and dilatancy (Li, 2005; Michalowski,1996; Noorzad & Zarinkolaei, 2015; Diambra, 2010; Wang et al., 2016).

There are 12 reinforced specimens (details shown in Table.1) tested in drained condition under the confining pressures varied from 50 kPa up to 300 kPa. A certain amount of Hostun sand is mixed with polypropylene fibres, and fibres content ranges from 0 % to 0.50%. All reinforced specimens are saturated to reach a B value above 0.97. The average void ratio for all reinforced specimens is $e = 0.80$.

Fig. 4.6 to Fig. 4.9 shows the axial strain-deviator stress and dilatancy response of fibre-reinforced sand, with different fibre content and confining pressure from 50 kPa up to 300 kPa. It is evident that for strain greater than a few percent, the deviatoric stress increases with fibre content. Higher fibre content indicates that they can generate more reinforcement to the soil. The observation has been shown in previous studies (Consoli et al., 2005; Diambra, 2010; Michalowski & Cermak, 2003). Besides, the initial stiffness of the FRS is affected by the fibre inclusion. Especially, fibres are found to reduce the initial stiffness of sand, although the initial stiffness reduction is found to be approximately the same in the samples with fibre content of 0.25% and 0.50%, respectively. This finding is consistent with the results reported by Gray and Al-Refeai (1986), where randomly distributed fibres in triaxial compression tests could cause a loss of compressive stiffness at the incipient state ($\varepsilon_a < 2\%$). A similar observation can be found in Michalowski and Cermak (2003), where the initial stiffness of the reinforced specimens (w_f = 1.5% and 2%) is significantly different from that of the pure-sand sample, which is smaller. In contrast, fibres affect less the initial stiffness of reinforced specimens reported in Heineck et al. (2005). Furthermore, with an increase

of fibre content, this would adversely affect the initial stiffness (Michalowski & Cermal, 2003; Wang et al., 2016).

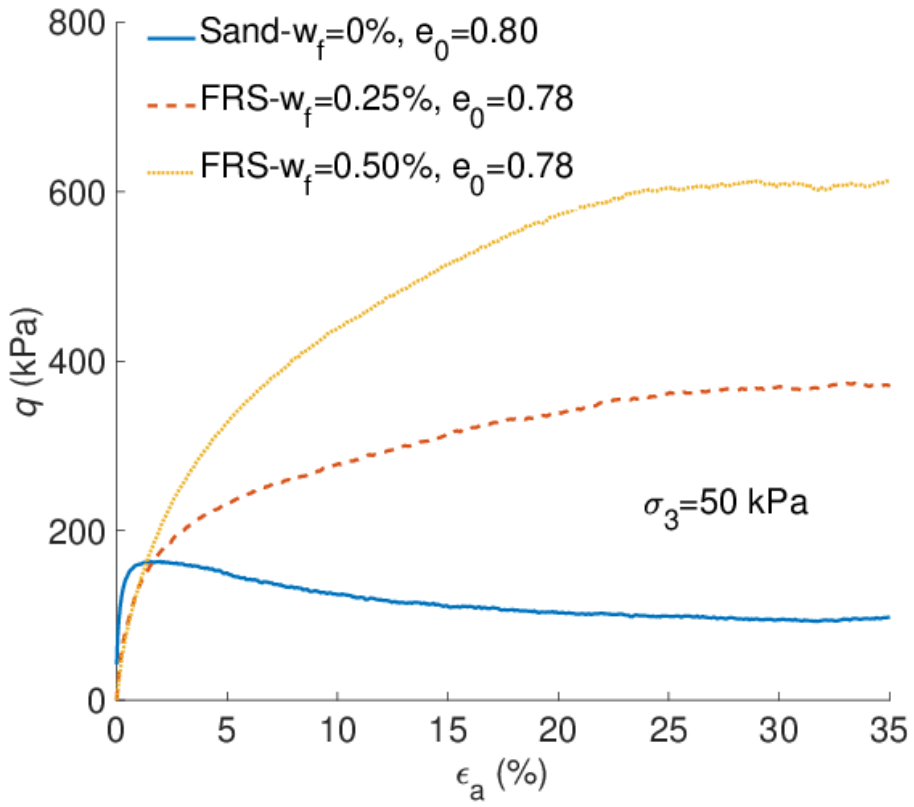

(a)

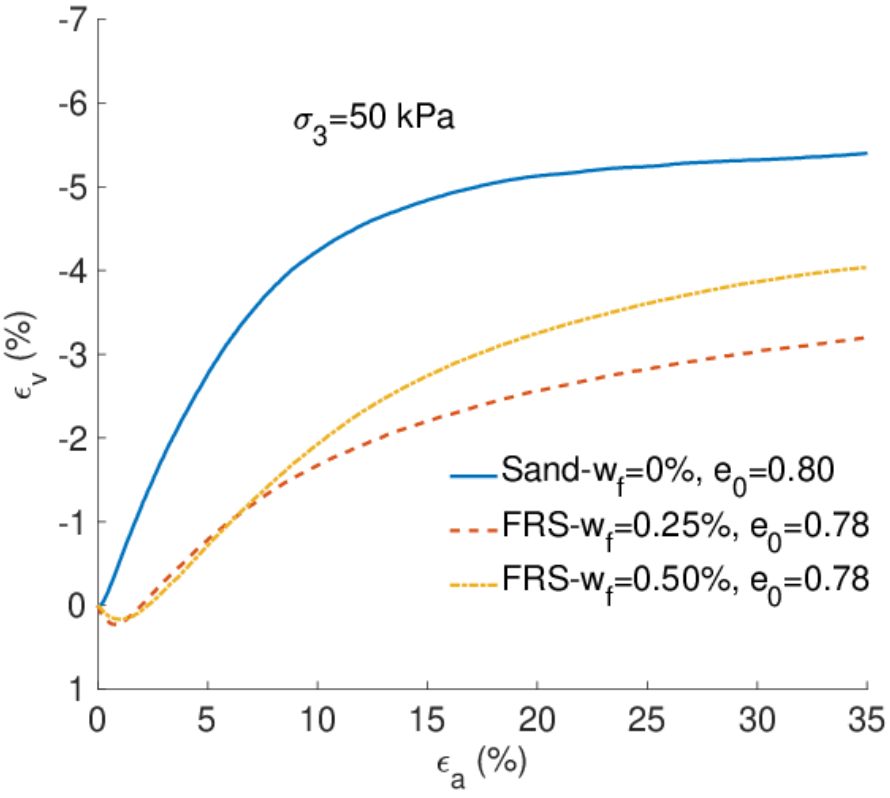

(b)

Fig. 4.6 The response of FRS tested at σ_3=50 kPa using different fibre contents ranging from 0% up to 0.50%

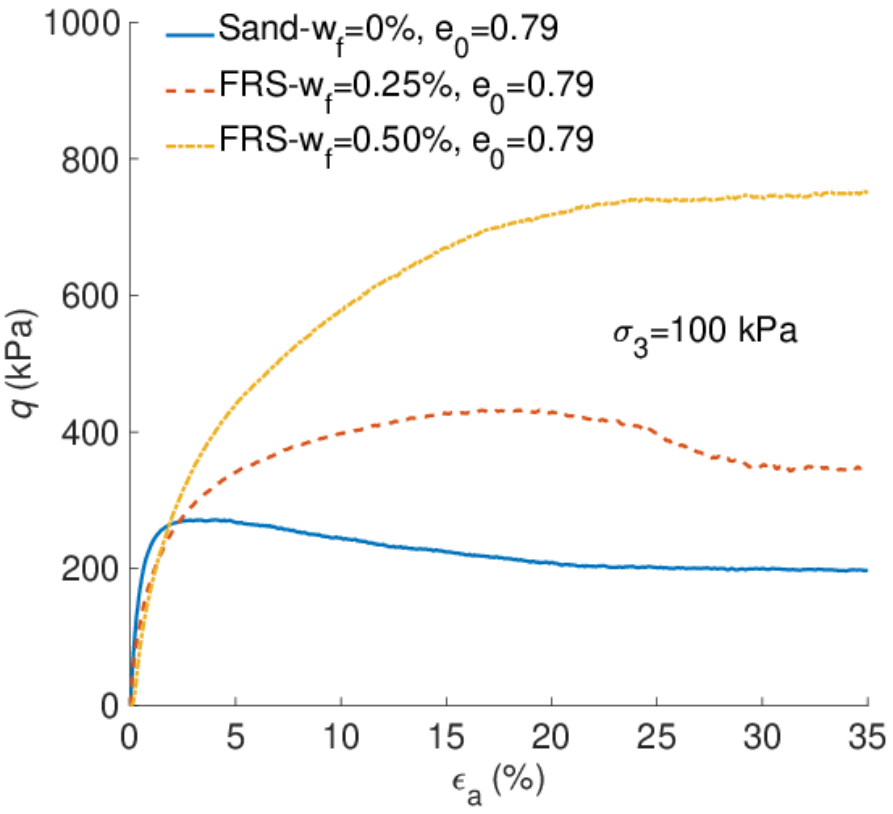

(a)

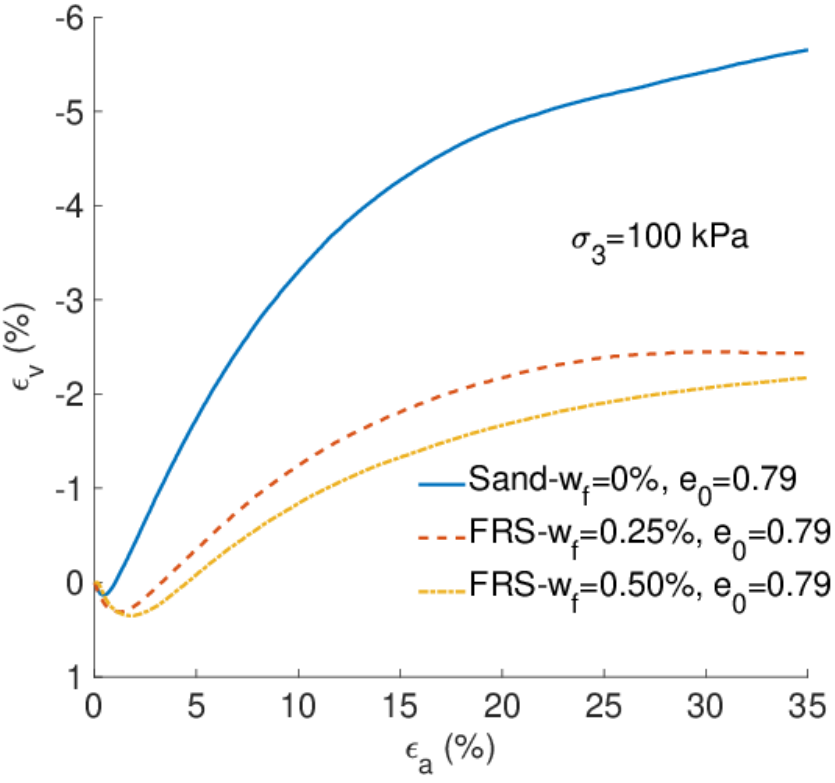

(b)

Fig. 4.7 The response of FRS tested at σ_3=100 kPa using different fibre contents ranging from 0% up to 0.50%

The test results in this study have some difference from the previous studies (Heineck et al., 2005; Li, 2005; Wood Muir et al., 2016; Wang et al., 2017). This would be attributed to various factors such as aspect ratio (η), fibre type, fibre length (l_f) and soil type. For instance, the results of the tests obtained from Michalowski et al. (1996) reported that the samples are prepared using steel fibres with different aspect ratios. As a result, the samples reinforced with steel fibres ($\eta = 85$) exhibit larger initial stiffness than the reinforced samples (η=40), which show the same initial stiffness as the unreinforced sample. Besides, increasing fibre length enhances the ductility of the FRS and enhances the initial stiffness. The specimen reinforced with 50mm of fibre length is significantly larger than the unreinforced samples, and the reinforced samples with shorter fibre length (l_f=25 mm), although the samples have the same fibre content, similar densities and tested under 140 kPa of confining pressure (Zornberg & Li, 2013). The use of different fibre types also affects the initial stiffness. For example, cement reinforcement increasing the soil stiffness and peak strength have been proven by Consoli et al. (1998). The effect of fibre inclusion has a pronounced influence on the glass fibre reinforced soil, where the tested samples are reinforced with three different types of glass fibres (Original glass fibres, recycled glass fibres and coated recycled glass fibres) (Ahmad et al., 2012). The recycled and coated recycled reinforcement causes a reduction in the initial sand stiffness.

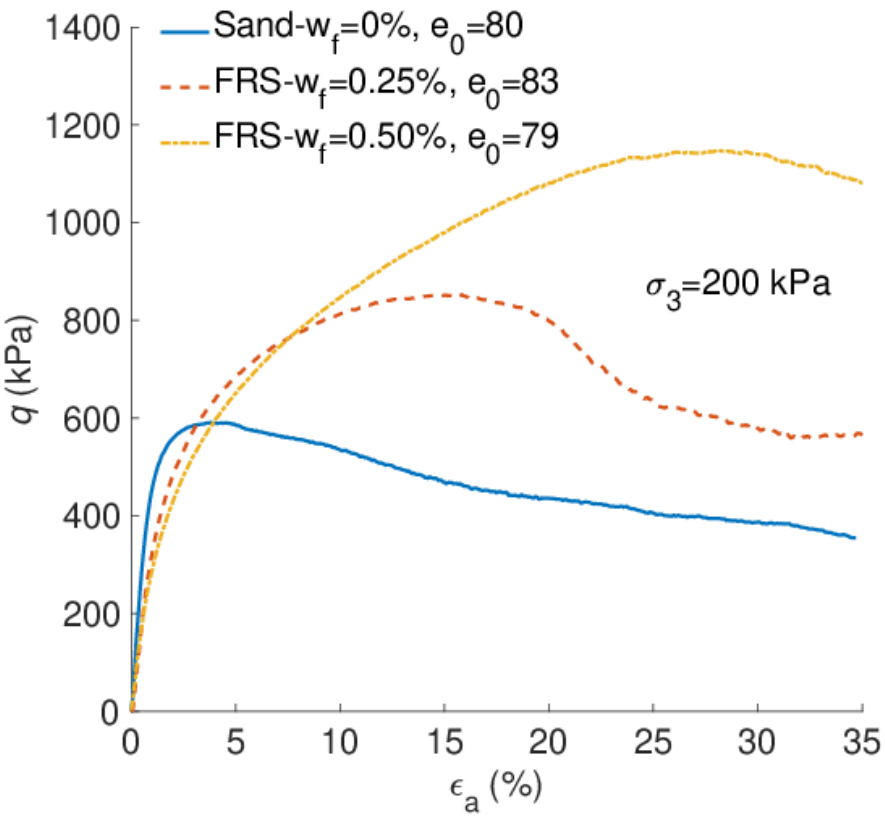

(a)

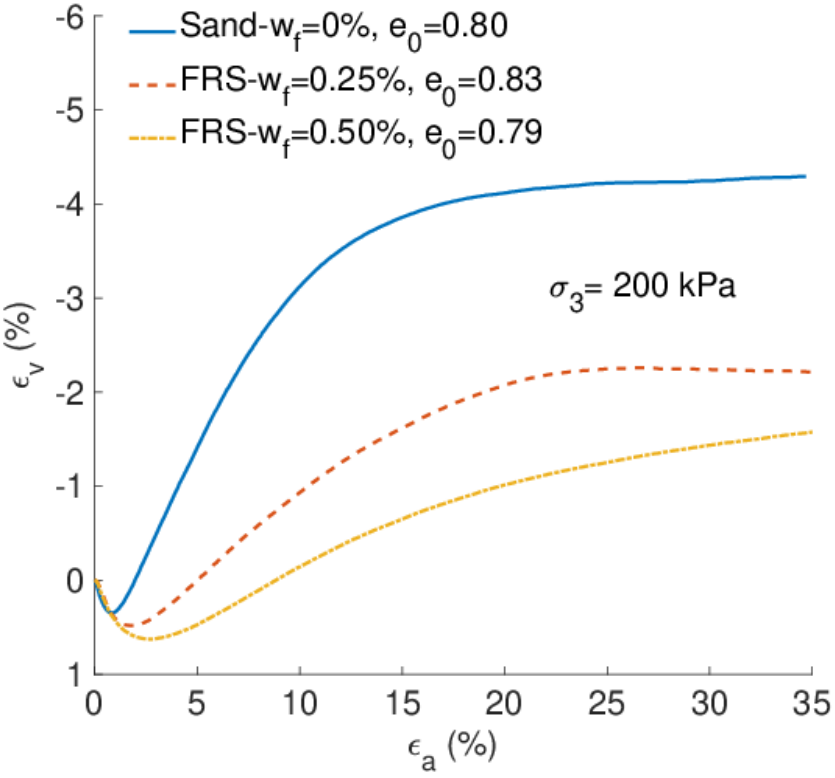

(b)

Fig. 4.8 The response of FRS tested at σ_3=200 kPa using different fibre contents ranging from 0% up to 0.50%

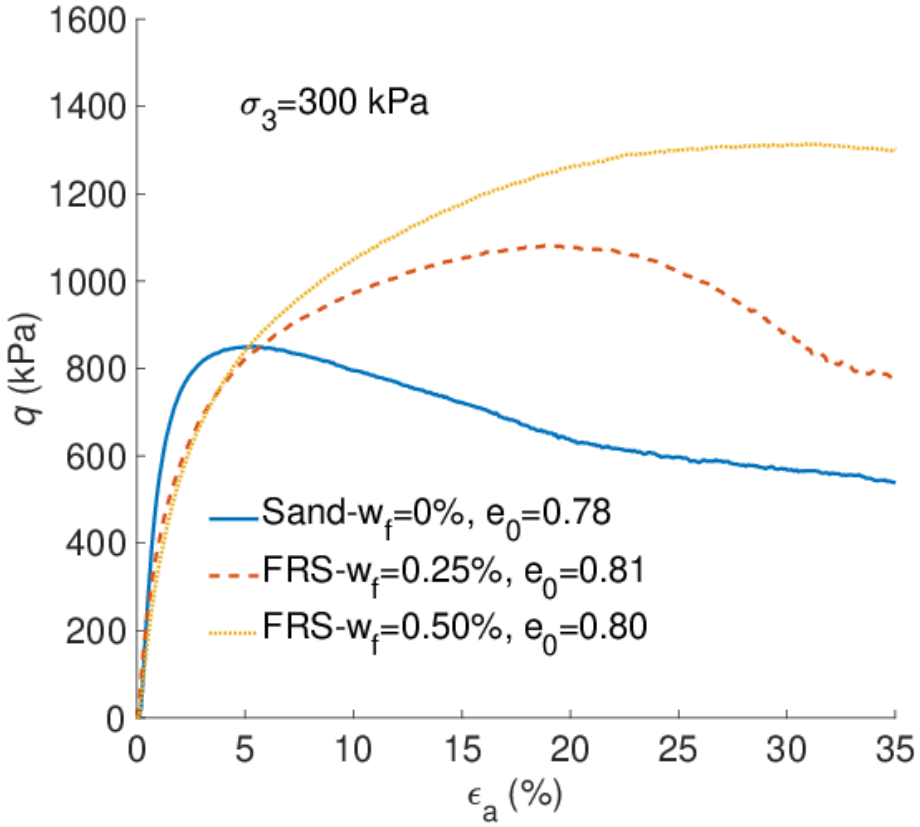

(a)

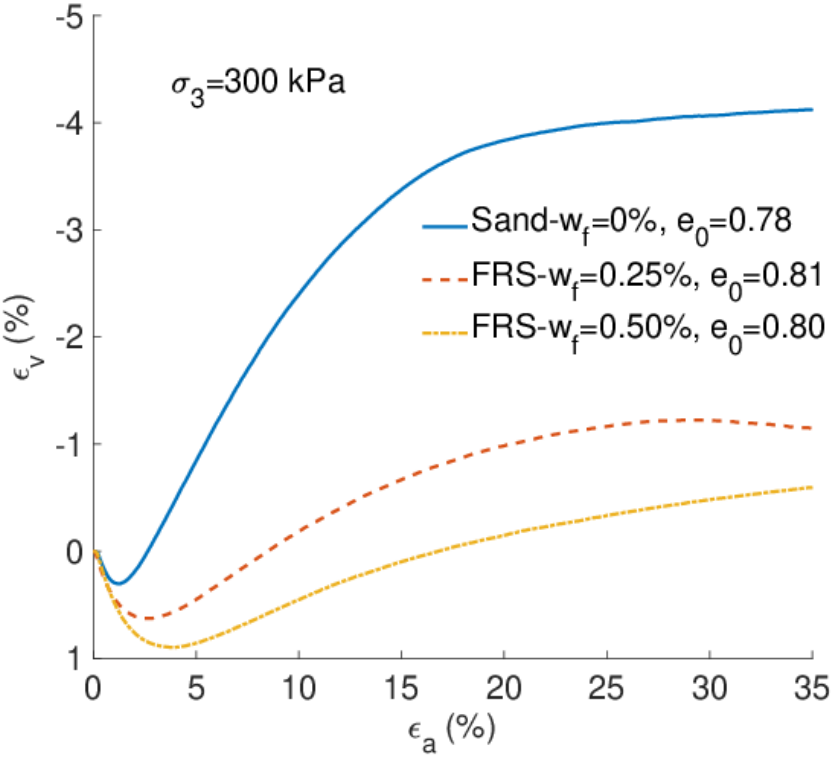

(b)

Fig. 4.9 The response of FRS tested at σ_3=300 kPa using different fibre contents ranging from 0% up to 0.50%

4.3 Shear Strength of FRS and Unreinforced Sand

In addition to the fibre inclusion affecting the initial stiffness, fibres inducing the softening behaviour of composite and limiting post-peak reduction have been studied (Li, 2005; Yetimoglu & Salbas, 2003; Gray & Ohashi, 1983). Generally, the softening behaviour is defined as a drop in the deviator stress after the peak. Bulging or shear band have been observed in the tests of this study. Apparent strain softening can be found in Fig. 4.6(a)-Fig.4.9(a). In these figures, excepting for the FRS samples with 0.25% of fibre content tested at 50kPa of confining pressure, the rests (Fig. 4.7(a)-Fig. 4.9(a)) show apparent softening behaviour at large axial strain (ε_a>20%). Compared with the above FRS, unreinforced samples tested under 100 kPa up to 300 kPa of confining pressure show a smoother softening behaviour. However, in percentage term, the post-peak drop is always greater for unreinforced samples. In contrast, the reinforced ones with 0.50% of fibre content respectively tested under 50, 100 and 300 kPa of confining pressure show an apparent hardening behaviour and the reduction of the peak strength cannot be observed (Fig. 4.6 (a), 4.7(a) & 4.9(a)), which mean higher fibre content causes higher ductility to the soil and thus reducing the occurrence of strain softening of soil. However, the FRS with 0.50% of fibre content tested at 200 kPa of confining stress (Fig. 4.8(a)) respectively show a loss in post-peak shear strength and a strain hardening at large strain. The main reason causing the strain softening is the internal structure of soil governed by fibres and the shear band occurrence. When fibres are randomly distributed in soil, more void spaces are produced between fibres and particles, meaning the sand matrix has changed. Consoli et al. (2009a) stated the specific range of aspect ratio of samples attributed to this strain behaviour. In Consoli's study, strain-softening or hardening behaviour is associated with the fibre length, where with shorter fibre, reinforced soils exhibit more apparent strain softening after peak strength, and the reinforced soils with longer fibres are causing strain hardening (Consoli et al., 2009a). In this study, the length of fibres ranges from 36 mm to 45 mm, indicating the ranges provide a wider aspect ratio. Therefore, the fibres with random

aspect ratios are randomly distributed in the soil, probably resulting in a reduction in the effectiveness of reinforcement. On the other hand, specimens having higher fibre content implies a larger strain is necessary to allow them fully yielding (Diambra, 2010; Li, 2005). However, this is also influenced by the sample preparation methods. More details regarding this will then be introduced in Chapter 6. For the unreinforced specimens, they seem to reach the peak strength at lower axial strain (ε_a<3%). After reaching the peak deviator stress, the trend of post-peak strength is tending to be a slight drop (Fig. 4.6(a)-Fig. 4.9(a)). Table 4.5 outlines the reduction of shear strength of unreinforced specimens, where the biggest loss of shear strength is found in the sample tested under 300 kPa of confining pressure.

Table 4.5 The peak and critical state deviator stress for unreinforced sand

Confining stress σ_3 (kPa)	Peak deviator stress (kPa)	Critical state deviator stress at ε_a=35%	Reduction of deviator stress during shear (kPa)
50	163.65	97.90	65.75 (40.2%)
100	271.61	198.07	73.54 (27.1%)
200	591.38	355.32	236.06 (39.9%)
300	850.86	535.44	315.42 (37.1%)

Furthermore, compared with the pure sand samples, fibre inclusion is found to be effective in reducing the loss of post-peak strength. Fig 4.6(a)-4.9(a) provide an apparent comparison in terms of limiting post-peak strength reduction. According to the test results obtained from Yetimoglu and Salbas (2003), a pronounced reduction in the loss of post-peak shear strength can be found at large strain and with higher fibre content for the reinforced specimens.

The expression of the brittleness index introduced by Consoli et al. (1998) is given below:

$$I_b = \frac{q_f}{q_u} - 1 \tag{4.1}$$

where q_f is the failure or peak deviatoric stress, while q_u is the ultimate deviator stress. Lower brittle index means more ductile response. The comparing results of the brittleness index between unreinforced and reinforced soils have been concluded in Table 4.6. As shown in the tables, due to fibre inclusion, I_b of FRS are apparently lower than unreinforced soil, which means a lower brittleness index caused by fibres inclusion indicates the material is more ductile.

Table 4.6: Brittleness index of unreinforced and FRS

Confining stress σ_3 (kPa)	Brittleness index I_b		
	Unreinforced soil	Fibre-reinforced soil (w_f=0.25%)	Fibre-reinforced soil (w_f=0.50%)
50	0.67	0.17	0.04
100	0.47	0.22	0.02
200	0.66	0.22	0.04
300	0.59	0.33	0.01

4.3.1 Shear Strength of Host Sand and FRS

The angle of internal friction and cohesion are the two essential soil parameters for measuring the shear strength of soils. Sands usually have very little cohesion compared with clays. The friction angle and cohesion of pure sand is shown in Table 4.7 and Table 4.8, respectively. Note that the cohesion and friction angle in these tables are obtained based on the peak deviator stress state. Notice that the values of friction angle and cohesion are probably slightly different under triaxial compression and extension as reported in Diambra (2010), which is due to the intermediate principal stress and anisotropy. As can be seen in these tables, the friction angle is different for the Hostun and Leighton Buzzard sand. This difference could be caused by the particle size/shape and the coefficient of uniformity C_u.

Table 4.7: Major and minor principle effective stress of the soil

Test ID	Soil type	void ratio after consolidation (e_0)	σ_1 (failure)	σ_3
Hos_100_080_MT	Hostun sand	0.789	368	100
Hos_200_080_MT		0.801	790	200
Hos_300_080_MT		0.780	1150	300
LB_100_080_MT	Leighton Buzzard sand	0.801	385	100
LB_200_080_MT		0.793	824	200
LB_300_080_MT		0.786	1265	300

Table 4.8 Peak friction angle and cohesion for Hostun and Leighton Buzzard sand

Soil Type	Soil density	Friction angle (φ), (°)	Cohesion (c), (kPa)	coefficient of uniformity (C_u)
Hostun	loose-medium (e_c=0.80)	36.24	0	1.4
Leighton Buzzard		39.09	0	2.13

The friction angle and cohesion for pure sand have been given above (Table 4.8). When fibres are added, the internal friction angle of the reinforced sample will be different. The friction angle of soil, in general, depends on the confining pressure and void ratio. However, under the limited confining conditions (50kPa-300 kPa in this study), it is mainly dependent on the reinforcing effect of fibres. Due to some of the test results of reinforced soils showing a hardening behaviour at the end of the tests, the stress at 20% of axial strain is defined as the failure stress (Diambra, 2010). The principal stress values used to calculate the internal friction angle of FRS have been listed in Table 4.9.

Table 4.9: Major and minor principle effective stress of tested reinforced sand

Test ID	Fibre content (w_f)	Void ratio after consolidation e_c	σ_1 (atε_a=20%)	σ_3
FRS_025_50	0.25	0.78	369	50
FRS_025_100		0.79	531	100
FRS_025_200		0.83	1050	200
FRS_025_300		0.81	1377	300
FRS_050_50	0.50	0.78	540	50
FRS_050_100		0.79	720	100
FRS_050_200		0.79	1316	200
FRS_050_300		0.80	1616	300

Furthermore, Table 4.10 shows that both the friction angle and cohesion increase with fibre content. Within the fibre content used in this study, there is obvious increase in the peak friction angle as fibre content increases. However, further increase in fibre content (w_f> 0.9%) could induce an opposite effect, because the fibres will reduce the contact areas between sand particles (Wang et al., 2016; Diambra, 2010).

Table 4.10: Effect of fibre content on the peak friction angle and cohesion of FRS

Fibre content (%)	0	0.25	0.50
Friction angle (°)	36.24	41.64	45.32
Cohesion (kPa)	0	38.33	73.14

It can thus be concluded that fibre inclusion increases the peak friction angle and cohesion of sand. However, the effect of fibre inclusion on cohesion is more significant. It is important to notice that the fibre orientation is a key factor that effects the shear strength of the FRS (Michalowski & Cermak, 2002; Ibraim et al., 2012). Generally, fibres oriented in the horizontal direction contribute more to the soil strength than those

with vertical orientation. Fig. 4.10 and Fig. 4.11 show the comparing results of the FRS specimen containing different fibre content under confining pressure from 50 kPa to 300 kPa. It is indicated that addition of fibre can significantly increase the shear strength, under the same testing condition (e.g., void ratio and confining stress). In particular, there is no softening behaviour observed in the FRS specimen with w_f=0.50%. Furthermore, it can be seen from Table 4.10 that both the peak friction angle and cohesion increase with fibre content.

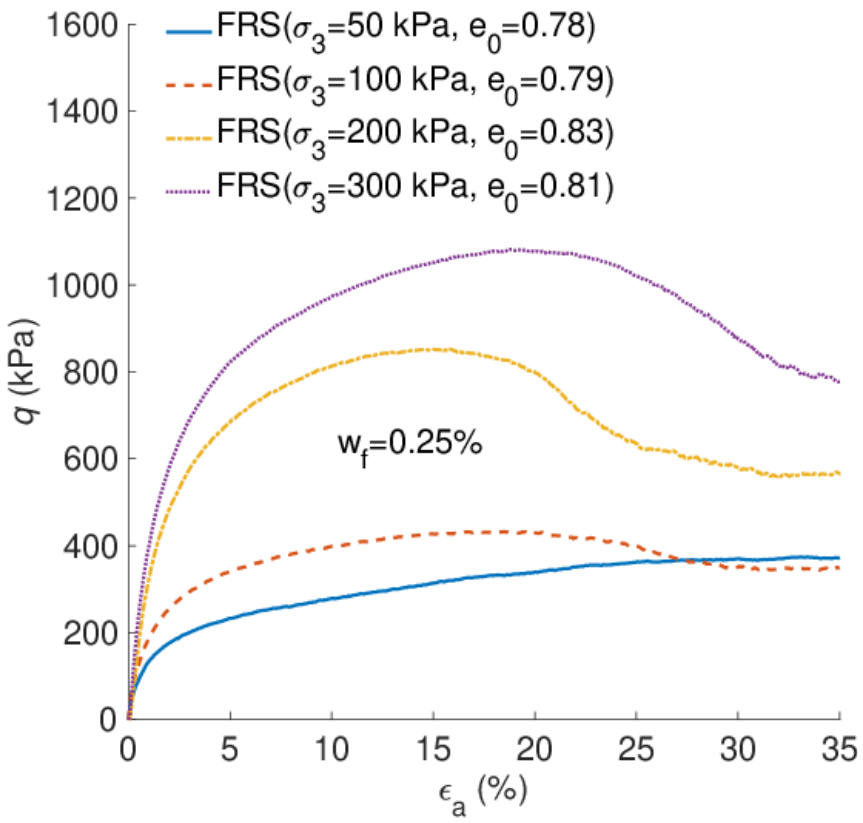

(a)

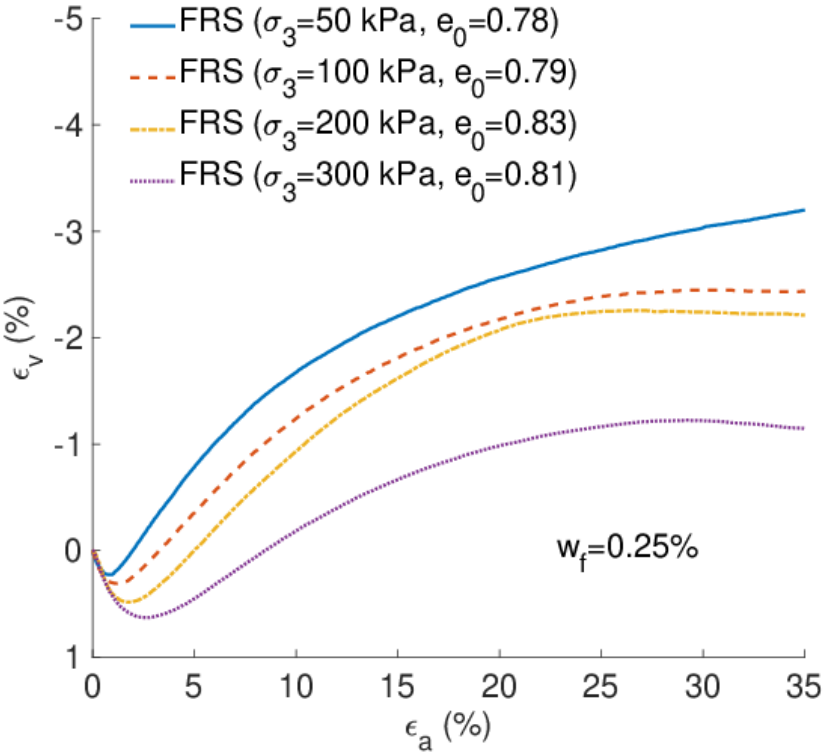

(b)

Fig. 4.10 The response of FRS with w_f=0.25% under confining pressure from 50 kPa to 300 kPa

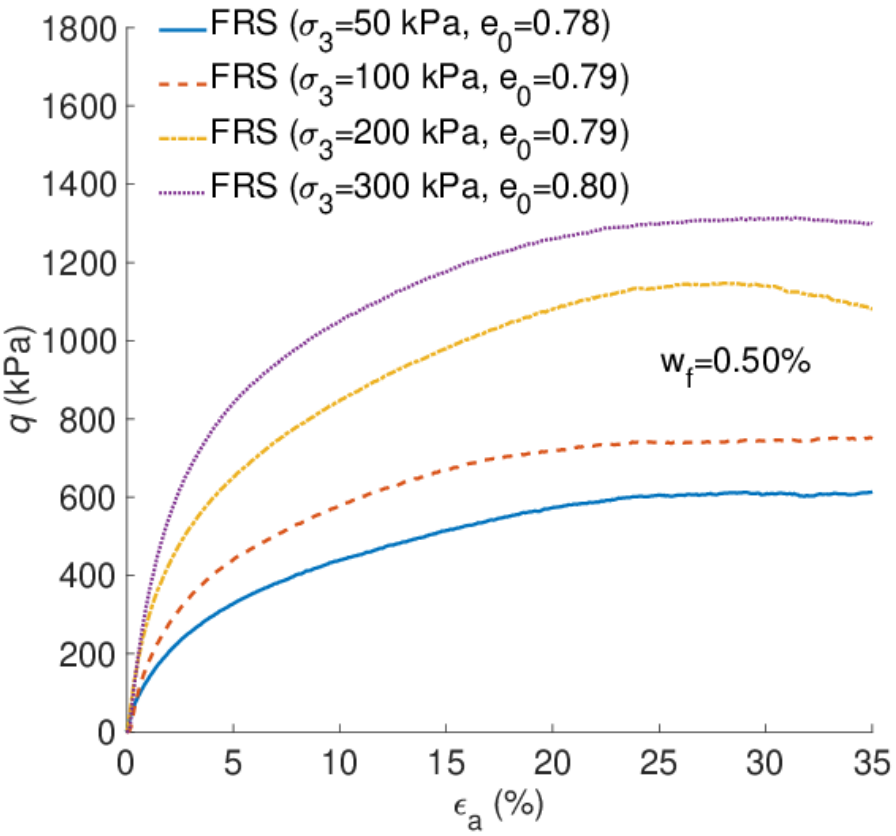

(a)

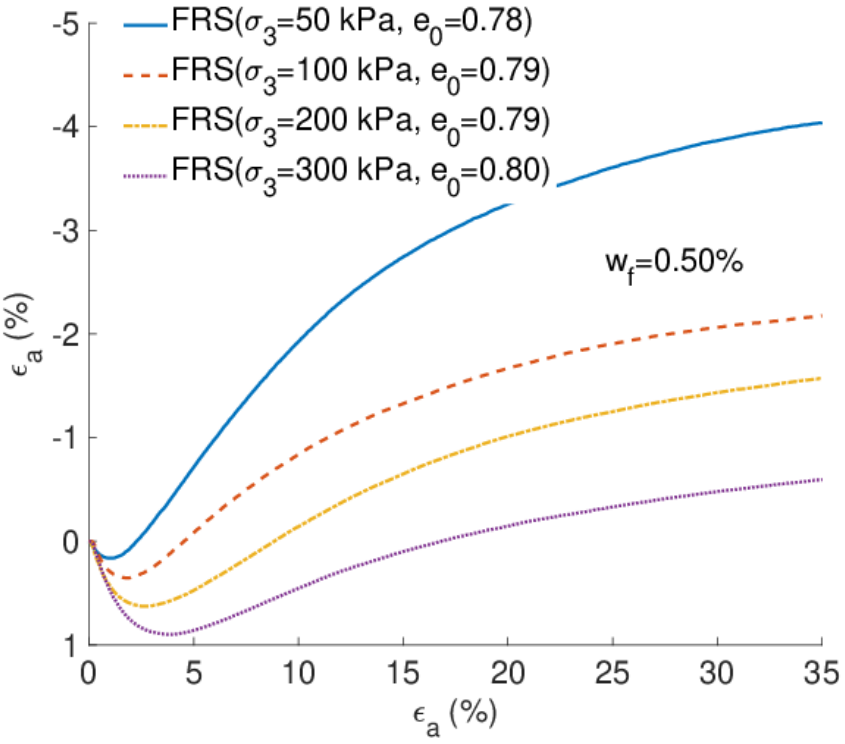

(b)

Fig. 4.11 The response of FRS with w_f=0.50% under confining pressure from 50 kPa to 300 kPa

Fig. 4.12 shows that the increase in failure deviator stress is proportional to the fibre content. This is more obvious when the confining pressure is below 200 kPa. Notice that the increase in shear strength is also dependent on the sand density. When the sand density is higher, there is more reinforcement to the soil strength at the same confining pressure and fibre content, which has been reported in the literature. Fig. 4.13 shows the comparison of strength envelopes between host and reinforced sand, where the failure envelopes move upwards as the fibre content increases.

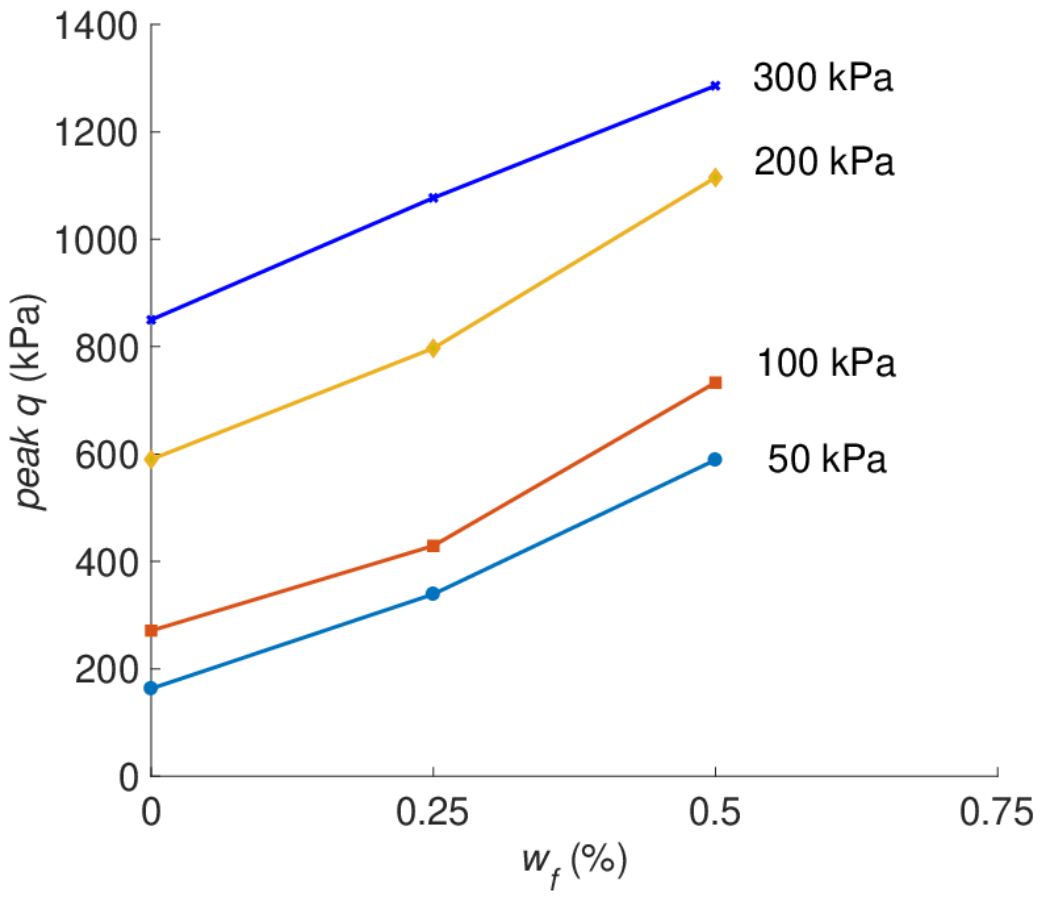

Fig. 4.12 The effectiveness of fibre inclusion on the peak deviatoric stress under different confining stresses from 50 up to 300 kPa

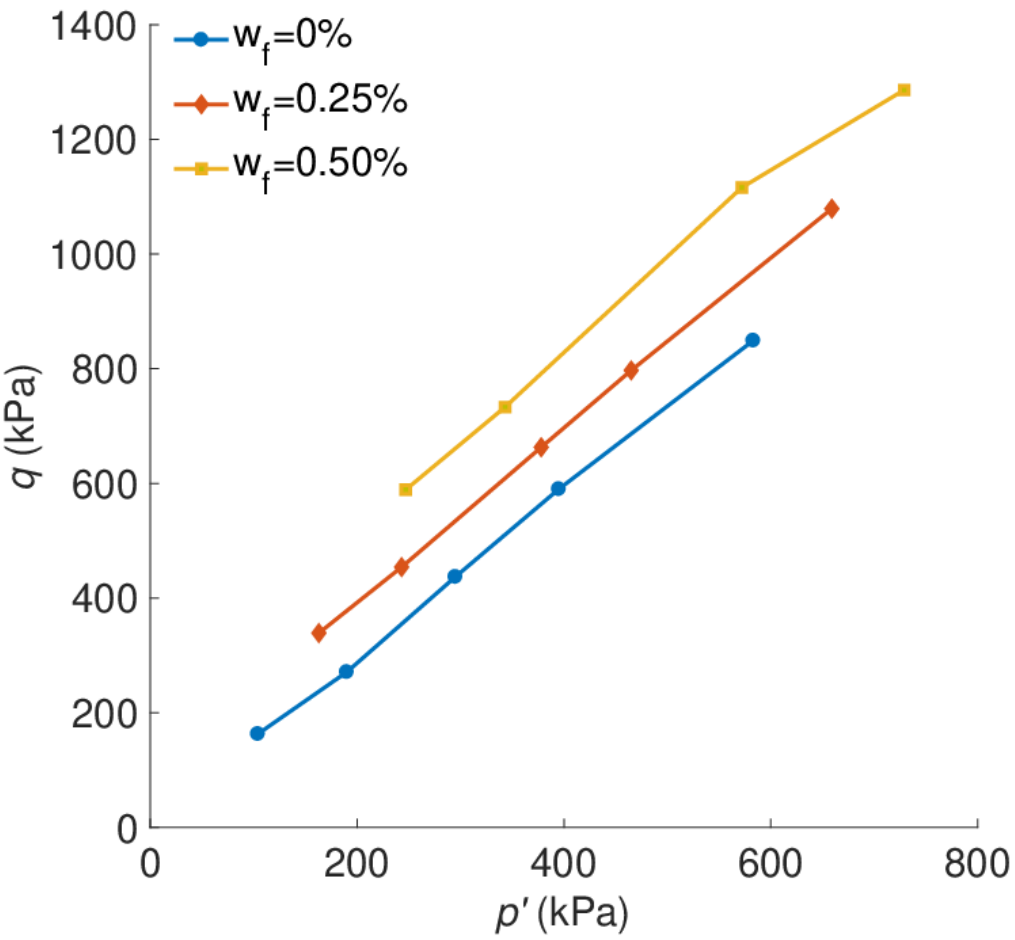

Fig. 4.13 The shear strength envelopes of axial strain of reinforced and unreinforced sand

4.4 Effect of Fibre Inclusion on Sand Dilatancy

Fig. 4.6(b) to Fig. 4.11(b) show the dilatancy of FRS with different fibre content (w_f=0%-0.5%). In general, the FRS with higher fibre content (w_f=0.5%) shows less dilative response. But the dilatancy response of the reinforced sample with σ_3=50 kPa shows a different trend (Fig. 4.6(b)), where the reinforced sample with w_f=0.25% shows more dilation than the reinforced sample with w_f=0.50%. This could be caused by test error. For instance, Wang (1995) pointed out the use of lubricated end platens might cause an error on void ratio correction. Besides, Omar and Sadrekarimi (2014) found that the volume change measurement is affected by the membrane thickness. More contractive response can be measured when a thinner membrane is used. Rowe and

Barden (1964) found that a thicker grease layer on the platens could influence specimen movement due to its viscous nature. When the sample is sheared to larger axial strain, more grease is extruded (Duncan and Dunlop, 1968). As a result, the drainage hole may be obstructed by the extrusion out of grease within the platens, which affects the volume change measurement.

Most existing studies have shown that the fibre inclusion makes the soil more contractive. This is due to that the fibres add extra confinement to the sand skeleton. Under otherwise identical conditions, the sand skeleton shows more contractive response when the confining pressure is higher. However, Diambra (2010) has shown that the FRS shows more dilative response than the host sand with the same confining pressure and void ratio. This is probably caused by the sample preparation method. In preparing the FRS with similar void ratio to that of pure sand, some of the sand is replaced by fibres in this study. In Diambra (2010), the same sand is used in the sample preparation instead. These two methods cause little difference in the void ratio, because the fibre content is very low. But more compaction energy would be required to prepare the FRS sample using the method reported in Diambra (2010), which eventually makes the FRS more dilative. Indeed, Diambra (2010) has used the stolen void ratio concept to explain such soil response.

4.5 Critical State

The steady state and the critical state have been employed in most studies to describe the behaviour of soils (Roscoe et al., 1958, Li, 2005; Diambra, 2010; Consoli et al., 2005). In fact, the two concepts are almost the same and the term critical state is used more frequently.

As mentioned above, the state parameter (ψ) is defined as the difference between the void ratio and the void ratio at critical state at the same value of mean effective stress:

$$\psi = e - e_c \tag{4.2}$$

where e and e_c are the current void ratio and the void ratio at critical state, respectively. Fig. 4.14 shows the CSL for Hostun sand and Leighton Buzzard sand in the $e - p'$ plot, where the CSL of Leighton Buzzard sand is lower than that of the Hostun sand.

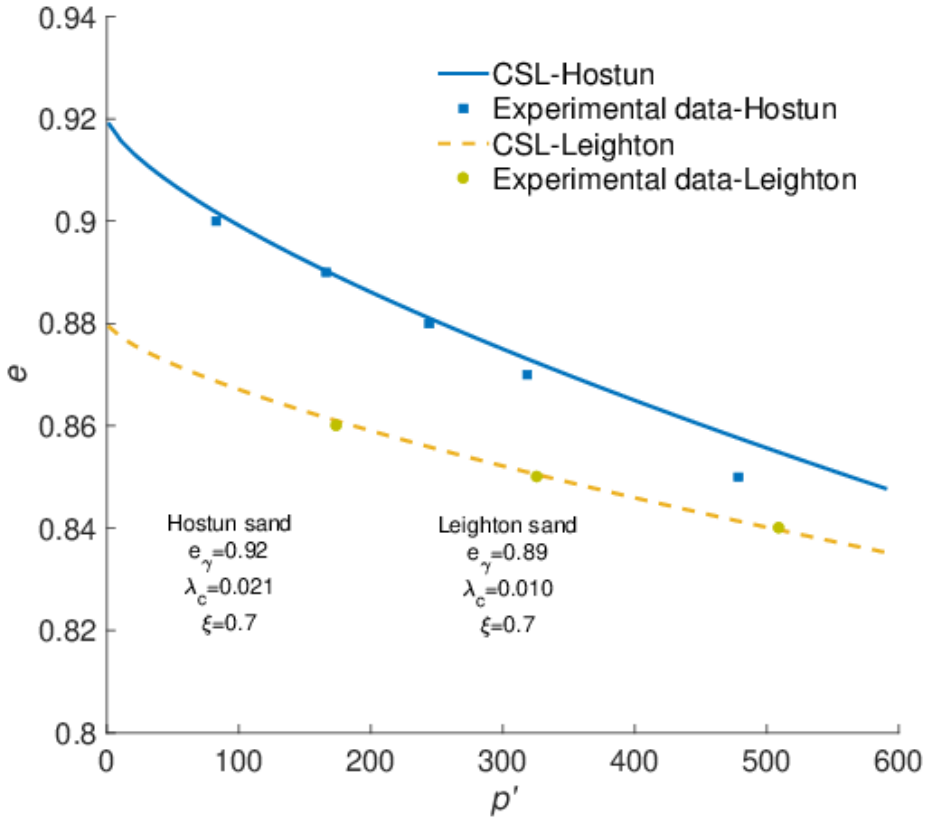

Fig. 4.14 Critical state line for Hostun and Leighton sand on the *e-p'* plane

It is found that both the shear strength and dilatancy of sand is affected by fibre inclusion, which means that the CSL of fibre-reinforced sand is different from that of host sand. Fig. 4.15 shows the difference of CSL between host and fibre-reinforced sand. It is obvious that the CSL of FRS lies in a lower position than that for host sand. This is due to that fibre inclusion makes the soil response more contractive under otherwise identical conditions. Fig. 4.16 shows the CSL in the $p' - q$ plot for both sand and fibre-reinforced sand. There is slight increase in the critical state stress ratio as the fibre content increases. Besides, the critical friction angle in the plot show a significant increase because of fibre inclusion.

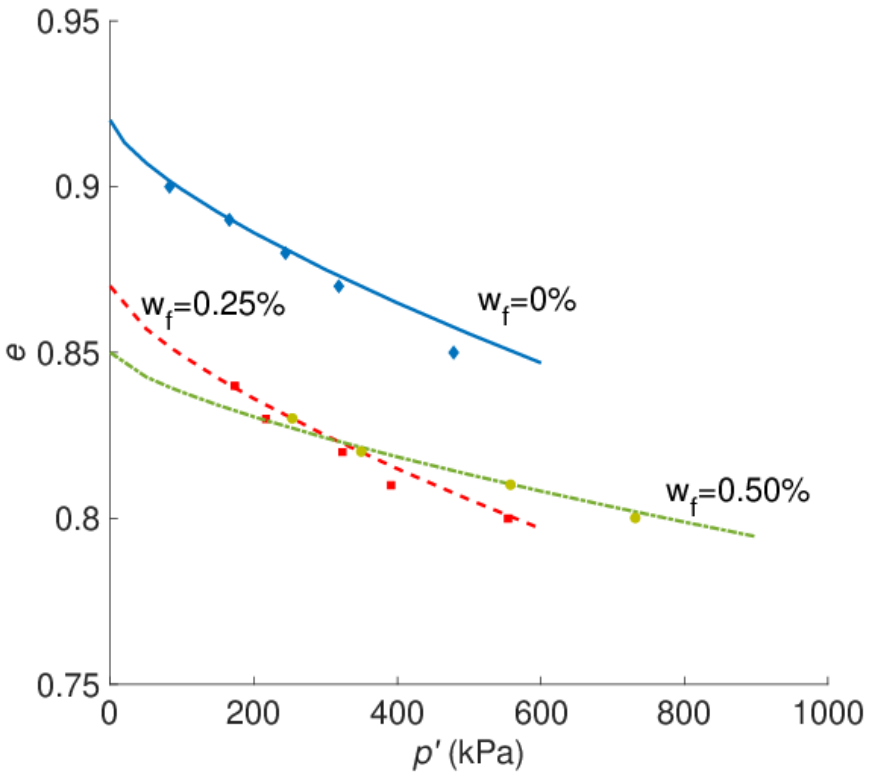

Fig 4.15 Effect of fibre inclusion on the deviatoric stress under different confining stresses from 50 up to 300 kPa.

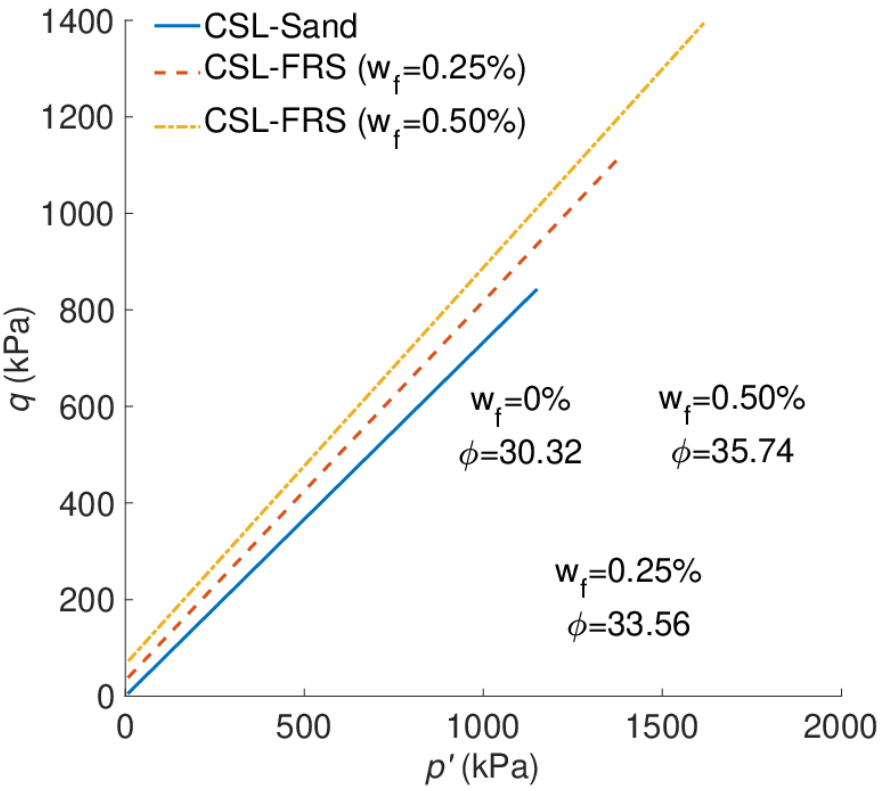

Fig. 4.16 Effect of fibre content on CSL

4.6 Summary

Stress-strain relationship of host sand and FRS have been described, where both the soil properties (i.e., mean diameter) and fibre characteristics (i.e., fibre content) affect the behaviour of soil. Repeatability of the test has been confirmed to improve the reliability of the test. It is found that volume change is an important characteristic for sand. It can be influenced by various factors such as sample preparation method, mean effective stress and density.

Soil type has effect on the stress-strain relationship because of different mean diameter, as higher mean diameter leads to higher shear strength. A clear comparison between Leighton-Buzzard (LB) samples and Hostun sand samples has been reported. The LB sand show higher shear strength, which has a higher mean diameter and coefficient of uniformity. The effect of confining pressure on the stress-strain relationship has been studied. The shear strength increases with confining pressure when other loading conditions are the same. There is less volume expansion in pure sand as the confining pressure increase.

The effect of void ratio on pure sand behaviour has been studied. Under the same confining pressure, the peak shear strength increases as the soil become denser. Meanwhile, dense sand shows more dilation under the same confining pressure. The effect of density and mean effective stress on pure sand behaviour can be described by the Li and Dafalias (2000) model with state-dependent dilatancy relationship and hardening law.

A series of drained triaxial compression tests have been done on FRS. The testing results show that the reinforced soil with greater than 0.3% of fibre content show strain-hardening response. FRS with higher fibre content has higher peak shear strength.

It is found that the initial stiffness of FRS is different from that of host sand, which is not consistent with some studies. Besides, compared with unreinforced soil, fibres can effectively increase the friction angle and cohesion of FRS. In addition, denser FRS

indicates more reinforcement generated to the soil.

The critical state line of FRS is different from that of pure-sand sample, as fibre inclusion causes more volume contraction in FRS.

Chapter 5: Modelling

5.1 Introduction to Constitutive Model

This model is developed based on the sand model of Li and Dafalias (2000) and the failure criterion of Gao and Zhao (2013). Both of them have been introduced in Chapter 2. The main features of the model will be discussed in Section 5.2. At present, the most accepted model for FRS is the one proposed by Diambra (2010). The main difference between the new model and Diambra (2010) is that it does not require the measurement of the stress-strain relationship of individual fibres. Instead, it uses the concept of effective skeleton stress and void ratio for modelling the FRS behaviour.

5.2 Effective Skeleton Stress and Void Ratio for Constitutive Modelling of Fibre-Reinforced Sand

The primary mechanism of the proposed constitutive modelling of fibre-reinforced sand is due to the fibre addition, where fibres would generate the stresses (noted as p^s and q^s) on the sand skeleton, thus strengthening the internal structure of sand. Meanwhile, fibres would change the void ratio space of the sand skeleton (noted as e^s). However, as shown in Fig 5.1, the effective stress ($p^s$and q^s) and effective void ratio $\mathrm{e^s}$ caused by the fibres are 'virtual', which are only used to reflect the effect of fibre on the sand skeleton and in modelling the dilatancy relation, plastic hardening and elastic moduli of FRS. In fact, the strain of an FRS element is only dependent on the deformation of the sand skeleton. Also, this method focuses on the global stress-strain relation of fibre-reinforced sand (FRS). However, it does not directly consider the interaction of sand and fibres at the micro-scale compared with the constitutive model introduced by Diambra (2013), highlighting the fibre orientation distribution in FRS cross-anisotropic due to compaction. The following study focuses on the behaviour of

FRS in triaxial compression wherein the major principal stress direction is perpendicular to the preferred fibre orientation plane.

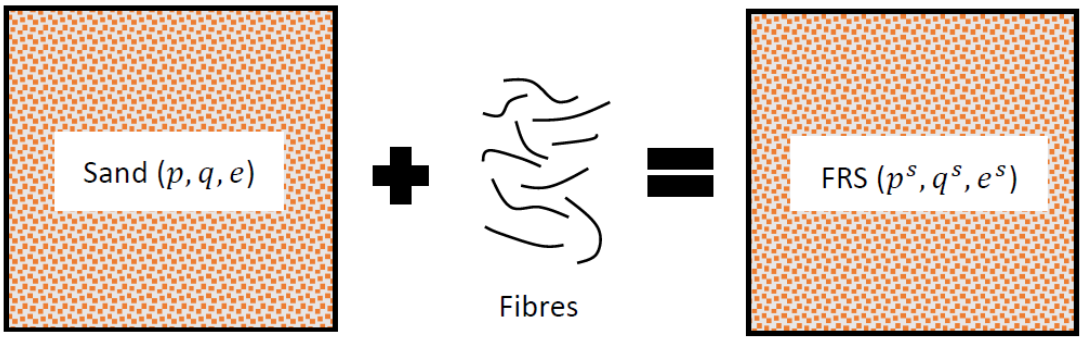

Fig 5.1 Illustration of variables used for constitutive modelling (Gao et al., 2020)

5.2.1 Effective Skeleton Stress p^s and q^s and Void ratio e_s

The expressions of p^s and q^s are defined based on the failure characteristics of FRS. As emphasised above, the purpose of this definition is modelling the overall stress-strain relation of FRS, rather than giving an accurate description in terms of the stress in fibres and its effect on the stress state of the sand skeleton. The failure of FRS cannot be observed in some cases, such as the effect of higher confining pressure or fibre content (Diambra et al., 2010; Michalowski, 1996). Therefore, the parameters for the expression of p^s have to be defined using an alternative method.

The failure at critical state of FRS in triaxial compression, which is shown by Gao and Zhao (2013) can be expressed as

$$q = M_c(p + p_c) \tag{5.1}$$

with

$$p_c = cp_a[1 - \exp(-\kappa p/p_a)] \tag{5.2}$$

Where M_c is the stress ratio (q/p) at critical state for sand, p_a is the atmospheric pressure (p_a=101 kPa); c and κ are two model parameters. Gao and Zhao (2013) stated c is a sensitive variable, which is varied with the fibre content and fibre aspect

ratio, while κ is insensitive to such factor. The general expression for c can be derived using a micromechanical approach. Many studies have reported further observation on c accounting for various factors such as fibre properties and sample preparation method (Michalowski & Cermak, 2002; Zonberg, 2002; Diambra et al., 2013). Therefore, the value of c would be determined by fibre content, even though other testing conditions are the same (e.g., sand type, fibre properties, void ratio and confining pressure).

Eqs. 5.1 and 5.2 indicate the mean effective stress of sand skeleton is $p + p_c$, which is greater than p, resulting in the shear strength of FRS higher than that of host sand. Hence, the following p^s and q^s can be used to describe the failure of FRS:

$$p^s = p + p_c \tag{5.3}$$

$$q^s = q \tag{5.4}$$

which renders $q^s = M_c p$ at failure. However, the critical state of sand has been studied, implying that effective stress does not always increase when the sand reaches the critical state. Meanwhile, there is no FRS sample deformation when added fibres are 'stretched' or critical, which means they no longer reinforce the sand skeleton. Experimental evidence shows that the reinforcement effect increases with the strain of FRS and finally reaches the maximum at the failure state when the fibres yield or pull out (Zornberg, 2002; Consoli et al., 2007; Diambra et al., 2013; Gao& Zhao, 2013). Based on those observations, the following expression for p^s can be used to account for the effect of strain level on fibre reinforcement, with q^s being expressed as Eq. 5.4:

$$p^s = p + p_f \tag{5.5}$$

where p_f is a strain-level dependent variable. p_f is varied from 0 at $\varepsilon_q = 0$ to p_c at sufficiently large ε_q, where ε_q $[= 2(\varepsilon_a - \varepsilon_r)/3]$ is the deviatoric strain, with ε_a and ε_r being the axial and radial strain, respectively. During the deformation of FRS specimen, the mean effective stress generated by fibres is gradually increased with the deviatoric strain ε_q, having $p_f = p_f + dp_f$. Evolution of p_f with ε_q is modelled using the following expression:

$$dp_f = \mu \frac{p_c - p_f}{1+e} \sqrt{\frac{p}{p_a}} d\varepsilon_q \quad (5.6)$$

where μ is a model parameter for FRS and e is void ratio. It is pointed out the term $p_c - p_f$ in Eq. 5.6 restrains the increment of p_f, which it would be a constant at large strain. On the other hand, the terms $1 + e$ and $\sqrt{p/p_a}$ in Eq. 5.6 enable the evolution of p_f with ε_q faster when the soil is denser, and p is higher (Silva Dos Santos et al., 2010; Diambra et al., 2010). As the fibres are regarded as part of the soil, the calculation of void ratio e can be expressed as:

$$e = v_v/(v_f + v_s) \quad (5.7)$$

where v_v, v_f and v_s are the volume of void, fibres and sand particles, respectively (Michalowski, 1996; Diambra et al., 2010). It should be considered when FRS specimen is subjected to shearing, p_f also changes with the volumetric strain ε_v, as some of the fibres are still subjected to tension with $d\varepsilon_v < 0$ (the fibres in extension provide reinforcement to the soil), while $d\varepsilon_q = 0$. Nevertheless, this is neglected for the sake of simplicity.

Although fibres 'occupy' the global volume of soil, which result in a negligible influence on the global void ratio e (Diambra et al., 2010), they affect the internal structure of the sand skeleton (Ibraim et al., 2012; Diambra et al., 2013; Diambra & Ibraim, 2015; Muir Wood et al., 2016). Consequently, the effective void ratio (e^s) of the sand skeleton is different from the global void ratio e. This concept has been used by Diambra et al. (2013) and Muir Wood et al. (2016) to describe such an effect. Based on their work, the relationship between the effective void ratio e^s and global void ratio e is assumed as below:

$$e^s = \left(1 + x\rho_f\right)e \quad (5.8)$$

Where e is the void ratio, x is a material constant, $\rho_f = {}^{v_f}/_{v_s}$ with v_f and v_s being the volume of fibres and dry sand, respectively. It is clear to observe from Eq. 5.8, a positive x can cause $e^s > e$, while a negative x gives $e^s < e$. It is found the value of x depends on sample preparation methods. Negative x can be obtained when FRS sample is prepared by adding fibres to a fixed volume of sand (e.g., Diambra

et al., 2010; Ibraim et al., 2012; Muir Wood et al., 2016). In contrast, positive x is observed when the FRS samples are prepared by keeping the overall solid volume constant (fibres and sand), such that fibres substitute sand in the FRS case (Michalowski & Zhao, 1996; Silva Dos Santos et al., 2010). More details regarding the material constant x will be discussed in the subsequent section in this chapter. In addition, ρ_f can be expressed in terms of the fibre weight content w_f (ratio of fibre and dry sand weight), which is more frequently used in the existing literature.

$$\rho_f = \frac{v_f}{v_s} = \frac{w_f G_s v_s / G_f}{v_s} = \frac{w_f G_s}{G_f} \tag{5.9}$$

where G_s and G_f denote the specific gravities of sand and fibres, respectively.

Overall, there are four model parameters c, κ, μ and x being employed to describe the effect of fibres on the sand skeleton. The effect of the model parameters on modelling the dilatancy of FRS will be discussed in the following section.

5.3 A simple constitutive model for fibre-reinforced soil

A simple constitutive model for FRS will be presented using the effective skeleton stress and void ratio, which the basic principles have been introduced in section 5.2. The host sand model is based on the work by Li and Dafalias (2000). The elasto-plastic based FRS model consists of four major elements, elastic moduli, yield function, flow rule and plastic hardening law. The yield function of the model is expressed in terms of p and q. The rest are obtained based on those for host sand by replacing the quantities associated with p, q and e with those associated with p^s, q^s and e^s, respectively.

5.3.1 Yield function and plastic flow rule

The yield function of this model is (Li & Dafalias, 2000)

$$f = q/p - H = 0 \tag{5.10}$$

where H is the hardening parameter whose evolution law will be given in the

subsequent section. The plastic flow rule can be expressed as:

$$d\varepsilon_q^p = \langle L \rangle \text{ and } d\varepsilon_v^p = \langle L \rangle D \tag{5.11}$$

where $d\varepsilon_q^p$ and $d\varepsilon_v^p$ are the plastic deviatoric and plastic volumetric strain increment, respectively. L is the loading index; $\langle \quad \rangle$ are the Macauley brackets such as $\langle L \rangle = L$ for $L > 0$ and $\langle L \rangle = 0$ for $L < 0$; D is the dilatancy relation expressed as

$$D = \frac{d\varepsilon_v^p}{d\varepsilon_q^p} \tag{5.12}$$

5.3.2 Dilatancy relation and hardening law

The dilatancy relation for FRS can be expressed as (Li & Dafalias, 2000)

$$D = d\left(M_c e^{m\psi^s} - \eta^s\right) \tag{5.13}$$

where d and m are two model parameters for pure sand; $\eta^s (= q^s/p^s)$ is the effective skeleton stress ratio; ψ^s $(= e^s - e_c^s)$ is the state parameter for FRS (Been & Jefferies, 1985), with e_c^s being the critical state void ratio corresponding to the current p^s. The critical state line in the $e^s - p^s$ plane has been studied by Li and Wang (1998)

$$e_c^s = e_\Gamma - \lambda_c (p^s/p_a)^\xi \tag{5.14}$$

where e_Γ, λ_c and ξ are three material constants. Similarly, for pure sand, the state parameter is $\psi = e - e_c$, where $e_c = e_\Gamma - \lambda_c (p/p_a)^\xi$.

The following hardening law (evolution of H) for FRS is given:

$$dH = \langle L \rangle r_H = \langle L \rangle \frac{G(1-\zeta e^s)}{p^s \eta^s}\left(M_c e^{-n\psi^s} - \eta^s\right) \tag{5.15}$$

where ζ and n are two model parameters for host sand; G is the elastic shear modulus and r_H is plastic modulus. The features of Eqs. 5.12 and 5.14 for pure sand have been extensively discussed in the existing literature (Li & Dafalias, 2000; Gao & Zhao, 2014), where it is suitable on modelling the critical state line of sand in the $e - p$ plane with a wide range of stress level, also, it can overcome some drawbacks in term of relationship between e_c and e_Γ. More discussion regarding the use of Eq.

5.8 for FRS will be carried out toward the end of this section. As the aim of this chapter is mainly focusing on introducing the constitutive model for FRS, therefore, the features of other equations will not be elaborated here. An extensive discussion regarding how Eqs. 5.13 and 5.15 describing the dilatancy and plastic hardening of FRS will be introduced toward the end of this section.

5.3.3 Elastic stress-strain relationship

The following empirical pressure-sensitive elastic moduli are employed for this model (Richard et al., 1970; Li & Dafalias, 2000; Gao et al., 2014):

$$G = G_0 \frac{(2.97-e^s)^2}{1+e^s}\sqrt{p^s p_a} \text{ and } K = G\frac{2(1+\nu)}{3(1-2\nu)} \quad (5.16)$$

where K is the elastic bulk modulus: G_0 is a material constant and ν is the Poisson's ratio, which is considered as a material constant independent of pressure, density and fibre inclusion. In conjunction with Eq. 5.16, the following hypoelastic stress-strain relationship is assumed for calculating the incrementally reversible deviatoric and volumetric strain increments $d\varepsilon_q^e$ and $d\varepsilon_v^e$:

$$d\varepsilon_q^e = \frac{dq}{3G} \text{ and } d\varepsilon_v^e = \frac{dp^s}{K} \quad (5.17)$$

According to Senetakis and Li (2017), Eq.5.17 probably fails to give accurate prediction for the elastic stiffness of FRS observed in laboratory tests. The present model is focusing on the soil response at a relatively large strain level, where the plastic strain is much larger than the elastic.

It is observed the model formulations in Eqs. 5.13-5.17 can be recovered to those for pure sand where there is no fibre inclusion with $p^s = p$, $q^s = q$ and $e^s = e$.

5.3.4 The constitutive equation

Based on the condition of consistency for the yield function (Eq. 5.10), flow rule (Eq. 5.11) and the elastic stress-strain relationship (Eq. 5.17), one can get the expression

for L as below:

$$L = \frac{3Gd\varepsilon_q - K\eta d\varepsilon_v}{p^s r_H + 3G - K\eta D} \tag{5.18}$$

where K and G are the elastic bulk modulus and shear modulus for sand, respectively, D is dilatancy, η is the stress ratio; The complete constitutive equation of this model is (Li & Dafalias, 2000):

$$\begin{Bmatrix} dq \\ dp \end{Bmatrix} = \left\{ \begin{pmatrix} 3G & 0 \\ 0 & K \end{pmatrix} - \frac{h(L)}{p^s r_H + 3G - K\eta^s D} \begin{pmatrix} 9G^2 & -3KG\eta \\ 3KGD & -K^2\eta D \end{pmatrix} \right\} \begin{Bmatrix} d\varepsilon_q \\ d\varepsilon_v \end{Bmatrix} \tag{5.19}$$

where $h(L)$ is the Heaviside function with $h(L) = 1$ for $L > 0$ and $h(L) = 0$ otherwise.

5.3.4 Effect of fibre inclusion on sand dilatancy

Diambra *et al.* (2013) and Wood et al. (2016) had carried out comprehensive experimental and theoretical investigations on the dilatancy of FRS. The result shows fibres occupy the void space of the sand skeleton. Namely, the void ratio of the sand skeleton is smaller than the global void ratio e. Consequently, under a similar void ratio and other loading condition, FRS samples exhibit more dilatancy response than a pure sand sample. However, some test results show the opposite trend (e.g., Michalowski, 1996; Michalowski & Zhao, 1996; Ahmad et al., 2010). Compared with those observations, the proposed new model is capable of showing both more dilative and contractive response for FRS, being described based on Fig. 5.2. In this figure, it can be seen that the dilatancy of FRS is dependent on x and the void ratio e. It is assumed the sand and FRS sample have the same e and the same stress state (p and q). If $x \geq 0$, it can get $e^s > e$, meanwhile, $\psi^s > \psi$ (as $p^s > p$) and $\eta^s < \eta$ are obtained (e.g., the dot with e^{s1} in Fig. 5.2). Besides, D_{frs} and D are used to describe the dilatancy of FRS and pure sand, respectively. $D_{frs} > D$ can be given based on dilatancy relation, meaning it will show more contractive for FRS. In contrast, when $x < 0$, the results show $e^s < e$, but the difference between ψ^s and ψ will be depending on the value of x and $p^s - p$. For example, as $\eta^s > \eta$ has confirmed,

with $\eta = {}^{q}/_{p}$, $D_{frs} > D$ can be true if x is sufficiently large (e.g. the dot with e^{s2} in Fig.5.2).

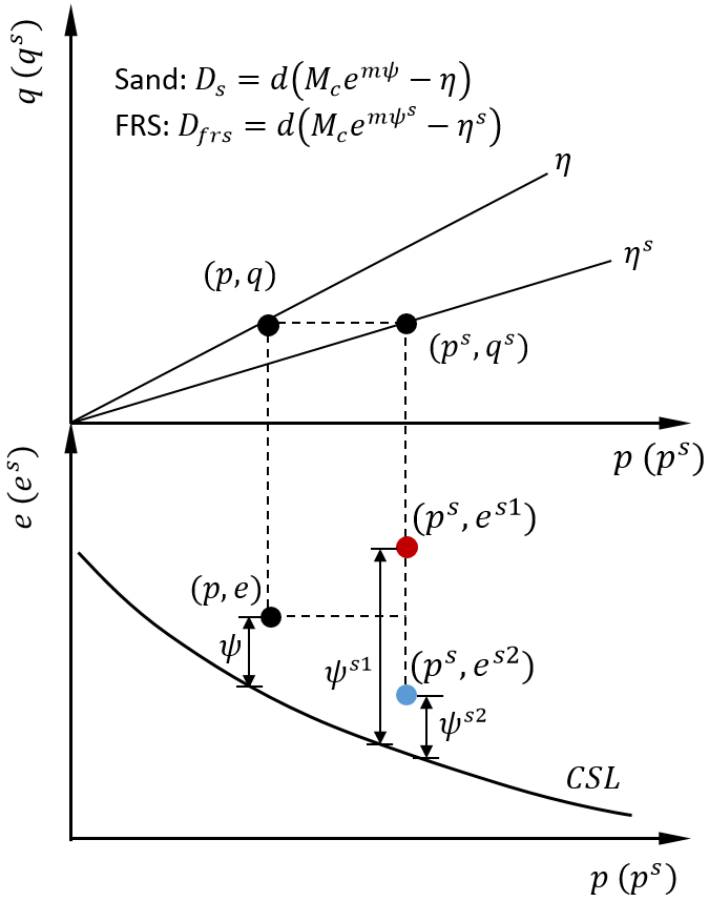

Fig. 5.2 Effect of x on modelling the dilatancy of FRS

The following figure is using Hostun RF(S28) sand to validate the assumption. Fig. 5.3a shows the effect of x on the stress-strain relationship of FRS in drained triaxial compression.

Fig. 5.3b shows the effect of x on stress against strain and volumetric strain against axial strain. It can be seen different x value can induce different performance of FRS. For example, the model gives a more contractive response when $x > 0$. In contrast, negative x implies FRS sample has a more dilative response because of the effect of ρ_f. However, a more dilative response of FRS is only observed at a sufficiently large negative x value (e.g., when $x = -5$).

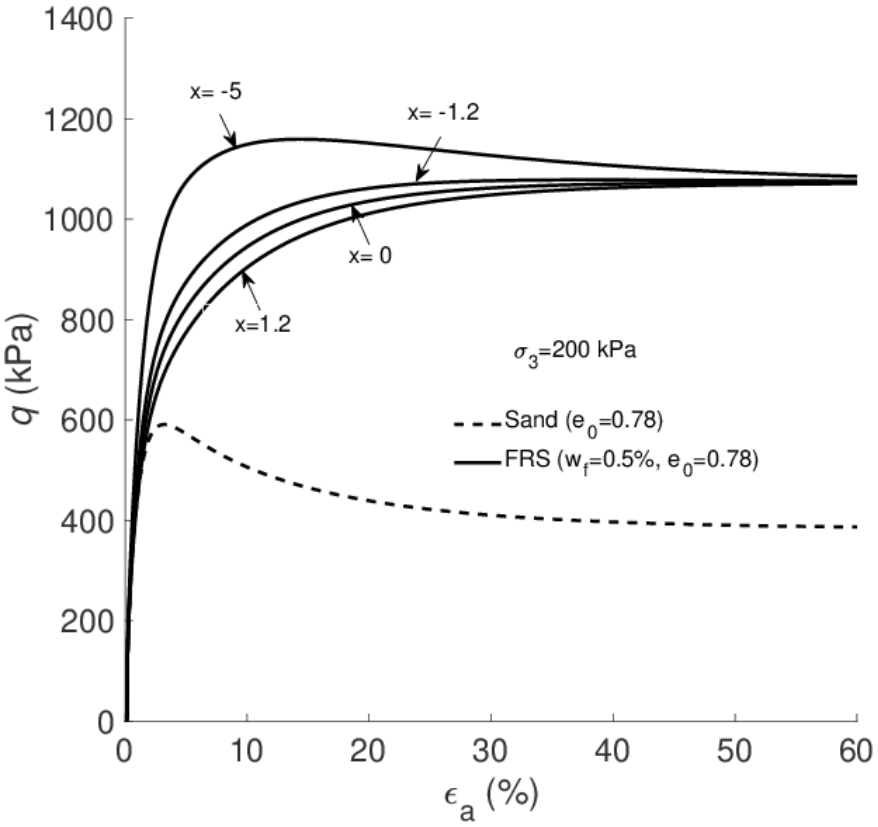

(a)

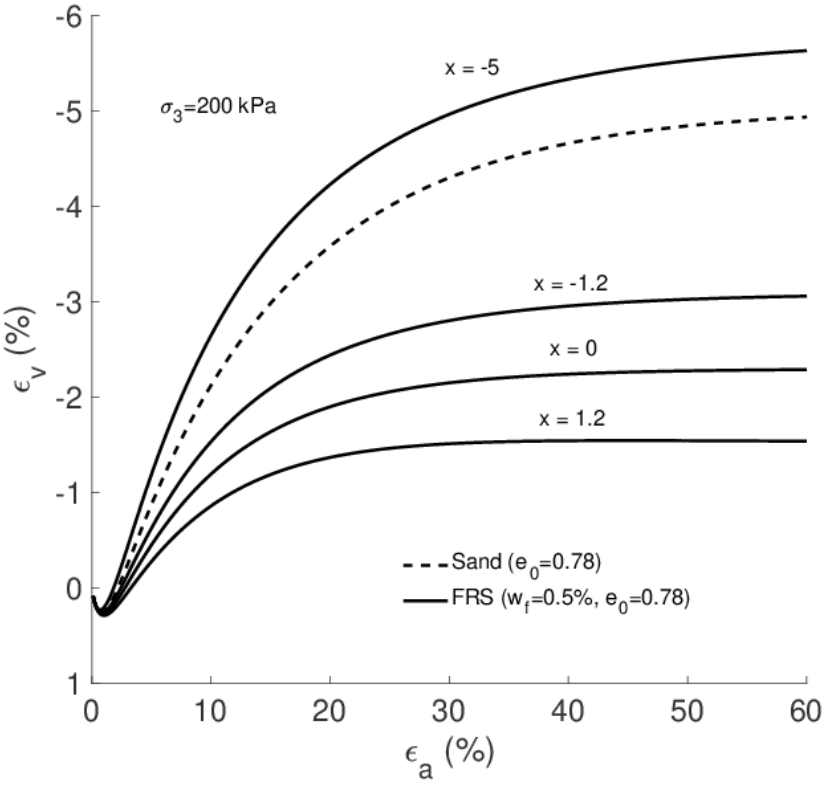

Fig. 5.3 Effect of the parameter x on stress-strain relationships for FRS in drained triaxial compression test

5.3.5 Effect of fibre inclusion on plastic hardening of sand

According to Eq. 5.15, it gives a 'virtual' peak stress ratio for FRS (expressed in terms of p and q) $M_f^p = M_c e^{-n\psi^s}(1 + p_f/p)$ attainable at the current state (where M_c is the critical stress ratio, n is model parameter for sand, p_f is mean effective principal stress given by fibres, ψ^s is the state parameter for FRS). M_f^p can be obtained as the stress ratio, which makes $r_H = 0$ (Li & Dafalias, 2000), where r_H is the plastic modulus. For pure sand, its 'virtual' peak stress ratio will be $M_s^p = M_c e^{-n\psi^s}$. Fig. 5.4 shows the development of the two 'virtual' peak stress ratio and r_H for both sand and FRS in a drained triaxial compression test. The parameters used in the plot is Hostun sand, and other parameters of sand have been displayed in Table 5.1. As can be seen from Fig. 5.4, M_f^p is initially smaller than M_s^p but gradually bigger than it. Otherwise, a slight difference observed between sand and FRS in terms of r_H at the initial loading stage ($\varepsilon_a < 2\%$), but r_H value of FRS is bigger throughout the test, meaning higher shear stiffness. This is indeed in agreement with the experimental observations, which can be seen in the model validation section. At the critical state, $r_H = 0$ for both sand and FRS. The reason why sand sample having negative r_H is due to strain softening response ($\varepsilon_a < 20\%$), where has been shown in Fig. 5.3.

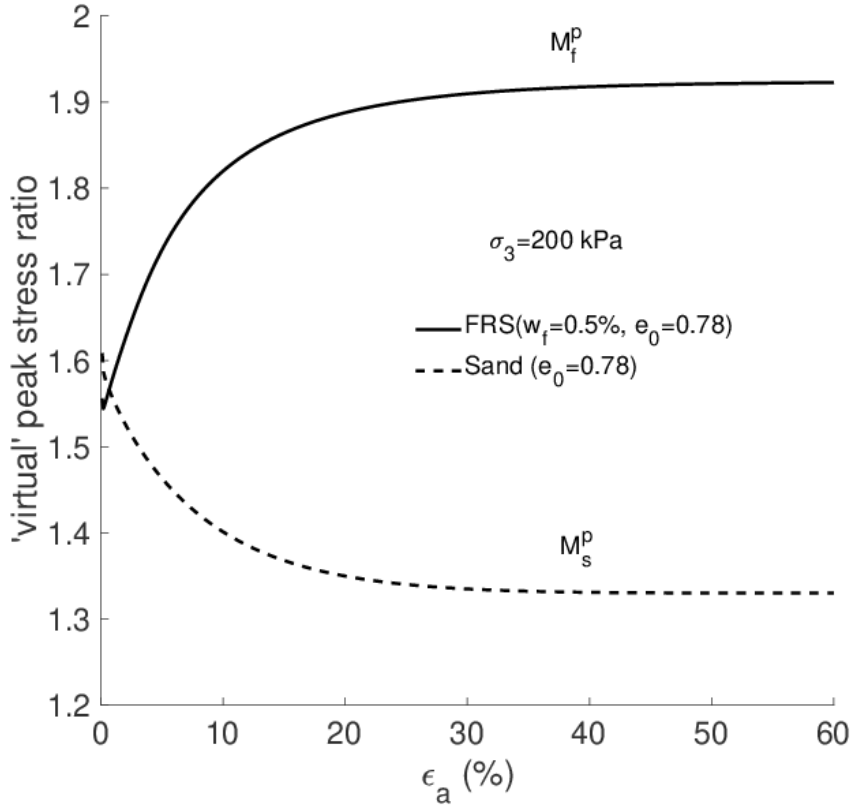

(a)

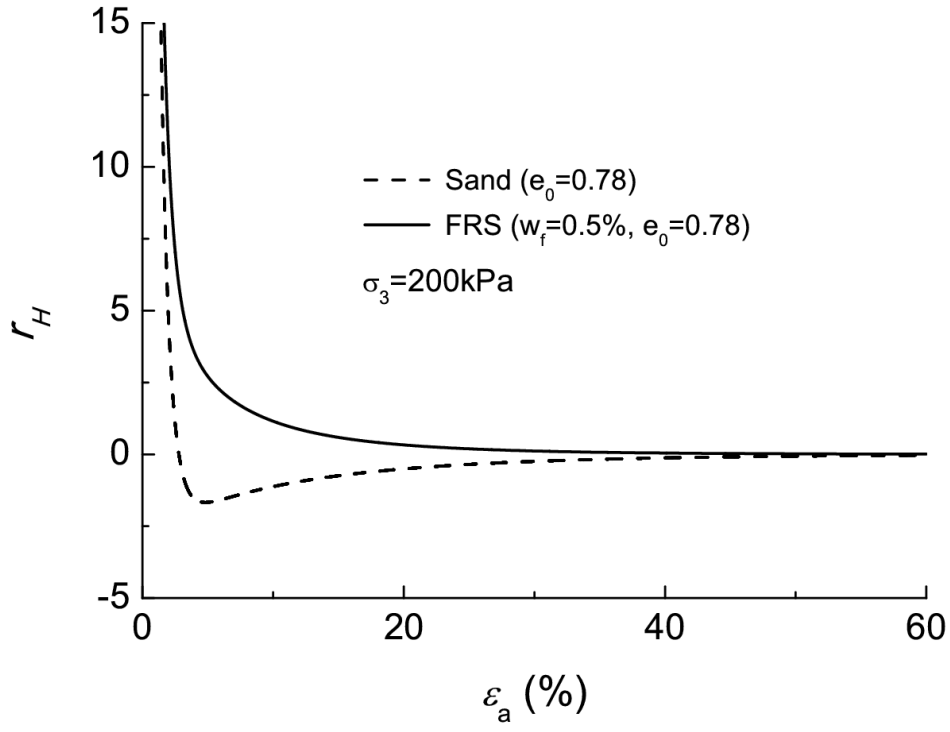

(b)

Fig. 5.4 Evolution of the 'virtual' peak stress ratio and r_H in a drained triaxial compression test

5.4 Model Validation

There are 14 parameters used in this model, 11 of which are for the host sand. Determination of the parameters has been discussed in previous papers (e.g., Li & Dafalias, 2000; Li & Dafalias, 2002; Gao et al., 2014). The four parameters characterising the fibre reinforcement can be determined based on the test results in triaxial compression. The following will be explained using the experimental results of Hostun sand conducted at the University of Glasgow:

(a) The failure condition of FRS predicted by this model in triaxial compression is expressed by Eq. 5.1. Therefore, c and κ can be determined based on the failure stress state in triaxial compression (Gao & Zhao, 2013). Fig. 5.5 illustrates the determination of parameter c and κ. It is noted different c value is applied for FRS with different fibre content.

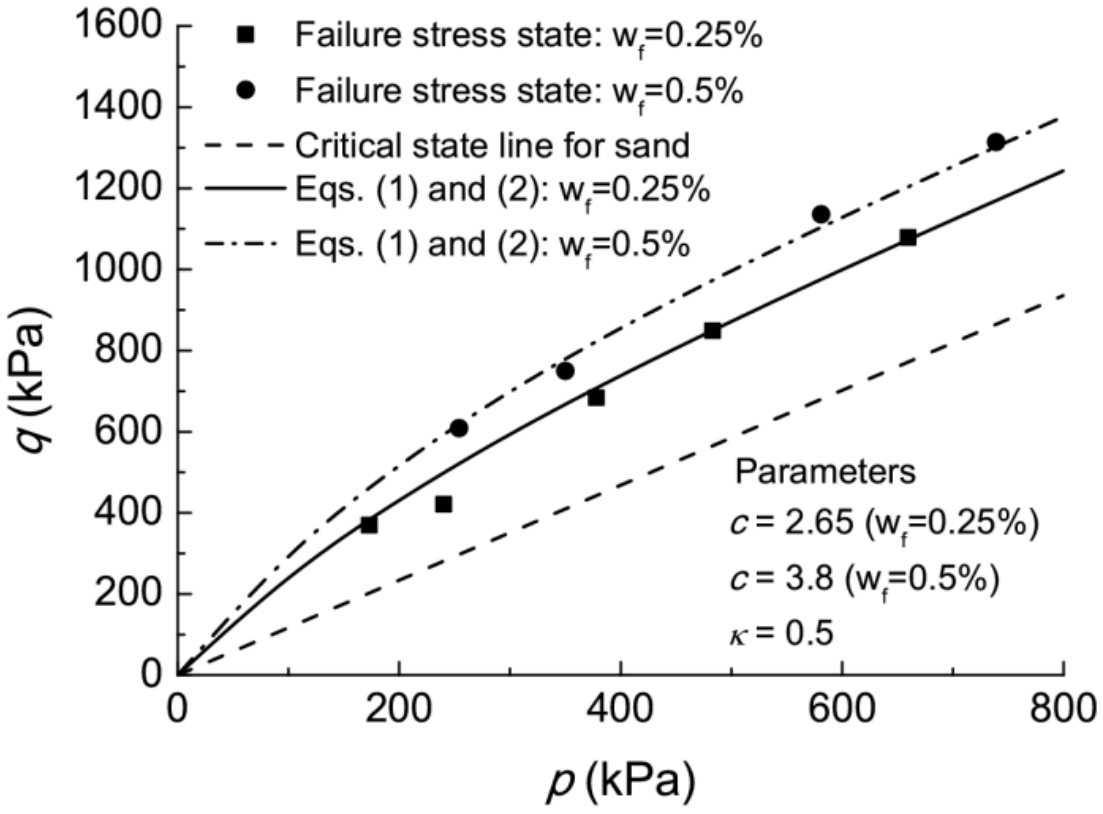

Fig. 5.5 Parameters c and κ for polypropylene-fibre-reinforced Hostun sand

(b) Once c and κ are determined, μ is then obtained by best fitting the $\varepsilon_a - q$ relationship of FRS with $x = 0$, and other model parameters (e.g., c and κ) are constant. As a result, it can be seen in Fig. 5.6, a significant effect of changing μ on stress-strain relation and less sensitive effect on $\varepsilon_a - \varepsilon_v$.

(c) Finally, before determining x, model parameter μ need to adjust to the best model simulation, as x also influences on the $\varepsilon_a - q$ relationship (Fig. 5.3). That is to say, repeatedly slightly adjusting μ is needed. It is recommended two tests or more for FRS are necessary for determining μ and x. For fibre-reinforced Hostun sand, they are determined using the tests shown in Fig. 5.7 with $\sigma_3 = 300$ kPa.

During calibration, it is found x and c are sensitive on triggering the trend of the curve on both $\varepsilon_a - q$ and $\varepsilon_a - \varepsilon_v$ Plane. In addition, c value, in general, has a positive relationship with the fibre content. It is noted once μ and κ are determined, they are no longer changed and only c and x can be modified with other conditions changed (e.g., water content, fibre content or sample preparation method).

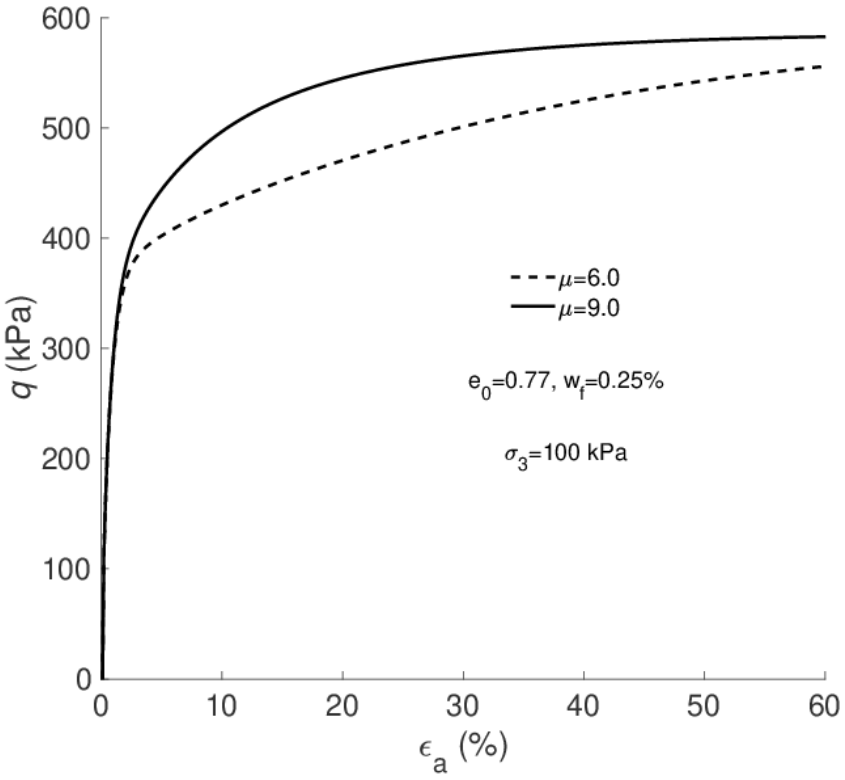

(a)

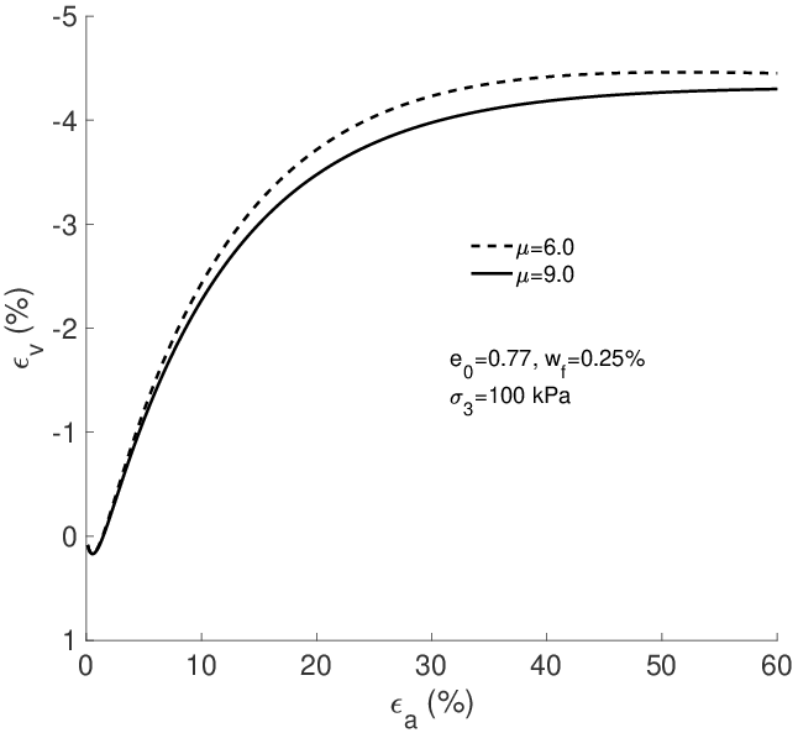

(b)

Fig. 5.6 Effect of the parameter μ on the simulated stress-strain relationship for FRS in drained triaxial compression test

Four different grains of sand are tested to validate the model, and their parameters are listed in Table 5.1.

Table 5.1 Model parameters

Paramters		Hostun sand	JH sand[a]	Osorios sand[b]	Hostun RF sand[c]
Sand	G_0 (Mpa)	135	135	120	80
	v	0.2	0.2	0.2	0.05
	M_c	1.17	1.42	1.16	1.4
	e_Γ	0.92	0.85	0.8	0.96
	ξ	0.7	0.7	0.7	0.7
	n	3.0	0.8	2.0	0.5
	ζ	0.2	0.3	0.1	0.3
	d	0.87	0.85	0.3	0.86
	λ_c	0.021	0.02	0.012	0.02
	m	0.5	3.6	2.0	0.5
FRS	c	2.65(w_f=0.25%) 3.8(w_f=0.5%)	0.5(w_f=0.41%) 1.3(w_f=1.25%)	6.0	1.6(w_f=0.3%) 2.6(w_f=0.6%)
	k	0.5	0.4	0.4	1.0
	μ	8.5	9.0	7.2	6.0
	x	1.2	1.3	-3.0	-5.2

a* Michalowski & Zhao (1996); b* Consoli et al. (2007); c* Diambra, (2010)

5.4.1 Polypropylene-fibre-reinforced Hostun sand

Several drained triaxial compression tests have been carried out for this sand at the University of Glasgow. Its major parameters have been concluded in Table 5.2. In addition, the sample diameter and weight were 40mm and 80mm, respectively. The sample was fabricated by moist tamping. In terms of fibre content, $w_f = 0.25\%$ and $w_f = 0.5\%$ were used in this experiment. Furthermore, because of the magnitude of the strain reached, natural strain ε_n calculated from the measured linear strain ε_l are used for both the axial strain ε_a and volumetric strain ε_v (Silva Dos Santos et al., 2010).

Table 5.2 Materials parameters for Hostun sand

	D_{50} (mm)	C_u	G_s	$e_{\max}$	$e_{\min}$
Sand	0.33	1.4	2.64	1.0	0.66
	G_f	l (mm)	D_f (mm)		
Fibre	0.91	35	0.088		

The comparisons between model simulation and experimental data with different testing conditions (e.g., confining pressure, void ratio and fibre content) have been shown in Fig. 5.7 to Fig. 5.9. The parameter x is found to be positive for this soil. In general, the model can give a satisfactory prediction for both $\varepsilon_a - q$ and $\varepsilon_a - \varepsilon_v$ relationships. However, it can be seen in these figures, the reinforced sample with $w_f = 0.25\%$ occurring strain softening towards the end of the test has not been captured. It is found the sudden decrease in q in these tests is caused by the development of a clear shear band (Fig. 5.7 to Fig. 5.8). It is assumed this development might be associated with the fabricated technique. In other words, if deformation remained uniform in the sample, there would not be such a sudden decrease in q. Most previous studies suggested the optimum fibre content (w_f) should be at least 0.3% to avoid localised soil failure for practical application (Michalowski, 1996; Consoli et al., 2007; Silva Dos Santos et al., 2010; Diambra et al., 2013).

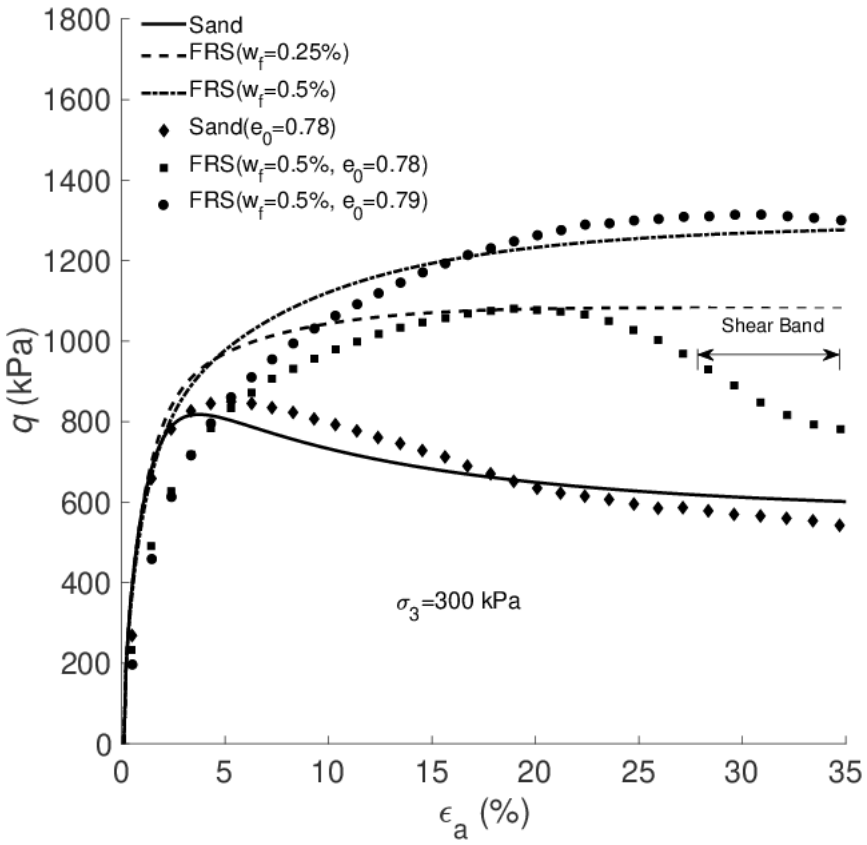

(a)

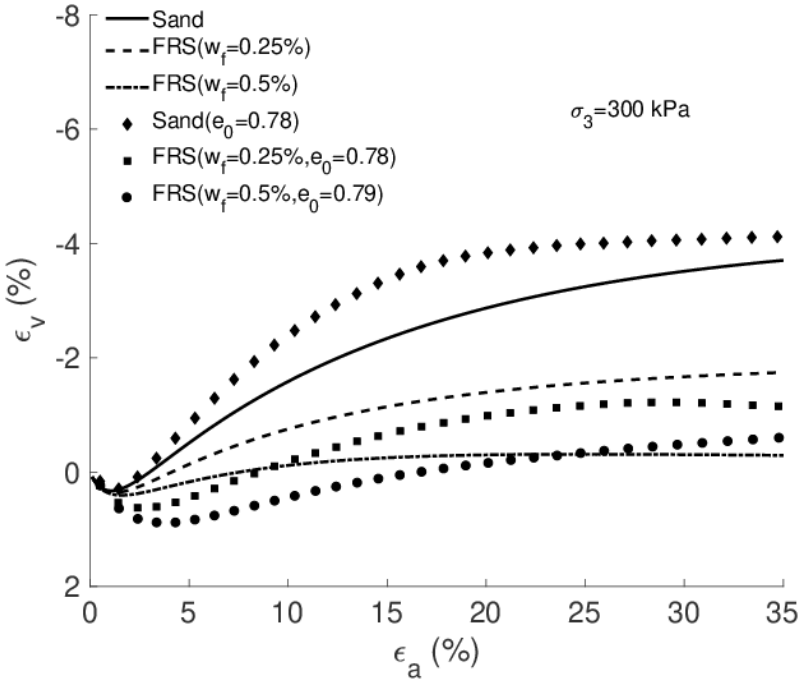

(b)

Fig. 5.7 Model predictions for the stress-strain relationship of polypropylene-fibre-reinforced Hostun sand in drained triaxial compression tests with $\sigma_3 = 300$ kPa

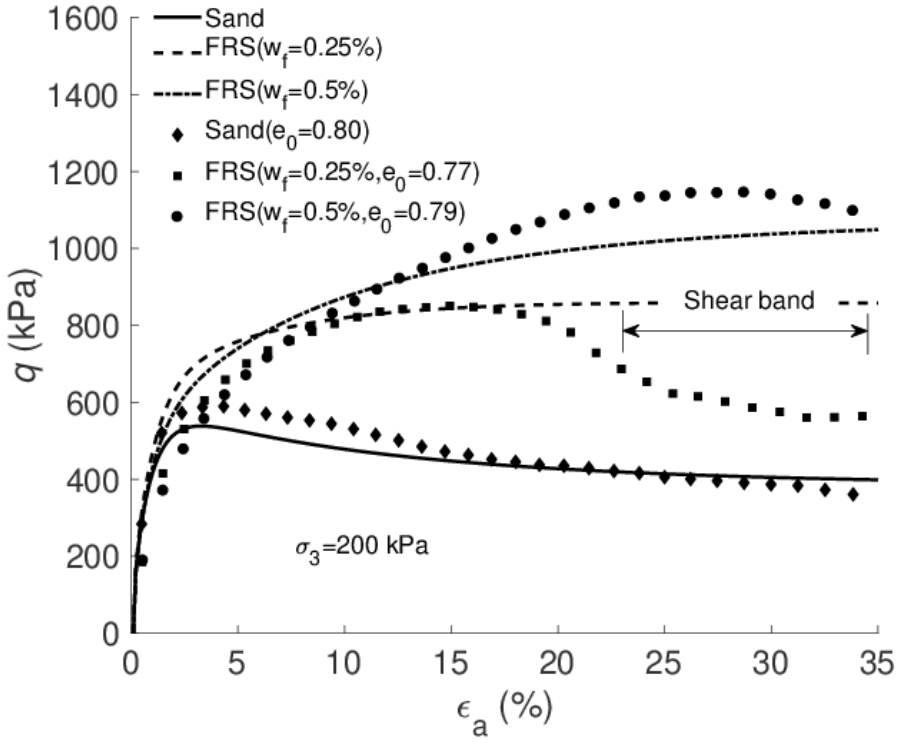

(a)

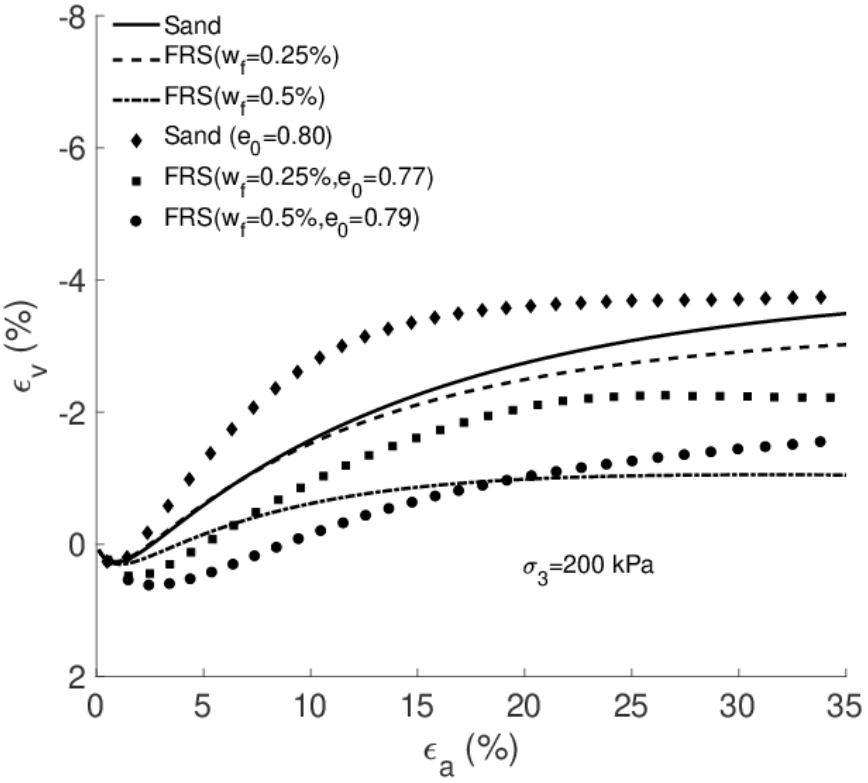

(b)

Fig. 5.8 Model predictions for the stress-strain relationship of polypropylene-fibre-reinforced Hostun sand in drained triaxial compression tests with $\sigma_3 = 200$ kPa

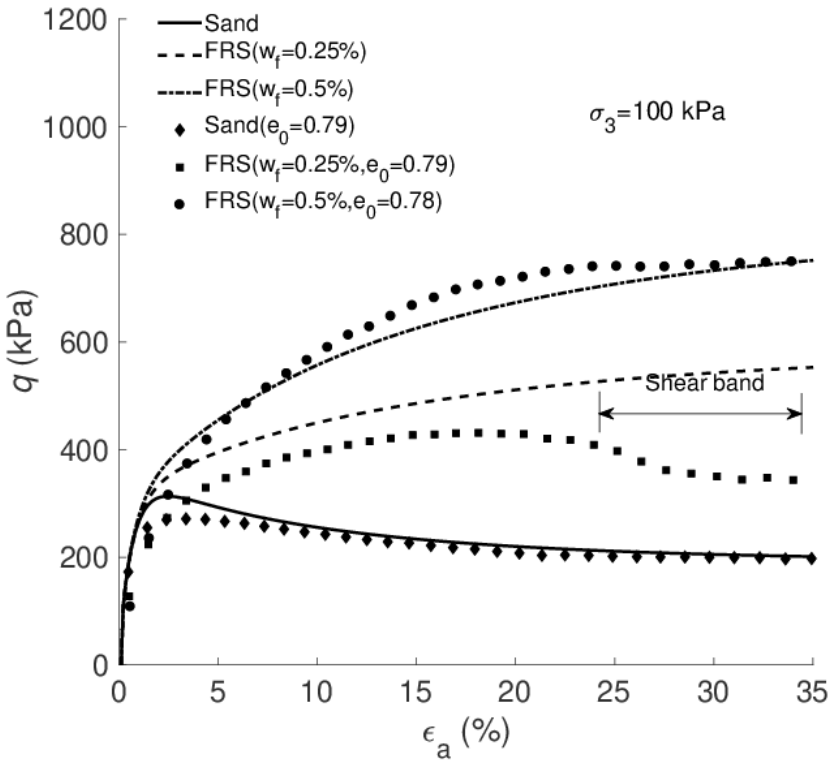

(a)

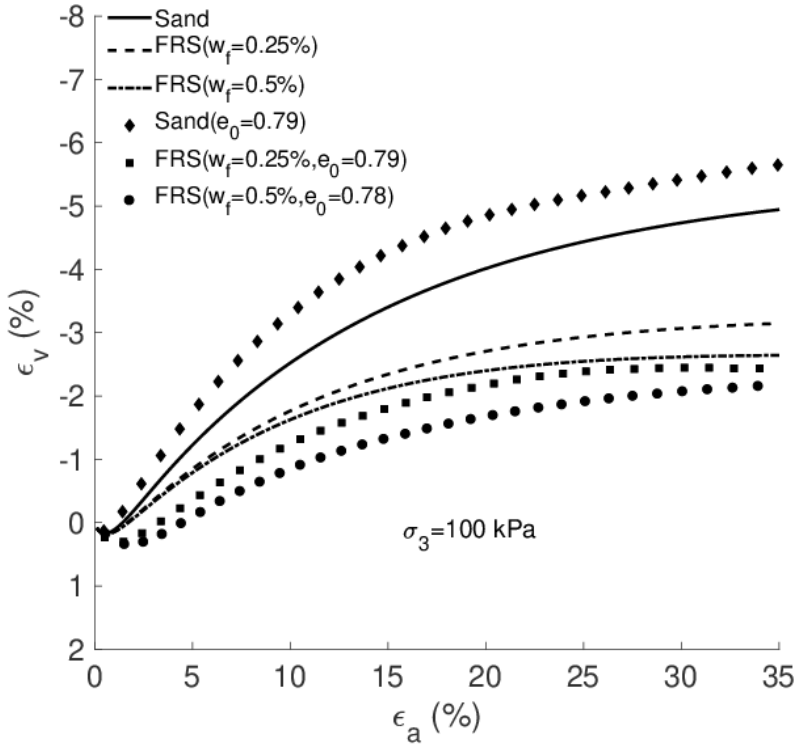

(b)

Fig. 5.9 Model predictions for the stress-strain relationship of polypropylene-fibre-reinforced Hostun sand in drained triaxial compression tests with $\sigma_3 = 100$ kPa

5.4.2 Steel-fibre-reinforced JH sand

Drained triaxial compression tests of this sand were conducted and reported by Michalowski & Zhao (1996). The sample preparation method was discussed in Michalowski & Zhao (1996) and Michalowski (1996). The related parameters for JH sand have been displayed in Table 5.3. Due to insufficient data for getting the position of the critical state line in the $e-p$ plane, λ_c and ξ are estimated based on the parameters of Hostun sand. Moreover, as all the pure sand samples show volumetric expansion towards the end of the test, the parameter e_Γ close to the $e_{\max}$ of this sand is proposed. The parameter of c and κ are determined based on the failure stress states reported by Michalowski (1996). Fig.5.10 and 5.11 respectively illustrate the comparison between the model predictions and test data with different fibre contents. They both have excellent agreement with the experimental data in $\varepsilon_a - q$ relation. Besides that, satisfactory prediction for the $\varepsilon_a - \varepsilon_v$ relation is also achieved, while the model mainly overestimating the volumetric expansion for the test with $\sigma_3 = 400\ \text{kPa}$ and $w_f = 2.0\%$.

Table 5.3 Materials parameters for JH sand

	D_{50} (mm)	C_u	G_s	$e_{\max}$	$e_{\min}$
Sand	0.89	1.52	2.65	0.56	0.89
	G_f	D_f (mm)	η_a=l_f/d_f		
Fibre	7.85	0.64	40		

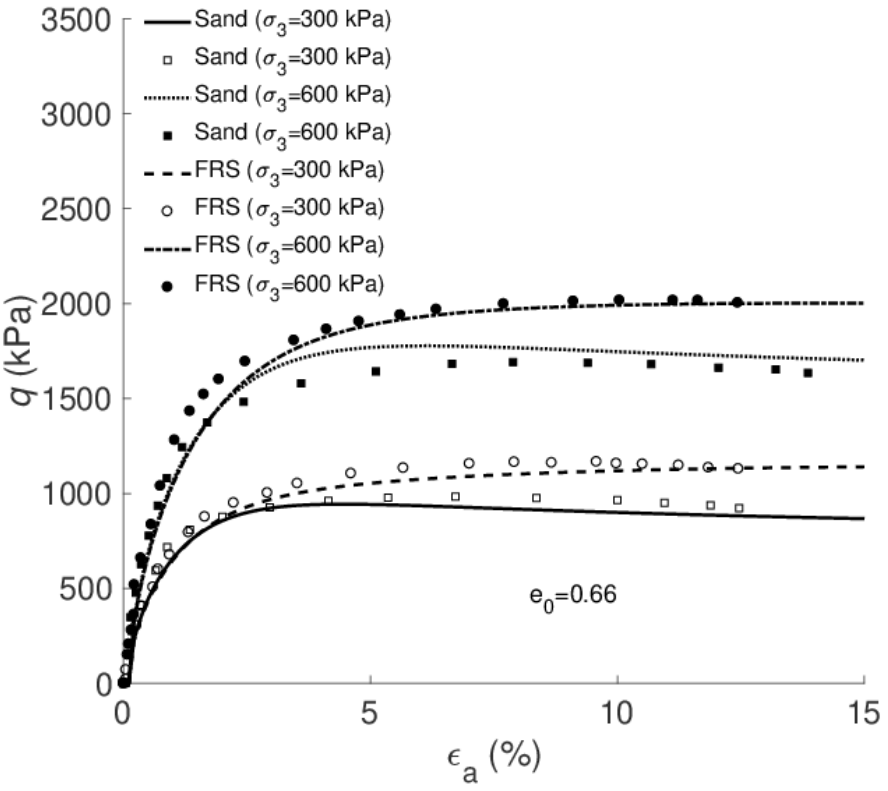

(a)

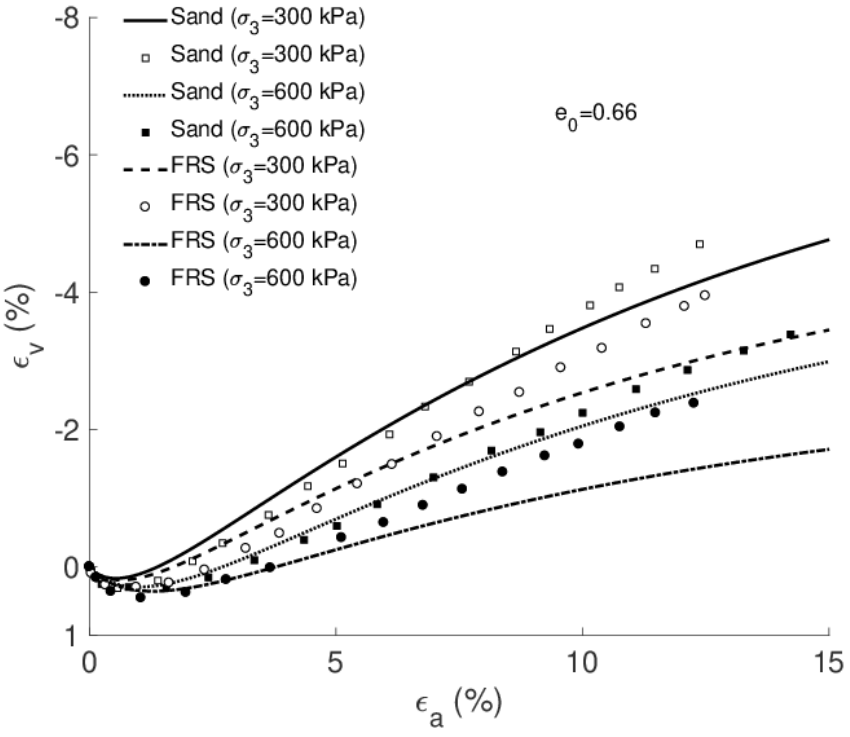

(b)

Fig.5.10 Comparison between model prediction and test results in stress-strain relation for steel-fibre-reinforced JH sand with $w_f = 6.0\%$. and $\eta_a = 40$ (Michalowski & Zhao, 1996)

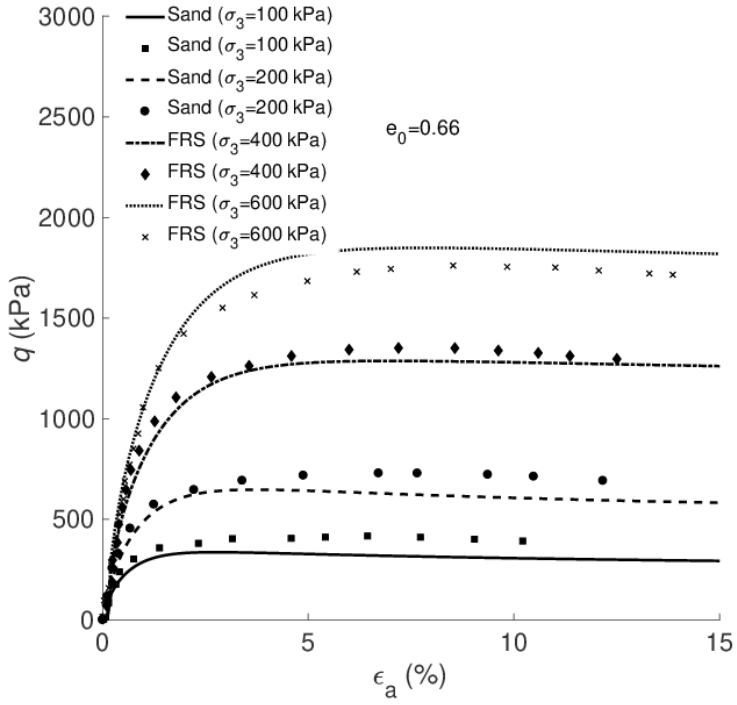

(a)

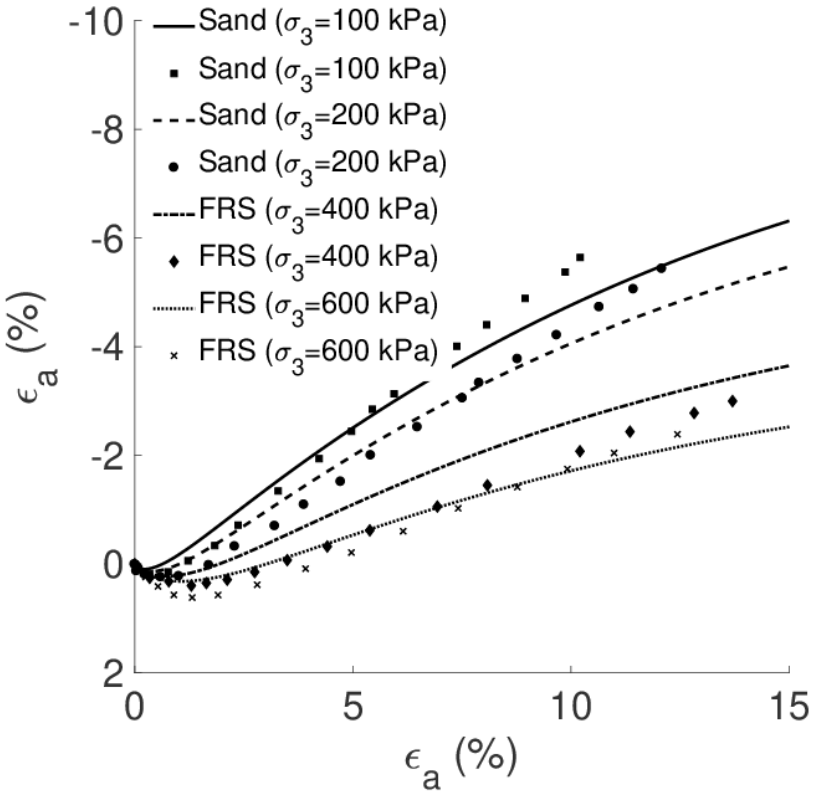

(b)

Fig.5.11 Comparison between model prediction and test results in stress-strain relation for steel-fibre-reinforced JH sand with $w_f = 2.0\%$. and $\eta_a = 40$ (Michalowski & Zhao, 1996)

5.4.3 Polypropylene-fibre-reinforced Osorio sand

Consoli et al. (2007) and Silva Dos Santos et al. (2010) have conducted a series of draind triaxial compression tests using Osorio sand reinforced by polypropylene fibres. The samples were prepared by moist tamping. Exclusive of the basic model parameters of this sand shown in Table 5.4, the parameters of c and κ are obtained based on the failure points in Santos study (Santos et al., 2010). Compared with Hostun and JH sand, this sand has a negative x, which is similar to the tests reported by Diambra et al. (2013).

Table 5.4 Materials parameters for Osorio sand

	D_{50} (mm)	C_u	G_s	$e_{\max}$	$e_{\min}$
Sand	0.16	2.1	2.62	0.6	0.9
	G_f	l (mm)	D_f (mm)		
Fibre	0.91	35	0.023		

The comparing results between model predictions and testing data have been shown in Fig. 5.12 and 5.13. It can be seen the model prediction has good agreement with the experimental data in Fig. 5.12, whereas there is an obvious discrepancy on the axial strain against volumetric strain relation. The possibility of this model itself needs to be improved by adjusting model parameters to obtain better predictions. Meanwhile, it is noted the experimental results displayed in Figs. 5.12 and 5.13 were conducted by different researchers. Although they followed the same test procedure, the samples might have slightly different internal structure caused by the distribution of fibres.

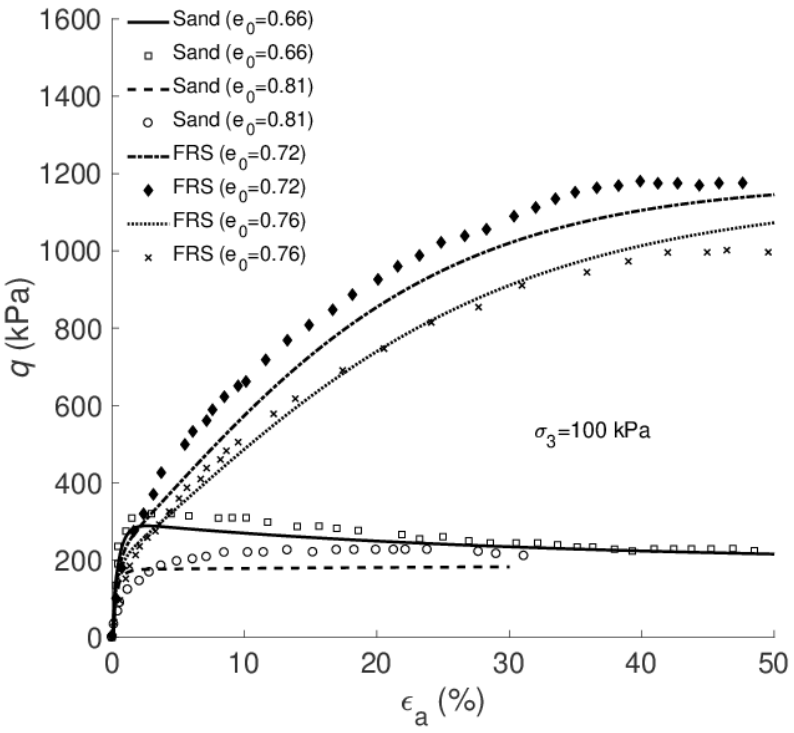

(a)

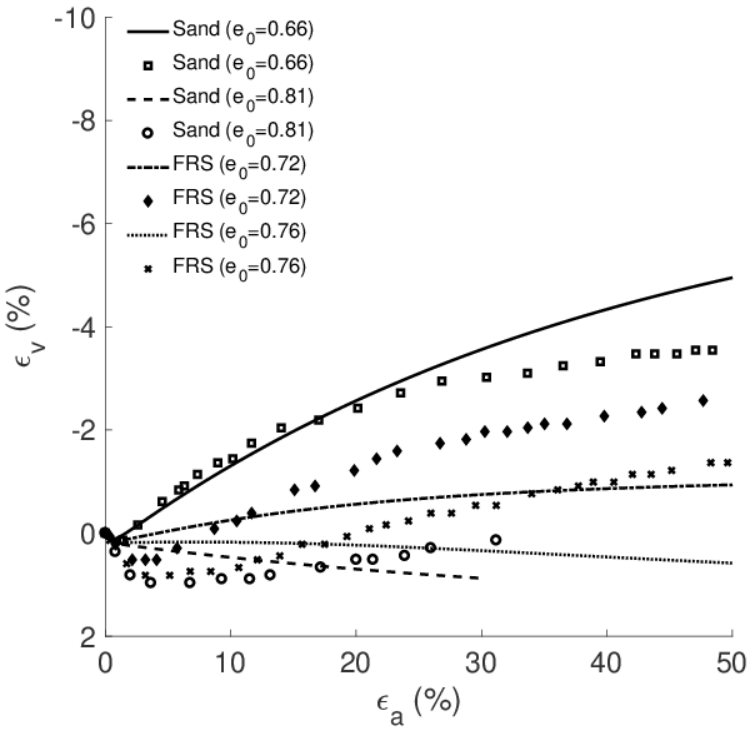

(b)

Fig. 5.12 Model predictions for the stress-strain relationship of polypropylene-fibre-reinforced Osorio sand in drained triaxial compression test with $\sigma_3 = 100$ kPa (Sila Dos Santos et al., 2010)

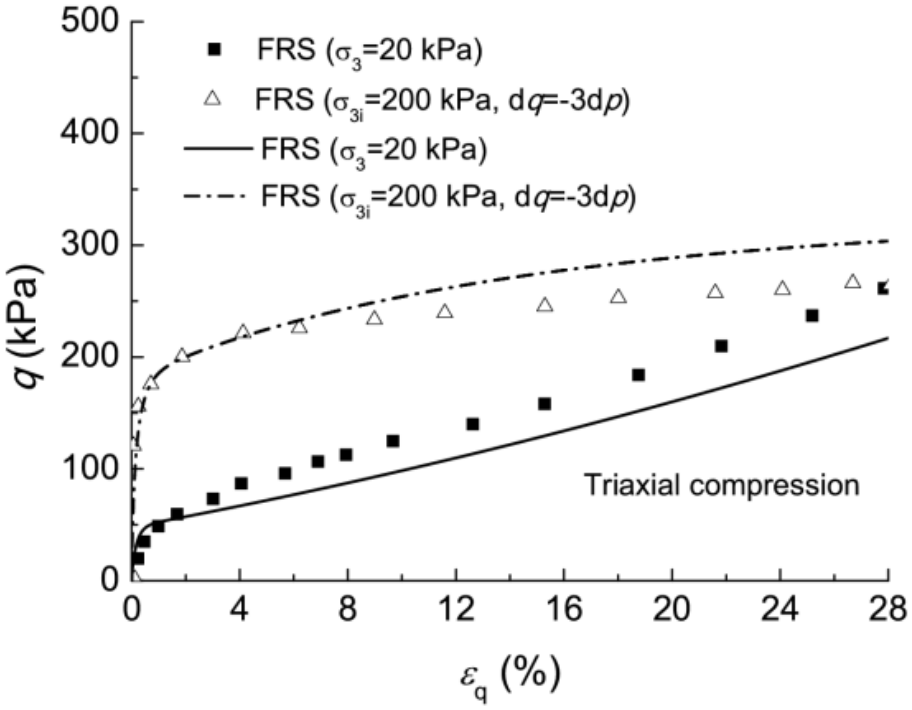

(a)

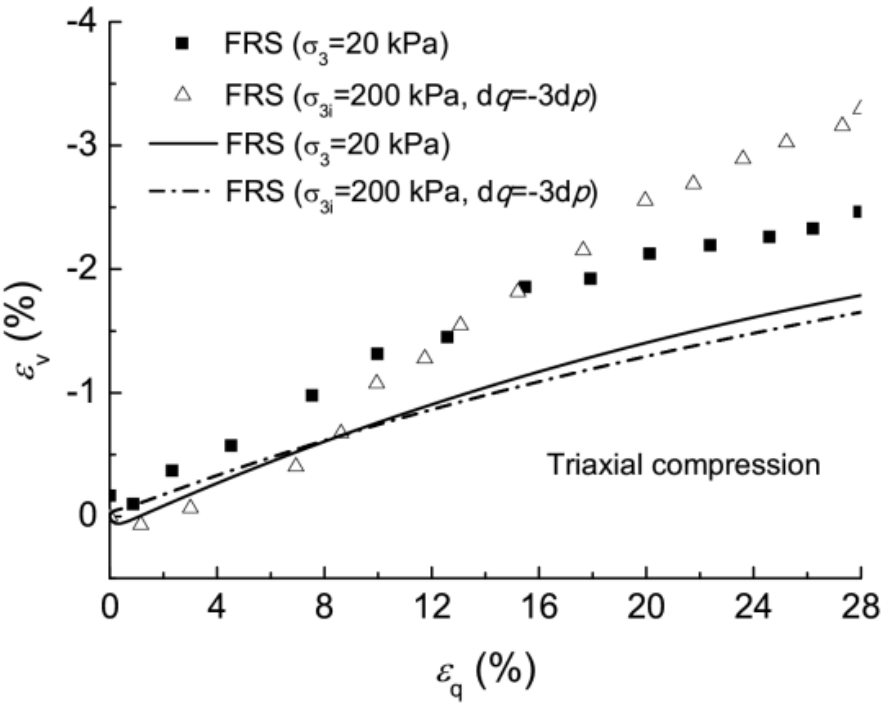

(b)

Fig. 5.13 Model predictions for the stress-strain relationship of polypropylene-fibre-reinforced Osorio sand in drained triaxial compression test with different stress paths (Consoli et al., 2007)

5.4.4 Polypropylene-fibre-reinforced Hostun RF (S28) sand

Hostun RF (S28) sand reinforced by $\mathrm{Loksand}^{\mathrm{TM}}$ fibres have conducted for both drained and undrained triaxial compression test (Diambra, 2010). The material parameters have been shown in Table 5.5. Compared with the experimental data done by several previous sand types, the FRS samples exhibit strain hardening even at the end of the test with large axial strain and no failure is observed, making it challenging to get c and κ for this soil from the test data directly. Therefore, assumptions for getting these parameters are necessary. First, $\kappa = 1.0$ is assumed. As discussed above, changing the value of μ affects the stress-strain relationship (Fig. 5.6), this FRS sample is expected to reach at a much higher axial strain level ($\varepsilon_a > 40\%$), hence a smaller $\mu(= 6.0)$ is assumed. c is then determined by best fitting the $\varepsilon_a - q$ relationship in Fig. 5.14. Finally, x is determined based on the $\varepsilon_a - \varepsilon_v$ relationship in Fig. 5.14.

Table 5.5 Materials parameters for Hostun (S28) sand

	D_{50} (mm)	C_u	G_s	$e_{\max}$	$e_{\min}$
Sand	0.38	1.9	2.65	0.648	1.041
	G_f	l (mm)	D_f (mm)		
Fibre	0.91	35	0.1		

The model simulations for the test data are shown in Figs. 5.14-5.17. Considerable discrepancies can be observed between model prediction and test data on soil dilatancy in Fig. 5.13b and 5.14b. Similar to Osorio sand, this might be due to the development of fibre-reinforcement, described by the evolution of p_f of the model, different from other FRS samples. In contrast, this model gives a good agreement with soil response in undrained triaxial tests. In addition, it is noted the model gives lower q compared with the FRS sample with w_f=0.3%, which could also be improved by using a different evolution law for p_f. Furthermore, Fig. 5.16 and 5.17 show the samples tend to regain some q at $\varepsilon_a > 15\%$. As $e_0 = 0.99$ is nearly approaching the

maximum void ratio of this sand (e_{max} in Table 5.5), a similar situation has been reported in many previous studies (Li & Dafalia, 2000; Gao et al., 2014). Therefore, there could be some experimental error in the tests.

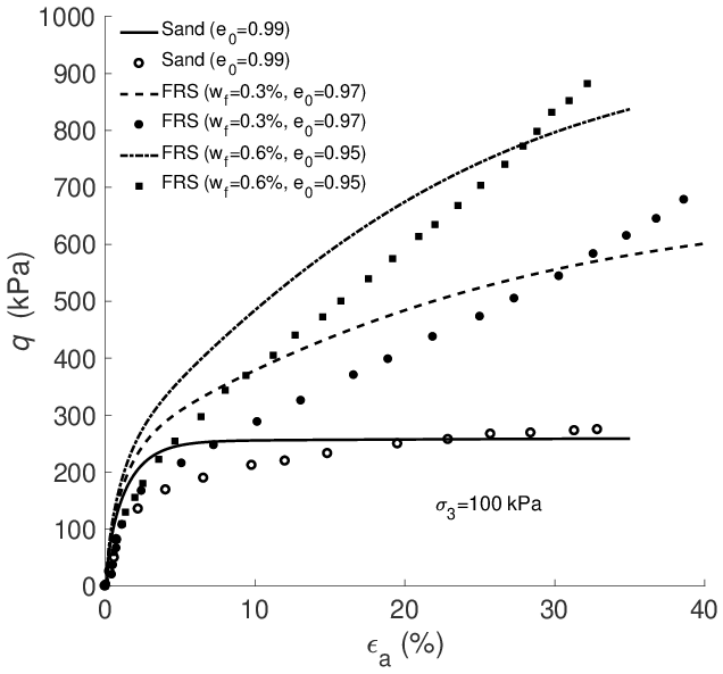

(a)

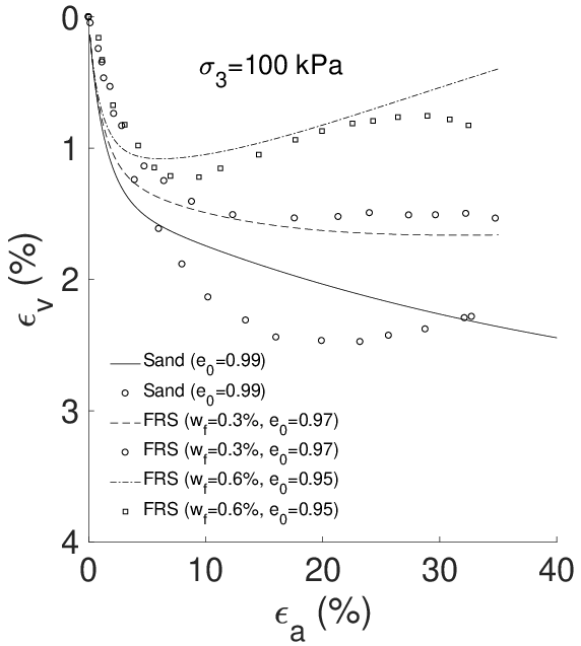

Fig. 5.14 Comparison between model and test data for polypropylene-fibre-reinforced Hostun RF sand (loose sand) in drained triaxial compression test (Diambra,2010)

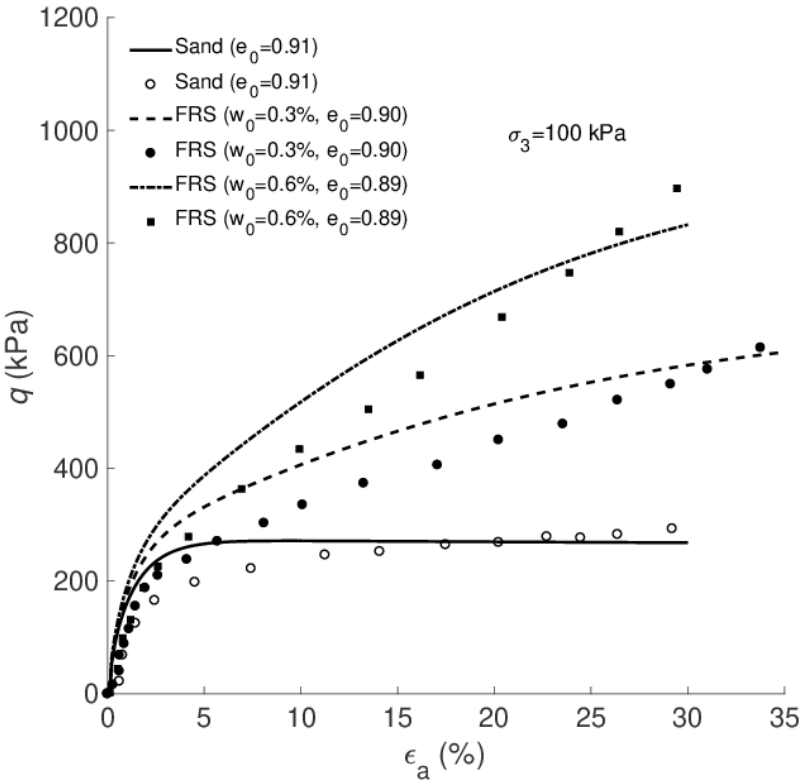

(a)

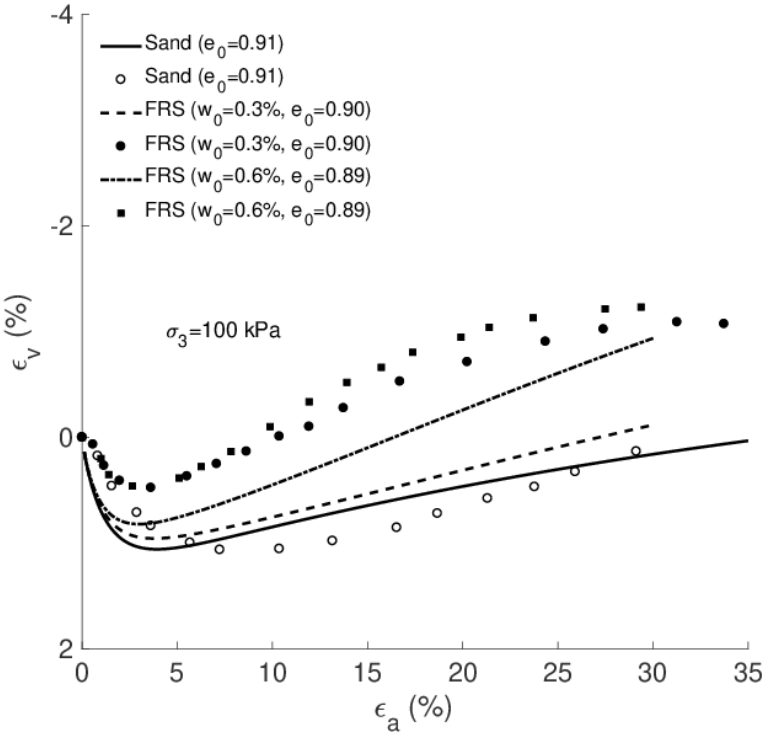

(b)

Fig. 5.15 Comparison between model and test data for polypropylene-fibre-reinforced Hostun RF sand (medium dense sand) in drained triaxial compression test (Diambra,2010)

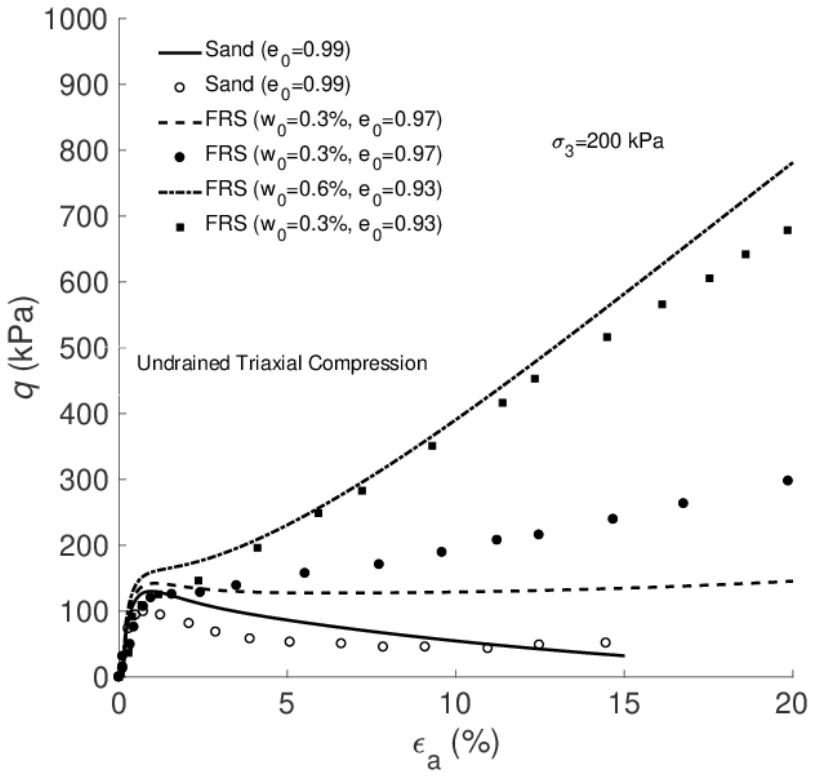

(a)

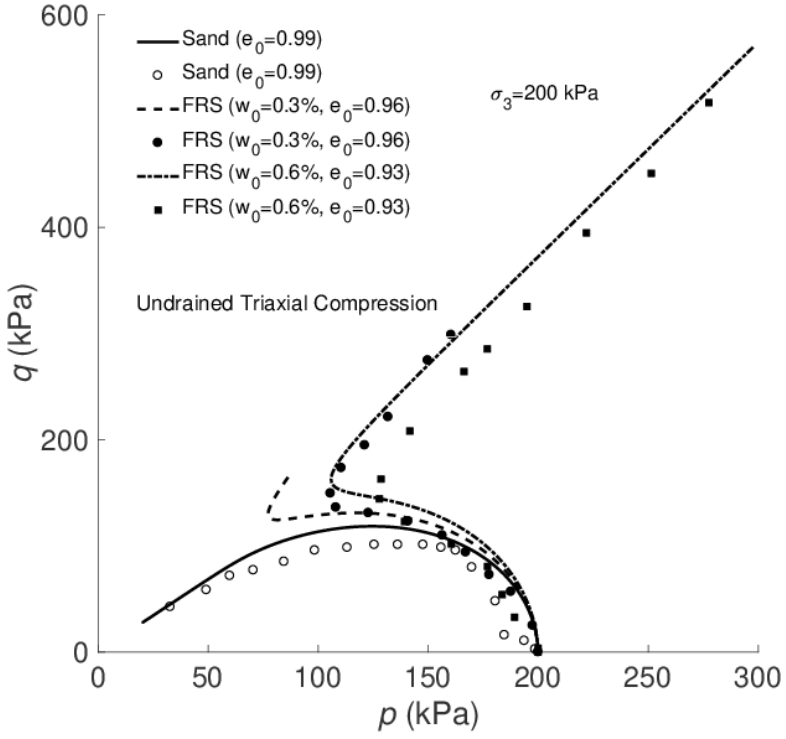

(b)

Fig. 5.16 Comparison between model and test data for polypropylene-fibre-reinforced Hostun RF sand in undrained triaxial compression test with $\sigma_3 = 200$ kPa (Diambra,2010)

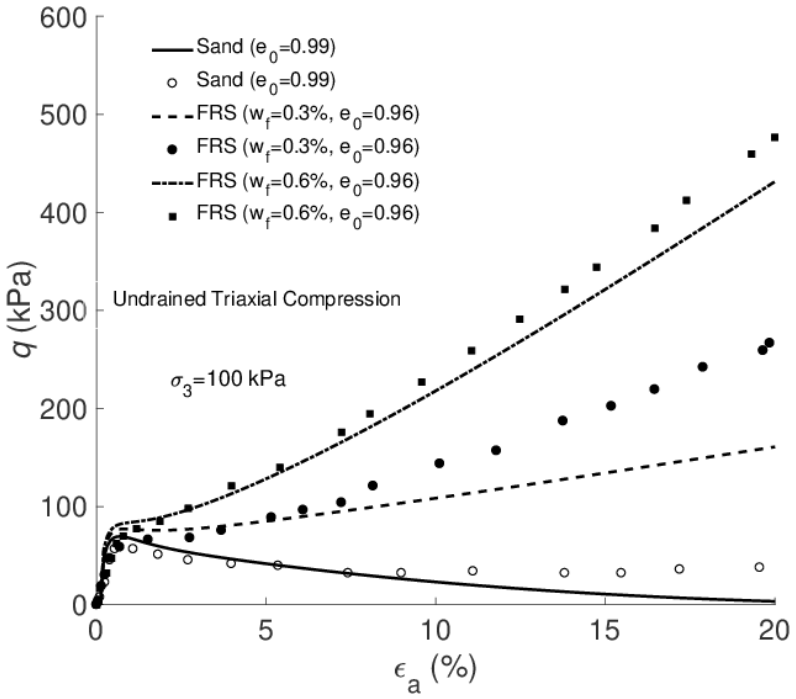

(a)

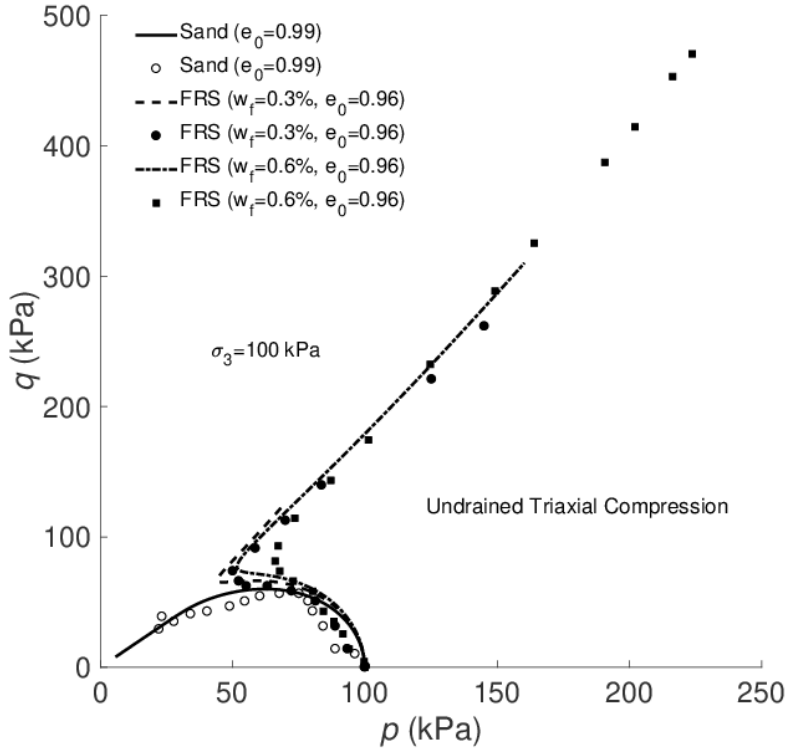

(b)

Fig. 5.17 Comparison between model and test data for polypropylene-fibre-reinforced Hostun RF sand in undrained triaxial compression test with $\sigma_3 = 100$ kPa (Diambra,2010)

5.5 Summary

A new model for the constitutive model of FRS has been introduced. It is assumed that the strain of FRS is dependent on the deformation of the sand skeleton, while the effective skeleton stress and void ratio are affected by fibre inclusion, which are evolving with the shear strain and dependent on fibre content, respectively.

In this new model, four model parameters (c, κ, μ and x) are the first introduced to characterise the fibre inclusion on the mechanical behaviour of sand. All of them can be easily determined based on the test data of triaxial test on FRS, without measuring the stress-strain relationship of individual fibres. In addition, it has been used to predict the stress-strain relationship for four different sands in both drained and undrained triaxial tests with different stress path. Overall, it would be better to be precise with the test data (35 tests in total).

This proposed constitutive model is expected to study how to model the mechanical behaviour of FRS using the concept of effective skeleton stress and void ratio. Hence, further works will be carried out for improving the constitutive model:

1. The parameter c needs to be specified for FRS with different fibre contents. Micromechanical analysis can be done to give a general expression for c, which can affect the properties of fibres and sand.
2. Due to discrepancy caused by the effect of $p_f$observed (e.g., comparison of $\varepsilon_a - \varepsilon_v$ relationship of Osorio sand), the evolution law of p_f needs to be improved.
3. More tests under undrained and extension condition should be considered, which can provide a wide range of different stress paths.
4. Fibre orientation in FRS is highly anisotropic, which having profound effect on the behaviour of FRS is not accounted for.
5. The model uses a Mohr-Coulomb type yield function which cannot describe the plastic deformation of FRS under compression.

6. The model is suitable for describing the FRS behaviour under monotonic loading. More works are needed to extend for cyclic loading.

Chapter 6: Sample Preparation Methods and Model Simulation

6.1 Introduction to Sample Preparation Method

It is well known that the mechanical behaviour of pure sand depends on the internal soil structure, which can be affected by sample preparation methods. Several studies state the internal soil structure caused by different preparation methods shows a remarkable difference in both static and dynamic deformation characteristics of sands (Ladd, 1974; Miura and Toki, 1982; Yamashita and Toki, 1993; Dai et al., 2016). For fibre reinforced sand (FRS), the sample preparation methods influence not only the internal structure of sand, but also the fibre distribution and sand-fibre interaction. For example, Sze and Yang (2014) implemented triaxial compression drained and undrained tests, in which the specimens were prepared by moist tamping (MT) and dry deposition (DD). Consequently, the specimens prepared by both methods exhibit a remarkable difference in stress responses (Fig. 6.1). In this section, some of the typical sample preparation techniques, especially for triaxial testing, will be introduced.

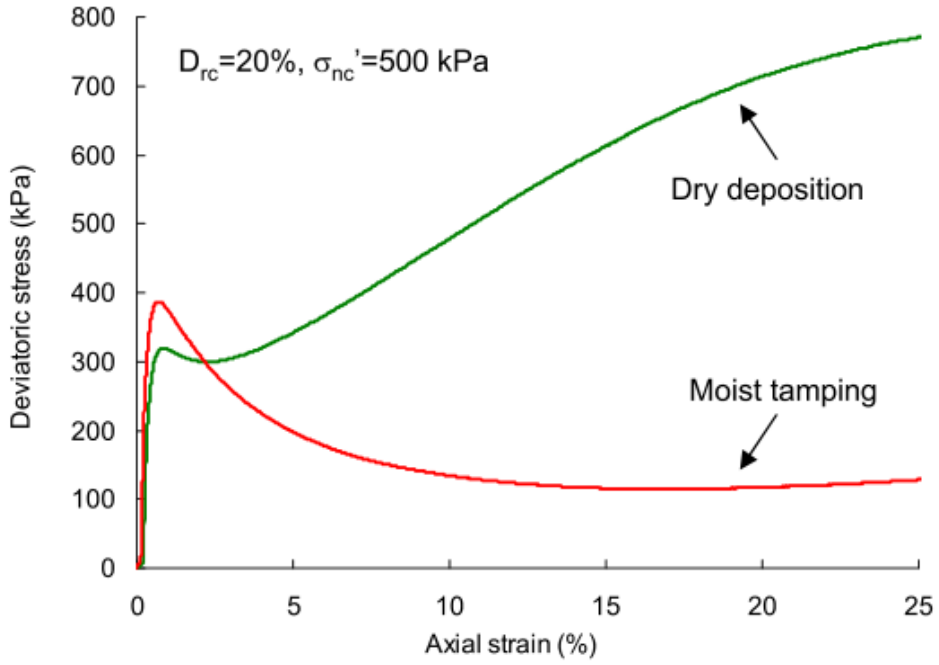

(a)

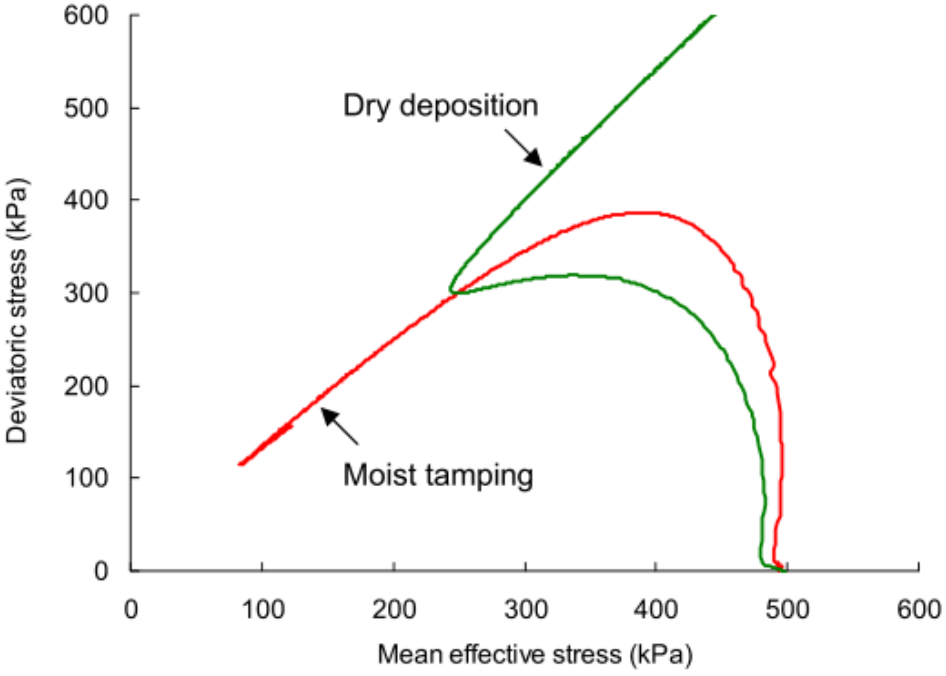

(b)

Fig 6.1 Comparing results of sample preparation for pure sand in (a) drained and (b) undrained tests, under the same relative density and confining stress (Sze and Yang, 2014).

Moist Tamping (MT)

Moist tamping is a proposed sample preparation technique to achieve a full range of densities (Chen and Chuang, 2001; Wang et al., 2016; Ibraim et al., 2012). Ladd (1978) was the first to introduce moist tamping technique. Due to its superiorities in term of relatively well-controlling specimen density and homogenous distribution of fibres, especially preventing fibre clumping or segregation, this technique has been widely used in many studies (Ibraim et al., 2012; Wang et al., 2016; Ishihara, 1993; Consoli et al., 2005). On the other hand, Vaid (1999) stated moist tamping, in general, was used to reconstituted very loose specimens, even looser than the maximum void ratio of the sand. On the contrary, Ishihara (1993) argued this method is capable of covering a wide density range of reconstituted specimens. However, in drained condition, these looser specimens often result in a contractive strain-softening response (Wanatowski & Chu, 2008). A consistent observation can be found in the following experimental results, which the loose samples prepared by MT show softening behaviour. Vaid and Sivathayalan (2000) explained the softening behaviour is caused as volume decreases, and the strain hardening behaviour is manifested as volume dilatancy.

Besides, the effect of sample preparation is relatively associated with the mechanical behaviour of the composite. For example, the specimens formed by MT are found to generate a more preferred horizontal orientation, which is anisotropic, whereas the ones prepared by dry deposition (DD) specimens are isotropic (Diambra et al., 2010; Sze & Yang, 2014). Therefore, a common observation in the triaxial compression test can be found at which the moist-tamped specimen exhibits less dilative response than that reconstituted by dry deposition, even though having the same confining stress and similar void ratios (Sze & Yang, 2014; Vaid et al., 1999). Furthermore, the sample preparation method affecting the steady state of granular soils has been studied. For instance, previous studies (e.g., Hird & Hassona, 1990; Ishihara, 1993) reported the position of critical state line (CSL) of sand is independent of the preparation method. In contrast, several researchers (Dennis, 1988; Chang et al., 2011) suggested the

specimen preparation method affected the slope of the CSL, meaning it was not independent of the initial fabric anisotropy caused by the sample preparation method.

Dry Deposition (DD)

In addition to the moist-tamping approach, dry deposition is also a concern in this study. Compared with the moist-tamping (MT) method, dry deposition (DD) method can achieve a more uniform sample. Nonetheless, Ishihara (1993) commented it is difficult for the samples to achieve a very loose density. Furthermore, although dry deposition is slightly different from the method which is so-called air pluviation, both methods share a similar principle, in which a funnel is required and maintained at a minimum drop height above the sand surface to allow sand to be deposited in a low-energy state (Wood et al., 2008; Sze & Yang, 2014). Otherwise, the stress-strain curve ($q - \varepsilon_a$) of the DD sample has a similar performance with the sample prepared by MT in drained condition. However, the volumetric change of the DD sample is not the same as the MT sample, at which the DD sample shows more dilation (Raghunandan et al., 2012). An opposite trend can be observed in this project, where the specimens prepared by both methods show a similar result in both stress planes.

Moist Vibration (MV)

Although dry deposition is one of the easier methods to prepare the sample, it is only suitable in preparing an unreinforced sample. The moist vibration (MV) method was first introduced by Ibraim et al. (2012). Similar to the MT technique, a certain amount of water is required but different in sample fabrication, in which a shaker with vibration frequency is required. As a result, the MT technique generating more near-horizontal fibres than MV technique is reported (*ibid*). For the MV method used to prepare the reinforced specimen, it is effective to avoid fibres' entanglement due to

the addition of water, and the tapping technique applied.

As discussed in Chapter 2, water content used in sample preparation has effect on the mechanical behaviour of FRS. The most important difference between the above methods is water content during compaction. Higher water content is required for moist tamping to well control specimen density and homogenous distribution of fibres. Zero water content for dry deposition has been used. Instead, the water content used in moist vibration is significantly less than MT. Different water content during compaction makes the soil structure different, which has influence on the mechanical behaviour of FRS. Different water content during compaction makes the soil structure different, which has influence on the mechanical behaviour of FRS.

This chapter presents new research on the effect of sample preparation methods on the mechanical behaviour of FRS using a series of drained triaxial compression tests. The samples are prepared using MT and Moist vibration (MV) methods. The shear stress-strain relationship and dilatancy of FRS are dramatically affected by the sample preparation methods. Besides, the testing results are also used to validate the versatility of the constitutive model. Potential reasons for the difference in FRS behaviour are then discussed.

6.2 Motivation and Experiments

Various methods have been used for preparing FRS samples in the laboratory. In Michalowski (1996), dry sand and fibres were dropped into the mould separately in five equal layers and then vibrated to reach the target density. Moist tamping (MT) is the most frequently used method for preparing FRS samples (Consoli et al., 2007; Ahmad et al., 2010; Ibraim et al., 2012; Kong et al., 2019). In this method, sand and fibres are first mixed at a certain water content to prevent the segregation of fibres. The mixture is then deposited in the mould in several equal layers and compacted to a target density. This method has also been used in airfield construction using FRS (Santoni and Webster, 2001). The sample preparation method directly affects the

internal structure of the sand skeleton, fibre distribution, and sand-fibre interaction.

Consequently, the stress-strain relationship of FRS is affected by the sample preparation methods. However, there is insufficient research in this regard. Ibraim et al. (2012) investigated loose FRS's mechanical behaviour prepared using MT and moist vibration (MV) methods. While the dilatancy of FRS was found to be affected by the sample preparation methods, the shear stress-strain relationship was not. This could be attributable to the fact that the two methods create a similar distribution of fibre orientation in FRS samples (Ibraim et al., 2012). More research is thus needed to explore the mechanical behaviour of FRS with significantly different internal structures.

For practical applications, it is also important to characterise the mechanical behaviour of FRS with a proper constitutive model. However, there is little research on how to model the effect of sample preparation methods on the stress-strain relationship of FRS. Some attempts have been made in modelling the fabric effect on the mechanical behaviour of pure sand (Yang et al., 2018; Zhao and Gao, 2016), where the difference in the initial sand fabric caused by the sample preparation methods is considered. The internal structure of FRS is affected by both the sand fabric and distribution of fibre orientation. Ibraim et al. (2012) used a model to describe the behaviour of FRS prepared using different methods in which only the soil fabric associated with the distribution of fibre orientation was considered. Since the sample preparation methods in that study were found to have a negligible influence on the shear stress and strain relationship of FRS, more research is needed to explore if this modelling assumption is proper when the effect of sample preparation methods is significant.

6.2.1 Materials and Sample Preparation Methods

Leighton Buzzard Sand

Leighton Buzzard (LB) sand is one of the coarse sand used in laboratory test in the UK. Its mean particle diameter (D_{50}) was found to be 0.53mm, which is larger than that of Hostun sand, which has been introduced in chapter 3. Other properties of LB sand are shown in Table 6.1 and Fig. 6.2.

Table 6.1: The properties of Leighton Buzzard Sand

Parameter	Value
Specific gravity G_s	2.81
Mean particle diameter D_{50}	0.53 mm
Uniformity coefficient C_u	2.13
Maximum void ratio e_{max}	0.90
Minimum void ratio e_{min}	0.63

$Loksand^{TM}$ Polypropylene fibres are used in the test, which the properties of fibres have been introduced in Chapter 3. The testing results of host sand and fibre-reinforced specimens prepared using moist tamping technique (MT) have been discussed in Chapter 3 and 4. Similar to MT, the samples prepared by dry deposition (DD) are assembled in a mould with 40 mm diameter and 80 mm length. The whole procedures of the two sample preparation methods (MT and DD) are shown in Fig. 6.3.

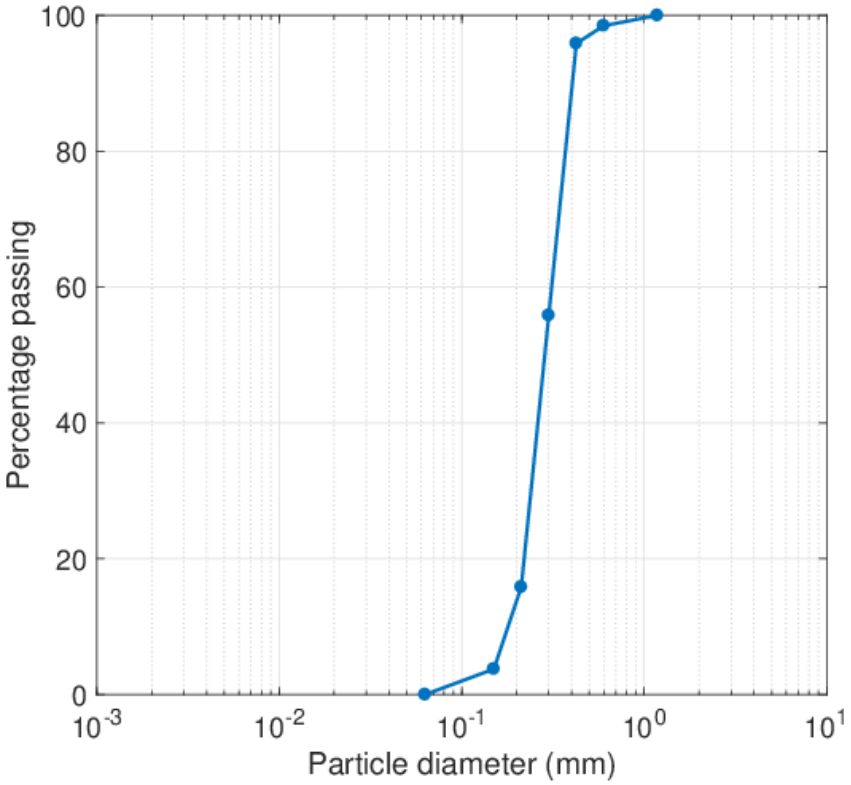

Fig. 6.2 Particle size distribution curve of Leighton Buzzard Sand

For both methods, sand and fibres are first mixed with a small amount of water (about 2% of the weight of dry sand) to prevent segregation of sand and fibres. All the samples are prepared in three layers. For the MT method, one-third of the sand-fibre mixture is deposited into the mould for each layer (Fig. 6.3a). Extra water (about 9% of dry sand weight) is then added to the mixture. Therefore, the water content of FRS samples prepared using MT is about 11% at the end of sample preparation.

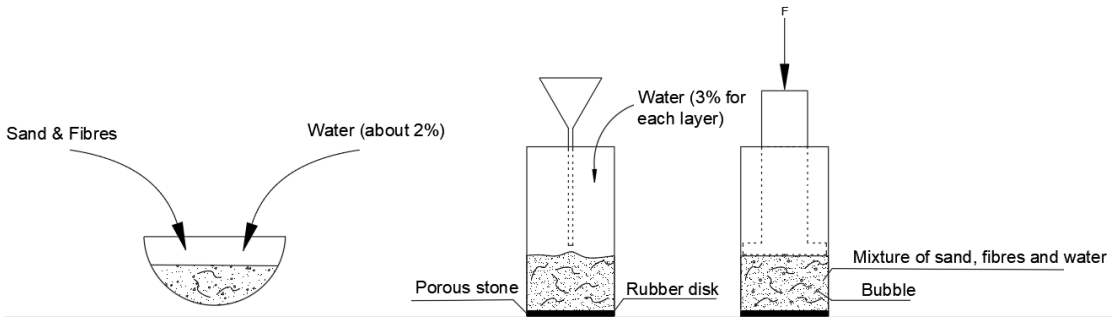

(a)

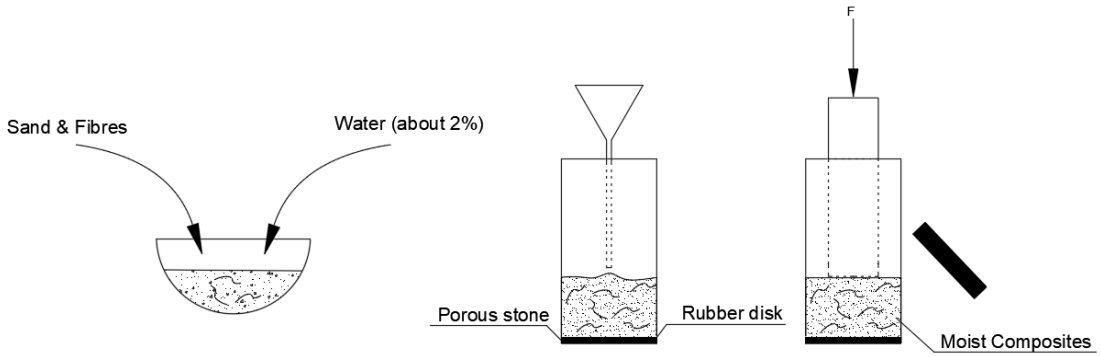

(b)

Fig. 6.3 Illustration of the sample preparation methods: (a) Moist tamping and (b) Dry vibration

During the sample preparation, slight vacuum pressure is applied to reduce the gap between the membrane and the mould (Fig. 6.4). Finally, vertical compaction is applied to achieve the required soil density for MT samples. When the samples are prepared using moist vibration, no extra water is added, and the soil is compacted by applying a fixed vertical load on the top and tapping on the side of the mould (Fig. 6.3b). Enlarged and lubricated end platens are applied to reduce the end constraint to the samples. The samples are flushed with CO_2 after they are set up in the triaxial cell. Saturation is then carried out by increasing the backpressure, ensuring the *B*-value reaches at least 0.97 for each specimen.

Fig. 6.4 Application of suction between the membrane and mould

6.3 Test Results

A total of 20 drained triaxial compression tests have been carried out for investigating the effect of the sample preparation method on soil behaviour (Table 6.2). The initial void ratio e_0, which is the void ratio at the beginning of triaxial compression, varies between 0.82 and 0.76. The effective confining pressure σ_r is between 50kPa and 200kPa (Table 6.2). The fibre weight content w_f (ratio of fibre and dry sand weight) is 0.25%. The repeatability of the tests is shown in Figs. 6.5 and 6.6, where ε_a is the axial strain, q is the deviator stress and ε_v is the volumetric strain. It is found that the repeatability of experimental results for FRS was only obtained with the adoption

of a certain number of layers (Mandolini, 2011; Mandolini et al., 2019). This is because segregation of fibres may happen within a thick layer, leading to sample inhomogeneity and leaving unreinforced bands within the sample. For the present study, it is found that good result repeatability can be achieved with three layers.

Table 6.2 List of tests

Test ID	Preparation method	w_f(%)	e_0	σ_3 (kPa)
CD50_M_080	MT	-	0.803	50
CD100_M_080			0.808	100
CD100_M_075			0.761	
CD200_M_080			0.817	200
CD200_M_080_01			0.811	
CD200_M_075			0.756	
CD50_M_080_025		0.25	0.811	50
CD100_M_080_025			0.823	100
CD100_M_075_025			0.762	
CD200_M_080_025			0.806	200
CD200_M_075_025			0.773	
CD50_D_080	MV	-	0.815	50
CD100_D_080			0.812	100
CD100_D_075			0.758	
CD200_D_080			0.803	200
CD200_D_075			0.755	
CD100_D_080_025		0.25	0.822	100
CD100_D_075_025			0.772	
CD200_D_080_025			0.806	200
CD200_D_075_025			0.761	

Figs. 6.7 and 6.8 show the effect of sample preparation methods on the stress-strain relationship of pure sand. In most cases, a small difference in the $\varepsilon_a - q$ and $\varepsilon_a - \varepsilon_v$ curves can be observed for pure sand. Nevertheless, the sample preparation method has been found to have a more dramatic influence on the stress-strain relationship of sand in undrained tests (Sze and Yang, 2014) because a small difference

in the soil dilatancy can cause a significant change in the effective stress path of an undrained test. These samples were tested in undrained conditions, a more significant difference in the stress-strain relationship would be expected. A direct comparison of the behaviour of sand and FRS is shown in Figs. 6.9 and 6.10. At the same initial void ratio and confining pressure, FRS shows much higher shear strength and less volume expansion.

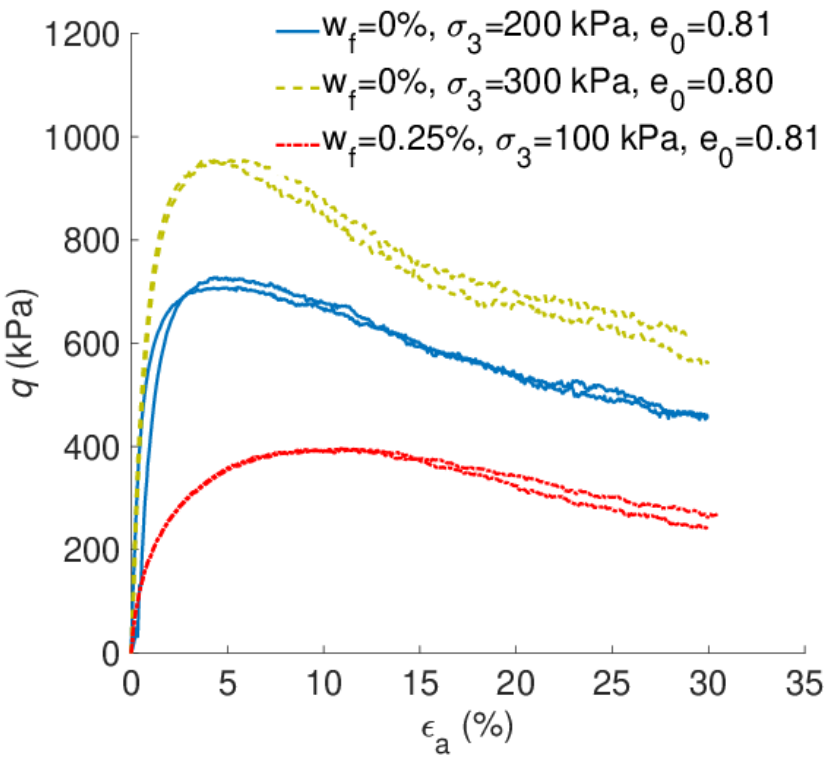

(a)

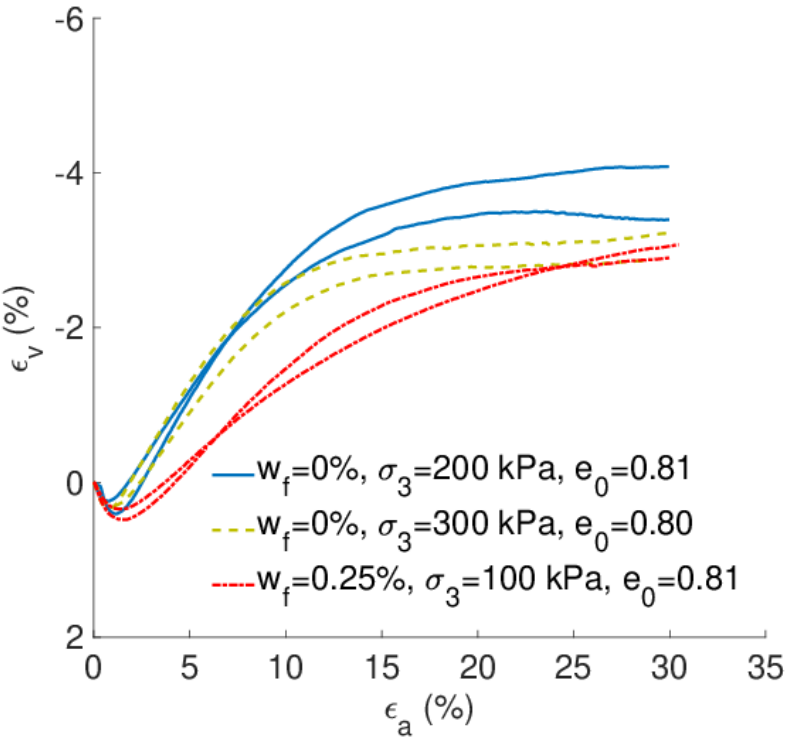

(b)

Fig. 6.5 Repeatability of the tests on MT samples with $\sigma_3 = 100 - 300$kPa: (a) the $\varepsilon_a - q$ relationship and (b) the $\varepsilon_a - \varepsilon_v$ relationship

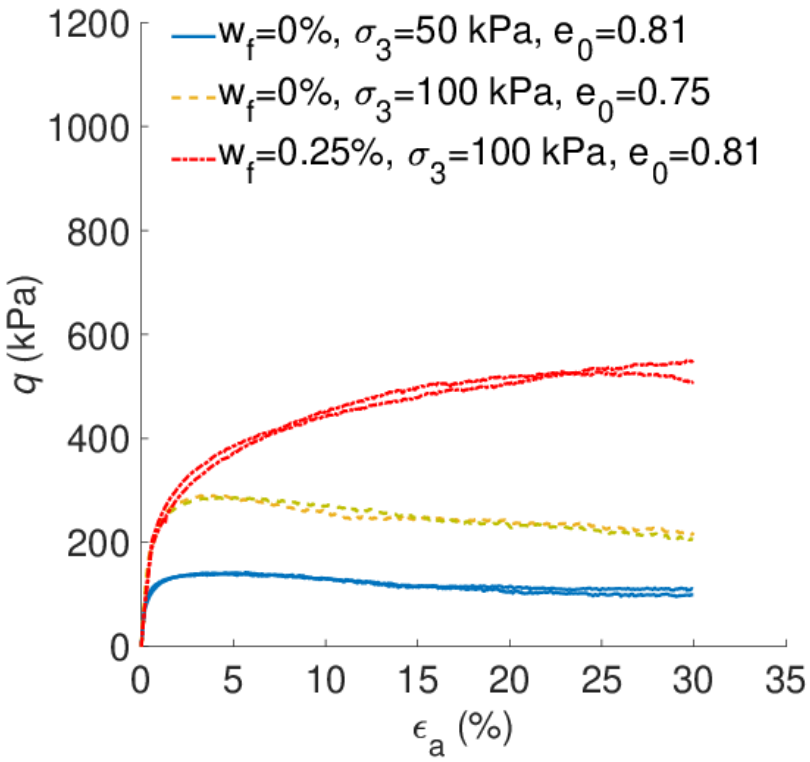

(a)

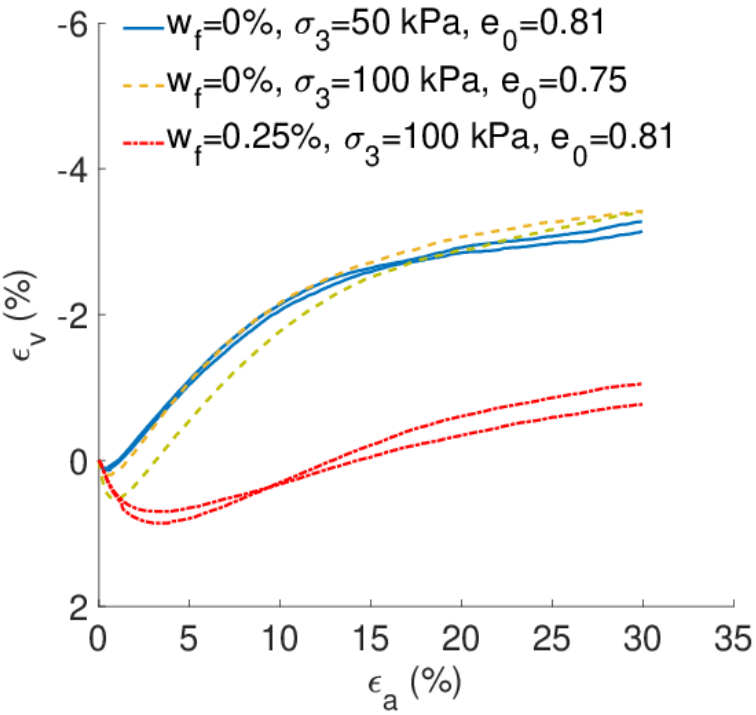

(b)

Fig. 6.6 Repeatability of the tests on MV samples with $\sigma_3 = 50 - 100$kPa: (a) the $\varepsilon_a - q$ relationship and (b) the $\varepsilon_a - \varepsilon_v$ relationship

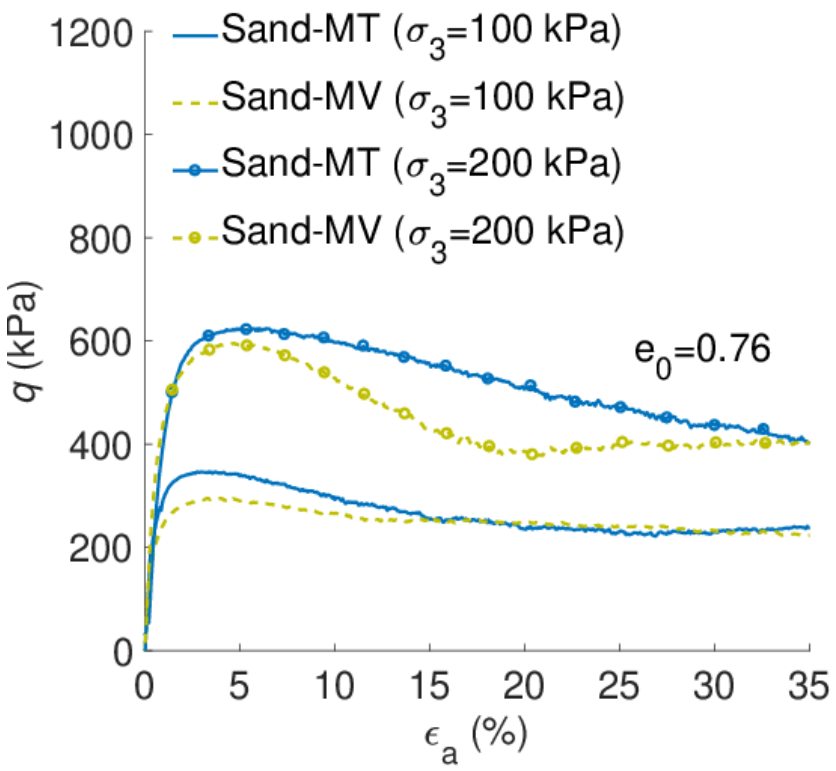

(a)

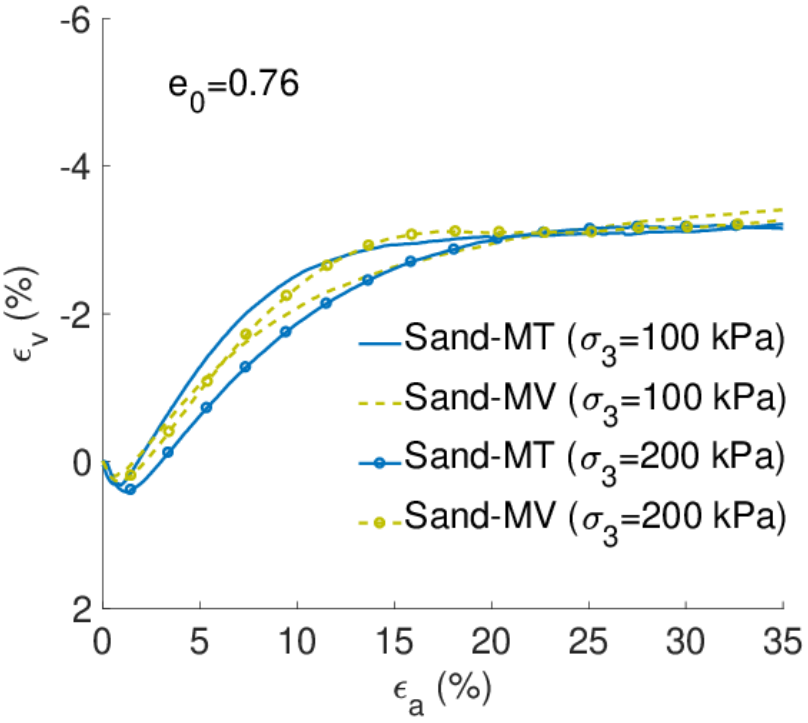

(b)

Fig. 6.7 Effect of the sample preparation method on mechanical behaviour of pure sand with $e_0 = 0.76$: (a) $\varepsilon_a - q$ relationship and (b) $\varepsilon_a - \varepsilon_v$ relationship

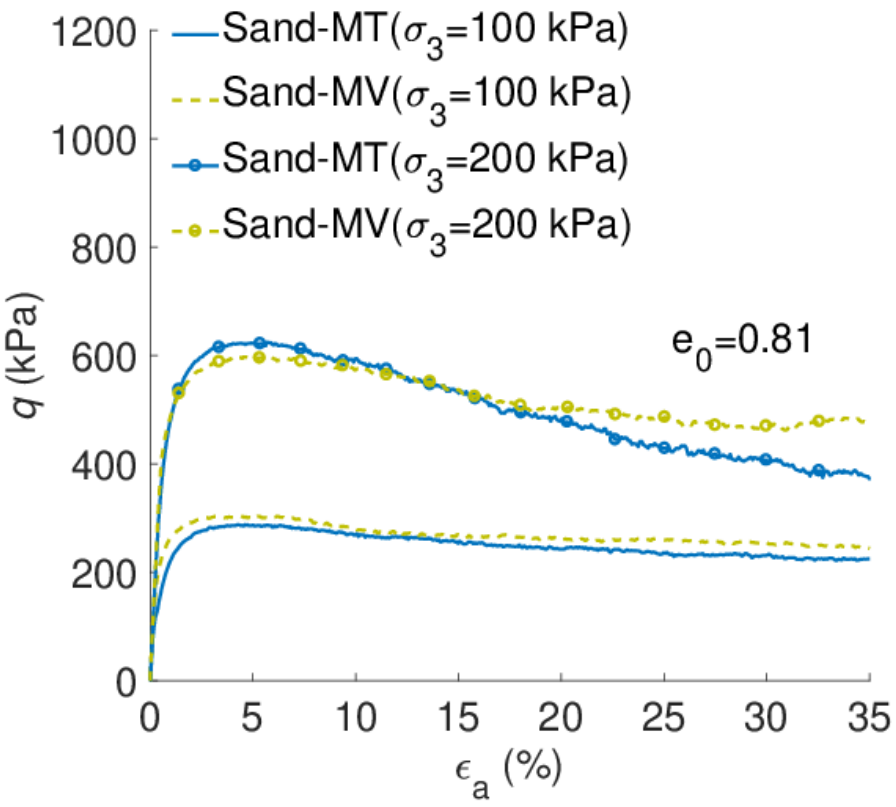

(a)

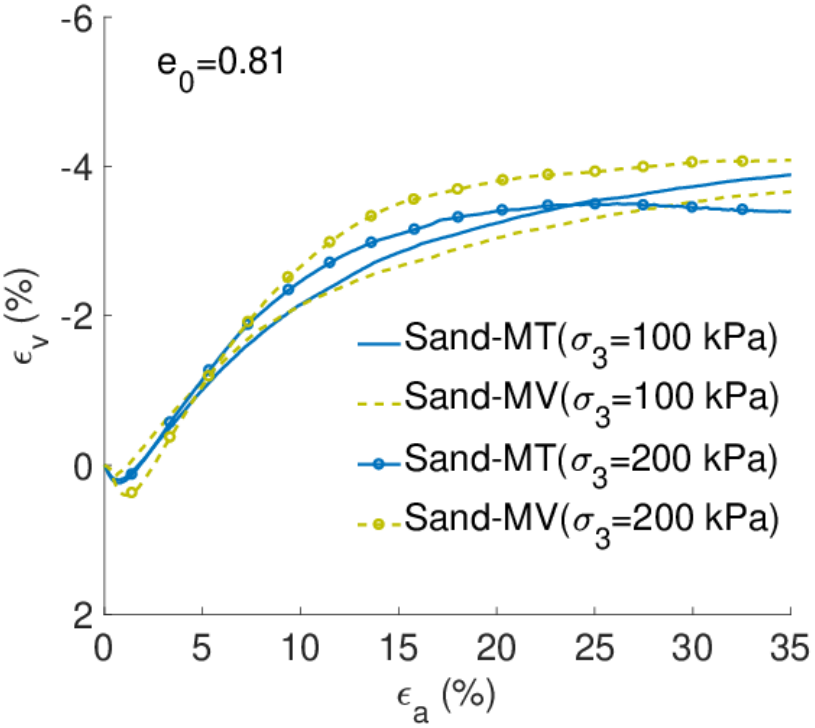

(b)

Fig. 6.8 Effect of the sample preparation method on the mechanical behaviour of pure sand with $e_0 = 0.81$: (a) $\varepsilon_a - q$ relationship and (b) $\varepsilon_a - \varepsilon_v$ relationship

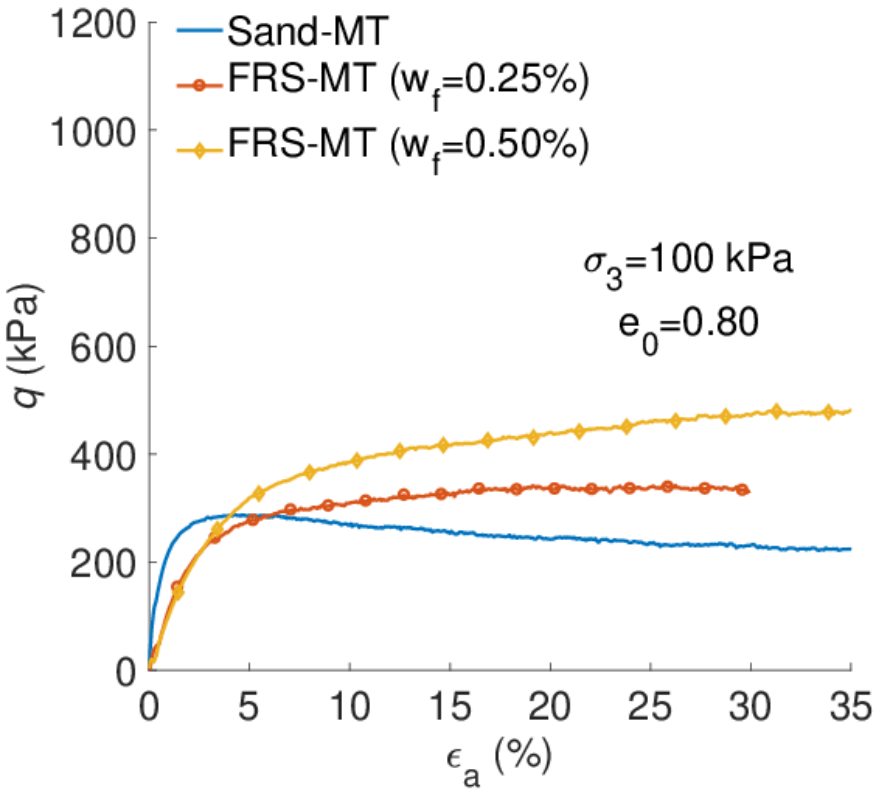

(a)

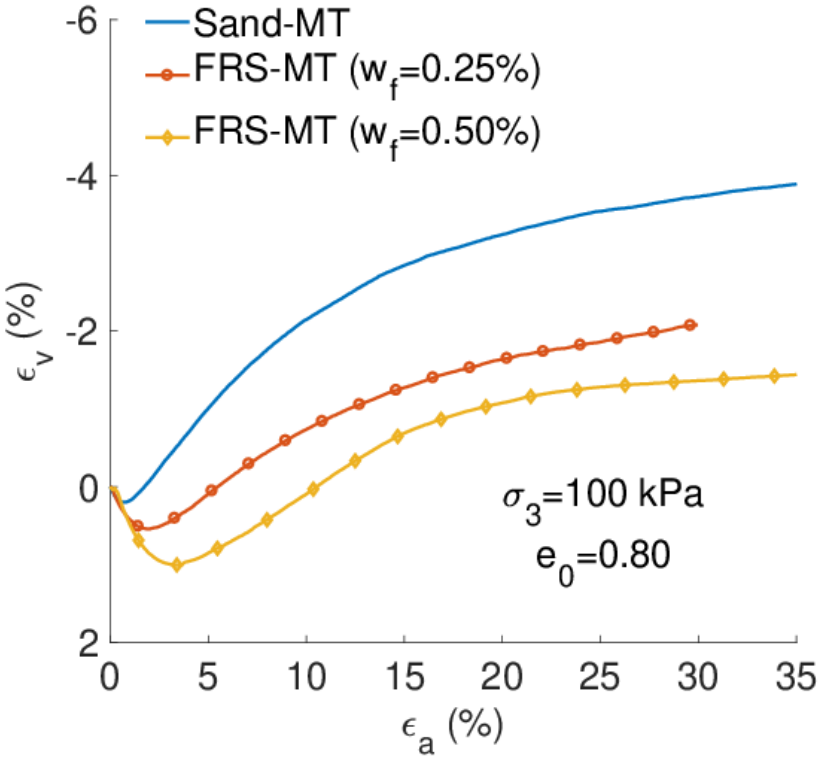

(b)

Fig.6.9 Effect of fibre content on the behaviour of fibre-reinforced sand prepared using the MT method: (a) $\varepsilon_a - q$ relationship and (b) $\varepsilon_a - \varepsilon_v$ relationship

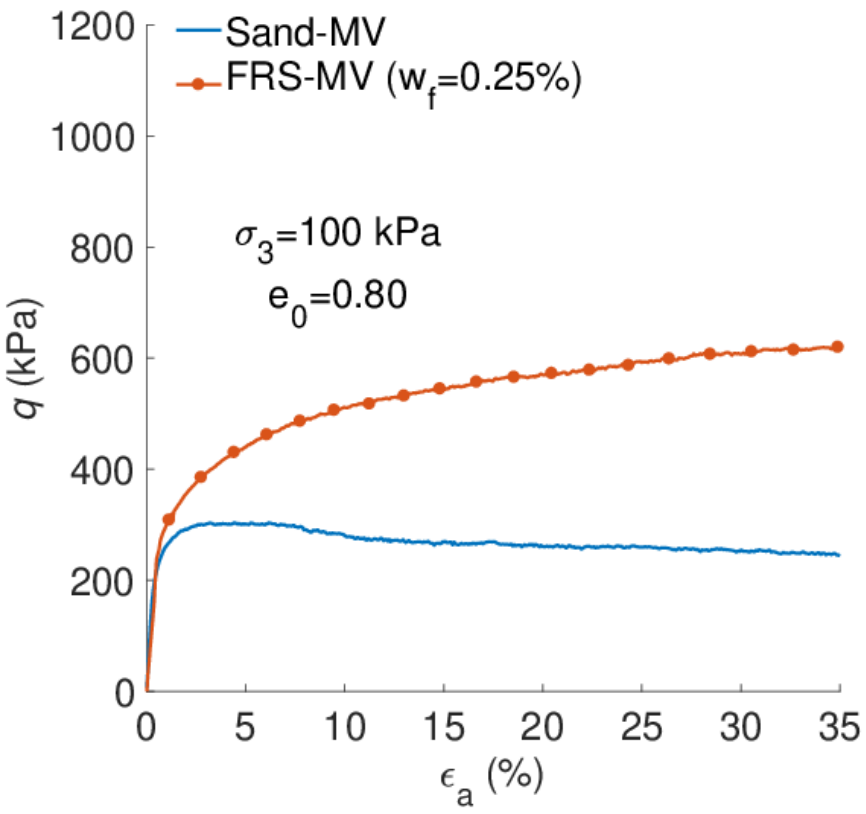

(a)

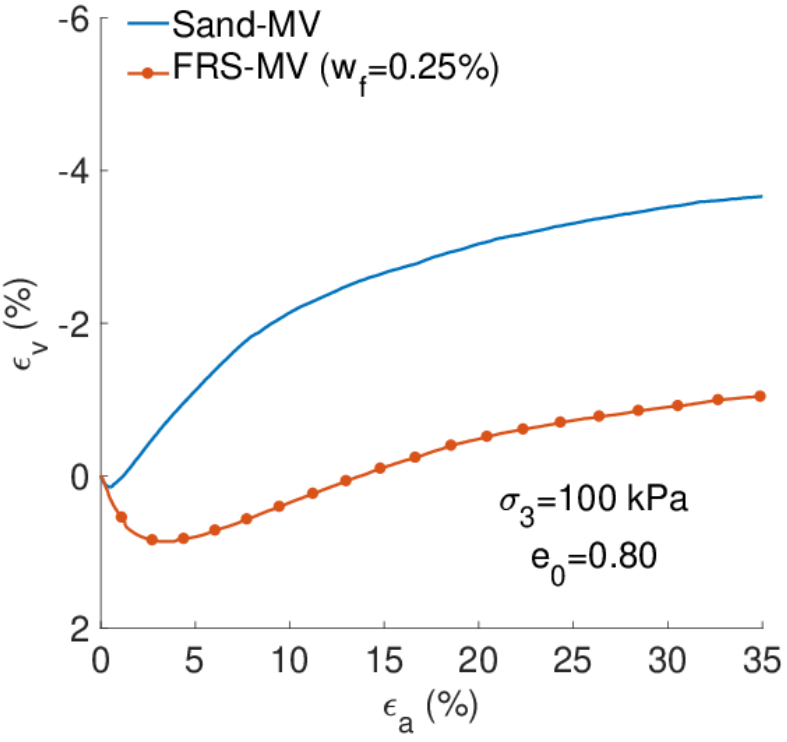

(b)

Fig. 6.10 Effect of fibre content on the behaviour of fibre-reinforced sand prepared using the MV method: (a) $\varepsilon_a - q$ relationship and (b) $\varepsilon_a - \varepsilon_v$ relationship

Figs. 6.11 and 6.12 show the stress-strain relationship of FRS with different sample preparation methods. There is a significant difference in both the $\varepsilon_a - q$ and $\varepsilon_a - \varepsilon_v$ relationships. Under the same initial condition, the MV samples show a less dilative response and much higher shear strength. The peak deviator stress of the MV sample is 30%-50% higher than that of the MT sample with the same initial stress state and void ratio. In particular, the ultimate strength for the MV sample with confining pressure of 100 kPa is almost the same as that of the MT sample with confining pressure of 200 kPa (Fig. 6.11). Most of the MV samples do not show strain softening at even very large axial strain. The shear stiffness of MV samples is also higher, indicating that the fibre-reinforcement to the soil stiffness and strength is more significant. This indicates that a method similar to the MV in this study should be used in compacting FRS in the field to achieve the largest possible increase in soil strength. Fig. 6.13 shows the failure envelope for FRS prepared using the MT and MV methods. It is well known that the failure envelope of FRS is curved, and the mobilised peak friction angle decreases as the mean effective stress increases (Diambra and Ibraim, 2015; Ibraim et al., 2012). Since all the tests have been carried out with the confining pressure over 100 kPa, the failure envelope of FRS at low mean effective stress cannot be obtained. Therefore, only the failure envelope with p >150 kPa is plotted in Fig. 6.13. More tests should be done to get the failure curves at low mean effective stress. Prediction of the failure criterion proposed by Gao and Zhao (2013) is also shown in Fig. 6.13. Two parameters c and κ in this failure criterion will also be used in the constitutive model below.

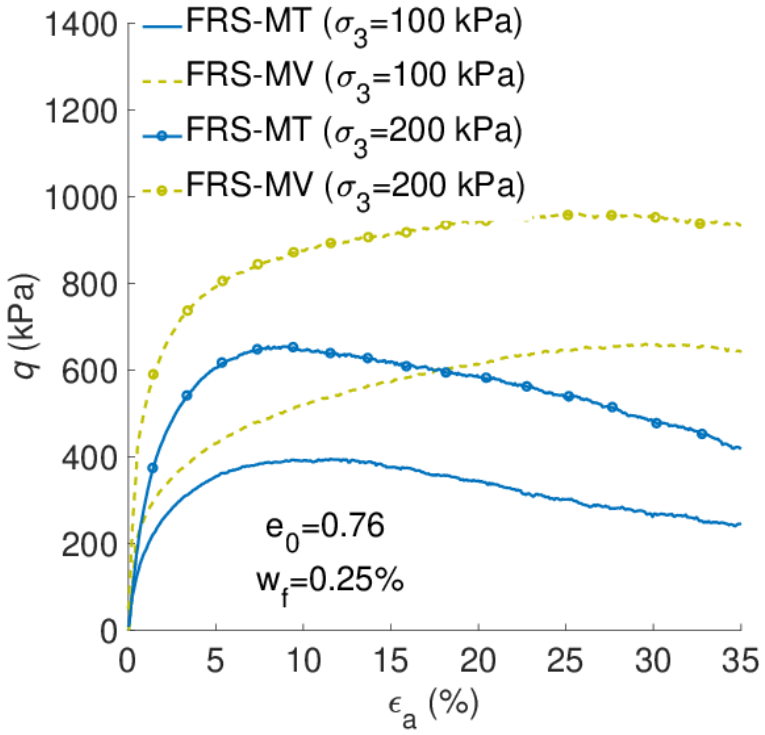

(a)

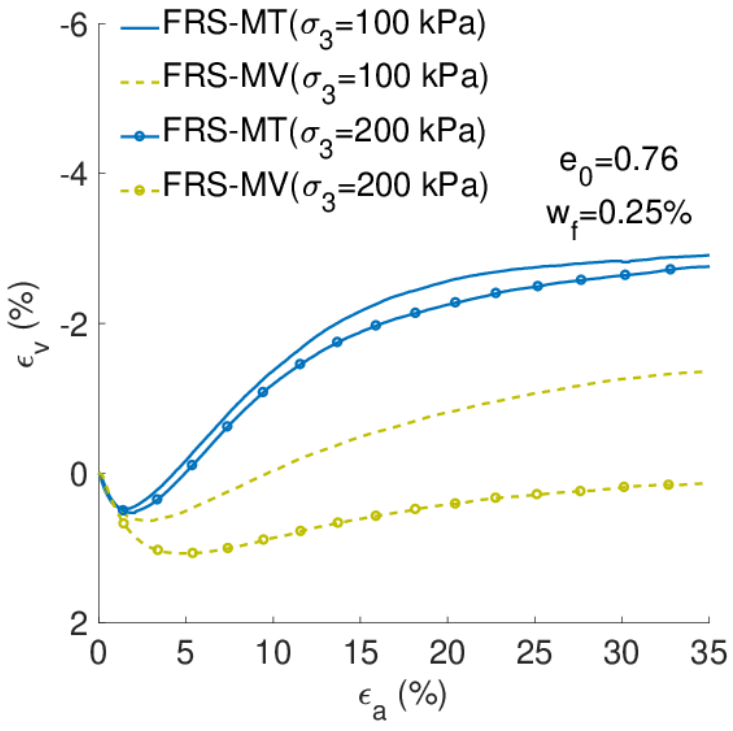

(b)

Fig. 6.11 The comparing results of FRS with different preparation methods under the confining pressure of 100 and 200 kPa ($e_0 = 0.76$): (a) the $\varepsilon_a - q$ relationship and (b) the $\varepsilon_a - \varepsilon_v$ relationship

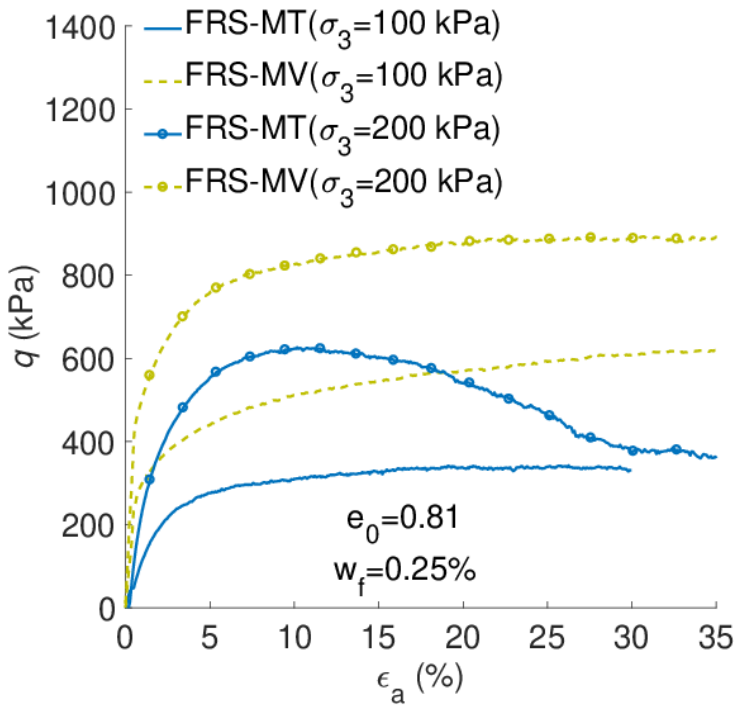

(a)

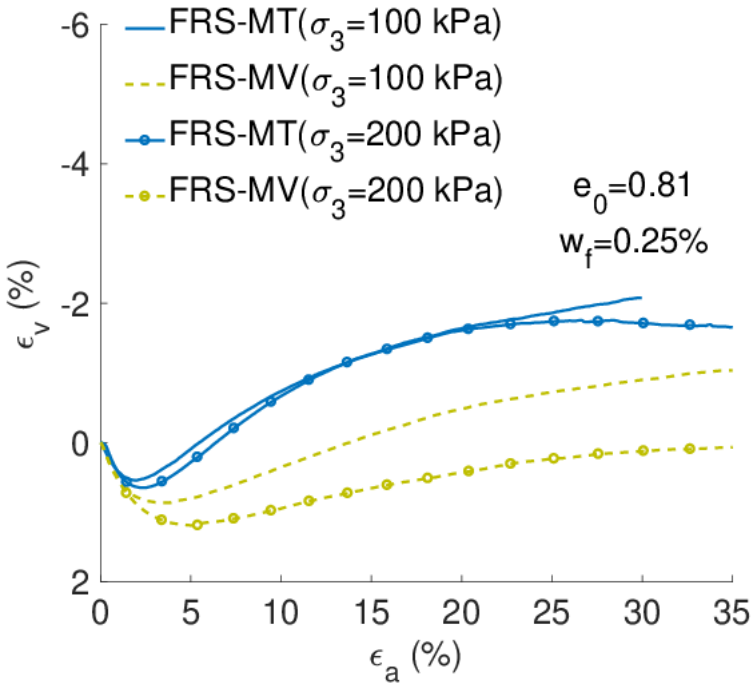

(b)

Fig. 6.12 The comparing results of FRS with different preparation methods under the confining pressure of 100 and 200 kPa ($e_0 = 0.81$): (a) the $\varepsilon_a - q$ relationship and (b) the $\varepsilon_a - \varepsilon_v$ relationship

The results in Figs. 6.11 and 6.12 are different from those in Ibraim et al. (2012), where a small difference in MT and MV samples' behaviour has been observed. While the MT method in the present study is similar to that used in Ibraim et al. (2012), the MV method is different. First, only 2% of water content is used during sample preparation in this study, compared to 10% in Ibraim et al. (2012). Secondly, the sample is densified by tamping the side of the mould with a fixed vertical loading on top of the soil in this present study. However, dynamic compaction in the vertical direction is used in Ibraim et al. (2012). Both the initial water content and compaction method can affect the fibre orientation, which affects the mechanical behaviour of FRS. Unfortunately, the fibre distribution in FRS has not been measured in the present study. Future work will be done to measure how the MT and MV methods used in this study affect the fibre orientation distribution using the method proposed by Ibraim et al. (2012). Thirdly, more fibres could be under tension at the end of sample preparation when the samples are prepared using the MV method in this study, as discussed in Consoli et al. (2005). This has a beneficial effect on the strength of FRS.

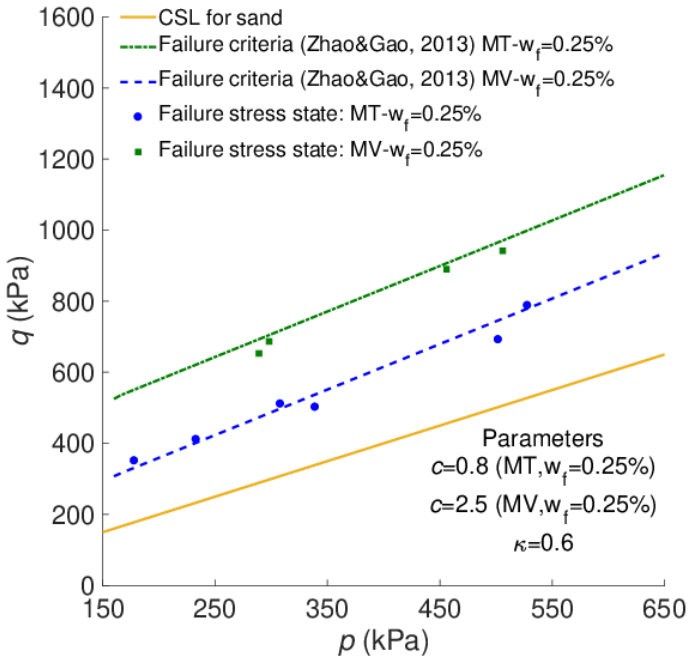

Fig. 6.13 The failure envelopes of FRS and prediction of the failure criterion proposed by Gao and Zhao (2013)

6.4 Model Simulation

Though the internal structure of FRS is affected by the fabric of both the sand skeleton and the fibres, the experimental evidence above shows that its mechanical behaviour is primarily affected by the fabric associated with the fibres. As introduced in Chapter 5, the model used in this study is developed based on the assumption that the strain of FRS is dependent on the deformation of the sand skeleton, while the effective skeleton stress (p^s and q^s) and effective skeleton void ratio e^s, which are only used for describing the mechanical response of FRS (dilatancy, plastic hardening and elastic stiffness).

There are 14 parameters used in this model, 11 of which are for the host sand (e.g., Li & Dafalias, 2000). Since the sample preparation method is found to have a negligible influence on the behaviour of pure sand, the same parameters are used for sand prepared using MT and MV. The method for determining the sand parameters can be found in Li and Dafalias (2000). Once the model parameters for pure sand have been determined, the rest can be determined based on the triaxial compression test results on FRS (Gao et al., 2020). Specifically, the parameters c and κ should be determined based on the strength of FRS. μ should be determined to fit the shear stress and strain relationship of FRS. Finally, the parameter x can be obtained based on the dilatancy of FRS. All the model parameters are listed in Table 6.3.

Table 6.3: Model parameters

Parameters		FRS (MT)	FRS (MV)
Sand	G_0	150	
	ν	0.2	
	M_c	1.28	
	p_a	101	
	e_Γ	0.89	
	λ_c	0.010	
	ξ	0.7	
	n	2.0	
	ζ	0.8	
	d	0.90	
	m	1.8	
FRS	x	7.3	8.8
	κ	0.6	0.6
	μ	6.0	9.0
	c	0.8	2.5

Figs. 6.14 to 6.16 show the model prediction of pure sand behaviour. In general, the model gives a satisfactory description of the experimental data. There is a slight overestimation of the volume expansion in some tests (Fig. 6.16). Better model predictions can be obtained by using different model parameters for MT and dry deposited sand (Yang et al., 2008). This will inevitably make the model more complex but may not improve FRS predictions, which is the focus of this study.

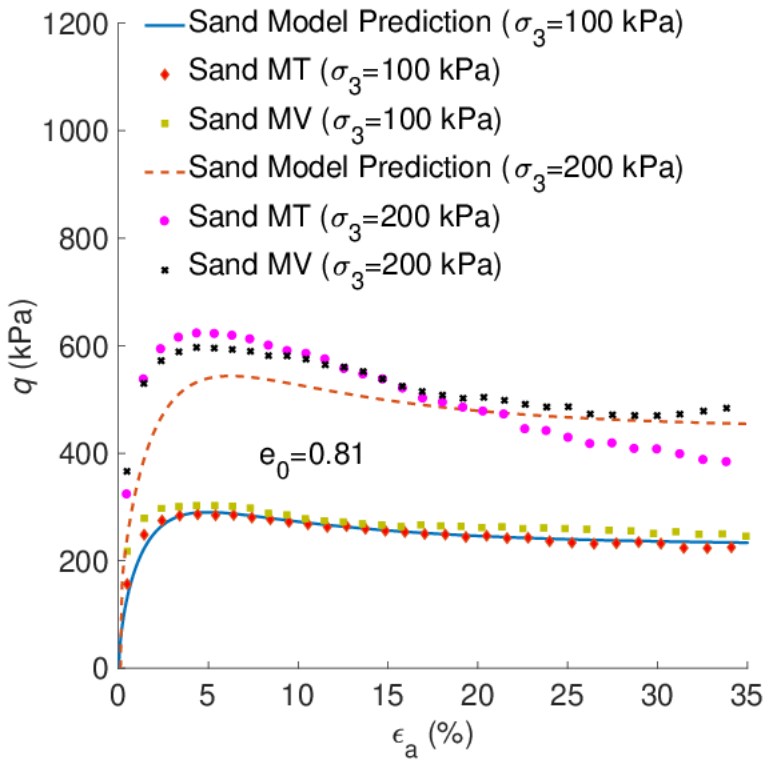

(a)

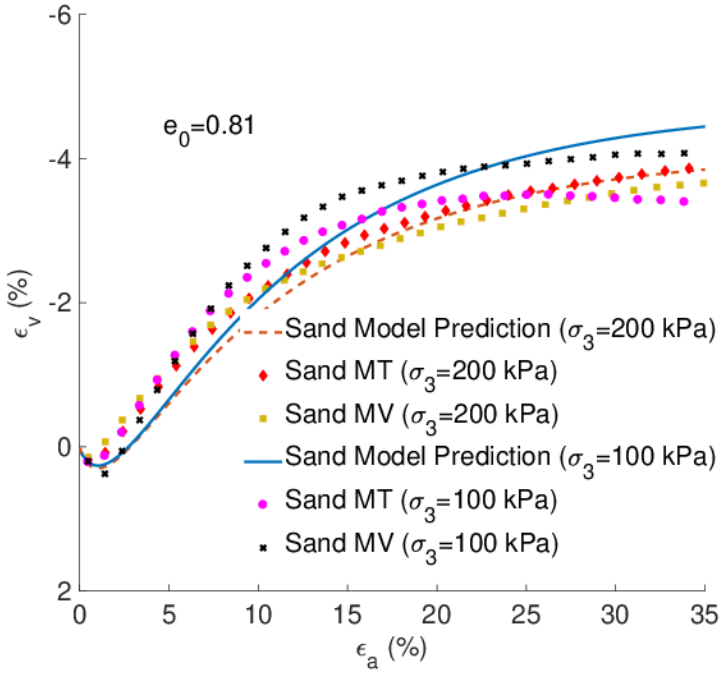

(b)

Fig. 6.14 Model prediction for the behaviour of pure sand in drained triaxial compression with $e_0 = 0.81$: (a) the $\varepsilon_a - q$ relationship and (b) the $\varepsilon_a - \varepsilon_v$ relationship

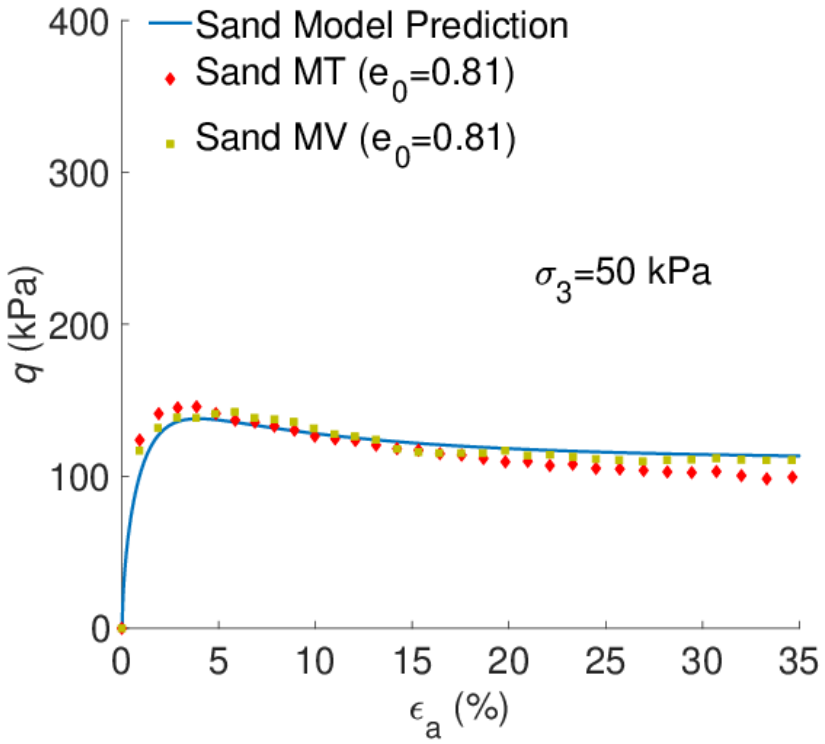

(a)

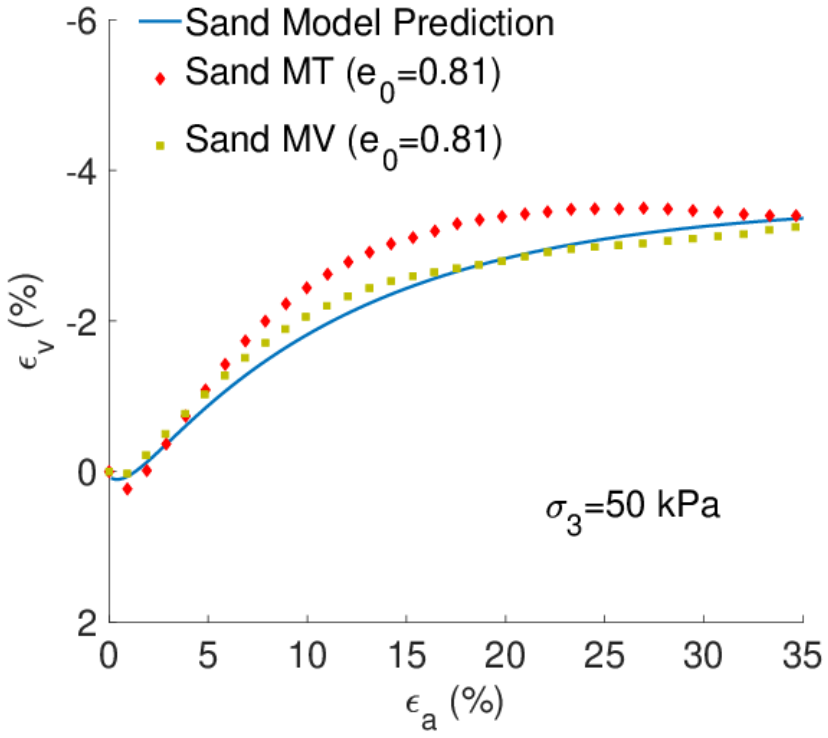

(b)

Fig. 6.15 Model prediction for the behaviour of pure sand in drained triaxial compression with $\sigma_3 = 50$kPa and $e_0 = 0.81$: (a) the $\varepsilon_a - q$ relationship and (b) the $\varepsilon_a - \varepsilon_v$ relationship

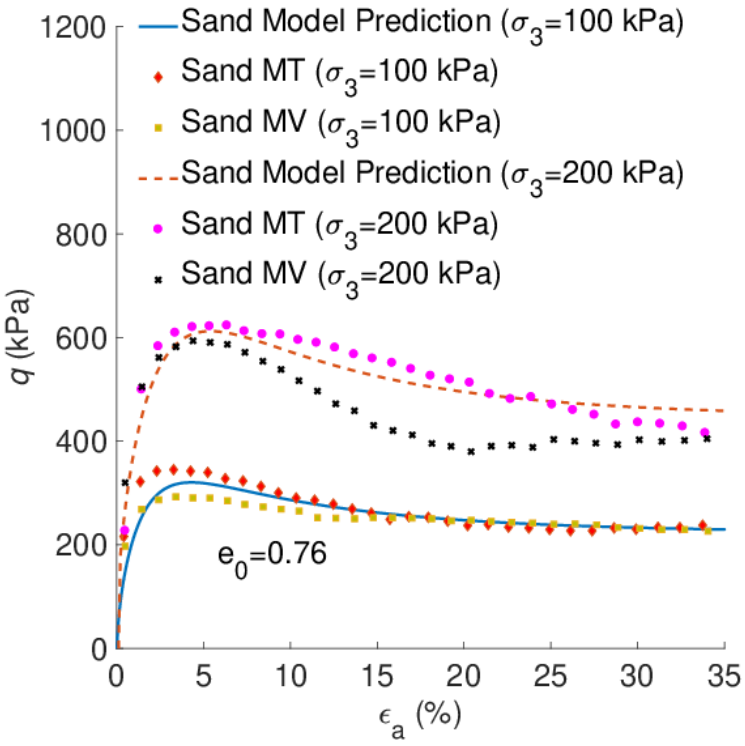

(a)

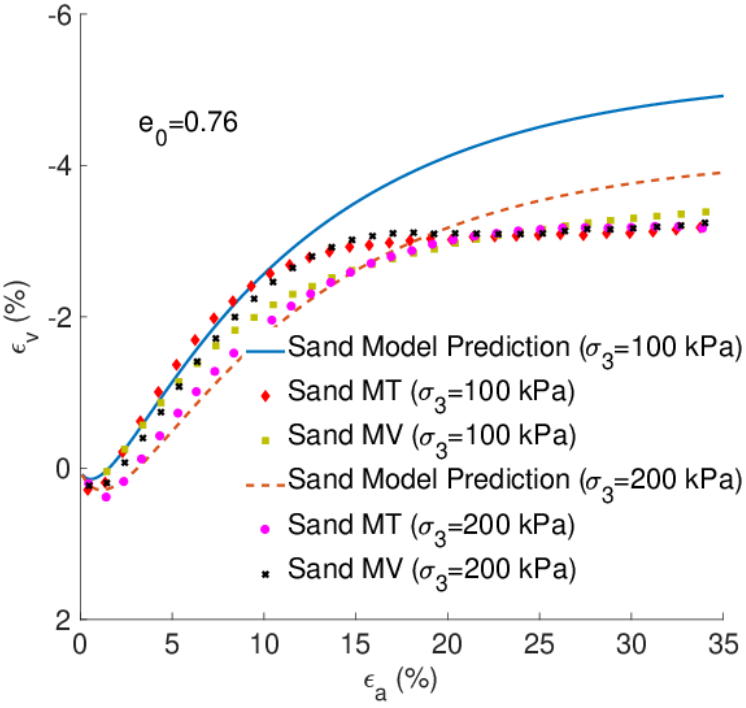

(b)

Fig. 6.16 Model prediction for the behaviour of pure sand in drained triaxial compression with $e_0 = 0.76$: (a) the $\varepsilon_a - q$ relationship and (b) the $\varepsilon_a - \varepsilon_v$ relationship

Figs. 6.17-6.20 show the comparison between test data and model prediction of FRS prepared using MT and MV. The model prediction is better for the MT samples. For the MV samples, the model tends to give lower deviator stress before failure. This could be due to the model not being able to describe the evolution of mean effective skeleton stress p_f with strain, which has also been discussed in Gao et al. (2020). The four parameters for FRS can be used to infer the difference in the internal structure of FRS (Table 6.5). The value of x is bigger for FRS prepared using the MV method, which means that the effective skeleton void ratio e^s is higher for the MV samples when the fibre content and global void ratio are the same (Gao et al., 2020). This could be caused by the structure of the sand skeleton and distribution of fibres, which can be better understood using X-ray computed tomography studies (Soriano et al., 2017). The parameters c and μ which describe the fibre reinforcement to soil strength and stiffness, are also higher for the FRS prepared using the MV method. A larger c means that a larger shear strength increase is achieved when the samples are prepared by the MV method (Figs. 6.17-6.20). A larger μ makes the shear stiffness of FRS higher, indicating faster development of the fibre-reinforcement. Both c and μ are mainly affected by the distribution of fibre orientation in FRS (Ibraim et al., 2012). They are bigger when more fibres orient in the horizontal direction. However, in the study of Ibraim et al. (2012), it was shown that the different preparation methods did not produce a significantly different distribution of fibre orientation. A micromechanical study is thus needed to find out the reason for the difference in these parameters here.

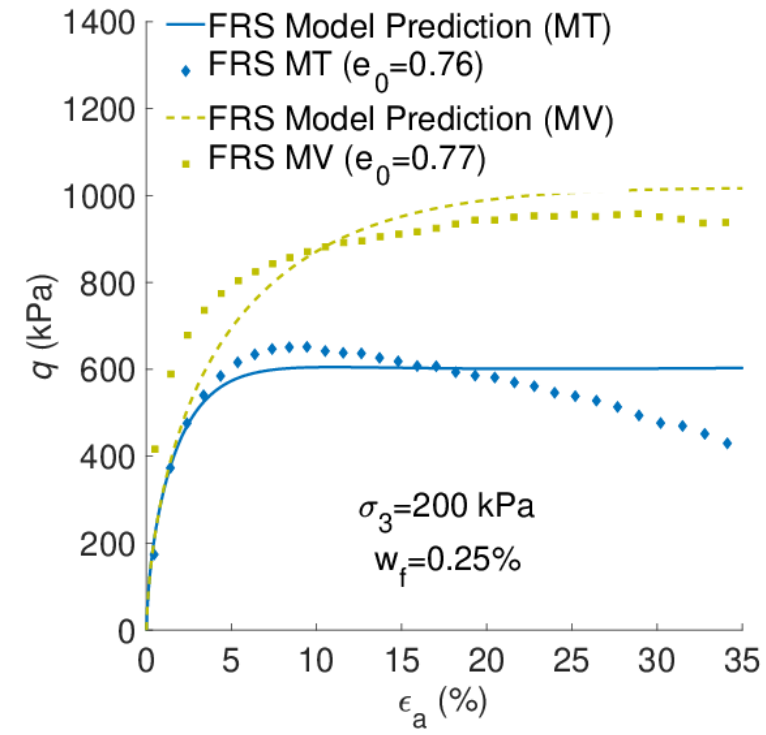

(a)

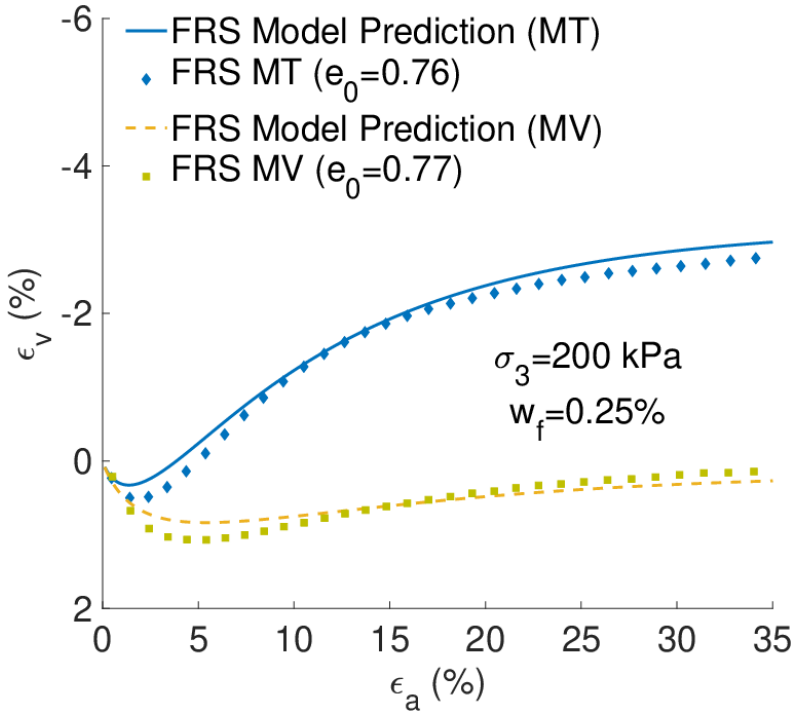

(b)

Fig. 6.17 Model prediction for the behaviour of FRS in drained triaxial compression with $\sigma_3 = 200$kPa and $e_0 \approx 0.76$: (a) the $\varepsilon_a - q$ relationship and (b) the $\varepsilon_a - \varepsilon_v$ relationship

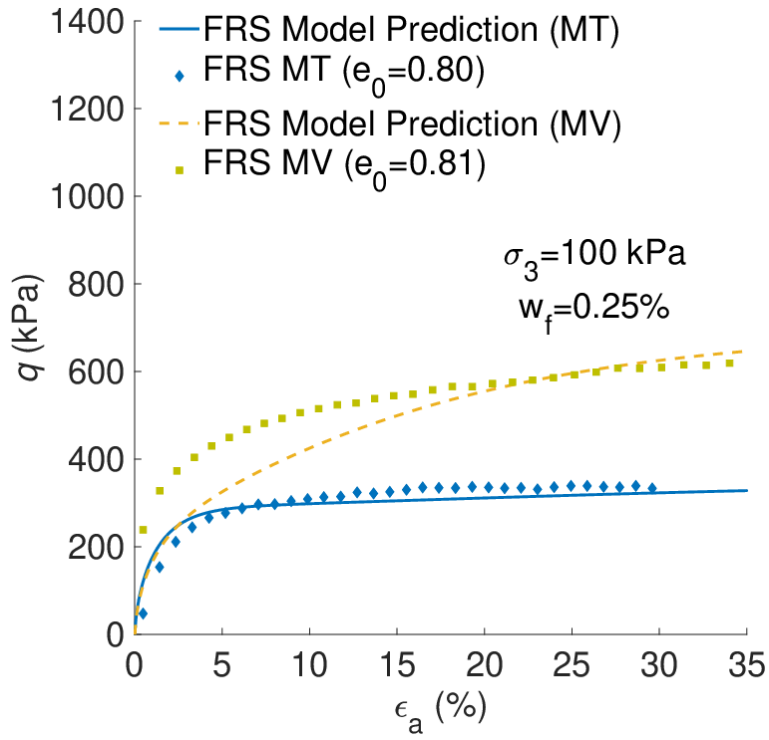

(a)

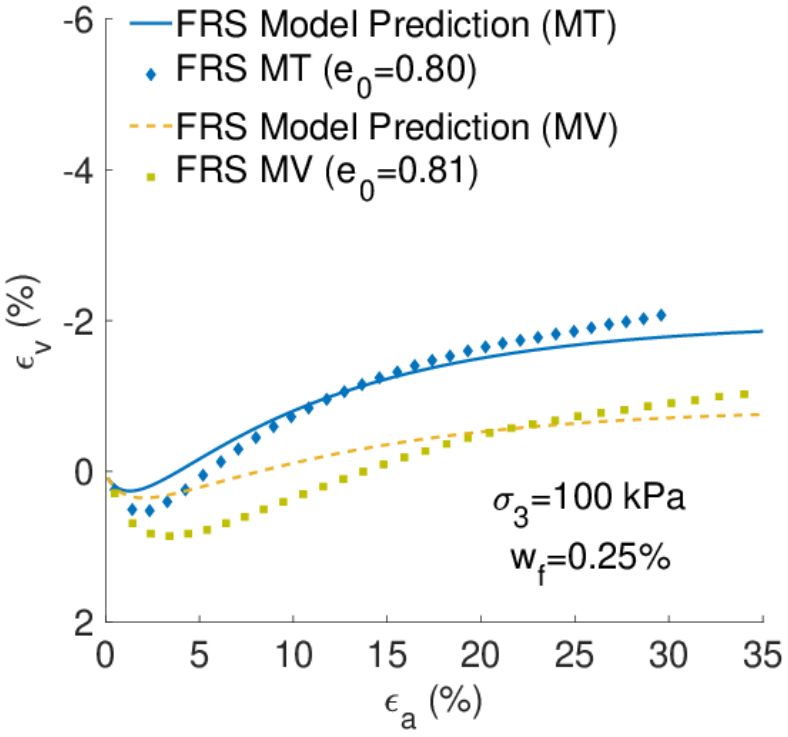

(b)

Fig. 6.18 Model prediction for the behaviour of FRS in drained triaxial compression with $\sigma_3 = 100$kPa and $e_0 \approx 0.81$: (a) the $\varepsilon_a - q$ relationship and (b) the $\varepsilon_a - \varepsilon_v$ relationship

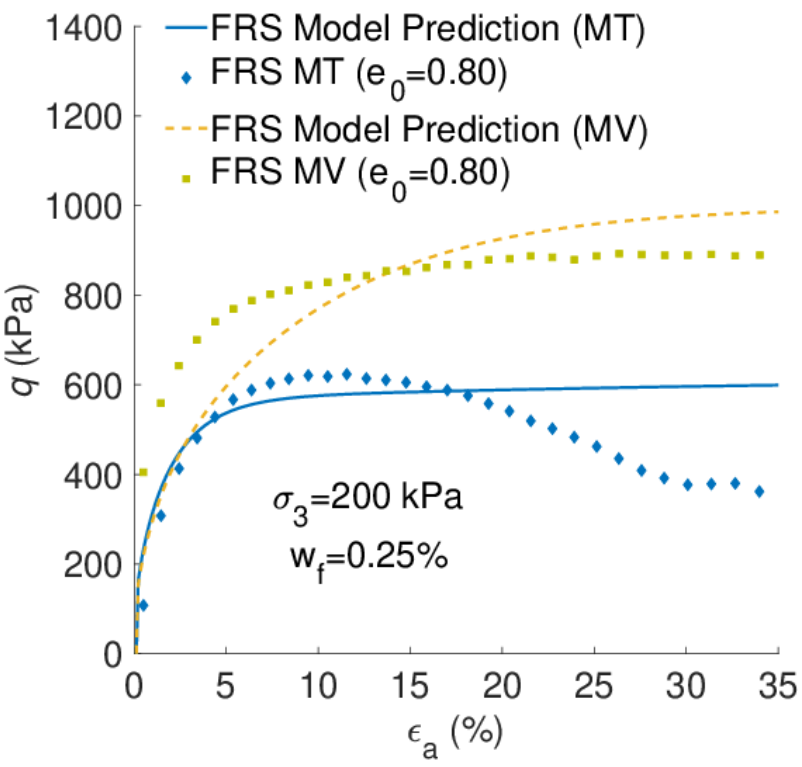

(a)

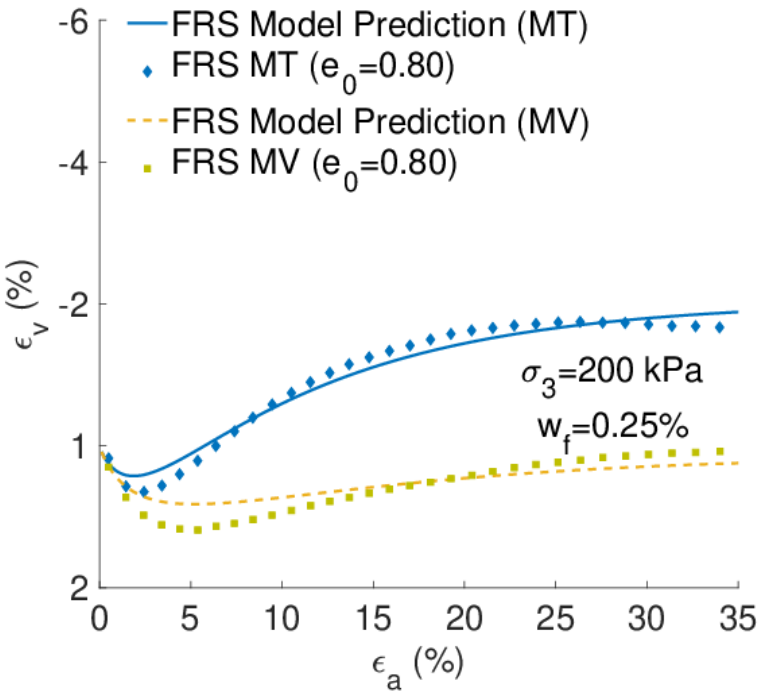

(b)

Fig. 6.19 Model prediction for the behaviour of FRS in drained triaxial compression with $\sigma_3 = 200$kPa and $e_0 \approx 0.80$: (a) the $\varepsilon_a - q$ relationship and (b) the $\varepsilon_a - \varepsilon_v$ relationship

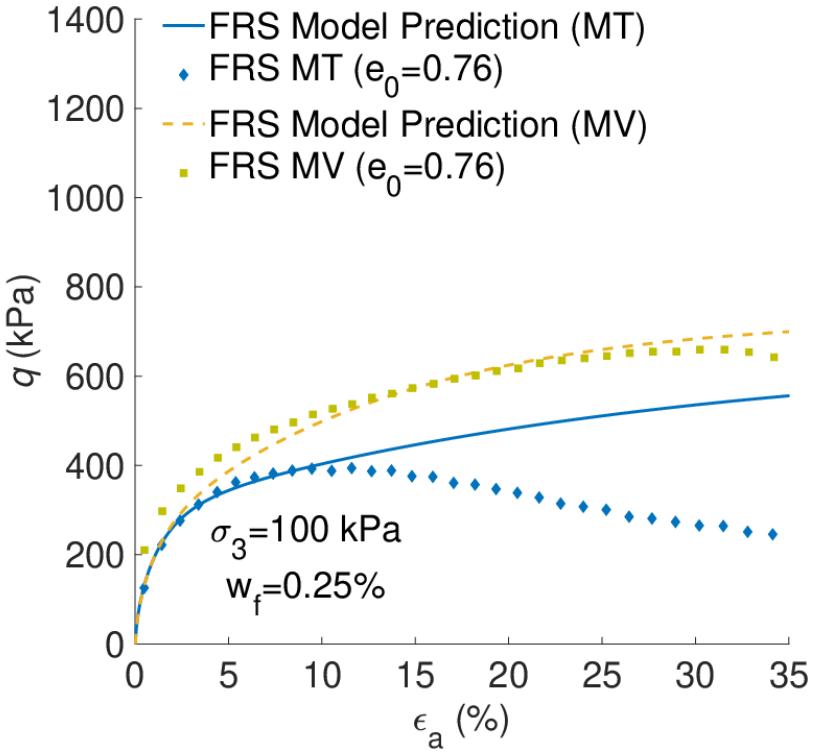

(a)

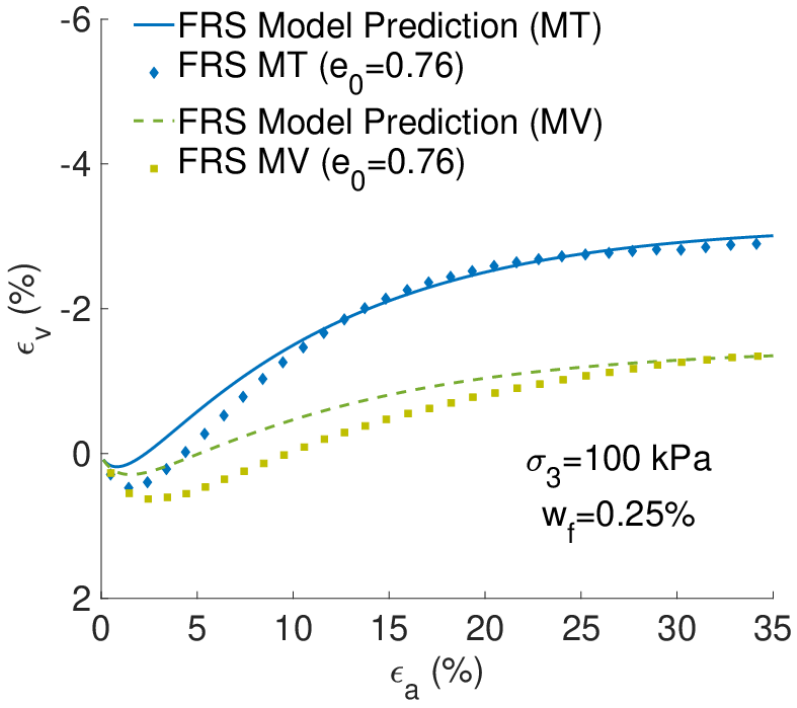

(b)

Fig. 6.20 Model prediction for the behaviour of FRS in drained triaxial compression with $\sigma_3 = 100$kPa and $e_0 = 0.76$: (a) the $\varepsilon_a - q$ relationship and (b) the $\varepsilon_a - \varepsilon_v$ relationship

6.5 Summary

The sample preparation method's effect on the mechanical behaviour of FRS has been studied using drained triaxial compression tests. The samples are prepared using MT and MV methods. The stress-strain relationship of pure sand appears to be insensitive to the sample preparation method. The mechanical behaviour of FRS is dramatically affected by the sample preparation methods, with the MV samples showing a less dilative response and higher shear strength under otherwise identical conditions. A newly developed constitutive model has been used to describe the stress-strain relationship of FRS. Some of the parameters for FRS have to be changed when the sample preparation method changes.

There are three main features for the proposed model compared with the previous constitutive model. As discussed in Chapter 2, most of models analyse the effect of fibre on the mechanical behaviour of FRS through the microstructure. Instead, the proposed constitutive model developed in this study analyse fibre based on the deformation of sand skeleton. Firstly, the proposed constitutive model can reflect other general factors that affect the mechanical behaviour of FRS such as sample preparation method, void ratio and fibre content through the parameter c and x. On the other hand, the model parameters used in the model can be easily obtained based on the testing data. Finally, the model can be suitable for most conventional triaxial test types (e.g., drained, undrained compression and extension).

Future research will be done on the following aspects. Firstly, research will be done on the internal structure of FRS at the microscale (interaction between sand particles and fibres and fibre distribution) using both experimental and numerical studies. These studies will help us understand how sample preparation methods affect the soil structure and stress-strain relationship. Additionally, the present research has focused

on the mechanical behaviour of saturated sand and FRS. But the unsaturated condition can be of importance in the field, where the soil is subjected to drying and wetting cycles. Therefore, research will be done to find out how the capillary force caused by unsaturation affects the behaviour of FRS (Yao et al., 2009; Melnikov et al., 2016; Liu et al., 2020).

Chapter 7: Conclusions

This thesis is divided into four main parts. Firstly, triaxial drained compression tests are conducted to understand the mechanical behaviour of host sand and fibre-reinforced soil (FRS). A new constitutive model is then introduced to describe the effect of fibres on the sand skeleton. Finally, the model is validated using the triaxial test data, and the effect of sample preparation methods on the behaviour of FRS is highlighted.

The literature review mainly focuses on the properties of fibre, soil and many constitutive models for FRS. Many of materials originating from natural, synthetics and waste sources can be used to reinforce the soil because of properties such as high shear resistance and low environmental impact. Therefore, FRS has been used in reinforcing embankments, slopes and roads. The effects of soil properties such as water content, particle size on the behaviour of FRS are highlighted. A change in those properties could induce significant changes in the behaviour of soil. Additionally, potential factors that may affect the reinforcement of the soil such as the range of fibre length and fibre content are discussed.

Many previous constitutive models have been introduced. Due to the complex internal structure of FRS, it can be analysed from several aspects, such as a simple force-equilibrium-based analysis, an energy-based homogenisation technique or kinematic-based analysis. These modelling analyses mainly focus on describing the relationship between fibre and soil particle through the microstructure. However, a complicated internal structure implies the original structure is changed, resulting in a series of change in other aspects (e.,g: void ratio, volume change). Therefore, those models that focus on analysing the fibre effect but neglecting the effect of the soil particle might not predict the evolution of FRS accurately.

Based on such observations in above constitutive models, fibre orientation has become a crucial direction to explore the internal interaction of FRS. Most studies indicate that different fibre orientation can induce different evolutions of FRS under

stress, especially in volume change. Although the structure of the constitutive model includes the analysis of fibre and soil particle, other physical impacts such as fibre entanglement and the use of lubrication technique are likely to be the main reasons of disagreement between experimental data and model predictions.

Hostun sand and polypropylene fibre are used in the experiments conducted in this study. All the testing samples including host sand and FRS are prepared using the moist-tamping technique (MT). During the test, the lubrication technique is applied to achieve homogeneous stress distribution and a uniform deformation of the sample. It is noted the effect of the membrane has been discussed but did not apply in the project, as the membrane correction has been included in the 'Clips Studio' software. The testing results are analysed through comparison in stress-strain relationship, shear strength, dilatancy and critical state. The findings are listed below:

1. Test repeatability can improve the reliability of the test results. The sensitivity of volume change has been proven in the repeated tests, in which a significant variability in volume change occurs, even though all the testing conditions are the same.
2. The mean diameter (D_{50}) and coefficient of uniformity (C_u) of soil also affect the shear strength. The friction angle and cohesion are different, depending on the sand type. However, both are changed with fibre content and water addition during sample preparation.
3. The confining stress affects the shear strength and volume change, where higher confining stress induces higher shear strength and less dilations.
4. The interaction between fibre and particle depends on the soil density and confining stress. A dense sample indicates more contact force generated between soil and fibre. Also, the strength improvement of soil is proportional to fibre content.
5. Fibre inclusion not only increases the shear strength of FRS, but also reduces the initial stiffness. Besides, the increase in shear strength is attributed to the increase of friction angle and cohesion caused by fibre.

6. The strain-softening behaviour is only observed at the reinforced sample with 0.25% of fibre content. Therefore, it is suggested higher fibre contents (w_f>0.3%) are used to avoid localised soil failure. Also, dilatancy is used to discuss the strain behaviour. It is found that strain behaviour exhibits softening when the volume change shows more dilation or otherwise.
7. The critical state line can be determined based on the testing results and exhibited through the $e - p'$ or $p' - q$ plane. The critical state line of FRS changes with fibre content due to fibre inclusion.

A new constitutive model for FRS has been introduced, using four model parameters: c, κ, μ and x, which are the first introduced to characterise the fibre inclusion on the mechanical behaviour of sand. However, the strain of FRS only depends on the deformation of the sand skeleton. There are 14 model parameters employed in the model, 10 of which are for host sand. All of them can be quickly determined based on triaxial test results. The determination of the rest of the model parameters (c, κ, μ and x) indicate that c and x are sensitive, as they are affected by many factors such as fibre content, fibre type and sample preparation method. Besides, it is noticed that the constitutive model for FRS is based on the model developed by Li and Dafalias (2000) for sand.

The model is validated by predicting the stress-strain relationship for four different sands in both drained and undrained triaxial tests with different stress paths. Most of the simulation results match the testing data well, even though some discrepancies are found in both the stress-strain and volume-strain relationship. In addition to external factors such as fibre entanglement and deviation in the void ratio, the evolution law of p_f is also the main reason for these discrepancies and will be the focus of future work.

Extensive work regarding the effect of sample preparation method on the mechanical response of FRS is carried out. The host and FRS samples are prepared using the moist-tamping (MT) and moist-vibration (MV) techniques, respectively. The testing results show the host sample prepared by the two methods, result in similar in shear stress

but slightly different in volume change behaviour. However, the mechanical behaviour of FRS is dramatically affected by the sample preparation methods, where MV samples showing a less dilative response and higher shear strength under identical conditions. The testing data is also used in validating the constitutive model. The simulation results show the model simulation can capture well the testing data partly. Meanwhile, it is found some of the model parameters for FRS have to be changed when the sample preparation method changed.

Based on these observations from the simulating results, it is concluded that for a given sand and fibre type, c appears to depend upon both fibre content and preparation method, μ and x appears to depend upon preparation method but not on fibre content, and κ appears to be independent of both fibre content and preparation method.

Recommendation for Further Work

This project's findings improve understanding of the fundamental mechanical response of FRS, knowing the basic mechanism of fibre to the soil. However, there are still several areas that need to be improved and developed:

Membrane Error

The effect of the membrane has been mentioned. The membrane thickness and elastic modulus have been studied previously, and these affect the deviatoric stress and volume change because of membrane penetration. Therefore, membrane correction should not be negligible, especially in triaxial undrained condition, in which a slight change in the void ratio would cause a remarkable change in $p' - q$ plane. Once membrane penetration is neglected, the volumetric change of the FRS sample cannot estimate the precise results, resulting in overestimating or underestimating the void ratio.

Otherwise, the test relating to the Young's modulus of membrane used in this project should be carried out. Meanwhile, those basic membrane parameters would be helpful in correcting the testing data.

Experimental Improvement

The testing results of the FRS sample prepared by MT and MV show different evolution in the stress-strain and volume-strain relationship compared with another study (Ibraim et al., 2012). Further work should investigate the distribution of fibre orientation by cutting the frozen FRS samples using a bench saw in the vertical and horizontal direction.

Theoretical Modelling

Although the model parameters c, κ, μ and x are the first employed in this study, there no formulation accounting for calculating the value accurately. For example, the parameter c can be modified for FRS with different fibre content or sample preparation method. Therefore, micromechanical analysis should be carried out to give a general expression for c.

Additionally, fibre orientation in FRS is highly anisotropic, which makes the mechanical behaviour of FRS dependent on the loading (or strain increment) direction. Therefore, a multiaxial model accounting for the effect of fibre orientation anisotropy should be developed.

This study has focused on the laboratory tests and constitutive modelling of FRS. The model is found to give reasonable prediction of FRS behaviour with different fibre content and host sand properties. The model can be implemented in an existing finite element software package like Abaqus to solve boundary value problems. Since the model is established based on the conventional plasticity theory, it can be implemented using some of the widely used stress integration methods, such as the

explicit or implicit stress integration methods (Potts et al., 2001). The numerical simulations can be better understanding how a slope or embankment built using FRS deforms. This information can then be used to improve the design, which will be the further work.

References

[1] Ahmad, F., Bateni, F., & Azmi, M. (2010). Performance evaluation of silty sand reinforced with fibres. *Geotextiles and Geomembranes, 28*(1), 93-99.

[2] Ahmad, F., Mujah, D., Hazarika, H., & Safari, A. (2012). Assessing the potential reuse of recycled glass fibre in problematic soil applications. *Journal of Cleaner Production*, *35*, 102-107.

[3] Al-Refeai, T. O. (1991). Behavior of granular soils reinforced with discrete randomly oriented inclusions. *Geotextiles and Geomembranes*, *10*(4), 319-333.

[4] Aggarwal, P., & Sharma, B. (2011). Application of jute fiber in the improvement of subgrade characteristics. *International journal on transportation and urban development*, *1*(1), 56-58.

[5] Ansal, A. M., & Erken, A. (1996). Posttesting correction procedure for membrane compliance effects on pore pressure. *Journal of geotechnical engineering*, *122*(1), 27-38.

[6] Asokan, P., Osmani, M., & Price, A. D. (2009). Assessing the recycling potential of glass fibre reinforced plastic waste in concrete and cement composites. *Journal of Cleaner Production*, *17*(9), 821-829.

[7] Axinte, E. (2011). Glasses as engineering materials: a review. *Material design*, 32,1717-1732.

[8] Azeiteiro, R. J., Coelho, P. A., Taborda, D. M., & Grazina, J. C. (2017). Critical state–based interpretation of the monotonic behavior of Hostun Sand. *Journal of Geotechnical and Geoenvironmental Engineering*, *143*(5), 04017004.

[9] Babu, G. S., & Vasudevan, A. K. (2007). Evaluation of strength and stiffness response of coir-fibre-reinforced soil. *Proceedings of the Institution of Civil Engineers-Ground Improvement*, *11*(3), 111-116.

[10] Baldi, G., Hight, D. W., & Thomas, G. E. (1988). State-of-the-art paper: a re-evaluation of conventional triaxial test methods. In *Advanced triaxial testing of soil and rock*. ASTM International.

[11] Baldi, G., & Nova, R. (1984). Membrane penetration effects in triaxial testing. *Journal of Geotechnical engineering*, *110*(3), 403-420.

[12] Been, K., & Jefferies, M. G. (1985). A state parameter for sands. *Géotechnique, 35*(2), 99-112.

[13] Been, K., Jefferies, M. G., & Hachey, J. (1991). The critical state of sands. *Geotechnique*, *41*(3), 365-381.

[14] Bishop, A. W., & Green, G. E. (1965). The influence of end restraint on the compression strength of a cohesionless soil. *Geotechnique*, *15*(3), 243-266.

[15] Biswas, S., Ahsan, Q., Cenna, A., Hasan, M. and Hassan, A. (2013). Physical and mechanical properties of jute, bamboo and coir natural fiber, *Fibers and Polymers*, *14* (10), 1762-1767.

[16] Bower, T. (2017). Constitutive modelling of soils and fibre-reinforced soils. PhD thesis, *Cardiff University*.

[17] Castro, A. (1969), Liquefaction of sands. Ph.D. thesis, Harvard University, Cambridge, Mass., *USA*.

[18] Chauhan, M. S., Mittal, S., & Mohanty, B. (2008). Performance evaluation of silty sand subgrade reinforced with fly ash and fibre. *Geotextiles and geomembranes*, *26*(5), 429-435.

[19] Chang, N., Heymann, G., & Clayton, C. (2011). The effect of fabric on the behaviour of gold tailings. *Géotechnique*, *61*(3), 187-197.

[20] Chen, Y. C., & Chuang, J. C. (2001, January). Effects of fabric on steady state and liquefaction resistance. In *The Eleventh International Offshore and Polar Engineering Conference*. International Society of Offshore and Polar Engineers.

[21] Colombo, P., Brusatin, G., Bernardo, E., and Scarinci, G. (2003). Inertization and reuse of waste materials by vitrification and fabrication of glass-based products. *Current Opinion in Solid State & Materials Science*, 7, 225-239.

[22] Consoli, N. C., Prietto, P. D., & Ulbrich, L. A. (1998). Influence of fiber and cement addition on behavior of sandy soil. *Journal of geotechnical and geoenvironmental engineering*, *124*(12), 1211-1214.

[23] Consoli, N. C., Casagrande, M. D., Prietto, P. D., & Thomé, A. N. (2003). Plate load test on fiber-reinforced soil. *Journal of Geotechnical and Geoenvironmental Engineering*, *129*(10), 951-955.

[24] Consoli, N. C., Casagrande, M. D., & Coop, M. R. (2005). Effect of fiber reinforcement on the isotropic compression behavior of a sand. *Journal of Geotechnical and Geoenvironmental Engineering*, *131*(11), 1434-1436.

[25] Consoli, N. C., Heineck, K. S., Casagrande, M. D. T., & Coop, M. R. (2007). Shear strength behavior of fiber-reinforced sand considering triaxial tests under distinct stress paths. *Journal of geotechnical and geoenvironmental engineering*, *133*(11), 1466-1469.

[26] Consoli, N. C., Vendruscolo, M. A., Fonini, A., & Dalla Rosa, F. (2009). Fiber reinforcement effects on sand considering a wide cementation range. *Geotextiles and Geomembranes*, *27*(3), 196-203.

[27] Consoli, N. C., Festugato, L., & Heineck, K. S. (2009a). Strain-hardening behaviour of fibre-reinforced sand in view of filament geometry. *Geosynthetics International*, *16*(2), 109-115.

[28] Consoli, N. C., Casagrande, M. D. T., Thomé, A., Dalla Rosa, F., & Fahey, M. (2009b). Effect of relative density on plate loading tests on fibre-reinforced sand. *Géotechnique*, *59*(5), 471-476.

[29] Dafalla, M. A., Al-Shamrani, M. A., Puppala, A. J., & Ali, H. E. (2012). Design guide for rigid foundation systems on expansive soils. *International Journal of Geomechanics*, *12*(5), 528-536.

[30] Dai, B., Yang, J., Zhou, C., & Luo, X. (2016). DEM investigation on the effect of sample preparation on the shear behavior of granular soil. *Particuology*, *25*, 111-121.

[31] Dennis, N. D. (1988). Influence of specimen preparation techniques and testing procedures on undrained steady state shear strength. In *Advanced Triaxial Testing of Soil and Rock*. ASTM International.

[32] Desrues, J., Chambon, R., Mokni, M., & Mazerolle, F. (1996). Void ratio evolution inside shear bands in triaxial sand specimens studied by computed tomography. *Géotechnique*, *46*(3), 529-546.

[33] Diambra, A., Russell, A. R., Ibraim, E., & Muir Wood, D. (2007). Determination of fibre orientation distribution in reinforced sands. *Géotechnique*, *57*(7), 623-628.

[34] Diambra, A. (2010). Fibre reinforced sands: experiments and constitutive modelling. PhD thesis. *University of Bristol*.

[35] Diambra, A., Ibraim, E., Russell, A. R., & Muir Wood, D. (2013). Fibre reinforced sands: From experiments to modelling and beyond. *International Journal for Numerical and Analytical Methods in Geomechanics, 37*(15), 2427-2455.

[36] Diambra, A., & Ibraim, E. (2015). Fibre-reinforced sand: Interaction at the fibre and grain scale. *Géotechnique, 65*(4), 296-308.

[37] di Prisco, C., & Nova, R. (1993). A constitutive model for soil reinforced by continuous threads. *Geotextiles and Geomembranes*, *12*(2), 161-178.

[38] Ding, D., & Hargrove, S. K. (2006). Nonlinear stress-strain relationship of soil reinforced with flexible geofibers. *Journal of geotechnical and geoenvironmental engineering*, *132*(6), 791-794.

[39] Doanh, T., & Ibraim, E. (2000). Minimum undrained strength of Hostun RF sand. *Géotechnique*, *50*(4), 377-392.

[40] Duncan, J. M., & Dunlop, P. (1968). The significance of cap and base restraint. *Journal of the Soil Mechanics and Foundations Division*, *94*(1), 271-290.

[41] Finno, R. J., Harris, W. W., Mooney, M. A., & Viggiani, G. (1996). Strain localization and undrained steady state of sand. *Journal of Geotechnical Engineering*, *122*(6), 462-473.

[42] Freilich, B. J., Li, C., & Zornberg, J. G. (2010, May). Effective shear strength of fiber-reinforced clays. In *9th International Conference on Geosynthetics, Brazil* ,1997-2000.

[43] Gao, Z., & Zhao, J. (2013). Evaluation on failure of fiber-reinforced sand. *Journal of Geotechnical and Geoenvironmental Engineering, 139*(1), 95-106.

[44] Gao, Z., Zhao, J., Li, X., & Dafalias, Y. F. (2014). A critical state sand plasticity model accounting for fabric evolution. *International Journal for Numerical and Analytical Methods in Geomechanics, 38*(4), 370-390.

[45] Gao, Z., & Diambra, A. (2020). A multiaxial constitutive model for fibre-reinforced sand.*Géotechnique* ,Accepted , 1-13.

[46] Gao, Z.W., Lu, D.C., Huang, M. (2020). Effective skeleton stress and void ratio for constitutive modelling of fiber-reinforced sand. Acta geotechnica,15(1), 2797-2811.

[47] Gary, D. H. (1970). Role of woody vegetation in reinforcing soils and stabilizing slopes. *Symposium on soil reinforcement and stabilizing techniques*, 253-306.

[48] Gajo, A., & Muir Wood, D., (1999) Severn-Trent sand: a Kinematic-hardening constitutive model: The q-p formulation. *Geotechnique, 49*(5), 595-614

[49] Gray, D. H., & Ohashi, H. (1983). Mechanics of fiber reinforcement in sand. *Journal of geotechnical engineering*, *109*(3), 335-353.

[50] Gray, D. H., & Al-Refeai, T. Behavior of fabric-versus fiber-reinforced sand. *Journal of Geotechnical Engineering*, *112*(8), 804-820 (1986).

[51] Greeuw, G., Adel, H. D., Schapers, A. L., & Haan, E. J. D. (2001). Reduction of axial resistance due to membrane and side drains in the triaxial test. In *Soft Ground Technology* (pp. 30-42).

[52] Gregory, G.H. & Chill, D.S. (1998) Stabilization of earth slope with fiber reinforcement. Proceedings 6th International Conference on Geosyntetics, *Atlanta*, 1073-1078

[53] Gregory, G. H. (1999). Theoretical shear-strength model of fiber-soil composite. In *Proceedings of* (Vol. 99, pp. 1-10).

[54] Gregory, G. H. (2006). Shear Strength, Creep and Stability of Fiber-Reinforced Soil Slopes. Ph.D. Dissertation, *Oklahoma State University, Stillwater, OK, USA*.

[55] Gregory, G. H. (2000). "Slope Reinforcement Simplified Design Guide Fiber-Reinforced Slope Over Firm Foundation," *Synthetic Industries, Inc*.

[56] Grogan, W. P., & Johnson, W. G. (1993). Stabilization of high plasticity clay and silty sand by inclusion of discrete fibrillated polypropylene fibers (Geofibers®) for use in pavement subgrades. *US Army Corps of Engineers Waterways Experiment Station*.

[57] Heineck, K. S., & Consoli, N. C. (2004). Discussion of 'discrete framework for limit equilibrium analysis of fibre-reinforced soil' by J.G. Zornberg. *Geotechnique, 54*(1), 72-73.

[58] Heineck, K. S., Coop, M. R., & Consoli, N. C. (2005). Effect of microreinforcement of soils from very small to large shear strains. *Journal of geotechnical and geoenvironmental engineering*, *131*(8), 1024-1033.

[59] Hejazi, S., Sheikhzadeh, M., Abtahi, S. & Zadhoush, A. (2012). A simple review of soil reinforcement by using natural and synthetic fiber. *Construction and Building Materials*, *30*, 100-116.

[60] Henkel, D. J., & Gilbert, G. D. (1952). The effect measured of the rubber membrane on the triaxial compression strength of clay samples. *Geotechnique*, *3*(1), 20-29.

[61] Hird, C. C., & Hassona, F. A. K. (1990). Some factors affecting the liquefaction and flow of saturated sands in laboratory tests. *Engineering Geology*, *28*(1-2), 149-170.

[62] Hatami, K., Gregory, G., Garland, G. S. (2018). Guidelines for the use of fibre-reinforced soil (FRS) in highway construction. PhD thesis. *The University of Oklahoma Norman.*

[63] Ibraim, E., Camenen, J., Diambra, A., Kairelis, K., Visockaite, L., & Consoli, N. C. (2018). Energy efficiency of fibre reinforced soil formation at small element scale: Laboratory and numerical investigation. *Geotextiles and Geomembranes, 46*(4), 497-510.

[64] Ibraim, E., Diambra, A., Muir Wood, D., & Russell, A. R. (2010). Static liquefaction of fibre reinforced sand under monotonic loading. *Geotextiles and Geomembranes, 28*(4), 374-385.

[65] Ibraim, E., Diambra, A., Russell, A. R., & Wood, D. M. (2012). Assessment of laboratory sample preparation for fibre reinforced sands. *Geotextiles and Geomembranes*, *34*, 69-79.

[66] Ishihara, K. (1993). Liquefaction and flow failure during earthquakes. *Geotechnique*, *43*(3), 351-451.

[67] Jefferies, M., & Been, K. (2015). *Soil liquefaction: a critical state approach*. CRC press.

[68] Ladd, R. S. (1974). Specimen preparation and liquefaction of sands. *Journal of Geotechnical and Geoenvironmental Engineering*, *100*(Proc. Paper 10857 Proceeding).

[69] Ladd, R. S. (1978). Preparing test specimens using undercompaction. *Geotechnical Testing Journal*, *1*(1), 16-23.

[70] Lade, P. V., & Wang, Q. (2011). Effect of boundary conditions on shear banding in true triaxial tests on sand. *Journal of Geotechnical Engineering Division, ASCE*, *42*(4), 19-25.

[71] Lee, K. L., & Vernese, F. J. (1978). End restraint effects on cyclic triaxial strength of sand. *Journal of Geotechnical and Geoenvironmental Engineering*, *104*(ASCE 13839 Proceeding).

[72] Li, C. L. (2005). Mechanical response of fibre-reinforced soil. Phd thesis. *University of Texas at Austin*.

[73] Li, J., Tang, C., Wang, D., Pei, X. & Shi, B. (2014). Effect of discrete fibre reinforcement on soil tensile strength. *Journal of Rock Mechanics and Geotechnical Engineering*, *6* (2), 133-137.

[74] Liu, X., Shao, L., & Guo, X. (2013). Local data analysis for eliminating end restraint of triaxial specimen. *Transactions of Tianjin University*, *19*(5), 372-380.

[75] Ling, H. I., Leshchinsky, D., & Tatsuoka, F. (Eds.). (2003). Reinforced soil engineering: advances in research and practice. *CRC Press*.

[76] Li, X. S., & Wang, Y. (1998). Linear representation of steady-state line for sand. *Journal of geotechnical and geoenvironmental engineering*, *124*(12), 1215-1217.

[77] Mandolini, A., Diambra, A., & Ibraim, E. (2019;2018;). Strength anisotropy of fibre-reinforced sands under multiaxial loading. *Géotechnique, 69*(3), 203-216.

[78] Maheshwari, K. V., Desai, A. K., & Solanki, C. H. (2011). Performance of fiber reinforced clayey soil. *Electronic Journal of Geotechnical Engineering*, *16*, 1067-1082.

[79] Maliakal, T., & Thiyyakkandi, S. (2013). Influence of randomly distributed coir fibers on shear strength of clay. *Geotechnical and Geological Engineering*, *31*(2), 425-433.

[80] Michalowski, R. L., & Zhao, A. (1996). Failure of fiber-reinforced granular soils. *Journal of geotechnical engineering*, *122*(3), 226-234.

[81] Michalowski, R. L. (1996). Micromechanics-based failure model of granular/particulate medium with reinforcing fibers. *Technical Report*, Air Force office of Scientific Research, USA.

[82] Michalowski, R. L., & Č ermák, J. (2002). Strength anisotropy of fiber-reinforced sand. *Computers and geotechnics*, 29(4), 279-299.

[83] Michalowski, R. L., & Čermák, J. (2003). Triaxial compression of sand reinforced with fibers. *Journal of geotechnical and geoenvironmental engineering*, *129*(2), 125-136.

[84] Michalowski, R. L. (2008). Limit analysis with anisotropic fibre-reinforced soil. *Geotechnique*, *58*(6), 489-501.

[85] Michalowski, R. L., & Čermák, J. (2002). Strength anisotropy of fiber-reinforced sand. *Computers and Geotechnics*, 29(4): 279-299.

[86] Miura, S., & Toki, S. (1982). A sample preparation method and its effect on static and cyclic deformation-strength properties of sand. *Soils and foundations*, *22*(1), 61-77.

[87] Mo, Y. X., Pang, J. Y., & Huang, J. K. (2019). Dynamic Mechanical Properties and Fractal Characteristics of Polypropylene Fiber-Reinforced Cement Soil under Impact Loading. *Advances in Materials Science and Engineering*, 2019.

[88] Nicholson, P. G., Seed, R. B., & Anwar, H. A. (1993). Elimination of membrane compliance in undrained triaxial testing. I. Measurement and evaluation. *Canadian Geotechnical Journal*, *30*(5), 727-738.

[89] Noyes H A. The effect on plant growth of saturating a soil with carbon dioxide[J]. *Science, 1914, 40*(1039): 792-792.

[90] Muir Wood, D., Diambra, A., & Ibraim, E. (2016). Fibres and soils: A route towards modelling of root-soil systems. *Soils and Foundations, 56*(5), 765-778.

[91] Omar, T., & Sadrekarimi, A. (2014). Effects of multiple corrections on triaxial compression testing of sands. *Journal of GeoEngineering*, *9*(2), 75-83.

[92] Pino, L. F. M., & Baudet, B. A. (2015). The effect of the particle size distribution on the mechanics of fibre-reinforced sands under one-dimensional compression. *Geotextiles and Geomembranes*, 43(3), 250-258.

[93] Potts, David M., et al. Finite element analysis in geotechnical engineering: application. Vol. 2. *London: Thomas Telford*, 2001.

[94] Puppala, A. J., & Musenda, C. (2000). Effects of fiber reinforcement on strength and volume change in expansive soils. *Transportation Research Record*, *1736*(1), 134-140.

[95] Raghunandan, M. E. (2011). Effect on cyclic response and liquefaction resistance due to desaturation of sand*,* Ph.D Thesis, *Indian Institute of Technology Bombay*, India.

[96] Raghunandan, M., Juneja, A., & Hsiung, B. (2012). Preparation of reconstituted sand samples in the laboratory. *International Journal of Geotechnical Engineering*, *6*(1), 125-131.

[97] Raghunandan, M. E., Sharma, J. S., & Pradhan, B. (2015). A review on the effect of rubber membrane in triaxial tests. *Arabian Journal of Geosciences*, *8*(5), 3195-3206.

[98] Raju, V. S., & Sadasivan, S. K. (1974). Membrane penetration in triaxial tests on sands. *Journal of the Geotechnical Engineering Division*, *100*(4), 482-489.

[99] Rao, G. V., & Balan, K. (2000). Coir geotextiles—Emerging trends, *Kerala State Coir Corporation Limited*.

[100] Ranjan, G., Vasan, R. M., & Charan, H. D. (1996). Probabilistic analysis of randomly distributed fiber-reinforced soil. *Journal of geotechnical engineering*, *122*(6), 419-426.

[101] Richart, F. E. Jr., Hall, J. R. & Woods, R. D. (1970). Vibrations of soils and foundations.

[102] Englewood Cliffs, NJ: Prentice-Hall.

[103] Roscoe, K. H., Schofield, A., & Wroth, A. P. (1958). On the yielding of soils. *Geotechnique*, *8*(1), 22-53.

[104] Rowe, P. W., & Barden, L. (1964). Importance of free ends in triaxial testing. *Journal of Soil Mechanics & Foundations Div*, *90*(Proc. Paper 3753).

[105] Santoni, R. L., Tingle, J. S., & Webster, S. L. (2001a). Engineering properties of sand-fiber mixtures for road construction. *Journal of geotechnical and geoenvironmental engineering*, *127*(3), 258-268.

[106] Santoni, R. L., & Webster, S. L. (2001b). Airfields and roads construction using fiber stabilization of sands. *Journal of transportation engineering*, *127*(2), 96-104.

[107] Senetakis, K., & Li, H. (2017). Influence of stress anisotropy on small-strain stiffness of reinforced sand with polypropylene fibres. *Soils and Foundations, 57*(6), 1076-1082.

[108] Scott, R. F. (1987). Failure. *Géotechnique*, *37*(4), 423-466.

[109] Sivakumar Babu, G. & Vasudevan, A. (2008). Strength and Stiffness Response of Coir Fiber-Reinforced Tropical Soil, *Journal of Materials in Civil Engineering*, *20*(9), 571-577.

[110] Skempton, A. H. (1954). The pore water coefficient A and B. *Geotechnique*, 4, 143-147.

[111] Sladen, J. A., & Handford, G. (1987). A potential systematic error in laboratory testing of very loose sands. *Canadian Geotechnical Journal*, *24*(3), 462-466.

[112] Sheng, D., Westerberg, B., Mattsson, H., & Axelsson, K. (1997). Effects of end restraint and strain rate in triaxial tests. *Computers and Geotechnics*, *21*(3), 163-182.

[113] Shewbridge, S. E., & Sitar, N. Deformation characteristics of reinforced soil in direct shear. *Journal of the Geotechnical and Geoenvironmental Engineering*, *115* (8), 1134-1147 (2001).

[114] Shukla, S. K. (2017). Fundamentals of Fibre-Reinforced Soil Engineering. *Springer Nature Singapore Pte Ltd*.

[115] Silva Dos Santos, A. P., Consoli, N.C., & Baudet, B. A. (2010). The mechanics of fibre reinforced sand. *Géotechnique*, *61*(10), 791-799.

[116] Soriano, I., Ibraim, E., Andò, E., Diambra, A., Laurencin, T., Moro, P., & Viggiani, G. (2017). 3D fibre architecture of fibre-reinforced sand. *Granular Matter, 19*(4), 1-14.

[117] Sze, H. Y., & Yang, J. (2014). Failure modes of sand in undrained cyclic loading: impact of sample preparation. *Journal of geotechnical and geoenvironmental engineering*, *140*(1), 152-169.

[118] Tang, C. S., Wang, D. Y., Cui, Y. J., Shi, B., & Li, J. (2016). Tensile strength of fiber-reinforced soil. *Journal of Materials in Civil Engineering*, 28(7), 04016031.

[119] Vaid, Y. P., and Thomas, J. (1995). Liquefaction and post-liquefaction behaviour of sand. *Journal of geotechnical engineering*, 121(2), 163-179.

[120] Vaid, Y. P., Sivathayalan, S., & Stedman, D. (1999). Influence of specimen-reconstituting method on the undrained response of sand. *Geotechnical Testing Journal*, *22*(3), 187-195.

[121] Vaid, Y. P., & Sivathayalan, S. (2000). Fundamental factors affecting liquefaction susceptibility of sands. *Canadian Geotechnical Journal*, *37*(3), 592-606.

[122] Verdugo, R., & Ishihara, K. (1996). The steady state of sandy soils. *Soils and foundation*, *36*(2), 81-92.

[123] Viswanadham, B. V. S., Phanikumar, B. R., & Mukherjee, R. V. (2009). Swelling behaviour of a geofiber-reinforced expansive soil. *Geotextiles and Geomembranes*, *27*(1), 73-76.

[124] Waldron, L. J. (1977). The shear resistance of root-permeated homogeneous and stratified soil. *Soil science society of American journal*, 41(3), 843-849.

[125] Wang, Y. X., Guo, P. P., Ren, W. X., Yuan, B. X., Yuan, H. P., Zhao, Y. L., ... & Cao, P. (2017). Laboratory investigation on strength characteristics of expansive soil treated with jute fiber reinforcement. *International Journal of Geomechanics*, *17*(11), 04017101.

[126] Wu, T. H., Mckinnel III, W. P., and Swanston, D. N. (1979). Strength of tree roots and landslides on Prince of Wales Island, Alaska. *Canadian geotechnical journal, 16*(1), 19-33

[127] Yamashita, S., & Toki, S. (1993). Effect of fabric anisotropy of sand during rotation of principal stress directions. *Soils and Foundations*, *33*(3), 92-104.

[128] Yetimoglu, T., & Salbas, O. (2003). A study on shear strength of sands reinforced with randomly distributed discrete fibers. *Geotextiles and Geomembranes*, *21*(2), 103-110.

[129] Yixian, W., Panpan, G., Shengbiao, S., Haiping, Y., & Binxiang, Y. (2016). Study on strength influence mechanism of fiber-reinforced expansive soil using jute. *Geotechnical and Geological Engineering*, *34*(4), 1079-1088.

[130] Zhao, J., & Gao, Z.W. 2016. Unified anisotropic elastoplastic model for sand. *Journal of Engineering Mechanics*, *142*(1).

[131] Zhang, H. (1997). Steady state behaviour of sands and limitations of the triaxial test. Ph.D. thesis, *University of Ottawa (Canada)*.

[132] Zhang, H., & Garga, V. K. (1997). Quasi-steady state: a real behaviour?. *Canadian Geotechnical Journal*, *34*(5), 749-761.

[133] Ziegler, S., Leshchinsky, D., Ling, H. I., & Perry, E. B. (1998). Effect of short polymeric fibers on crack development in clays. *Soils and Foundations*, *38*(1), 247-253.

[134] Zornberg, J. G. (2002). Discrete framework for limit equilibrium analysis of fibre-reinforced soil. *Géotechnique*, *52*(8), 593-604.